NMR RELAXATION AND SELF DIFFUSION STUDIES OF THALLIUM COMPOUNDS.

A thesis submitted by

KEVIN JEFFREY KITTLE

in candiature for the degree

of Doctor of Philosophy

of the University of London.

The Bourne Laboratory,
Royal Holloway and Bedford New College,
University of London,
Egham Hill,
Egham,
Surrey.

September 1987

ProQuest Number: 10096451

All rights reserved

INFORMATION TO ALL USERS
The quality of this reproduction is dependent upon the quality of the copy submitted.

In the unlikely event that the author did not send a complete manuscript
and there are missing pages, these will be noted. Also, if material had to be removed,
a note will indicate the deletion.

ProQuest 10096451

Published by ProQuest LLC(2016). Copyright of the Dissertation is held by the Author.

All rights reserved.
This work is protected against unauthorized copying under Title 17, United States Code.
Microform Edition © ProQuest LLC.

ProQuest LLC
789 East Eisenhower Parkway
P.O. Box 1346
Ann Arbor, MI 48106-1346

ABSTRACT

^{205}Tl NMR relaxation and self-diffusion measurements were applied to study the probe qualities of thallium cations in sucrose/solvent systems.

The value of variable field/variable temperature relaxation measurements in defining relaxation behaviour was demonstrated.

The relaxation of the dimethylthallium(III) cation in 60% sucrose/D_2O (w/w) solution is dominated by the CSA mechanism at both high and low field. It was necessary to use a temperature dependent Fuoss-Kirkwood distribution of correlation times to rationalise the R_1 data and this analysis gave the shielding anisotropy of the cation as 5588 ± 173ppm, in keeping with previous studies. Similar behaviour was noted for the diethylthallium cation in sucrose/DMSO-d^6 solutions (>10% concentration) and a concentration dependence in the distribution width parameter was observed.

The ^{13}C relaxation in aqueous sucrose solution at 60% concentration similarly showed complex behaviour.

Self-diffusion and relaxation studies on thallium(I) ion in sucrose/D_2O solutions showed the cation to be a good diffusional probe in viscous solutions, but a poor probe of reorientational motion. Studies on the self-diffusion of the dimethylthallium(III) cation in D_2O were consistent with a solvent structure-limited model for translational motion. Further studies in sucrose/D_2O

solutions showed the dimethylthallium(III) cation to be limited to studying solutions < 30% concentration.

Studies of $Tl(I)^+$ ion in aqueous TANOL solutions showed an inverse frequency dependence of R_1 and R_2 and a dominant electron-nuclear scalar relaxation mechanism was proposed.

Finally, ^{205}Tl and ^{203}Tl R_1 measurements in neat and diluted thallium(I) ethoxide showed that in the neat solution the rates for both nuclei were equal at high field and were dominated by the CSA mechanism. At low field, ^{203}Tl R_1 > ^{205}Tl R_1 and a dominant scalar mechanism was proposed. In dilute solution the rates were equal at both high and low field and no CSA contribution was observed.

ACKNOWLEDGEMENTS.

The author would like to thank Dr Duncan Gillies for his interest, guidance and encouragement during the course of this work and Dr Mark Forster for many helpful discussions.

Thanks are also due to Dr Ray Matthews for the supply of thallium compounds and to Dr Geoff Hawkes and the staff of the University of London Intercollegiate Research Services for experiments performed on the Bruker WH-400 spectrometer.

The receipt of a research studentship from the Science and Engineering Research Council is gratefully acknowledged.

In addition, the author would like to thank the staff and research students of the Bourne Laboratory for making the author's stay a very happy one.

Finally the author wishes to thank his family and Miss Alison Patten for their support, particularly during the latter stages of this work.

To The Memory of

My Father

CONTENTS

CONTENTS continued PAGE

CONTENTS continued PAGE

CONTENTS continued PAGE

CONTENTS continued

CONTENTS continued.

LIST OF FIGURES.

LIST OF Figures continued

LIST OF FIGURES continued.

LIST OF TABLES.

CHAPTER FOUR

LIST OF TABLES continued

LIST OF TABLES continued

LIST OF TABLES continued

LIST OF TABLES continued.

CHAPTER ONE - INTRODUCTION.

Section 1.1 NMR basic principles.

1.1.1 Quantum Mechanical Formalism.

The nuclei of interest in the NMR experiment are those that possess the property of spin angular momentum. This property is quantised in units of $\hbar$ and its magnitude may be specified in terms of a spin quantum number I. Nuclei that have an odd atomic mass number possess half integral spin where I = $\frac{1}{2}$, $\frac{3}{2}$, $\frac{5}{2}$ .. The spin I = $\frac{1}{2}$ nucleus is a very common example and is the class of nucleus of interest in the studies presented in this work.

The magnetic moment μ associated with the nuclear spin angular momentum is either parallel or antiparallel to it, and is proportional in magnitude. This may be expressed as

$$\mu = \gamma \underline{I} \qquad (1 - 1)$$

Thus γ, the magnetogyric ratio, is a scalar quantity associated with each nucleus and may be either positive or negative. Clearly the magnetic moment will be also quantised along a component direction (Z) since the allowed values of $\hat{I}_z$ are $m_I\hbar$, where m_I takes on the 2I+1 values from -I, -I+1, ... +I.

When a static magnetic field B_o is applied along the Z direction the classical interaction energy of the magnetic moment,

$$E = -\underline{\mu} \cdot \underline{B}, \qquad (1-2)$$

reduces to

$$E = -\mu_z \cdot B_o. \qquad (1-3)$$

In quantum mechanical terms

$$\hat{\mathcal{H}} = -\hat{\mu}_z \cdot B_o. \qquad (1-4)$$

Therefore it follows that the (2I+1) allowed energies (eigenvalues) are,

$$E = -\gamma \hbar m_I B_o \qquad (1-5)$$

and the separation between the energy levels ΔE is

$$|\gamma \hbar B_o|. \qquad (1-6)$$

In the NMR experiment the transitions between energy levels are induced by a radiofrequency field. The resonance condition is derived from the Einstein relation, $\Delta E = h\upsilon$ and hence,

$$\upsilon_o = \frac{\gamma B_o}{2\pi}. \qquad (1-7)$$

The description of the NMR experiment to this stage has been based on the quantum mechanical formalism. However, if we wish to describe relaxation phenomena, the quantum mechanical approach proves to be complex. The situation is more readily understood by a classical treatment of the motion of magnetic moments in a magnetic

field. This approach was first described by Bloch[1].

1.1.2 The Bloch equations.

If the sample is considered to be comprised of a number of non interacting identical spins, then the total magnetic moment or magnetisation is the sum of the individual moments,

$$\underline{M} = \Sigma_i \underline{\mu}_i . \qquad (1 - 8)$$

When the sample is placed in a magnetic field the spins experience a torque that changes the angular momentum, $\underline{P}$. The rate of change is given by,

$$\frac{d \underline{P}}{d t} = - \underline{B} \times \underline{M} \qquad (1 - 9)$$

The magnetisation is related to the total spin angular momentum by the relation,

$$\underline{M} = \gamma \underline{P} , \qquad (1 - 10)$$

where γ is the magnetogyric ratio for the nucleus. Hence it follows that

$$\frac{d \underline{M}}{d t} = - \gamma \underline{B} \times \underline{M} . \qquad (1 - 11)$$

Equation (1 - 11) describes the motion of the magnetisation in the presence of a static magnetic field B_o. The solution to this equation shows that the motion

takes the form of a precession about the B_o axis with an angular frequency $\omega_o = \gamma B_o$. This is known as Larmor precession, and ω_o is the Larmor frequency.

The nuclei may be aligned either against, or in the direction of the static field B_o. At thermal equilibrium, the Boltzmann distribution dictates that the lower energy state will be more populated. Therefore more nuclei are aligned with the static field and so the net magnetisation $\underline{M}$ is along the positive z' axis. At this point, there is no phase coherence of the magnetic moments along the x' and y' axes , and so the net transverse magnetisation is zero thus,

$$\underline{M} = (0,0,M_o) \qquad (1-12)$$

To observe the NMR spectrum, one must perturb the system by applying a small, time dependent, magnetic field, $2B_1 \cos \omega t$ along the x direction and as ω approaches ω_o, the x and y components of the magnetisation become non zero.

The perturbing field may be resolved into components rotating in opposite directions in the xy plane. The component that rotates in the same direction as the Larmor precession provides the only significant interaction, and so the second component may be neglected.

The total magnetic field, B experienced by the nucleus may now be written in terms of the unit vectors $\underline{i}$, $\underline{j}$, $\underline{k}$, in the x,y, and z directions.

$$B = B_1 \cos \omega t \, (\underline{i}) - B_1 \sin \omega t \, (\underline{j}) + B_0 \, (\underline{k})$$

(1 - 13)

As yet, no account has been taken of the processes of nuclear spin relaxation that lead to internal realignment of the nuclear spins to the Boltzmann equilibrium populations, following a perturbation of the magnetisation. Bloch assumed that the longitudinal and transverse components of the magnetisation both decayed exponentially to their equilibrium values, but with different time constants T_1 and T_2 respectively. Thus the full equations of motion, the Bloch equations are given by,

$$\frac{d M_x}{d t} = \gamma (M_y B_0 + M_z B_1 \sin \omega t) - \frac{M_x}{T_2}$$

(1 - 14)

$$\frac{d M_y}{d t} = \gamma (M_z B_1 \cos \omega t - M_x B_0) - \frac{M_y}{T_2}$$

(1 - 15)

$$\frac{d M_z}{d t} = \gamma (M_x B_1 \sin \omega t + M_y B_1 \cos \omega t) - \frac{(M_z - M_0)}{T_1}$$

(1 - 16)

1.1.3 Nuclear spin relaxation.

The Bloch equations allow for a quantitative description of nuclear spin relaxation .

The description in physical terms at the molecular level was first provided by Bloembergen, Purcell and Pound (BPP)[2]. In their model, nuclear spin relaxation of spin $\frac{1}{2}$ nuclei arises as a result of the nucleus experiencing a magnetic interaction from its surroundings which is modulated, in a random manner, by the random molecular (Brownian) motion. The microscopic fluctuating field, b may be resolved into components b_x, b_y, and b_z along the x,y, and z axes. The interaction of the macroscopic magnetisation $\underline{M}$ with the microscopic field $\underline{b}$ is given by,

$$(\underline{b} \times \underline{M}) = \underline{i} (b_y M_z - b_z M_y) + \underline{j} (b_z M_x - b_x M_z) + \underline{k} (b_x M_y - b_y M_x). \qquad (1 - 17)$$

Thus it is apparent that for random fluctuating fields, the component oscillating in the x direction will interact with M_y and M_z and may cause relaxation of these components. Similarly the component in the y direction will interact with M_z and M_x and the component in the z direction will interact with M_y and M_x. Therefore it is the b_x and b_y components of the fluctuating microscopic field that are efficient for both spin-lattice (longitudinal) and spin-spin (transverse) relaxation.

If we consider the rotating frame of reference, the entire axis system is assumed to rotate at the Larmor frequency ω_o about the z' axis. The components of the microscopic magnetic fields b_x,b_y, and b_z oscillating at

ω_o are seen to be static in the reference axis system. A static component b_z in the rotating frame is also observed to be static in the laboratory frame and so there is a frequency independent contribution to the transverse relaxation. However static components along the x' and y' axes in the rotating frame are seen to oscillate at the larmor frequency in the laboratory frame, and will thus provide a frequency dependent contribution to both spin-spin and spin-lattice relaxation.

Only those components oscillating at the larmor frequency can effect nuclear spin-lattice relaxation, and so the efficiency of the relaxation process is dependent on the relationship between the timescale for molecular motion and the resonance frequency in the experiment. The detailed effects of the dependence of nuclear spin relaxation on molecular motion and resonance frequency are discussed in section {2.2.1}.

Section 1.2 Thallium NMR.

1.2.1 NMR Properties.

The intrinsic nuclear properties of thallium suggest that it has particularly useful application to NMR studies. There are two naturally occuring isotopes of thallium, both of which are spin $\frac{1}{2}$ nuclei, these are ^{205}Tl which is 70.5% abundant and ^{203}Tl which is 29.5% abundant. The ^{205}Tl nucleus has a relative receptivity of 0.1355 with respect to a proton receptivity of one and is the third most receptive spin $\frac{1}{2}$ nucleus after ^{1}H and ^{19}F. These properties enable one to readily observe the thallium nucleus by NMR spectroscopy.

The magnetogyric ratios of the ^{205}Tl and ^{203}Tl nuclei are in the ratio ^{205}Tl : ^{203}Tl = 1.0098, hence the resonance frequencies show a similar ratio. Therefore observation of either nucleus gives essentially the same information.

For a reference sample of aqueous thallium(I) nitrate, the extrapolated infinite dilution ^{205}Tl resonance frequency is reported to be 57,683,833Hz[3] in a magnetic field in which the protons of TMS resonate at exactly 100MHz.

The chemical shifts and coupling constants are particularly sensitive to the electronic environment surrounding the thallium nucleus and so thallium spectroscopy is particularly appropriate for the study of chemical and physical interactions both in the solid and

liquid state and has aroused much interest in this field.

1.2.2 Thallium NMR studies.

Initial thallium NMR spectra in both the solid[4] and liquid[5] state were reported as early as 1953 and since then, extensive studies on thallium species have been made. Thallium has an outer electronic configuration of $d^{10}\ 6s^2\ 6p^1$ and thus exists in both the (+1) and (+3) states.

The $Tl(I)^+$ ion has a chemical shift range greater than 3400 ppm and has found primary use in the study of ion solvent and ion pairing interactions in the solution state. The dependence of the ^{205}Tl chemical shift on the concentration of the thallium species and the nature of its anion has been extensively studied in many different systems [3,6-23]. Some of these studies [3,15,16,23] have extended the probe qualities of the cation to the study of ion-solvent interactions in mixed solvent systems and the ^{205}Tl chemical shift for $TlNO_3$ in a number of binary systems has been analysed in terms of preferential solvation of the $Tl(I)^+$ by either solvent component[24].

The ionic radius of the $Tl(I)^+$ ion is about 140pm and is similar in size to both $Na(I)^+$ and $K(I)^+$ ions. Hence, the $Tl(I)^+$ ion has been considered as a probe ion to study the function of $Na(I)^+$ and $K(I)^+$ ions in biological systems[25-34].

The interaction of the $Tl(I)^+$ ion with complexing ligands has also been studied by ^{205}Tl NMR, and complexes

with ethylendiamine[35], cryptands[36], and crown ethers[18,37,38] have been discussed.

In addition to chemical shift studies, the nuclear spin relaxation behaviour of the $Tl(I)^+$ ion has also been studied. For $Tl(I)^+$ ion in aqueous solution, the ^{205}Tl relaxation rates have been reported[35,39] to be insensitive to changes in concentration, anion, solvent isotope (H_2O and D_2O) and resonance frequency, yet sensitive to changes in temperature. The dominant mechanism was proposed to be the spin-rotation mechanism[35,39,40] and this was further discussed by Schwartz[41] who noted the importance of the transient spin-rotation mechanism.

Further ^{205}Tl relaxation studies on $Tl(I)^+$ ion in n - butylamine[40], methanol[35], and DMSO[42] have shown that the ^{205}Tl R_1 is solvent dependent.

The strong sensitivity of the ^{205}Tl R_1 to added paramagnetic ions has been observed in studies on aqueous $Tl(I)^+$ ion solutions in the presence of oxygen[35,39,43,44], *TANOL[45], and $Fe(CN)_6^{3-}$ ion[46]. By an analysis of the effect of dissolved oxygen on the ^{205}Tl R_1 of $Tl(I)^+$ ion, Hinton et al.[47] derived useful solution structure information on Tl(I)-antibiotic complexes based on information gained from relaxation studies reported in earlier work[31-34].

^{205}Tl NMR studies on Tl(III) compounds have been mostly confined to the studies of organothallium(III)

derivatives due to the instability of Tl(III) salts. However a number of ^{205}Tl NMR studies on these systems have been made[14, 34, 48-50, 51].

^{205}Tl chemical shifts have been reported for $(CH_3)_3Tl$[14, 48, 52], $(C_2H_5)_3Tl$[14], $(CH_3)_2Tl^+$ [14, 35] and CH_3Tl^{2+}[53]. In addition, the ^{205}Tl chemical shift of a number of organothallium(III) compounds have been studied and are reported in the thesis of Brady[54].

^{205}Tl chemical shift studies on dimethyl and monomethyl cations have been made as a function of temperature, concentration, anion and solvent[53, 55-57]. The results show that the ^{205}Tl chemical shift has a significant temperature dependence, yet changes in concentration and anion have little effect. For the $(CH_3)_2Tl^+$ cation, the temperature dependence is in the order of 0.44 ppm/K and the cation has been proposed[58] and used for temperature measurement in variable temperature ^{205}Tl NMR studies[43].

Arylthallium derivatives have been studied by Koppel et al.[14], who have reported thallium chemical shifts for $Ph\ TlCl_2$ and its complexes with PPh_3 and dipyridine in pyridine and methanol solvents. Additional studies were made on Ph_2TlBr in DMSO and Ph_3Tl in ether. Other workers have provided further studies in this area: Hildebrand and Dreeskamp[52] have reported the ^{205}Tl chemical shift for Ph_2TlCl in liquid ammonia; Hinton and Briggs[56] have provided ^{205}Tl chemical shift data for a series of aryl-thallium(III)

Bis (trifluoroacetates) in a number of solvents and finally Brady[54] has reported ^{205}Tl chemical shifts for a number of diarylthallium(III) compounds.

Initial ^{205}Tl relaxation studies on organothallium compounds were reported by Chan and Reeves[35], who noted that the ^{205}Tl R_1 for the $(CH_3)_2Tl^+$ cation in a degassed aqueous solution, was independent of anion, concentration, solvent isotope composition (H_2O or D_2O), thallium isotope and resonance frequency. The apparent lack of frequency dependence in the ^{205}Tl R_1 was later found to be in error by Forster et al.[59], who noted that the ^{205}Tl R_1 of the $(CH_3)_2Tl^+$ cation and other dialkylthallium cations had a strong positive field dependence, indicating a contribution from the CSA mechanism. A further study[60] on the ^{205}Tl R_1 for the cation in aqueous glycerol solution similarly showed a very strong positive field dependence and a dominance of the CSA mechanism was suggested.

The presence of dissolved oxygen was found to enhance the ^{205}Tl R_1 of the $(CH_3)_2Tl^+$ cation in aqueous solution. However the effect was noted to be not as great as for the $Tl(I)^+$ ion.

^{205}Tl relaxation rates have been measured as a function of temperature for a wider range of mono and diorganothallium compounds, and are reported in the thesis of Brady[54]. In addition, Forster[43] has furthered the work of Brady to discuss the temperature and field

dependence of the ^{205}Tl R_1 values of Ph_2TlCl in DMSO-d^6 and $((CH_3)_3CCH_2)_2$ TlCl in pyridine-d^5.

Finally, thallium NMR spectroscopy has provided important information to determine the structure of thallium(I) alkoxides in solution. From the observation of ^{205}Tl and ^{203}Tl spectra, Schneider and Buckingham[48] were able to determine the tetrameric nature of thallium(I) ethoxide in both neat liquid and cyclohexane solution. Gillies et al.[61] used the technique in a later study to prove that the tetrameric structure was also prevalent in several other thallium alkoxides in toluene and benzene solutions.

There are a number of studies on thallium NMR spectroscopy that have not been covered in this review, indeed, the information gained from measured thallium spin-spin coupling constants has not been discussed. However, the review is designed to cover the areas of interest in the studies presented in later chapters and has therefore related to the relaxation properties of the thallium species and their ion-solvent, ion-complex interactions. More extensive reviews on thallium NMR has been provided by Hinton et al.[47,62] and less extensive reviews are provided in the theses of Forster[43], Brady[54] and Burke[63].

* 4-hydroxy-2,2,6 tetramethylpiperidine-1-oxyl

References for CHAPTER ONE.

1. F.Bloch, Phys. Rev.,70, 460 (1946)
2. N.Bloembergen, E.M.Purcell and R.V.Pound, Phys. Rev., 73, 679 (1948)
3. J.F.Hinton and R.W.Briggs, J. Magn. Reson. 19, 393, (1975)
4. N.Bloembergen and T.J.Rowland, Acta Metal, 1, 731 (1953)
5. H.S.Gutowsky and B.R.McGarvey, Phys. Rev., 91, 81 (1953)
6. T.D.Gierke and W.H.Flygare, J. Amer. Chem. Soc., 94, 7277 (1972)
7. R.P.H.Gasser and R.E.Richards, Mol. Phys., 2, 357 (1959)
8. R.Freeman, R.P.H.Gasser, R.E.Richards and D.H.Wheeler, Mol. Phys., 2, 75 (1959)
9. E.B.Baker and L.W.Burd, Rev. Sci. Instr., 34, 238 (1963)
10. D.Herbison-Evans, P.B.P.Phipps and R.J.P.Williams, J. Chem. Soc., 6170 (1965)
11. R.Freeman, R.P.H.Gasser and R.E.Richards, Mol. Phys., 2, 301 (1959)
12. R.W.Vaughan and D.H.Anderson, J. Chem. Phys., 52, 5287 (1972)
13. S.Hafner and N.H.Nachtreib, J. Chem. Phys. 42, 631 (1965)
14. H.Koppell, J.Dallorso, G.Hoffman and B.Walther, Zeit. Anorg. Allg. Chem., 427, 24 (1976)
15. J.J.Dechter and J.I.Zink, Inorg. Chem. 15, 1690 (1976)
16. J.J.Dechter and J.I.Zink, J. Amer. Chem. Soc., 97, 2937 (1975)
17. J.J.Dechter and J.I.Zink, J. Chem. Soc. Chem.Commun.,. 96 (1974)

18. J.J.Dechter and J.I.Zink, J. Amer. Chem. Soc., 98, 845 (1976)

19 J.F.Hinton and R.W.Briggs, J. Magn. Reson., 25, 379 (1977)

20. J.J.Dechter, Diss. Abstr. Int B, 36, 3944 (1976)

21. R.W.Briggs, K.R.Metz and J.J.Hinton, J. Solution Chem., 8, 479 (1979)

22. J.F.Hinton and K.R.Metz, J. Solution Chem., 9, 197 (1980)

23. R.W.Briggs and J.F.Hinton, J. Solution Chem. 6, 827 (1977)

24. R.W.Briggs and J.F.Hinton, J. Solution Chem., 8. 519 (1979)

25 J.Reuben and G.J.Kayne, J. Biol. Chem., 246, 6227 (1971)

26. F.J.Kayne and J.Reuben, J. Amer. Chem. Soc., 92, 220 (1970)

27. C.M.Grisham, R.K.Gupta, R.E.Barnett and A.S.Mildvan, J. Biol. Chem. 249, 6738 (1974)

28. J.F.Hinton, G.L.Turner and F.S.Millett, J. Magn. Reson., 45, 42 (1981)

29. J.F.Hinton, G.Young and F.S.Millett, Biochemistry, 21, 651 (1982)

30. G.L.Turner, J.F.Hinton and F.S.Millett, Biochemistry, 21, 646 (1982)

31. R.W.Briggs, F.A.Etzkhorn and J.F.Hinton, J. Magn. Reson., 37, 523 (1980)

32. R.W.Briggs and J.F.Hinton, J. Magn. Reson. 32, 155 (1978)

33. R.W.Briggs and J.F.Hinton, J. Magn. Reson., 43, 363 (1979)

34. R.W.Briggs and J.F.Hinton, Biochemistry, 17, 5576 (1978)

35. S.O.Chan and L.W.Reeves, J. Amer. Chem. Soc., 96,

404 (1974)

36. D.Gudlin and H.Schneider, Inorg. Chim. Acta, 33, 205 (1979)

37. M.Shamispur, G.Rounaghi and A.Popov, J. Solution Chem., 9, 701 (1980)

38. C.Srivinavit, J.I.Zink and J.J.Dechter, J. Amer. Chem. Soc. 99, 5876 (1977)

39. M.Bacon and L.W.Reeves, J. Amer. Chem. Soc., 95, 272 (1973)

40. J.F.Hinton and R.W.Briggs, J. Magn. Reson., 25, 379 (1977)

41. R.N.Schwartz, J. Magn. Reson., 24, 205 (1976)

42. J.F.Hinton and K.H.Ladner, J. Magn. Reson. 32, 303 (1978)

43. M.J.Forster, Ph.D. Thesis, University of London

44. B.W.Bangerter, J. Magn. Reson., 28, 141 (1977)

45 B.W.Bangerter and R.N.Schwartz, J. Chem. Phys., 60, 333 (1974)

46. R.P.H.Gasser and R.E.Richards, Mol. Phys. 2, 357 (1959)

47. J.F.Hinton, K.R.Metz and R.W.Briggs, Ann. Rep. NMR Spectry., 13, 211 (1982)

48. W.G.Schneider and A.D.Buckingham, Disc. Faraday Soc., 34, 147 (1962)

49. B.N.Figgis, Trans. Faraday Soc., 55, 1075 (1959)

50. J.Glaser and U.Henriksson, J. Amer. Chem. Soc. 103, 6642 (1981)

51. G.M.Sheldrick and J.P.Yesinowski, J. Chem. Soc. Dalton, 870 (1975)

52. K.Hilderbrand and H.Dreeskamp, Zeit. Phys. Chem., 69, 171 (1970)

53. C.S.Hoad, R.W.Matthews, M.M.Thakur and D.G.Gillies, J. Organometal. Chem., 124, C31 (1977)

54. F.Brady, Ph.D. Thesis, Polytechnic of North London

(1980)

55. P.J.Burke, D.G.Gillies and R.W.Matthews, J. Chem. Res., 5, 124 (1981)

56. J.F.Hinton and R.W.Briggs, J. Magn. Reson. 22, 447 (1976)

57. P.J.Burke, R.W.Matthews and D.G.Gillies, J.Chem. Soc. Dalton, 1, 132 (1981)

58. M.J.Forster, D.G.Gillies and R.W.Matthews, J. Magn. Reson., 65, 497 (1985)

59. F.Brady, R.W.Matthews,M.J.Forster and D.G.Gillies, Inorg. Nucl. Chem. Lett., 17, 155 (1981)

60. M.J.Forster and D.G.Gillies, Mol. Phys., in press.

61. P.J.Burke, R.W.Matthews and D.G.Gillies, J. Chem. Soc. Dalton, 1439 (1980)

62. J.F.Hinton and R.W.Briggs in NMR and the Periodic Table, Editors R.K.Harris and B.Mann, Academic Press (1978)

63. P.J.Burke, Ph.D. Thesis, Polytechnic of North London 1979

CHAPTER TWO MOLECULAR MOTION AND RELAXATION MECHANISMS.

Section 2.1 Diffusion.

The addition of thermal energy to a liquid system results in an overall increase in the rates of molecular motion. These motions are exhibited by the whole molecule as an overall translation or reorientation, and within the molecule itself as atomic vibrations or rotations about a bond. The theory of diffusion allows one to discuss the nature of translational and reorientational motion in both a quantitative and qualitative manner.

2.1.1 Translational diffusion

The translational motion of molecules may be affected in the first instance by the driving force of a gradient established within the system. This gradient may arise from differences in, for example, temperature, molecular velocity, concentration, and electric potential in different parts of the solution. Fick[1] studied the binary component system and assumed that the driving force for translational motion was the concentration gradient and thus formulated the relationships known as Fick's first and second laws of diffusion.

If we consider the case where a solute is added to a pure solvent, or similarly where a solution is added to another solution of lower concentration, then a concentration gradient is formed. The net transport of

matter due to the interdiffusion of the two components is given by Fick's first law,

$$J = -D_{ij} \frac{dc}{dx} , \qquad (2 - 1)$$

where J represents the flow of matter across a reference plane per unit area per unit time, $\frac{dc}{dx}$ represents the concentration gradient, and D_{ij} represents the mutual diffusion coefficient.

This equation explains the interdiffusion of solute and solvent molecules assuming a constant gradient is maintained in solution and thus describes time independent processes. For the case where the boundary between the two components gradually becomes more diffuse as molecules translate from the higher to lower concentration regions, a time dependent diffusion process is observed. The concentration gradient relaxes in time until the solution has uniform concentration throughout. The rate of change of concentration for a time dependent concentration gradient $\frac{\delta c}{\delta t}$ is given by Fick's second law

$$\frac{\delta c}{\delta t} = D_{ij} \frac{\delta^2 c}{\delta x^2} . \qquad (2 - 2)$$

Here we observe that $\frac{\delta c}{\delta t}$ is proportional to the second derivative, or curvature of, the concentration dependence on the distance. If the concentration changes rapidly between points, then the rate of change of concentration with time is correspondingly rapid.

In a pure liquid that has uniform concentration throughout, the molecules translate via a random walk process induced by the thermal energy in the system and have an equal opportunity to take up any position within the total volume of liquid. By labelling a molecule in the liquid in some way that does not change its properties, the translational diffusion of that molecule within a sea of unlabelled similar molecules would be observed to be the true self diffusion of the molecule. If we consider a multicomponent system, one may add some labelled molecules of one of the components to form a concentration gradient of labelled and unlabelled species within a uniform environment. One can then apply equation (2 - 2) to the interdiffusion of labelled and unlabelled species to define a self diffusion coefficient D_s.

The NMR spin echo technique discussed in Chapter 3 enables one to label nuclei without changing their physical properties, and observe the interdiffusion between labelled and unlabelled species. Similarly, isotopic labelled tracer techniques allow one to add a trace of labelled species to an otherwise uniform environment of unlabelled species and by monitoring the decay of the initial concentration gradient with time, the tracer diffusion coefficient D_{tr} may be calculated. This coefficient is approximately equal to the self diffusion coefficient and only differs because of the slight difference in the mass of the labelled species.

Equation (2 - 2) is a differential equation that may be solved to describe the diffusive motion of particles. The solution is given for practical purposes as a radial distribution function rather than an explicit solution for individual molecules. For a molecule that is initially at a position r_o , the probability of finding the same molecule at a position r after a time t is given by

$$P(r_o,r,t) = (4\pi Dt)^{-3/2} \exp [- (r-r_o)^2 / 4Dt]. \qquad (2 - 3)$$

Where D is the diffusion coefficient in m^2s^{-1}. As time progresses the radial distribution function increases in width and the concentration of particles gradually spreads through the material. This concentration may be predicted at any point in the system, at any time, by the use of equation (2 - 3). Similarly this equation may be used to calculate the mean square random walk distance $\langle d^2 \rangle$ for the unrestricted Brownian motion of the molecules and thus,

$$\langle d^2 \rangle = 6Dt, \qquad (2 - 4)$$

where t is the timescale for diffusion, and the brackets < > signify a time average.

The timescale over which the molecule is allowed to undergo the diffusional random walk is very significant. If the time, t is sufficiently long such that the value of

$\langle d^2 \rangle$ is significantly larger than the dimensions of some macromolecule under study, the diffusion that one measures is due to the true centre of mass motion. However if $\langle d^2 \rangle$ is shorter than the macromolecular dimension then it is possible that one is observing the non-Fickian diffusion processes arising from the co-operative segmental rotations.

In the discussion presented later the NMR pulsed field gradient technique used for the determination of the self diffusion coefficients in liquid systems, monitors the motion over a timescale that is typically in the range of 1 to 1000 milliseconds. If we consider that typical self diffusion coefficients for molecules in non viscous solutions at room temperature are of the order of 1×10^{-9} $m^2 sec^{-1}$ and for typical high molecular polymers in solution the self diffusion coefficient is of the order of 1×10^{-12} $m^2 sec^{-1}$, then it is clear from equation (2 - 4) that the NMR self diffusion experiment monitors molecular displacements that are several orders of magnitude larger than the radius of a typical molecule.

A further point to note in relation to the diffusion timescale concerns the restricted diffusion of molecules in a system that contains barriers to diffusion. If the timescale of measurement is such that the value of $\langle d^2 \rangle$ corresponds to a value of (d) that is larger than the dimensions of the restrictive cavity that encloses the molecule under study, the molecule will be reflected back

from the wall of the cavity. Therefore the displacement $\langle d^2 \rangle$ will be less than the value predicted by equation (2-4) and the measured diffusion coefficient will be apparently smaller. These effects were first noted by Woessner[2] for the steady field gradient spin echo measurements of the self diffusion of benzene in rubber.

Restrictive diffusion may be characterised by measuring the self diffusion coefficient D_s as a function of the timescale over which the diffusion is measured. The value of D_s will thus apparently alter with the change in diffusion timescale when restricted diffusion or non random walk processes are prevalent. By analysis of this behaviour one may determine the short range diffusion, and the barrier spacings[3,4].

2.1.2 Hydrodynamic theory of diffusion.

The diffusion coefficient is formally described by the Einstein relation

$$D = \frac{k_b T}{f} , \qquad (2 - 5)$$

where k_b is the Boltzmann constant in JK^{-1}, T is the temperature in K and f represents a frictional constant.

The factor f has been calculated[5] for a sphere of radius a moving in a continuous medium of viscosity η by classical hydrodynamics and is given by the Stokes equation,

$$f = 6\pi\eta a \left[\frac{1 + 2\eta / \beta a}{1 + 3\eta / \beta a} \right], \qquad (2 - 6)$$

where β represents the coefficient of friction between the diffusing molecule and its surroundings. If we consider the two limiting forms of β

a) as β tends to zero

This represents the 'stick' limit in which the diffusing sphere is assumed to drag a contact solvent layer through the medium as it translates. This behaviour is typical of systems in which the diffusing sphere is large in comparison to the molecules of the surrounding medium. In this limit equation (2 - 6) reduces to

$$f = 6\pi\eta a \ , \qquad (2 - 7)$$

and this gives the Stokes - Einstein equation

$$D = \frac{k_b T}{6\pi a \eta} \qquad (2 - 8)$$

b) as β tends to infinity

This represents the 'slip' limit, in which the molecule is considered to diffuse through the medium without exerting a viscous drag on the surrounding molecules. This limit is typically approached when a molecule diffuses through a medium of similarly sized molecules. for this case equation (2 - 6) reduces to

$$f = 4\pi\eta a \qquad (2-9)$$

and the diffusion coefficient is thus given by

$$D = \frac{k_b T}{4\pi a \eta} . \qquad (2-10)$$

2.1.3 Rotational diffusion.

The effects of Brownian motion have so far been discussed as the cause of the random fluctuations in the position of molecules leading to molecular translational diffusion. By a similar argument, Brownian motion may lead to random fluctuations in the orientation of the principal axis of the molecule and thus give rise to a thermally induced random reorientational process.

If we consider a simple two dimensional reorientation, the orientation of the molecule may be defined by the angle ϕ that the principle axis makes with a reference axis system. The probability that a molecule will lie at an angle between ϕ and $(\phi + \Delta\phi)$ at a time t is represented by the quantity $P(\phi_t)$. Under conditions of random orientation, the value of $P(\phi_t')$ will be independent of ϕ' as the molecule has an equal probability of exhibiting any angular orientation. However if we apply some orienting force then both $P(\phi_t')$ and $\frac{\delta P(\phi_t')}{\delta \phi'}$ become dependent upon ϕ'. When the orienting force is switched off, the molecules with fixed orientation will relax to a random orientation. If we can, define a flux quantity J_{rot} as the number of

molecules per unit time whose principle axes cross the direction of a vector lying at an angle ϕ' to the fixed reference axis, then one may describe this process by analogous equations to the diffusion equations (2 - 1) and (2 - 2) such that,

$$J_{ROT} = - D_R \frac{\delta P}{\delta \phi'} , \qquad (2 - 11)$$

and

$$\frac{\delta P}{\delta t} = D_R \frac{\delta^2 P}{\delta \phi'^2} , \qquad (2 - 12)$$

where D_R is the rotational diffusion coefficient in rad^2 s^{-1}.

Thus we have the concept that reorientation may be regarded as a diffusional process. Debye[6] considered isotropic reorientation in three dimensions for a sphere reorienting in a continuous viscous medium. The orientation of the sphere is defined by the polar angles θ,ϕ of a vector v to some fixed direction and thus the reorientation in three dimensions is described by the probability function $P(\theta,\phi,t)$ that the vector will have polar angles θ, ϕ to the fixed axis at a time t. This function similarly obeys the equations (2 - 11) and (2 - 12).

If we consider a point I on the surface of a spherical molecule, this will be observed to undergo a thermally

induced random walk over the surface, as the molecule reorients due to the fluctuating torques exerted on the molecule as a result of Brownian motion. The reorientational motion is thought to occur through a series of very small displacements induced by molecular collisions. These displacements are both rapid and frequent, and for a significant change in orientation the molecule must experience a high number of displacements.

Additional models have been proposed to account for more complex molecular reorientational motion and some of these are discussed further in the study presented in Chapter 4.

2.1.4 Relation with $\tau_{\ell,m}$

The rotational diffusion coefficient D_R is inversely proportional to the rotational correlation time $\tau_{\ell,m}$. Where ℓ is the order of the spherical harmonic whose decay determines the relaxation. The general expression is given by[7],

$$\tau_\ell = \frac{1}{\ell(\ell+1)D_R} \quad . \qquad (2-13)$$

For correlation times that are derived from NMR relaxation, Raman light scattering, and fluorescence depolarisation experiments, the spherical harmonic $Y_{2,o}$ is of second order

$$Y_{2,0}(\theta, \phi) = \frac{1}{2}(3\cos^2\theta(t) - 1), \qquad (2-14)$$

and thus equation (2 - 13) gives the relation

$$\tau_{2,0} = \frac{1}{6 D_R}. \qquad (2-15)$$

However, for dielectric and IR relaxation the spherical harmonic is of the first order

$$Y_{1,0}(\theta, \phi) = \cos\theta(t), \qquad (2-16)$$

and equation (2 - 13) gives

$$\tau_{1,0} = \frac{1}{2 D_R}. \qquad (2-17)$$

Therefore, it is clearly observed that the relationship between the correlation times derived from these methods is given by,

$$\tau_{1,0\,(diel),(IR)} = 3\tau_{2,0\,(NMR)}. \qquad (2-18)$$

The magnitude of the rotational diffusion coefficient is given formally by the Stokes-Einstein equation

$$D_R = \frac{k_b T}{8\pi a^3 \eta} . \qquad (2 - 19)$$

It follows from equations (2 - 13) and (2 - 19) that the reorientational correlation time is related to the viscosity of the medium by

$$\tau_{\ell, m} = \frac{8\pi a^3 \eta}{\ell (\ell + 1) k_b T} . \qquad (2 - 20)$$

Thus for the NMR correlation time $\tau_{2,0}$ we obtain,

$$\tau_{2,0} = \frac{4\pi a^3 \eta}{3 k_b T} . \qquad (2 - 21)$$

This is known as the Stokes-Einstein-Debye model which provides a fundamental theory of the liquid state. The equation implies that $\tau_{2,0}$ and η/T have the same temperature dependence. Other models provide modifications to this basic model and these will be discussed further in section (4.2.10), where the hydrodynamic theory is tested over a wide range of viscosities.

Section 2.2 Correlation functions

2.2.1 Single correlation time model

In a liquid system a molecule may exhibit many motional properties involving translational, reorientational and vibrational modes. It is usual to express these properties in terms of a time dependent autocorrelation function $G(\tau)$. The normalised autocorrelation function for a time dependent function $f(\tau)$ is defined as[8]

$$G(\tau)=\frac{\langle f(0)\, f^{*}(\tau)\rangle}{\langle f(0)^{2}\rangle} \qquad (2-22)$$

where the brackets $\langle\ \rangle$ denote an ensemble average and * a complex conjugate.

The autocorrelation function describes how long a particular property of a system persists until it is averaged out by microscopic molecular motion.

Molecular reorientation provides an important mechanism for NMR relaxation. The treatment, originally due to Debye[6] defines the orientation of a molecule in polar co-ordinates (θ,ϕ) and allows these to vary in a random fashion with time, thus the time dependent functions, $f(t)$, are the normalised spherical harmonics, $Y_{l,m}(\theta, \phi)$[8].

Typically $G(\tau)$ is an even function dependent upon τ but independent of the time origin t. The value of $G(\tau)$ is 1 at $\tau = 0$, and decays to zero at $\tau = \infty$. In general $G(\tau)$

must obey the inequality ,

$$-1 \leq G(\tau) \leq 1. \qquad (2 - 23)$$

It is apparent from this inequality, that it is possible for the correlation function to take on a negative value as τ increases. However this behaviour is not observed directly by NMR relaxation measurements as they do not give information on the form of the autocorrelation function, but rather, a quantity τ_c equal to the area under the curve

$$\tau_c = \int_0^\infty G(\tau)\, dt. \qquad (2 - 24)$$

This arises because NMR relaxation is on a very much larger timescale than molecular reorientation.

In equation (2 - 24) we have introduced the motional property measureable by NMR relaxation studies, τ_c. This is the average correlation time and is the characteristic time for the decay of the autocorrelation function. Often it is assumed that the decay is exponential and the correlation function then takes the form.

$$G(\tau) = \exp (-| \tau | / \tau_c). \qquad (2 - 25)$$

The function $G(\tau)$ is related to the spectral density function $J(\omega)$ by a Fourier transformation,

$$J(\omega) = \int_{-\infty}^{\infty} G(\tau) \exp(i\ \omega\ t)\ d\tau. \qquad (2-26)$$

$J(\omega)$ is a frequency spectrum for molecular fluctuations and is of particular interest to relaxation studies when ω corresponds to the relevant transition frequency ω_0. Here $J(\omega_0)$ becomes a measure of the power available to effect nuclear spin relaxation, and so appears as an important term in the relaxation rate equation.

If the correlation function, $G(\tau)$ has the exponential form given by equation (2 - 25), then the Fourier transform gives a Lorentzian spectral density function,

$$J(\omega_0) = \frac{2\ \tau_c}{1 + \omega_0^{\ 2}\ \tau_c^{\ 2}} \qquad (2-27)$$

It is of interest to note the behaviour of $J(\omega_0)$ as a function of $\omega_0\tau_c$. In figure (2 - 1) the function is plotted for three different situations, a) where $\omega_0\tau_c \ll 1$, b) where $\omega_0\tau_c \sim 1$ and c) where $\omega_0\tau_c \gg 1$.

In most liquids of low viscosity the correlation time τ_c is typically very short ($\sim 10^{-12}$s) whilst ω_0 has a value in the order of 10^8. Therefore in this situation $\omega_0\tau_c \ll 1$ and this is known as the extreme narrowing limit. This situation is represented in figure (2 - 1) by curve (A). Here $J(\omega)$ covers the widest range of motional frequencies and indicates that relaxation (at $J(\omega_0)$) at

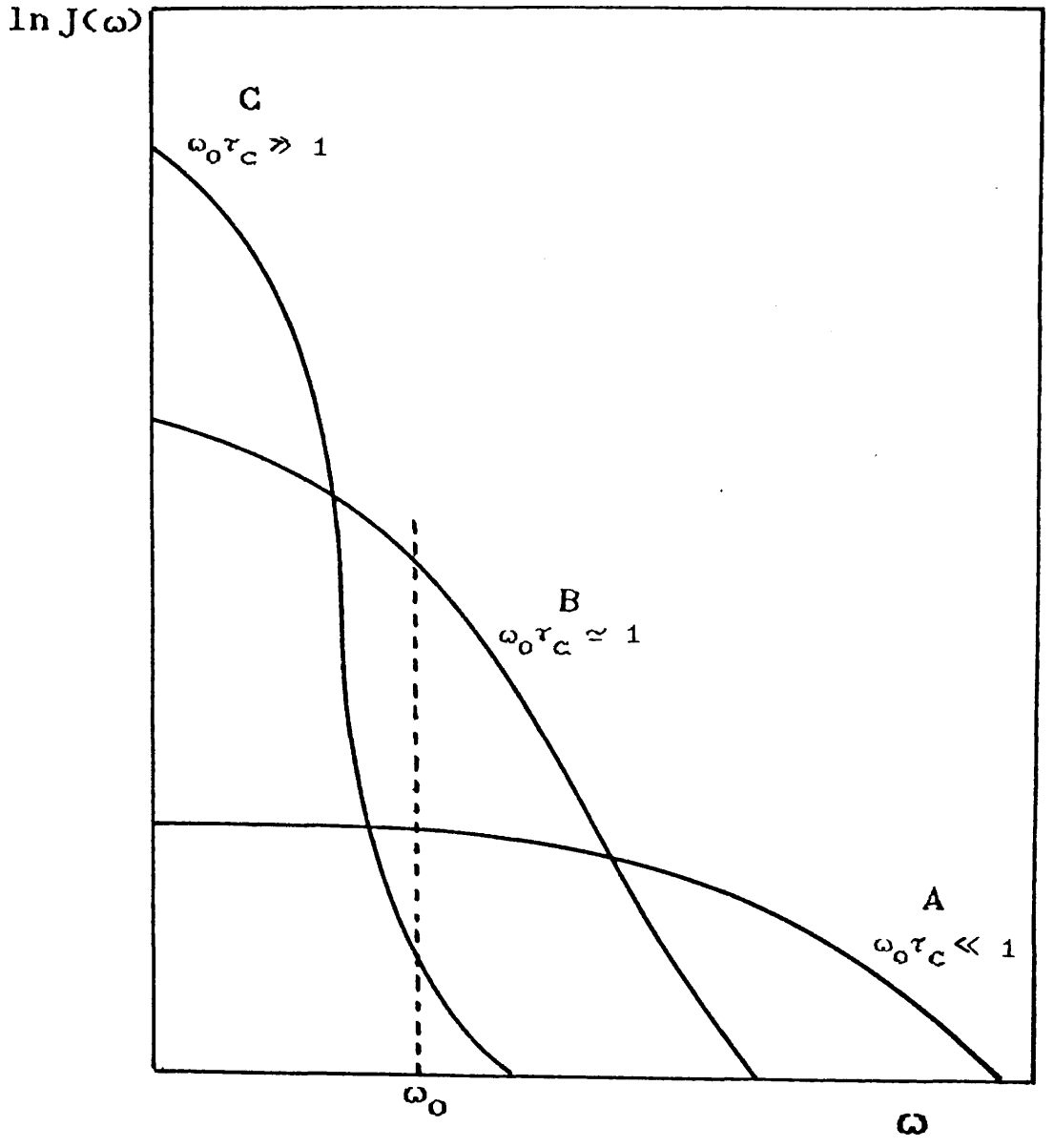

Figure (2-1) Plot of ln J(ω) as a function of ω.

accessible magnetic fields will be relatively inefficient and frequency independent. In highly viscous systems, the molecular motion is slow and $\omega_0\tau_c \gg 1$ and this situation is represented by curve (C). Here $J(\omega)$ extends to much higher values, but these are spread over a smaller range of (low) motional frequencies and the components at high frequency are consequently reduced. Therefore the contribution at the resonance frequency is similarly small. However, in the intermediate situation where $\omega_0\tau_c = 1$ (curve B), the components of $J(\omega)$ are largest at the resonance frequency ω_0 and thus the relaxation is at its most efficient.

Therefore as the molecular motion is slowed down outside the extreme narrowing limit, the contribution of $J(\omega_0)$ will be seen to go through a maximum value and then decrease as the motion is slowed further. This has a direct effect on the magnitude of the spin-lattice relaxation rate, R_1, and thus one expects to observe an R_1 maximum.

2.2.2 Distribution of correlation times.

The single, exponential correlation function does not necessarily apply to the reorientation of molecules in all systems. For example, in many polymer solutions the large chains of molecules may undergo many types of motion involving the relatively slow reorientation of large chain sections and the fast reorientation of small end groups and therefore the molecular motion may be defined by a

range of possible correlation times. Similarly, the solution may contain a distribution of chain lengths, and if the reorientation of these chains is a function of their size, a similar distribution of correlation times will be observed. Therefore it is necessary to modify $J(\omega)$ to include a distribution width parameter to reflect this behaviour.

NMR correlation times often cover a very wide range of motional frequencies and so they are best defined on a logarithm scale. For this purpose a variable, S may be defined by

$$S = \ln \left(\frac{\tau_c}{\tau_o} \right), \qquad (2 - 28)$$

where τ_o is the centre of the distribution of correlation times.

The distribution is described by a density function $F(s)$ which must be normalised, thus

$$\int_{-\infty}^{\infty} F(s)\, ds = 1. \qquad (2 - 29)$$

The new correlation function $G'(\tau)$ may therefore be written as the simple exponential function, $G(\tau)$, weighted by the density function $F(s)$,

$$G'(\tau) = \int_{-\infty}^{\infty} F(s) \exp\left[- | \tau | / \tau_0 \exp(s) \right].$$

(2 - 30)

This is related to the spectral density $J(\omega)$ by the Fourier transformation and so we obtain the function,

$$J(\omega) = 2 \int_{-\infty}^{\infty} \frac{F(s)\, \tau_0 \exp(s)\, ds}{1 + \omega_0^2 \tau_0^2 \exp(2s)} .$$

(2 - 31)

Statistical continuous distributions (as opposed to discrete) have been formulated and applied to rationalise relaxation data in many polymeric and associated liquid systems. Many were originally applied to the discussion of dielectric relaxation behaviour and later adapted to the NMR relaxation case.

A typical example is the Cole-Cole distribution[9] that has a density function $F(s)$ defined by

$$F(s) = \frac{1}{2\pi} \frac{\sin \beta \pi}{\cosh \beta s + \cos \beta \pi}, \qquad (2 - 32)$$

where β is the distribution width parameter that lies in the range $0 < \beta \leq 1$ such that when $\beta = 1$, the single correlation time limit applies. Inserting this density function into equation (2 - 30) and performing the Fourier

tranform, we obtain the spectral density,

$$J(\omega) = \frac{1}{\omega} \frac{\cos\left[(1-\beta)\, \pi/2 \right]}{\cosh\left[\beta \ln(\omega \tau_0) \right] + \sin\left[(1-\beta)\, \pi/2 \right]} \qquad (2-33)$$

The Cole-Cole distribution is symmetrical about a central correlation time τ_0 and therefore the average correlation time is equal to τ_0. Other symmetrical distributions have been formulated and these include the Fuoss-Kirkwood[10], the Gaussian[11], and rectangular[12] distributions. An alternative treatment is to bias the weighting of the distribution towards either longer or shorter correlation times and thus to apply an asymmetrical distribution model. A typical example is the Cole-Davidson distribution[13] that has a density function given by,

$$F(s) = \frac{\sin \beta\pi}{\pi} \left(1 - e^{-s} \right)^{-\beta} \qquad \text{for } (\tau < \tau_0) \qquad (2-34)$$

$$\text{and } F(s) = 0 \qquad \text{for } (\tau > \tau_0) \qquad (2-35)$$

The distribution width is denoted, by β and lies in the range $0 < \beta \leq 1$. However the correlation time, τ_0 in this example is defined as the limiting correlation time which is assumed to be the longest correlation time that the molecules may exhibit at each temperature. The average correlation time given by this model is

$$\tau_c = \beta \tau_o. \qquad (2 - 36)$$

It is apparent from equations (2 - 34) and (2 - 35) that the Cole-Davidson distribution is skewed with a tail towards shorter correlation times. An alternative approach is provided by the log χ^2 distribution[14] which has a tail towards longer correlation times and this has been suggested to be more appropriate for the relaxation of polymers in solution.

More detailed discussions on the formalism of the distribution of correlation times model have been presented in review articles by Connor[15] and Heatley[16].

Distribution of correlation times models will be discussed in Chapter 4, where the applicability of symmetrical and asymmetrical distributions to account for ^{205}Tl and ^{13}C relaxation data is fully tested.

Section 2.3 Nuclear spin relaxation mechanisms.

2.3.1 Chemical shift anisotropy

The Zeeman interaction of a nuclear spin I with a static magnetic field B_0 is given by,

$$\hat{\mathcal{H}}_z = -\hbar \gamma \underline{B}_0 . (\underline{\underline{1}} - \underline{\underline{\sigma}}) . \hat{\underline{I}}, \qquad (2 - 37)$$

where γ is the magnetogyric ratio for the spin I, and $\underline{\underline{\sigma}}$ is the shielding tensor that describes the contribution of the local electronic environment of the spin to the total magnetic field. If the principle axes of the shielding tensor are fixed in the molecular frame then σ will be characterised by three unique values σ_{XX}, σ_{YY}, and σ_{ZZ}.

For molecules undergoing rapid molecular reorientation, the shielding tensor is averaged to the isotropic value σ_{iso} which is equal to one third of the trace,

$$\sigma_{iso} = \frac{1}{3} (\sigma_{xx} + \sigma_{yy} + \sigma_{zz}). \qquad (2 - 38)$$

If the shielding tensor has spherical symmetry, then $\sigma_{xx}=\sigma_{yy}=\sigma_{zz}$. However, if the shielding tensor lacks spherical symmetry, then σ_{xx}, σ_{yy} and σ_{zz} are not all equal and we can define a traceless tensor $\underline{\underline{\delta}}$ with components δ_{jj}, where,

$$\delta_{jj} = \sigma_{jj} - \sigma_{iso}. \qquad (2 - 39)$$

The shielding tensor is said to be anisotropic and molecular reorientation results in the nucleus experiencing a time dependent fluctuation in the Zeeman energy provided by the traceless components of the shift tensor. This fluctuating magnetic field provides a mechanism for nuclear spin relaxation, commonly termed chemical shift anisotropy (CSA).

The full expressions for the spin-lattice and spin-spin relaxation rates are given by[17],

$$R_{1CSA} = \frac{1}{15} \gamma^2 B_0^2 \Delta\sigma^2 \left(1 + \frac{\eta^2}{3} \right) \left[\frac{2 \tau_c}{1 + \omega_0^2 \tau_c^2} \right] \qquad (2 - 40)$$

$$R_{1CSA} = \frac{1}{15} \gamma^2 B_0^2 \Delta\sigma^2 \left(1 + \frac{\eta^2}{3} \right) \left[\frac{4 \tau_c}{3} + \frac{\tau_c}{1 + \omega_0^2 \tau_c^2} \right], \qquad (2 - 41)$$

where η is the parameter that reflects the asymmetry of the shielding and is defined by

$$\eta = \frac{(\delta_{xx} - \delta_{yy})}{\delta_{zz}}, \qquad (2 - 42)$$

and $\Delta\sigma$ is the anisotropy defined by

$$\Delta\sigma = \sigma_{zz} - \frac{1}{2} (\sigma_{xx} + \sigma_{yy}). \qquad (2 - 43)$$

When the molecular motion is within the extreme narrowing limit, such that $\omega_0\tau_c << 1$, equations (2 - 40) and (2 - 41) reduce to

$$R_{1CSA} = \frac{2}{15} \gamma^2 B_0^2 \Delta\sigma^2 (1 + \eta^2/3) \tau_c, \qquad (2 - 44)$$

$$R_{2CSA} = \frac{7}{45} \gamma^2 B_0^2 \Delta\sigma^2 (1 + \eta^2/3) \tau_c. \qquad (2 - 45)$$

Here it is apparent that in this limit, the ratio $R_{2CSA}/R_{1CSA} = \frac{7}{6}$. However, this ratio is dependent upon $\omega_0\tau_c$ and becomes greater than $\frac{7}{6}$ when the molecular motion is outside the motional extreme narrowing limit.

Inspection of equations (2 - 40) and (2 - 41) shows that the term B_0^2 gives rise to a strong positive field dependence. Clearly a study of the field dependence of relaxation rates at, as low and high fields as possible provides an unambiguous test for the contribution of this mechanism, and this technique is widely used in the work presented in later chapters.

Finally, from studies presented later, it is noted that the chemical shift anisotropy mechanism is found to be important for the nuclear spin relaxation of the dimethylthallium(III) and diethylthallium(III) cations.

These cations are assumed to be axially symmetric, and for this case the asymmetry parameter η becomes zero, and the anisotropy $\Delta\sigma$ is given by

$$\Delta\sigma = \sigma_{\parallel} - \sigma_{\perp}, \qquad (2 - 46)$$

where $\sigma_{\parallel} = \sigma_{zz}$ and $\sigma_{\perp} = \sigma_{xx} = \sigma_{yy}$.

2.3.2 Dipole-dipole mechanism.

The dipole-dipole (DD) relaxation mechanism is often the dominant contributor to the relaxation of spin $\frac{1}{2}$ nuclei in the liquid state. The most common example is in ^{13}C relaxation where there are bonded proton(s) that normally provide a dominant intramolecular DD mechanism.

If we consider two nuclear spins I and S on the same molecule, the spin I will experience a total magnetic field comprising of the laboratory field, B_0 and the local field from the magnetic moment of the spin S, B_{LOC}. The interaction between the magnetic moments of the two nuclei is dependent upon the distance between the spins, r_{IS}, and also the relative orientation, (θ,ϕ) of the internuclear vector, to the field B_0. Random molecular reorientation leads to a time dependency in (θ,ϕ) and this in turn leads to a time dependency in the local field at the I spin and thus provides the fluctuating magnetic field necessary for relaxation

At this point it should be noted that in the situation where the I and S spins are on different molecules there is an intermolecular DD mechanism to be considered. In

this case the internuclear distance, r changes as well as the angular term, and clearly this mechanism is dependent upon translational as well as reorientational motion. Normally this mechanism is only relevant for proton-proton interactions at higher concentrations.

In passing it may be noted that the tensor expression for the DD mechanism, which is analogous to equation (2 - 37) given for the CSA mechanism, is

$$\hat{\mathcal{H}} = -\hbar \, \hat{\underline{I}} \cdot \underset{\sim}{D} \cdot \hat{\underline{S}} , \qquad (2 - 47)$$

where $\underset{\sim}{D}$ is the dipolar coupling tensor.

For the intramolecular mechanism the following expressions[18, 19] apply for spin $I = \frac{1}{2}$ nuclei, when I is relaxed by the interaction with S.

$$R_{1DD} = \frac{n_S}{20} \left(\frac{\mu_0}{4\pi} \right)^2 \frac{\gamma_H^2 \gamma_C^2 \hbar^2}{r^6} \left[\frac{\tau_C}{1+(\omega_S - \omega_I)^2 \tau_C^2} + \frac{3\tau_C}{1 + \omega_I^2 \tau_C^2} + \frac{6 \tau_C}{1 + (\omega_S + \omega_I)^2 \tau_C^2} \right]$$

(2 - 48)

$$R_{2DD} = \frac{n_S}{20}\left(\frac{\mu_0}{4\pi}\right)^2 \frac{\gamma_H^2\gamma_C^2\hbar^2}{r^6}\left[4 + \frac{\tau_C}{1+(\omega_S-\omega_I)^2\tau_C^2} + \frac{3\tau_C}{1+\omega_I^2\tau_C^2} + \frac{6\tau_C}{1+\omega_S^2\tau_C^2} + \frac{6\tau_C}{1+(\omega_S+\omega_I)^2\tau_C^2}\right],$$

(2 - 49)

where n_S is the number of S nuclei, μ_0 is the permeability of free space, equal to $4\pi \times 10^{-7}$ H m^{-1}, r is the internuclear distance and τ_C is the correlation time for reorientational motion about an axis perpendicular to the internuclear vector. These equations simplify in the limit of extreme narrowing to,

$$R_{1DD} = R_{2DD} = \left(\frac{\mu_0}{4\pi}\right)^2 \frac{\gamma_H^2\gamma_C^2\hbar^2 n_S \tau_C}{r^6}.$$

(2 - 50)

2.3.3 Spin-rotation mechanism.

The spin-rotation (SR) mechanism arises from a nucleus experiencing a magnetic field generated by molecular rotation. The interaction arises from a coupling of the nuclear spin angular momentum to the molecular rotational angular momentum. The magnitude of the coupling is called the spin-rotation constant.

Molecular collisions alter the magnitude and direction of the angular momentum vector associated with the rotation of the molecule[20] and therefore the nucleus

experiences a fluctuating localised magnetic field which gives rise to a relaxation mechanism.

The Hamiltonian for the spin-rotation mechanism is given by,

$$\hat{\mathcal{H}} = - \hbar \, \hat{\underline{I}} \, . \, \underset{\sim}{C} \, . \, \hat{\underline{J}} \, , \qquad (2 - 51)$$

where $\underset{\sim}{C}$ is the spin-rotation tensor and $\hat{\underline{J}}$ is the angular momentum operator.

The terms $\underline{I}$, $\underset{\sim}{C}$ and $\underline{J}$ may all show a time dependence. $\underset{\sim}{C}$ is affected by changes in molecular orientation and $\underline{J}$ is affected by changes in the molecular rotational state. Similarly $\underline{I}$ has a time dependence, as nuclear spin relaxation leads to a change in the nuclear spin state.

The magnitude of $\underline{J}$ increases as the molecular rotation becomes faster and therefore the relaxation by this mechanism is anticipated to be more efficient for small, rapidly rotating molecules at higher temperatures, and particularly in the vapour phase.

The relaxation rate for a species exhibiting rapid isotropic reorientation is given by[21],

$$R_{1SR} = (2 \, k_b T / \hbar^2) \, I_m \, C_{eff}^2 \, \tau_{SR} \qquad (2 - 52)$$

where I_m is the moment of inertia, τ_{SR} is the spin-rotation correlation time, and C_{eff} is the spin-rotation tensor given by,

$$C^2_{eff} = (2C_\perp{}^2 + C_\parallel{}^2) / 3 \qquad (2 - 53)$$

The spin-rotation correlation time reflects the persistence of a given angular momentum and increases with increasing temperature, a temperature dependence which is opposite to that of the reorientational correlation time, τ_C. Hubbard[20] and McClung[22] have shown that for spherical molecules with diffusion controlled processes, τ_{SR} is inversely proportional to τ_C,

$$\tau_C \, \tau_{SR} = \frac{I_m}{6 \, k_b T} \quad . \qquad (2 - 54)$$

The increased relaxation rate at higher temperature provides a convenient means of separation of the SR contribution from the other spin relaxation mechanisms.

2.3.4 Scalar relaxation mechanism.

The interaction Hamiltonian for the scalar coupling between two nuclear spins I and S is given by,

$$\hat{\mathcal{H}}_{SC} = J \, \hbar \, \hat{\underline{I}} \, . \, \hat{\underline{S}} \qquad (2 - 55)$$

where J is the scalar coupling constant.

A modulation of the scalar coupling interaction may lead to relaxation of the nuclear spin I and this may arise by one of two processes; firstly J may become time dependent as a result of chemical exchange, and secondly $\hat{\underline{S}}$ may become time dependent due to relaxation. These

processes lead to scalar relaxation of the first and second kind respectively.

The relaxation rates for the scalar relaxation of nucleus I by either mechanism are given by[23],

$$R_{1Sc} = \frac{8\,\pi^2\,J^2\,S(S+1)}{3}\left[\frac{\tau_{Sc}}{1+(\omega_I-\omega_s)^2\,\tau_{Sc}^2}\right] \quad (2-56)$$

$$R_{2Sc} = \frac{4\,\pi^2\,J^2\,S(S+1)}{3}\left[\tau_{Sc}+\frac{\tau_{Sc}}{1+(\omega_I-\omega_S)^2\,\tau_{Sc}^2}\right] \quad (2-57)$$

where ω_I and ω_S are the resonance frequencies of the I and S spins in rad s^{-1} and S is the quantum number of the coupled spin. τ_{Sc} is the scalar correlation time which is equal to either the chemical exchange time constant τ_{ex} or proportional to the relaxation time of the spin S,

The scalar relaxation mechanism does not often contribute to the R_1 owing to the typically large values of $\Delta\omega^2\tau_c^2$ which is a result of the poor matching of timescales. The mechanism is more likely to contribute significantly to R_2 since the zero frequency term in the R_2 equation does not rely on this value of $\Delta\omega^2\,\tau_c^2$ to be ≤ 1, to be efficient.

There are exceptions to this rule. The scalar relaxation mechanism may be observed to contribute to the

R_1 of nucleus I in systems where the relaxation rate of the nucleus S is large. Thus the mechanism may be efficient if S is for instance a quadrupolar nucleus. Alternatively, the mechanism may be efficient if the difference in resonance frequencies, $\Delta\omega$ is small as for the ^{13}C-^{79}Br group.

2.3.5 Quadrupolar relaxation.

Nuclei with spin $I > \frac{1}{2}$ possess an electric quadrupole moment, Q due to their non spherical nuclear charge distribution. In the presence of an electric field gradient at the nucleus there will be an interaction with the electric quadrupole moment which will be modulated by molecular reorientational motion. This provides a relaxation mechanism which arises from fluctuating electric field gradients.

The Hamiltonian for this interaction is given by

$$\hat{\mathcal{H}} = \hat{\underline{I}} \cdot Q \cdot \hat{\underline{I}} , \qquad (2 - 58)$$

where $\underset{\sim}{Q}$ is the quadrupole coupling tensor.

The relaxation rates in the extreme narrowing limit have been derived[23] and are given by

$$R_{1Q} = R_{2Q} = \frac{3}{40} \frac{(2I+3)}{I^2 (2I-1)} \left[1 + \frac{\eta^2}{3} \right] \left(\frac{e^2 Q q}{\hbar} \right) \tau_2 \qquad (2 - 59)$$

where e q is the electric field gradient at the nuclear

site, η is the asymmetry in the field gradient tensor and $(e^2Q\ q\ /\ \hbar)$ is the quadrupole coupling constant in frequency units.

This mechanism dominates the relaxation of all spin I $> \frac{1}{2}$ nuclei that have a large electric field gradient and can result in very large nuclear spin relaxation rates.

References for CHAPTER TWO

1. A.Fick, Pogg. Annln, 94, 59 (1855)
2. D.E.Woessner, J. Phys. Chem., 67, 1365 (1963)
3. J.E.Tanner, Ph.D. Thesis, University of Wisconsin (1966)
4. J.E.Tanner, J. Chem. Phys., 69, 1748 (1978)
5. G.G.Stokes, Trans. Camb. Phil. Soc., 9, 8 (1951).
6. P.Debye, "Polar Molecules". Chapter 5, Dover Publications (1945).
7. G.R.Alms, D.R.Bauer, J.L.Brauman and R.Pecora, J. Chem. Phys., 58, 5570 (1973).
8. A.Carrington and A.D.McClachlan, "Introduction to Magnetic Resonance". Harper and Row. (1967).
9. K.S.Cole and R.H.Cole, J. Chem. Phys., 9, 341 (1941).
10. R.M.Fuoss and J.G.Kirkwood, J. Amer. Chem. Soc., 63, 385 (1941).
11. W.A.Yager, Physics, 7, 434 (1936).
12. D.W.McCall, D.C.Douglass and E.W.Anderson, J. Chem. Phys., 30, 1272 (1959).
13. D.W.Davidson and R.H.Cole, J. Chem. Phys., 19, 1484 (1951).
14. J.Schaefer, Macromolecules, 6, 882 (1974).
15. T.M.Connor, Trans. Faraday. Soc., 60, 1574 (1964).
16. F.Heatley, Prog. Nucl. Magn. Reson. Spectrosc., 13, 47 (1979).
17. H.W.Spiess, "Rotation of Molecules and Nuclear Spin Relaxation in NMR. Basic Principles and Progress", Vol 15. Springer Verlag.
18. J.R. Lyerla and G.C.Levy, Top. C-13 NMR Spectrosc., 1, 79 (1974).
19. D.Doddrell, V.Glushko and A.Allerhand, J. Chem. Phys., 56, 3683 (1972).
20. P.S.Hubbard, Phys. Rev. 131, 1155 (1963).

21. D.M.Grant, C.H.Wang and J.R.Lyerla Jr., J. Chem. Phys., 55, 4674 (1971).

22. R.E.D.McClung, J. Chem. Phys., 51, 3842 (1969).

23. A.Abragam, "The Principles of Nuclear Magnetism." O.U.P (1964).

CHAPTER THREE EXPERIMENTAL TECHNIQUES

Section 3.1 Spectrometer systems

The nuclear spin relaxation rates and self diffusion coefficients presented in later chapters, were all derived from the spectra provided by three spectrometer systems. High field measurements at a field strength of 9.40 T were performed on a Bruker WH-400 spectrometer, which is under the control of the University of London Intercollegiate Research Service (ULIRS) situated at Queen Mary College. All other work was done at Royal Holloway and Bedford New College. Measurements at a field strength of 2.11T were carried out using a Jeol FX90Q spectrometer and low field measurements at a field strength of 0.89T were performed using a modified Varian XL-100/15 spectrometer.

The Bruker WH-400 spectrometer system with a 10mm dedicated Thallium probe allowed for the observation of ^{205}Tl and ^{203}Tl nuclei at frequencies of 231.6 MHz and 229.2 MHz respectively. All spectra were obtained without proton decoupling. The system was used to measure Thallium nuclear spin relaxation times T_1, T_2 and $T_{1\rho}$. The typical 90^{o} pulse length was 14 μs and satisfactory spectra for all thallium samples were obtained in only a few pulses. However as the ^{205}Tl and ^{203}Tl relaxation times were typically very short at this field strength, only short pulse delays were necessary, and so 100-200 pulses were applied for all measurements. Typical experimental times

were in the order of 10 minutes.

For temperature measurement purposes (section 3.3) it was necessary to observe routine proton spectra at 400MHz and these spectra were observed through the decoupler coils of the thallium probe insert.

The system was used to perform ^{13}C R_1 measurements and ^{13}C -{^1H} nuclear Overhauser enhancement experiments in 60% sucrose/D_2O solution at a frequency of 100.6MHz. For these measurements a 10mm dedicated ^{13}C probe insert was used and the typical 90^o pulse length was 23μs. All spectra used for T_1 measurements were accumulated in 32 pulses under full proton decoupling conditions and overall experimental times were in the order of 10 minutes. For ^{13}C - {^1H} nOe measurements, spectra were obtained in 72 pulses giving similar experimental times.

In all measurements at this field strength, field/frequency locking was achieved by locking to the deuterium resonance either in the solvent or in a sample held in a concentric sample tube

The Jeol FX90Q spectrometer system allowed for the observation of ^{13}C, ^1H, ^{205}Tl and ^{203}Tl nuclei. The ^1H nucleus was observed at 90MHz and the spin echoes arising from the PGSE pulse sequence (see section 3.5) were used for the determination of the self diffusion coefficients for the dimethylthallium(III) cation (0.8M) in D_2O. The typical 90^o pulse length was 23μs and suitable spectra were obtained in 4 pulses giving overall experimental

times of 30 minutes.

The ^{13}C R_1 measurements were performed under full proton decoupling conditions at 22.5MHz using a 10mm ^{13}C /^{1}H dual insert. The typical 90^{o} pulse length was 65μs and satisfactory spectra for a 60% sucrose/D_2O solution were obtained in 96 pulses giving overall experimental times of 30 minutes.

^{205}Tl and ^{203}Tl nuclei were observed at 51.84MHz and 51.74MHz respectively using the standard multinuclear probe with 5mm insert

The specifications of the multinuclear probe and wide band amplifier do not include observation at the thallium frequencies, but are restricted to ^{1}H and ^{19}F observation and the range of frequencies up to and including the ^{31}P frequency of 36.4MHz. However, on frequency band 2, frequencies in the range of 51 MHz may be tuned to, but the sample does not receive the full excitation power as the probe is not fully tuned and matched to accept these frequencies. The consequent increase in 90^{o} and 180^{o} pulse lengths to 180μs and 360μs respectively enables one to perform limited ^{205}Tl R_1 measurements.

However, The long 180^{o} pulse lengths are often significant in systems that exhibit short ^{205}Tl relaxation times in the order of a few milliseconds. Many organothallium compounds show high contributions from the CSA relaxation mechanism for the relaxation of the thallium nucleus and this mechanism is often very

efficient at 51.8MHz, therefore relaxation measurements at this frequency are not always tenable.

The system was used to measure the ^{205}Tl R_1 in neat thallium(I) ethoxide. Spectra were obtained in 200 pulses and experimental times were typically 15 minutes. In contrast ^{203}Tl R_1 values in thallium(I) ethoxide were found to be too short to measure by this technique.

The system was later used to perform the ^{205}Tl PGSE experiment to measure self diffusion coefficients for the $Tl(I)^+$ ion in aqueous sucrose solutions. Spectra adequate for analysis were obtained in 4 pulses and the duration of each experiment was typically 15 minutes.

Field / frequency locking in ^{205}Tl R_1 and self diffusion measurements was achieved by locking to the external ^7Li lock of the spectrometer and ^{13}C R_1 measurements were made by locking to the ^2H signal from the solvent D_2O.

The Varian XL-100/15 spectrometer system has been modified and so requires a brief description. The system was originally designed for multinuclear observation using the Varian Gyrocode observe facility at 2.35 T.

For the measurements performed in this thesis, low field observation of the ^{205}Tl and ^{203}Tl nuclei was required and so the spectrometer was operated at a reduced field strength of 0.89 T. The ^{205}Tl and ^{203}Tl frequencies were observed in the spectrometer Gyrocode observe mode at 21.96MHz, and 21.74MHz respectively and the typical 90^o

pulse lengths were 28μs and 19μs respectively. Field/frequency locking was achieved by locking to the ^{31}P resonance in an 85% phosphoric acid solution at 15.4 MHz, which is the frequency that would normally be used for the deuterium lock when the spectrometer is operating at 2.35T.

The proton decoupling frequency was generated by a Schlumberger FSX 3006S frequency synthesiser. The output was passed via an attenuator to an Amplifier Research Type 10LA broad band amplifier and then via a Texscan Type 3BD 38 band pass filter to the probe.

The thallium resonance frequency was measured using a Hewlett Packard Type 52452 frequency counter which was referenced to the 1 MHz crystal in the Schlumberger FSX 3006S frequency synthesiser. Thus the thallium frequency may be referenced to the proton decoupler frequency.

The spectrometer was interfaced via a 10 bit analogue to digital converter to a PDP-11/20 computer. The software, which was written by I.D Cresshull and I.C Moon operated the pulse sequence used for the measurement of spin-lattice relaxation times (section 3.4.1) and gave the facility to store up to ten FID 's under one file name. All data were acquired using a phase alternated pulse sequence and each FID was stored on a Dual Dec RX01 floppy disc drive. The pulse times were controlled by a separate timer unit which consists of five digital timers which were assigned to the 90^{o} pulse length, the 180^{o} pulse

length, the time period between these two pulses, the digitisation rate and the pulse delay. The spectrometer mode of operation was changed between normal spectral accumulation and the T_1 pulse sequence by simply connecting the 180^o pulse timer unit. The timer unit allowed one to manually set the time τ between the 180^o and 90^o pulses, but when applying the T_1 pulse sequence, this time was under software control.

For data processing, the FID was recalled, the cosine apodisation and exponential multiplication functions were applied and then a Fourier transform of up to 8K points was made. The spectra were displayed on an oscilloscope for phasing and then plotted using a Bryans XY plotter.

The experimental conditions varied with the type and concentration of thallium compound under study and the quality of spectra required. Typically, for an organothallium compound at 0.3M concentration in viscous solution, ^{205}Tl spectra adequate for accurate spin-lattice relaxation measurements were obtained in ~ 2000 pulses and the overall experiment took ~ 2.5 hours. However for thallium(I) nitrate in aqueous solution (0.246M), adequate spectra were obtained in only 30 pulses giving typical experimental times of 45 minutes.

For neat thallium(I) ethoxide, spectra were obtained in under 100 pulses and T_1 measurements took on average 10 minutes. The number of pulses necessary to observe thallium spectra of thallium(I) ethoxide diluted with

cyclohexane to 17 mole% was significantly increased to 8000 pulses for the ^{205}Tl nucleus and 16000 pulses for the ^{203}Tl nucleus, giving experimental measurement times of approximately 3.5 hours and 7 hours respectively.

Section 3.2 Sample preparation

For the study of thallium cations in aqueous sucrose solutions, each solution was made by a standard procedure. The weighed amount of sucrose was added to a weighed amount of D_2O then sealed in a boiling tube. The sucrose was then dissolved by gentle warming in hot water. Following this, the thallium salt was added and dissolved in a similar manner. The solution was then transferred to a thick walled tube with an NMR tube sidearm, for the solvent degassing procedure.

Degassing was achieved by the freeze-pump-thaw technique. For this procedure the sample is frozen, then the air above the solvent is evacuated to a pressure of ~ 5×10^{-5} Torr. The air pump is then disconnected and the sample is allowed to thaw. During the thawing time the dissolved oxygen comes out of the solvent. The freeze-pump-thaw cycle is then repeated until no more air bubbles are observed to come out of the solvent. This procedure typically took ~ 11 cycles in viscous solutions and ~ 7 cycles in non-viscous solutions. After degassing, argon was introduced into the sample tube to a pressure of 610mm/Hg and the sample was then sealed.

A modified procedure was used to incorporate a sealed capillary of dimethylthallium(III) nitrate in D_2O (0.8M) in samples containing diethylthallium(III) nitrate in sucrose/DMSO-d^6 solutions. The sample in the capillary tube could not be frozen, as this destroyed the tube, and

so, once the DMSO-d^6 solvent had been degassed by the freeze-pump-thaw technique, the sample tube was filled with argon, then the capillary tube was inserted. The sample tube was then evacuated briefly without freezing and then argon was reintroduced to a pressure of 610mm/Hg and the sample was sealed.

For the study of $TlNO_3$ in aqueous TANOL solutions, each sample was degassed in the usual manner for aqueous samples.

For the study on neat thallium(I) ethoxide, the sample was put in a NMR tube under a nitrogen atmosphere in a glove box, in order to protect the air sensitive thallium(I) ethoxide. The sample was then degassed by the freeze-pump-thaw technique and sealed.

Finally, for the study on thallium(I) ethoxide diluted with cyclohexane, the sample was made by adding thallium(I) ethoxide to degassed cyclohexane in a glove box and under a nitrogen atmosphere. The sample was then degassed and sealed.

Section 3.3 Temperature measurement.

3.3.1 Introduction

In the work presented in later chapters, nuclear spin relaxation and self-diffusion measurements are made as a function of temperature. The measurements are made for the purpose of deriving motional parameters in order to test models that have been proposed to account for the molecular motion, and to define relaxation mechanisms pertinent to the system under study.

Evidently, the errors associated with temperature measurement will eventually appear as uncertainties in the derived activation parameters and so it becomes necessary to make accurate measurements both quickly and easily, so that it may be practical in routine experiments.

3.3.2 Experimental arrangement

The simplest method of measurement available was to have a thermocouple inserted into the probe to measure the temperature of the gas flow that heats the sample. However this was thought to be unsatisfactory as this technique does not measure the actual temperature within the sample. The preferred technique was to contain the thermometer, which in this case was a thermometric liquid, in a concentric tube within the sample tube itself. When this was impractical the thermometric liquid was placed in an outer concentric tube.

For some measurements, the only practical method of temperature measurement was to substitute the study sample

with a tube containing the thermometric liquid. In principle, this is a more inaccurate method as the temperature may be perturbed in some way by change of the sample and in addition, errors may be incurred through differences in sample volumes. However in tests using the concentric tube and sample substitution techniques, the difference in the temperature measured by each technique was found to be within the error limits of ± 0.5K. The arrangement for temperature measurement in each study is mentioned when appropriate.

3.3.3 Temperature measurement in ^{205}Tl and ^{203}Tl studies.

When measurements of ^{205}Tl and ^{203}Tl relaxation rates were made as a function of temperature, the thermometric liquid was a sample of dimethylthallium(III) nitrate in D_2O (0.8M). This sample was originally proposed as a ^{205}Tl chemical shift thermometer by Forster et al.[1].

At a frequency of 21.96MHz the temperature calibration equation for the ^{205}Tl chemical shift in the range 0^oc to 100^oc is given by the equation,

$$t(^oc) = 2.492 \times 10^{-5}\Delta\upsilon^2 + 0.01817\Delta\upsilon - 60.30, \qquad (3-1)$$

where t is the temperature in degrees celsius and $\Delta\upsilon$ is the observed ^{205}Tl frequency minus 21,962,783 Hz. The field/frequency lock used in the measurement of ^{205}Tl chemical shifts to derive this equation, was provided by

locking to the ^{31}P resonance in a sample of 85% phosphoric acid which was assumed to be temperature invariant(2)

The studies discussed in later sections involve the measurement of ^{205}Tl spin relaxation rates over a range of temperatures, at different field strengths. It is therefore necessary to scale the calibration equation (3 - 1) to the appropriate operating frequency. The field strength at which the calibration equation was derived was determined independently of the field/frequency sample locking configuration by a $^{205}Tl-\{^{1}H\}$ double resonance experiment. The ^{205}Tl spectrum was observed whilst the ^{1}H CW decoupling frequency was altered to give the optimum decoupling. This was taken to be the central frequency for the protons in dimethylthallium(III) nitrate. This frequency was found to be,

$$\upsilon_H = 37,943,718 \pm 2 \text{ Hz}. \qquad (3 - 2)$$

Therefore, a knowledge of the proton and thallium resonance frequencies on any spectrometer system, calibrated to a common reference, enables temperature calculation at that field by a simple scaling of equation (3 - 1) by the ratio of the proton frequency of the operating spectrometer, to υ_H.

To establish the field strength at a ^{205}Tl frequency of 231.6 MHz, it was necessary to calibrate the proton frequency. This was achieved by introducing a radiofrequency spike at a known frequency into the

observed proton spectrum. The radiofrequency was generated by a General Radio 1061 frequency synthesiser which was referenced to the 10 MHz master crystal of the spectrometer.

At high field, The proton frequency was found to vary slightly with change in temperature due to the temperature dependence of the D_2O which was used as a field/frequency locking material. Therefore, at each temperature, the proton spectrum was observed and the frequency was measured.

The thallium frequency was calibrated in a similar manner to the proton frequency by generating a radiofrequency spike in the observed thallium spectrum.

This technique allows for simple, routine temperature measurement under fully coupled or decoupled conditions and may be quoted to an accuracy within ± 0.5K.

3.3.4 Temperature measurement in ^{13}C relaxation studies.

For the ^{13}C R_1 studies in 60% sucrose/D_2O (w/w) solution, the temperature measurement was achieved by observation of the peak separation between the ^{13}C resonances of cyclooctane and diiodomethane in a 1:5 v/v mixture. The method was proposed by Vidrine and Peterson[3] and is applicable over the temperature range 20^oc to 100^oc. The peak separation $\Delta\delta$ has been calibrated and is given by the equation,

$$\frac{1}{T} = 0.0220027 - 0.000223362 \; . \; \Delta\delta \qquad (3 - 3)$$

The method offers particular advantages to the measurement of temperatures in variable temperature ^{13}C studies. The technique observes the ^{13}C NMR resonance and so it is not necessary to change the probe, or retune to different frequencies between ^{13}C relaxation measurements and this enables measurements to be made in a simple and routine manner. In addition the spectra of the thermometric liquid is observed under full proton decoupling conditions and therefore the temperature is measured under the same conditions experienced by the sample under study.

The resonance peaks due to the thermometric liquid appear to low frequency of many organic compounds and this was found to be true for the ^{13}C spectrum of sucrose at both field strengths of interest. Thus the thermometric liquid may be sealed within the sample and there is no need for sample substitution.

The accuracy of the temperature measured by this technique has been quoted to be, at best, $\pm$ 0.15K[3] but the technique becomes less accurate if the signal to noise ratio is low or if it is necessary to apply a large sensitivity enhancement function to the FID.

In the studies presented later, a suitable ^{13}C spectrum of the thermometric liquid was obtained in ~ 50

pulses and the necessary line broadening led to uncertainties in temperature measurement within ± 0.5K.

For field dependent relaxation studies, the use of an NMR thermometer with its own internal reference, such as that used in this study, was found to be more convenient than thermometers that require a knowledge of the absolute frequency[4]. Such a thermometer necessitates the calibration of the spectrometer frequency at each magnetic field strength and this may lead to error in the measured temperature.

3.3.5 Temperature measurement in self diffusion studies.

The technique used for temperature measurement in all of the self-diffusion studies reported in this thesis involved measuring the separation of the ^1H peaks due to the aliphatic and hydroxyl protons in a sample of methanol or ethylene glycol. The sample of methanol was used to measure temperatures in the range 220K to 330K and the calibration equation at 60 MHz is given by[5],

$$T = 435.5 - 1.193 \mid \Delta\upsilon \mid - 29.3 \cdot \left[\frac{\Delta\upsilon}{100}\right]^2, \qquad (3-4)$$

where $\Delta\upsilon$ is the separation in Hz between the methyl and hydroxyl proton resonances.

For the temperature range 310K to 410K the calibration equation for ethylene glycol at 60 MHz is given by[6],

$$T = 466.0 - 1.694 \mid \Delta\upsilon \mid \qquad (3 - 5)$$

where $\Delta\upsilon$ corresponds to the peak separation in Hz between the methylene an hydroxyl proton resonances.

Becker et al.[6] have provided calibration equations for both these compounds at 220MHz and showed that the equations due to Van Geet may be successfully scaled to higher field without significant increase in error. Thus equations (3 - 4) and (3 - 5) were simply scaled to an operating frequency of 90MHz for the present study.

Section 3.4 T_1, T_2 and nOe measurements.

3.4.1 T_1 pulse sequence.

The spin-lattice relaxation time (T_1) measurements presented in this thesis were made by applying the Inversion Recovery Fourier Transform (IRFT) technique[7]. The pulse sequence is given by,

$$\{ 180^{o} - \tau - 90^{o} - W \}_{n}. \qquad (3-6)$$

Before the pulse sequence is applied, the macroscopic spin magnetisation has a thermal equilibrium value M_o and is aligned along the (+) z' axis, parallel to the magnetic field B_o. The application of a 180^{o} pulse turns the magnetisation onto the (-) z' axis. Once perturbed, the magnetisation begins to return to the equilibrium value and is allowed to do so for τ seconds. After this time, a 90^{o} pulse is applied which turns the partially relaxed magnetisation onto the (-) y' axis where it may be observed. The resulting free induction decay is collected and Fourier transformed in the usual way.

The observed spectra may appear either positive or negative depending upon whether the delay time τ before the 90^{o} pulse, is long enough for the magnetisation to pass through zero on its return to equilibrium. Thus for short τ times ($\tau < T_1 \ln 2$), the resulting spectra will appear negative whilst for long τ times ($\tau > T_1 \ln 2$), the spectra will appear positive and this typical behaviour is shown in the representative T_1 spectra in

figure (3 - 1). For perfect 90^{o} and 180^{o} pulses, the magnetisation will be nulled if a delay time, $\tau = T_1 \ln 2$, is allowed and thus a T_1 null is often used to provide a quick estimation of the T_1 value.

The term W in the pulse sequence is the wait time allowed for the magnetisation to return to equilibrium before the next 180^{o} pulse is applied. Typically this time is set to $5T_1$ or greater and this can often result in very long experimental times especially if the nucleus under study has long T_1 values and low sensitivity, for example ^{13}C and ^{15}N .

Canet et al.[8] proposed a modification of the IRFT technique in which the wait time W is shorter than $5T_1$ but long enough to allow for the transverse magnetisation to fully decay. The technique is known as the Fast Inversion Recovery Fourier Transform (FIRFT) technique and offers much more rapid data accumulation at the expense of some dynamic range. The optimal wait period for this experiment has been studied and was suggested to be in the range [9],

$$0.5T_1 \leq W \leq 2T_1. \qquad (3 - 7)$$

The spin-lattice relaxation rates presented in this thesis were obtained using the IRFT technique and where necessary, the FIRFT technique was used.

3.4.2 Analysis of T_1 data

Having applied the IRFT pulse sequence, for a series of τ values ranging from very short time to $5T_1$, one

Figure (3-1) ^{205}Tl IRFT spectra of $TlNO_3$ in aqueous TANOL solution ($5 \times 10^{-5}M$), at 230.8MHz. 4 scans, 1Hz. linebroadening sweep width = 2000Hz, temperature = 296K.

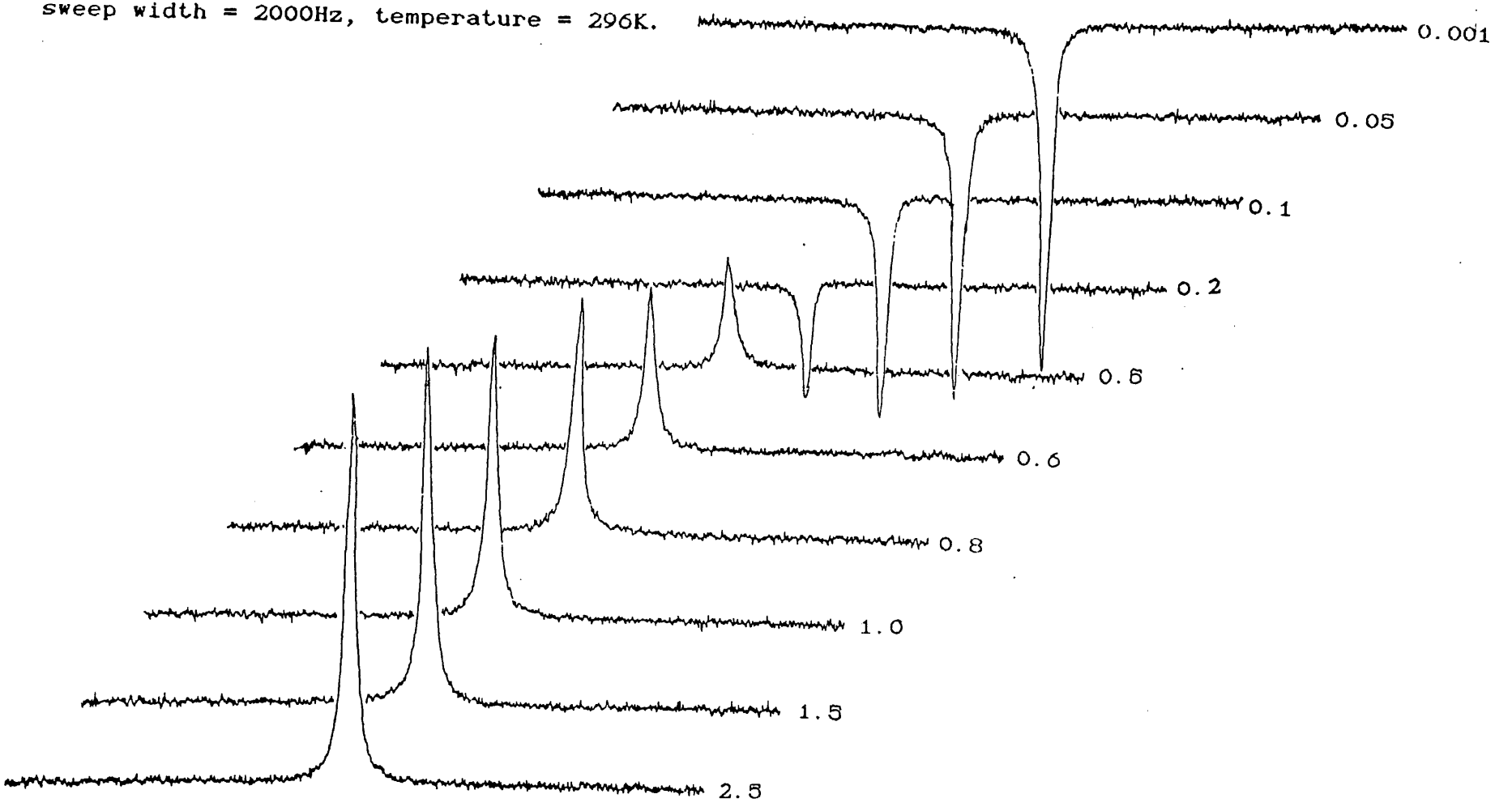

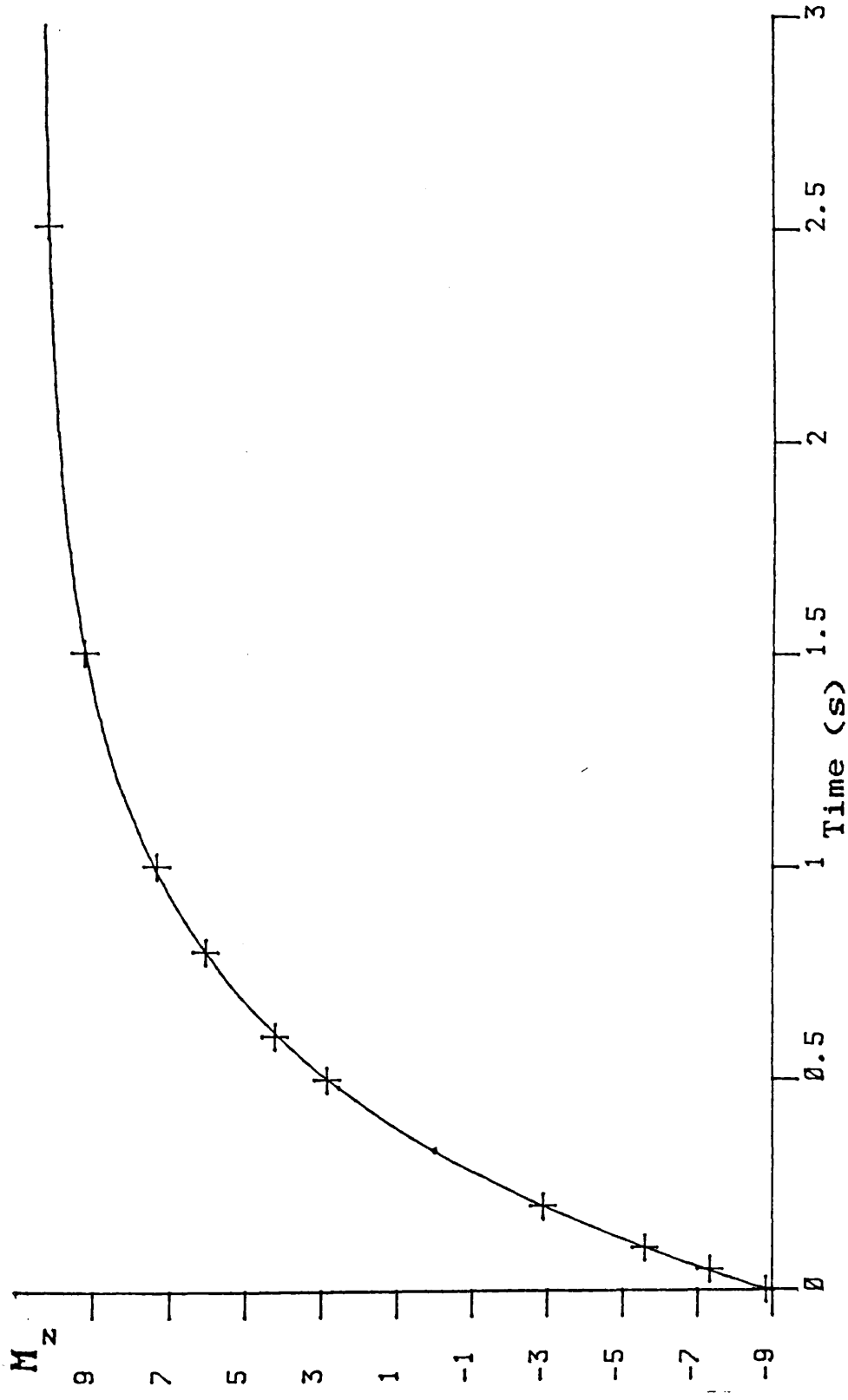

Figure (3-2) Exponential T_1 recovery curve for the IRFT data given in figure (3-1).

obtains a series of spectra reflecting the recovery of the inverted magnetisation to the equilibrium value M_0 (figure(3 - 1)). This recovery is described by the equation,

$$M(\tau) = M_\infty \mid 1 - 2 \exp(-\tau/T_1) \mid . \qquad (3 - 8)$$

To obtain a value for T_1, the simplest approach is to rearrange equation (3 - 8) to give.

$$\ln(M_\infty - M(\tau)) = \ln(2M_\infty) - \tau/T_1. \qquad (3 - 9)$$

If one applies a linear least squares fitting procedure to a plot of $\ln(M_0 - M(\tau))$ against τ, the slope of the plot obtained is equal to $-1/T_1$. This procedure is known as the semi-logarithm plot method.

A more accurate method of analysis was proposed by Sass and Ziessow[9]. Here the T_1 values are calculated by an iterative non linear least squares fitting procedure to the equation,

$$M(\tau) = A_1 + A_2 \exp(\tau . A_3) \qquad (3 - 10)$$

Where A_1 corresponds to the equilibrium magnetisation M_∞, A_2 to the value $(M_0 - M_\infty)$ and A_3 gives the value for $(-1/T_1)$.

This method has been shown[10] to provide calculated

T_1 values with less error than the alternative semi-logarithm plot method. In addition, the error in T_1 is much less sensitive to the frequency offset and to slight errors in the set 90^o and 180^o pulse lengths. Finally, the non linear least squares fitting procedure has the advantage that it may be used to analyse both IRFT and FIRFT data whereas the semi-logarithm plot method is limited to the analysis of IRFT data alone.

The iterative fitting procedure was used to calculate all of the T_1 values reported in later chapters. An example of the best fit curve to the plot of signal intensity against τ delay time is presented in figure (3 - 2).

3.4.3 Measurement of T_2.

The spin-spin relaxation times, T_2 presented in this work were measured using the Hahn spin echo technique[11]. The pulse sequence is given as follows,

$$\{ 90^o - \tau - 180^o - \tau - (\text{spin echo}) - W \} \qquad (3 - 11)$$

After an initial 90^o pulse, the magnetisation is turned into the y' axis of the rotating frame of reference. The slight inhomogeneities in the magnetic field B_o cause the magnetic vectors in different portions of the sample to precess with different larmor frequencies and thus they are observed to fan out with respect to the axes rotating at the larmor frequency. After a wait period

of τ seconds, a second pulse is applied which has the effect of rotating all the vectors through 180^{o} about the x'axis, here they continue to move in the same direction and after a further time τ , refocus to give a spin echo. If no T_2 relaxation has occured during this sequence of pulses, then the echo signal would be equal to that from a simple 90^{o} pulse, however T_2 decay processes do occur and therefore the decrease in echo amplitude is a function of the wait period, τ.

3.4.4 Analysis of T_2 data

The intensity of the Fourier transformed spin echo is observed to decay to zero as the wait interval τ is increased. This decay is exponential and is given by the equation,

$$S_{\tau} = S_0 \exp (-2\tau / T_2) \qquad (3 - 12)$$

Where S_{τ} is the spin echo intensity for a wait time of τ seconds and S_0 is the intensity at zero time.

Equation (3 - 12) may be used in an iterative non linear least squares fitting procedure to the intensity : τ time data. The procedure optimises the values of S_0 and T_2 in order to rationalise the observed echo decay behaviour and thus provides a best estimate for the value of T_2.

3.4.5 Measurement of $T_{1\rho}$.

The measurement of the spin-lattice relaxation time in the rotating frame, $T_{1\rho}$, utilises the spin locking technique. At first, a 90^{o} pulse is applied long the x'

axis to tip the magnetisation through 90^{o} onto the y' axis. Following this, the phase of the RF pulse is shifted by 90^{o} so that its magnetic component, B_1 is applied along the y' axis. The magnetisation therefore becomes spin locked along this axis and, in effect, is now held in a magnetic field of magnitude B_{1y}. Consequently the spin-lattice relaxation that occurs under this condition will occur at a very low field. Hence the $T_{1\rho}$ experiment is essentially a zero field experiment and thus provides further useful information to aid the study of field dependent relaxation mechanisms.

The experiment is performed by spin locking the magnetisation along the y' axis for a duration of τ seconds. The spin locking field B_{1y} is then released and the FID is collected and Fourier transformed. The signal S_τ is observed to decay as a function of the spin locking period τ according to the relation,

$$S_\tau = S_0 \exp (-\tau / T_{1\rho}) \qquad (3 - 13)$$

where S_0 is the signal intensity at zero time.

Thus one may obtain a series of signal intensities at different spin locking times, τ and these may be used in an iterative non-linear least squares fitting procedure to equation (3 - 13), to deduce the best fit parameters for S_0 and $T_{1\rho}$.

The experiment however, is often difficult to perform

due to the limitations of the spectrometer. The technique requires the RF power amplifier to maintain a spin locking field at a constant power level over the full range of τ times. As a result, the duration of the spin locking field τ may be limited to short times by the power handling capabilities of the probe.

This problem may be alleviated by the spectrometer software facility to reduce the power of the RF pulse during the spin locking period. However, the Bruker WH-400 spectrometer used for the measurement of $T_{1\rho}$ in this work does not have such a facility and therefore measurements were performed using the DANTE[12] sequence to provide the spin locking pulse.

The DANTE sequence employs a train of m pulses of duration Δt seconds, which are spaced at intervals of τ seconds (typically $\Delta t \ll \tau$). This appears in the frequency domain as a series of Sinc functions that are $1/\tau$ Hz apart with a width of excitation between zero crossing points, equal to $1/m\tau$ Hz.

The effect of the sequence is similar to that of a low power RF pulse with an effective B_1 given by the relation,

$$B_1^{eff} = B_1 \times \frac{\Delta t}{\Delta t + \tau} \qquad (3 - 14)$$

However, there is a limit to the application of this technique. The condition for spin locking requires that the spin locking field must satisfy the condition,

$$\Delta\omega << \gamma B_1 \qquad (3 - 15)$$

where $\Delta\omega$ is the spread of resonance frequencies that must be spin locked by the field B_1. Therefore, as the resonance linewidth is increased, the condition given by equation (3 - 15) becomes increasingly difficult to satisfy.

For the measurements of $T_{1\rho}$ for aqueous thallium(I) nitrate in the presence of TANOL free radicals, presented in Chapter 6, the effect of TANOL was to enhance the ^{205}Tl spin-spin relaxation of the $Tl(I)^+$ ion, significantly broadening its resonance linewidth and thus limiting the measurement of $T_{1\rho}$.

The experiment used an effective field corresponding to a ^{205}Tl resonance frequency in the rotating frame of 40Hz and thus the condition (3 - 15) could only be satisfied in the $1 \times 10^{-5}M$ and $5 \times 10^{-5}M$ TANOL solutions, where the linewidth was below 30Hz.

3.4.6 NOE measurements.

The nuclear Overhauser enhancement for a nucleus, A coupled to a nucleus, X may be obtained in principle, simply by comparing the intensity of the A resonance in the presence and absence of full decoupling of the X nucleus. If several pulses need to be applied to obtain greater signal to noise and experimental accuracy, then a sufficiently long pulse interval must be used to avoid partial saturation of the resonance.

This method is often inconvenient as the coupled

spectrum often appears as a series of overlapping multiplets. In order to circumvent this problem, nOe measurements in this study have been made using the gated decoupling technique[13,14]. This technique is performed by switching the decoupler on at the time of the 90° pulse during data acquisition. Decoupling of X occurs instantaneously whilst the associated nOe effect for A develops with a time constant of the spin-lattice relaxation time T_1. The decoupler is then switched off for a wait period before the next pulse so that any nOe that has built up may decay to zero. Thus one obtains a fully decoupled spectrum without the associated nOe effect which may be compared with the spectrum obtained with the decoupler on over the entire experiment.

The conditions required for accurate use of this method have been investigated by Harris and Newman[15]. They noted that for a $^{13}C-\{^1H\}$ nOe experiment, for an isolated ^{13}CH group, the required delay time between pulses was different for the fully decoupled and gated decoupled spectrum. For the fully decoupled spectrum the ^{13}C nucleus is relaxing under proton decoupling conditions and therefore the delay time need only be in the order of $5 \times T_1$. For gated decoupling conditions the ^{13}C and ^1H nuclei are relaxing together according to the coupled differential equations for a multispin system and the result of this is that the nOe continues to operate after the decoupler is turned off, until the proton

magnetisation has returned to its equilibrium value and unless

$$T_1(^1H) \ll T_1(^{13}C), \qquad (3-16)$$

the ^{13}C magnetisation will overshoot its equilibrium value. It therefore takes longer to reach thermal equilibrium and the required pulse length must be of the order of at least $10 \times T_1$.

If the protons are relaxed by a mechanism other than via the ^{13}C nucleus, then this delay time may be reduced to $6-8 \times T_1$

3.4.7 NOE Data analysis.

The intensity of the signal following an A-{X} double resonance experiment, S_A^* is related to the corresponding signal in the absence of a decoupling RF, S_A^o , by the following relationship derived from the Solomon equations[16],

$$\frac{S_A^*}{S_A^o} = 1 + \frac{\gamma_X}{\gamma_A} \left(\frac{W_2 - W_0}{W_2 + 2W_{1A} + W_0} \right) \qquad (3-17)$$

where W_0, W_1 and W_2 correspond to the transition rate for a zero, single and double quantum transition respectively. These transitions are shown for the two spin case in figure {3 - 3}.

Figure (3 - 3) Transition rates for an AX spin system.

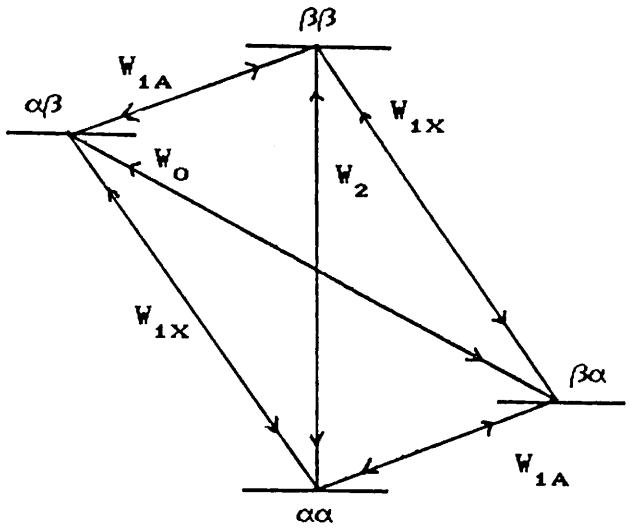

For dipolar relaxation, these probabilities are given by,

$$W_0 = (1/20)\,(2\pi R)^2\, J(\omega_X - \omega_A) \qquad (3 - 18)$$

$$W_{1A} = (3/40)\,(2\pi R)^2\, J(\omega_A) \qquad (3 - 19)$$

$$W_{1X} = (3/40)\,(2\pi R)^2\, J(\omega_X) \qquad (3 - 20)$$

$$W_2 = (3/10)\,(2\pi R)^2\, J(\omega_X + \omega_A) \qquad (3 - 21)$$

Where R is the dipolar interaction constant given by, $(\mu_0/4\pi)\gamma_A\gamma_X(\hbar/2\pi)r_{AX}^{-3}$, and $J(\omega)$ are the spectral densities at the appropriate frequencies. Substituting equations (3 - 18) to (3 - 21) into equation (3 - 17) gives the frequency dependent general expression for the A-(X)

heteronuclear nOe, this is,

$$\frac{S_A^*}{S_o} = 1 + \frac{\gamma_X}{\gamma_A} \left[\frac{6\,J(\omega_X + \omega_A) - J(\omega_X - \omega_A)}{6\,J(\omega_X + \omega_A) + 3\,J(\omega_A) + J(\omega_X - \omega_A)} \right] \qquad (3 - 22)$$

$= 1 + \eta$, where η is the enhancement factor.

It is noticeable that the nOe is strongly dependent upon $\omega_o\tau_c$ when the motion becomes outside the extreme narrowing limit, and this equation is more important in viscous situations. In mobile liquids, where the extreme narrowing limit applies, the expression reduces to,

$$\frac{S_A^*}{S_o} = 1 + \frac{\gamma_X}{2\gamma_A}. \qquad (3 - 23)$$

Thus for the $^{13}C-\{^1H\}$ nOe experiment, the maximum nOe for a full contribution from the dipole-dipole mechanism is predicted to be 2.99.

It is necessary to note that, as it is only the dipole-dipole mechanism that contributes to all W_o, W_1, and W_2 in equation (3 - 17), it is the only mechanism that will give rise to a positive nOe. The scalar mechanism contributes to W_o only, giving rise to a negative bracketed term in equation (3 - 17) and thus if the scalar mechanism dominates, the signal intensity would be decreased. The remaining relaxation mechanisms only contribute to W_1 and thus no intensity change is observed if these mechanisms dominate.

Section 3.5 Measurement of Self-diffusion coefficients.

3.5.1 The basic experiment.

The Hahn spin echo sequence is utilised for the measurement of self-diffusion coefficients by field gradient techniques.

The magnetic field is purposely made inhomogenous by the application of a linear magnetic field gradient. The inhomogeneity ensures that the nuclei in different spacial positions are each labelled with a position dependent precession frequency.

It has been shown that the Hahn spin echo experiment refocusses resonant spins following a 90^{o}-180^{o} pulse sequence. However this is only possible if the spins maintain the same precession frequency throughout the experiment. Diffusion of a nuclear spin to a different spacial position in an inhomogenous magnetic field will result in a change in its frequency and consequently will not be refocussed to a spin echo at the same time as the spins that maintain an effectively constant spacial position.

It is important to note that the self-diffusion experiment does not directly monitor the individual spin self-diffusion, but rather the overall probability distribution for the translational motion of spins along the direction of the linear field gradient.

For the NMR self-diffusion experiment, the echo

amplitude $M(2\tau)$, depends[11] on the T_2 of the nucleus and the diffusion coefficient D. For diffusion in a steady field gradient[17],

$$\frac{M_y(2\tau)}{M_y(0)} = \exp\left[\frac{2\tau}{T_2} - \frac{2\gamma^2 D G^2 \tau^3}{3} \right] \quad (3-24)$$

where τ is the duration between the 90^o and 180^o pulses in the Hahn spin echo sequence, $M(2\tau)$ is the intensity of the spin echo after 2τ seconds, $M(0)$ is the initial spin echo intensity, D is the diffusion coefficient in m^2s^{-1} and G is the field gradient strength in Gauss m^{-1}.

The effect of a time dependent magnetic field gradient on the spin echo has been discussed by Stejskal and Tanner[18], and the relation is given by,

$$M_y(2\Delta) = M_y(0) \exp\left[-\frac{2\Delta}{T_2} - (\gamma G \delta)^2 D\left(\Delta - \frac{\delta}{3} \right) \right] \quad (3-25)$$

where δ is the duration of the field gradient pulse and Δ is the total time duration between 90^o and 180^o pulses.

3.5.2 The PGSE experiment.

The self-diffusion coefficients reported in this work have all been derived by use of the Pulsed field Gradient Spin Echo (PGSE) technique. As noted in the previous section, the technique utilises the modified Hahn sequence and this is best understood by reference to the pulse

timing diagram in figure (3 - 4).

After an initial 90^{o} pulse, the spins begin to precess in the x'y' plane of the rotating frame of reference. During this time, a linear field gradient is applied across the sample in a single pulse of duration δ ms, along one direction only. A 180^{o} refocussing pulse is then applied and this is followed by a second linear field gradient pulse, identical to the first. The spins continue to refocus to form a spin echo at a time equal to 2Δ. The spin echo is then Fourier transformed to separate the contributions from different components in the system.

By reference to the equation for spin echo attenuation in the presence of an applied pulsed field gradient, (equation (3 - 25)) one can derive a procedure for performing the experiment. The spin echoes may be measured as a function of the duration of the field gradient pulse, δ or as a function of the strength of the applied field gradient G[19]. Typically it is more convenient to maintain a constant field gradient strength and vary the duration of the pulse, and this procedure is applied in the study presented later.

If the wait interval PI, in the pulse diagram shown in figure (3 - 4), is maintained at a constant value throughout the experiment, then by successive increases in the duration of the field gradient pulse the value of Δ will successively increase. During this time period, the echo will decay due to the effects of diffusion and T_2

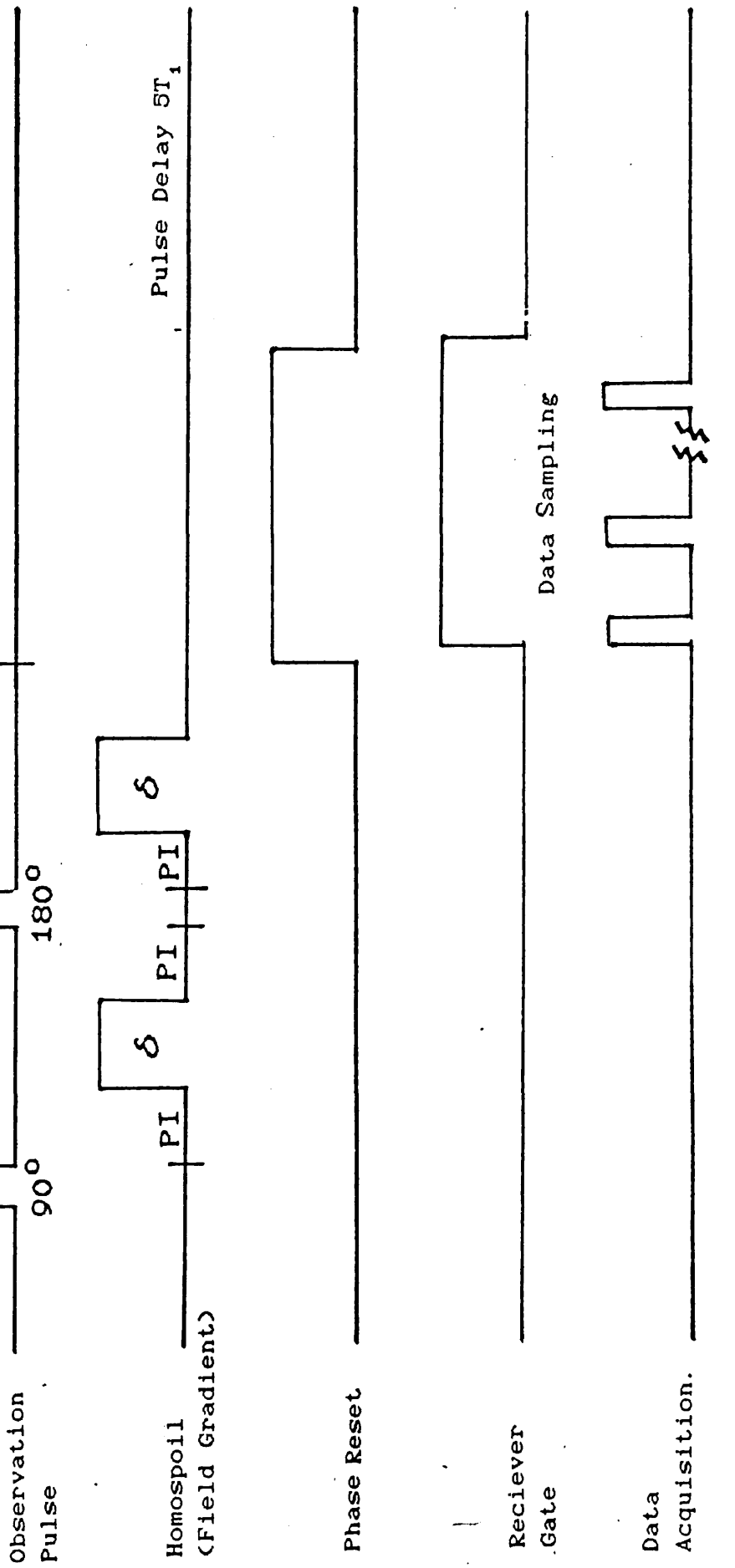

Figure (3-4) PGSE pulse timing diagram.

processes. In order to separate these effects one typically performs the experiment in the presence and absence of the field gradient. This gives the spin echo attenuation due to natural T_2 processes and the total spin echo attenuation due to the combined effects of diffusion and T_2 decay. For data analysis this procedure will be termed method (a).

Alternatively, if the spectrometer software allows, then for each increment of the field gradient pulse, the wait period, PI is similarly decreased such that the time period Δ does not alter between successive experiments. In this experiment the attenuating effect we are observing with increasing field gradient pulse length, is the effect due to diffusion only. If we assume that attenuation due to natural T_2 decay does not occur during the millisecond timescale that the field gradient pulse is applied, then it is unnecessary to apply an experiment to correct for T_2. This is particulary of use in situations where the T_2 decay is very small over the full range of Δ values and eliminates the problems caused by J-modulation effects. This method is denoted method (b).

The magnetic field gradient applied across the sample is generated by passing an electric current through a set of coils which may be of the quadrupole[20] or opposed Helmholtz type[21]. The sample under study is placed in the centre of the coil arrangement in order that the sample experiences a linear magnetic field gradient

This field gradient must be uniform over the sample region and sample volumes are kept low for this reason.

The homospoil pulse coils of the Jeol FX90Q NMR spectrometer consist of an opposed Helmholtz arrangement through which computer controlled field gradient pulses in the order of 2 G cm^{-1} may be generated, and this is satisfactory to measure accurate self-diffusion coefficients in the $10^{-9}m^2s^{-1}$ range. This lower limit may be reduced to an estimated $2 \times 10^{-11}m^2s^{-1}$ if the T_2 of the nucleus under study is $\geq 0.3s$[22].

It is necessary to calibrate the applied field gradient before proceeding with the experiment. The errors associated with field gradient calibration will ultimately manifest themselves as errors in the final calculation of the diffusion coefficient and are indeed the major source of error. therefore it is necessary to use a method of calibration that accurately reflects the effective field gradient experiencd by the nuclei under study. Several methods are in general use. The field gradient may be calculated by analysing the band shape of the spin echo in a steady[17] or pulsed[23] field gradient, where the echo shape gives a quantitative measure of the background field gradient if the sample geometry is known. Wider applications of these techniques have been discussed by Fukishima and Roeder[24].

Other techniques include direct mapping of the magnetic field[25] or by the analysis of the spin echo

attenuation of a PGSE experiment on a sample of known diffusion coefficient. This is the generally preferred technique and is utilised in the study presented later.

3.5.3 Experimental procedure.

For all measurements the samples were kept static in the Jeol FX90Q 5mm probe insert. For ^{1}H self-diffusion measurements, the dual $^{13}C/^{1}H$ probe insert was used, whilst for ^{205}Tl measurements, the 5mm multinuclear probe insert was used. Field/frequency locking was achieved by using the external ^{7}Li lock on account of its stability and lack of oscillation during and after the application of the field gradient pulse[22].

The experiment was applied using the pulse sequence shown in appendix (1) which was a modified version of that due to Stilbs and Moseley[22]. This sequence allowed for longer field gradient pulses to be applied, which is a necessity in self-diffusion studies in viscous liquids.

The calibration of the field gradient was performed using a 5mm sealed sample of dried benzene for which the self-diffusion coefficient at a given temperature may be interpolated from the data given by Collings and Mills[26]. The PGSE pulse sequence was applied to the sample and the echo attenuation was analysed in a similar manner to the standard procedure for obtaining self-diffusion coefficients from echo attenuation data, and hence a value of G was deduced from a knowledge of D. Typical error limits over a series of four readings for

the field gradient were ± 2%.

Typical parameters for ^{1}H PGSE studies in aqueous solution are as follows (refer to pulse timing diagram, figure (3 - 4)). For a constant PI value of 30 to 40 ms, the duration of the pulsed linear field gradient was varied between 5 and 30ms at lower temperatures, and between 5 and 15ms at temperatures greater than 330K. All sequence recycle times were greater than $5T_1$. A spin echo was obtained for each different field gradient pulse length, the height of which decreased with increasing pulse length. The homospoil of the Jeol FX90Q spectrometer was then switched off so that the field gradient pulse duration time, δ, operated purely as a time delay. This gave a series of spin echoes which were unaffected by an applied field gradient.

An example of the ^{1}H PGSE spectra obtained by this procedure is shown in figure (3 - 5), where the methyl protons in a sample of dimethylthallium(III) nitrate in D_2O (0.8M) were studied in the presence and absence of a 2.18 G cm^{-1} pulsed linear field gradient.

For the ^{205}Tl PGSE study of $Tl(I)^{+}$ cations in more viscous, aqueous sucrose solution, the wait period PI was varied with increasing field gradient pulse duration such that the time parameter Δ was always kept constant. The duration of applied field gradient varied up to values of 70ms. The significant increase in these values reflects not only the slower diffusional motion in these systems,

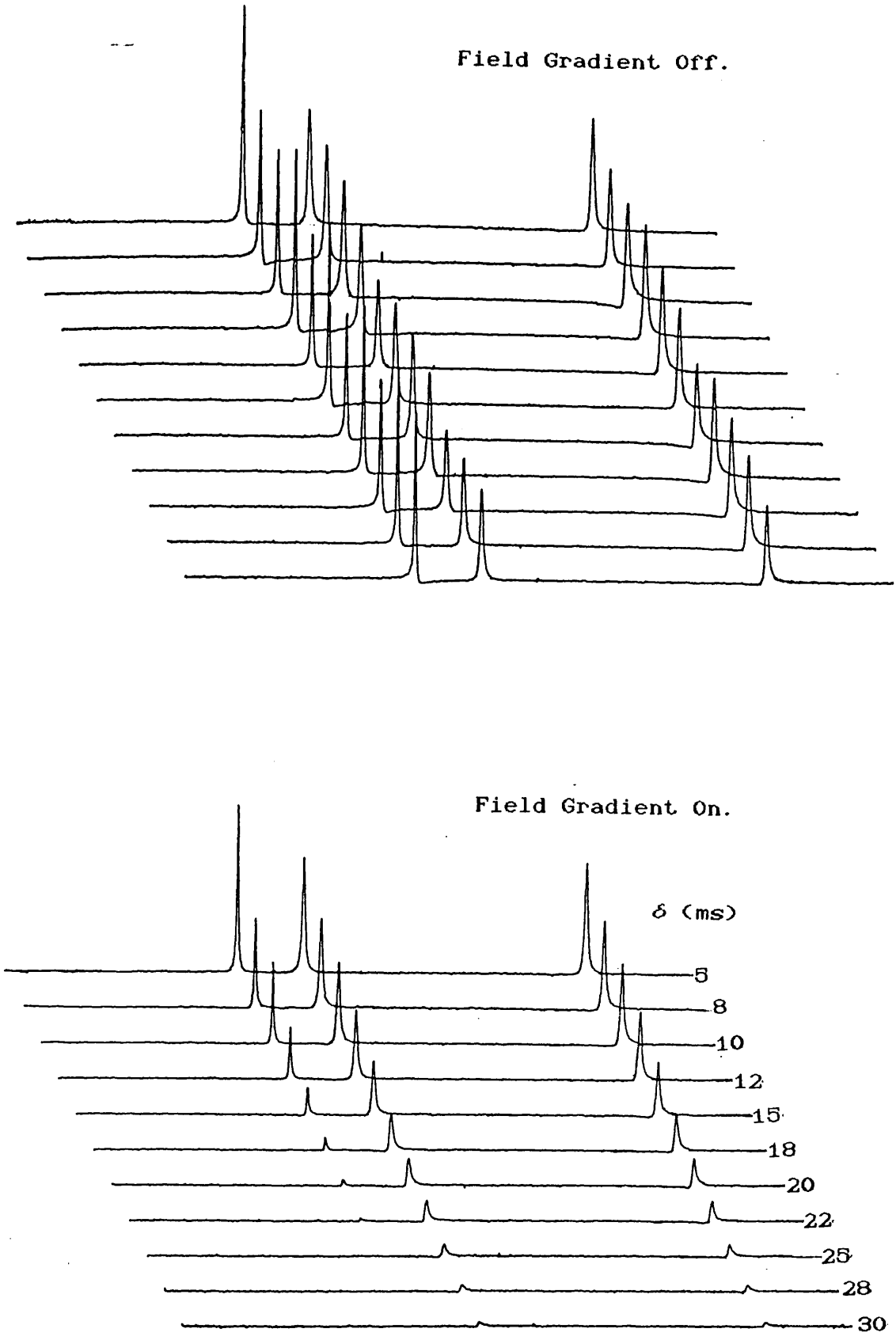

Figure (3-5) ^{1}H PGSE spectra for $(CH_3)_2Tl^+$ in D_2O
4 scans, no linebroadening, sweep width = 1000Hz.,
temperature 329.6K, field gradient = 2.18 G cm^{-1}.

but also the decrease in the effect of the field gradient on the ^{205}Tl nucleus which has a lower magnetogyric ratio than the ^{1}H nucleus (proportional to γ^2).

3.5.4 Data analysis.

As a result of applying the experimental method (a), one obtains a series of spectral intensities M(2Δ) in the presence and absence of an applied field gradient, for different pulse duration times. In the absence of the pulsed field gradient (g = 0), the spectral decay is given by

$$M_y(2\Delta)_{g=0} = M_y(0)\exp(-2\Delta/T_2), \qquad (3-26)$$

whereas the spectral decay under an applied pulsed field gradient is given by equation (3 - 25). thus we may write,

$$\ln\left[\frac{M_y(2\Delta)}{M_y(2\Delta)_{g=0}}\right] = -\gamma^2G^2D\,\delta^2\,(\Delta - \delta/3). \qquad (3-27)$$

Thus a plot of $\ln [M_y(2\Delta) / M_y(2\Delta)_{g=0}]$ against $\delta^2(\Delta-\delta/3)$ will yield a straight line, to which a regression analysis may be applied to give a value for the slope, equal to $-\gamma^2G^2D$. A value of G is known from the calibration procedure and therefore D may be derived.

From experimental method (b), one obtains a series of spin echo intensities for different field gradient pulse lengths. The echo attenuation due to natural T_2 decay is constant for each spin echo and so a plot of $\ln [M_y(2\Delta)]$ against $\delta^2(\Delta - \delta/3)$ will give a straight line with the same gradient.

References for CHAPTER THREE.

1. M.J.Forster, D.G.Gillies and R.W.Matthews, J. Magn. Reson., 65, 497, (1985).
2. M.D.Gordan and L.d.Quin, J. Magn. Reson., 22, 149 (1976).
3. D.R.Vidrine and P.E.Peterson, Anal. Chem. 48, 1301 (1976).
4. J.T.Bailey, G.C.Levy, and D.A.Wright, J. Magn. Reson., 37, 353 (1980).
5. A.L.Van Geet, Anal. Chem., 40, 2227 (1968).
6. P.S.Raford, C.L.Fisk and E.D.Becker, Anal. Chem., 51, 2050 (1979).
7. R.L.Vold, J.S.Waugh, M.P.Klein and D.E.Phelps, J. Chem. Phys., 48, 3831 (1968).
8. D.Canet, G.C.Levy and I.R.Peat, J. Magn. Reson., 18, 199 (1975).
9. M.Sass and D.Ziessow, J. Magn. Reson., 24, 263 (1977).
10. G.S.McDonald and J.S.Leigh Jr., J. Magn. Reson., 9, 358 (1973).
11. E.L.Hahn, Phys. Rev., 80, 580 (1950).
12. G.A.Morris and R.Freeman, J. Magn. Reson., 29, 433 (1978).
13. K.F.Kuhlmann and D.M.Grant, J. Chem. Phys., 55, 2998 (1971).
14. R.Freeman, H.D.W.Hill and R.Kaptein, J. Magn. Reson., 7, 327(1972).
15. R.K.Harris and R.H.Newmann, J. Magn. Reson., 24, 449 (1976).
16. I.Solomon, Phys. Rev., 99, 559 (1955).
17. H.Carr and E.M.Purcell, Phys. Rev., 94, 630 (1954).
18. E.O.Stejskal and J.E.Tanner, J. Chem. Phys., 42, 288 (1965).
19. P.T.Callaghan, K.W.Jolley and C.M.Trotter, JEOL

News, 16A, 12 (1980).

20. I.Zupancic and J.Pirs, J. Phys., (London), E9, 79 (1976).

21. J.E.Tanner, Ph.D. Thesis, University of Wisconsin (1966).

22. P.Stilbs and M.E.Moseley, Chemica Scripta, 15, 176 (1980).

23. M.I.Hrovat and C.G.Wade, J. Magn. Reson., 28, 157 (1977).

24. E.Fukishima and S.W.Roeder, "Experimental Pulse NMR; A Nuts and Bolts Approach", Addison-Wesley Publishing Co., Reading. Mass. (1981).

25. P.T.Callaghan, K.W.Jolley and C.M.Trotter, J. Magn. Reson., 34, 39 (1979).

26. A.F.Collings and R.Mills, Trans. Faraday. Soc., 66, 2761 (1970).

CHAPTER FOUR ^{205}Tl AND ^{13}C RELAXATION STUDIES IN SUCROSE / SOLVENT SYSTEMS.

Section 4.1 Previous studies on sucrose solutions.

4.1.1 Relaxation Studies.

The use of ^{13}C spin lattice relaxation measurements to characterise the motional properties of sucrose molecules was first described by Allerhand et al.[1]. In this work ^{13}C spin lattice relaxation times (T_1) and nuclear Overhauser enhancements (nOe) were measured for sucrose (2M and 0.5M) in both H_2O and D_2O at 15.08 MHz. It was concluded that the two sugar rings behaved as a single rigid entity reorienting isotropically, whilst the CH_2OH side chains showed evidence of internal reorientation. A maximum value for the nOe indicated that the ^{13}C -^{1}H dipole-dipole mechanism was responsible for the relaxation of all the ^{13}C nuclei, and work in D_2O showed that the dipole-dipole relaxation contribution from the solvent protons was negligible.

In a series of papers by Suggett and co-workers[2-4] NMR and dielectric relaxation studies were performed to characterise the molecular motions and interactions in aqueous carbohydrate solutions. The dielectric studies[2] were predominately made at a 1.4M concentration of sucrose in water and it was found that a single Debye type relaxation process could not account for the observed data and, instead, a three process model was required. This

modification was justified by assigning the three processes to different reorientation rates of the solute, the bulk solvent and the solvent in the solute hydration sphere. A two process model arising from differing solute and solvent reorientation was also discussed with the possibility that each of these processes could include a distribution of correlation times of the Cole-Cole type[5]. It was concluded that the data obtained from solutions with concentrations lower than 1M were best fitted by a two process model and could adequately be explained by each process being of the Debye type, whereas, higher concentrations required the three Debye type process model to fit the observed relaxation data.

The complementary use of dielectric and NMR relaxation measurements in the study of aqueous carbohydrate solutions was discussed by Suggett[4]. The correlation times of the solute molecules derived from dielectric relaxation data compared unfavourably with those derived from NMR relaxation data. This was explained by considering that the dielectric relaxation of sugar molecules is not purely determined by the overall molecular reorientation rate, but rather due to the coupled motions of the side chain and the ring. Both dielectric, and NMR relaxation techniques were applied to study the solvent, H_2O and both relaxation rates were in good agreement when a two process model was assumed to apply to the dielectric relaxation data.

Many workers have assumed the motion of the sucrose molecule to be isotropic. McCain and Markley[6], however have noted that the sucrose molecule is not perfectly spherical and suggested that this would give rise to anisotropic reorientation. The crystal structure[7,8] obtained by neutron diffraction techniques confirms that sucrose is non spherical having dimensions of 1 x 0.8 x 0.4nm. For the anisotropic case the reorientation of the molecule may not be described by a simple spectral density function, but rather by a modified function featuring two or more different rotational correlation times[9,10]. The use of a single correlation time model to explain the results obtained for sucrose in low concentrations was justified[6] by averaging the motions of the eight differently oriented C-H vectors to calculate a single correlation time for the whole molecule which more closely resembles isotropic motion than that of a single C-H vector. Further justification lies in the fact that the rotational motion of sucrose has been shown to be only slightly anisotropic[11,12] and the correlation times are almost equal to each other. In the limit when anisotropic correlation times are equal, the spectral density becomes a function of a single correlation time.

The rigid molecule assumption has also been found to be slightly incorrect. Bock and co-workers[11,13] deduced from their studies using molecular dynamics calculations and NMR, that there was a slight flexing of the furanoid

ring.

McCain and Markley[6] later assumed that the internal motions of atoms within the ring structure of sucrose gave rise to a reduced spectral density at the NMR resonance frequencies of ^{13}C nuclei. The measurement of ^{13}C R_1 and nOe values in aqueous sucrose solutions ($\leq$ 1M) showed that the correlation times derived from nOe experiments were consistently longer than those derived from R_1 measurements. The nature of this discrepancy indicated a multiplication factor that was independent of both temperature and correlation time and so the scaled Lorentzian spectral density model proposed by Levy et al.[14], and discussed in section (4.3), was used to rationalise the data. This model was able to fit the data obtained at four different field strengths and several concentrations, by reducing the value of $J(\omega_0)$ to 89% of its full theoretical value. Thus it was concluded that the rapid fluctuations of atoms in the ring structure accounted for an 11% loss in the value of $J(\omega_0)$.

4.1.2 Effect of concentration on sucrose conformation.

The ^{13}C relaxation data for the highly concentrated sucrose solution, to be reported later, suggest a definite overall change in motional behaviour from the simple isotropic reorientational model invoked for less concentrated solutions. It will also be seen later that this is reflected in the motional behaviour of both the

dimethylthallium(III) and diethylthallium(III) cations in the sucrose/D_2O, and sucrose/DMSO-d^6 solutions respectively.

Anomolous behaviour at high sucrose concentrations has been noted previously by other workers and has been explained by the concentration effect on the conformation and association of sucrose molecules in solution. Schneider et al.[15] studied the viscosity of sucrose solutions at different concentrations and concluded that it is possible that the molecules undergo a rearrangement at ~ 30-40% concentration (w/w) which corresponds to a transition from the hydrated sucrose molecules to sucrose - sucrose associates.

A similar concentration effect was later noted by Sapronova et al.[16] in NMR studies on the structure of sugar solutions. They observed the existence of a hydration equilibrium in sucrose solutions at concentrations ≤ 30% giving way to molecular association at ~ 30 - 40% concentration (w/w) and becoming more pronounced at higher concentrations.

Tikhomiroff[17] studied supersaturated sucrose solutions by several techniques (density, viscosity, and thin layer chromatography) and the existence of associated groups of sucrose molecules was demonstrated.

A Raman study on the effect of sucrose on the water structure carried out by Walrafen[18] noted that, at high concentration (58% w/w) no intramolecular Raman bands of

sucrose were indicated and also the intermolecular bands from water were decreased in intensity. This was later justified by Mathlouthi et al[19] by assuming that sucrose - sucrose association occured at these concentrations, releasing water of hydration.

Lower sucrose concentrations have been studied extensively and there is some disagreement over the concentration dependence of the conformation of the sucrose molecule. Bock and Lemieux[11,20] have studied dilute solutions of sucrose in both D_2O and DMSO-d^6 (0.1M and 0.3M) by molecular modelling techniques and by NMR. They concluded that the conformation of sucrose in solution is concentration independent and is similar to the conformation preferred in the crystalline state, but for the loss of one intramolecular hydrogen bond from O -6^f to O -5^g (see figure 4-1), and the slightly different conformation of the furanoid ring. McCain and Markley[12] extended the study over a wider range of temperatures and concentrations ($\leq$ 1M). Their conclusions were in agreement with those of Bock and Lemieux suggesting the conformation of sucrose to be concentration independent over the range 0.1M to 1M.

However Mathlouthi and co-workers[21-23] suggest that the conformation of sucrose in H_2O is concentration dependent. Following laser Raman[21,22] studies on sucrose concentrations 10-66% (w/w), they noted that up to 35% concentration, the sucrose molecules exist as single

hydrates and at concentrations of ~ 35% the molecules begin to form regions of localised order that eventually lead to full sucrose-sucrose molecular association at concentrations of 66%. In this region the CH_2OH group of the D - fructofuran ring participates in intramolecular hydrogen bonding, whilst the D - glucosyl ring participates in intermolecular association.

Similar results were found in a further study on aqueous sucrose solutions in concentrations 10-82% (w/w), using the X-ray diffraction technique[23]. In this work sucrose hydrates were found to exist at concentrations less than 22.3%. In the intermediate range, 22.3% < C < 65.3% the sucrose molecules were found to become more ordered and draw closer to each other, and at concentrations greater than 65.3%, short range intermolecular forces between these molcules were apparent.

These studies led to a proposed picture of the conformational behaviour of sucrose as a function of concentration (see figure (4 - 1)) : In dilute solutions, the sucrose molecule lacks intramolecular hydrogen bonds, but as the concentration is increased the molecule undergoes a twisting about the glycosidic linkage $C-1^g - O - C-2^f$. At intermediate concentrations the molecule has the form suggested previously with one intramolecular hydrogen bond between $O-1^f$ and $O-2^g$ but this conformation changes at higher concentration to the form

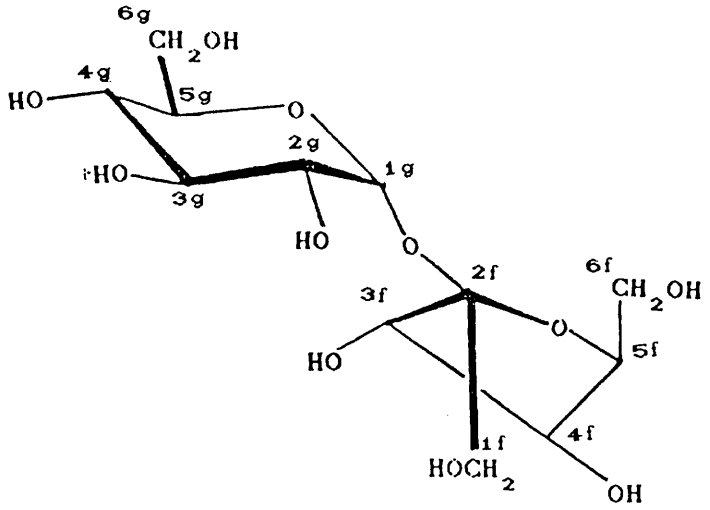

A)

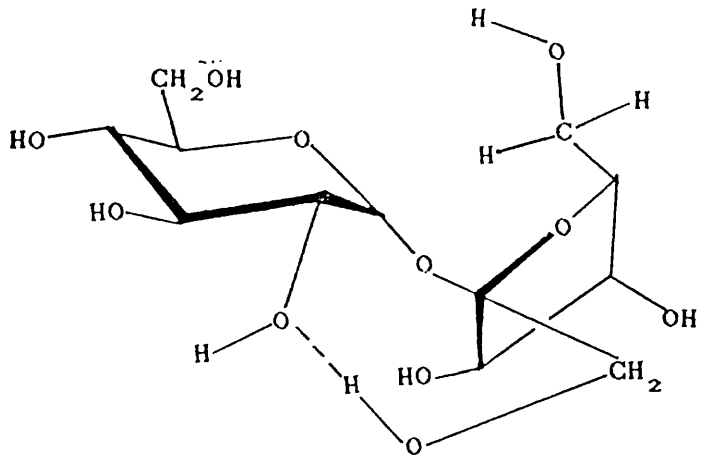

B)

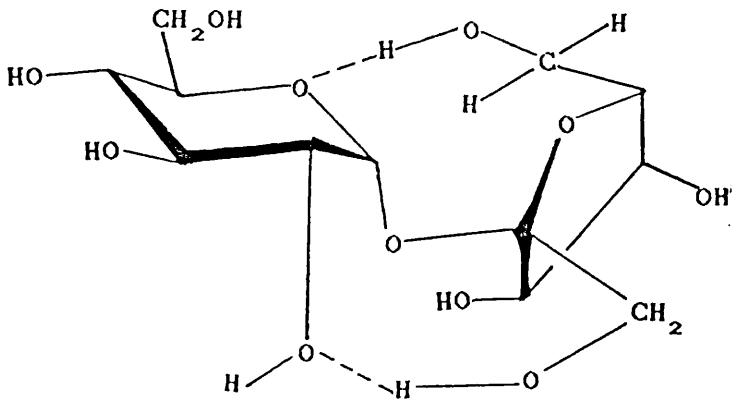

C)

Figure (4-1) Change in sucrose conformation[23] as a function of concentration. a) low (<22.3%), b) medium (<65.3%), c) high (>65.3%)

found in the crystalline state which has two intramolecular hydrogen bonds

Section 4.2 ^{205}Tl relaxation studies on Dimethylthallium(III) nitrate in 60% sucrose/D_2O (w/w) solution.

4.2.1 The dimethylthallium(III) cation.

The study proposed involves the application of the dimethylthallium(III) cation as a probe molecule to study the motion of ions, at the microscopic level, in highly concentrated, aqueous sucrose solution.

The addition of dimethylthallium(III) nitrate to aqueous solution generates the dimethylthallium(III) cation and it has been shown by ^{205}Tl NMR chemical shift studies[24], supported by conductivity data[25], that the dissociation is almost complete over the studied concentration range ($\leq$ 1.5 mol%). The cation has other favourable qualities, the ^{205}Tl R_1 for dimethylthallium(III) nitrate has been shown to be concentration independent over the range 0.04M to 0.8M and is also unaffected by the change in anion from nitrate to acetate[26]. The structure of the cation has been shown by Raman and infrared studies to consist of a linear C-Tl-C backbone and so may be considered to take the shape of an ellipsoid in solution for the purpose of testing theories of the liquid state.

The application of the dimethylthallium(III) cation to

the study of concentrated aqueous sucrose solution is an extension of the work of Forster et al.[26,27] who studied the ^{205}Tl relaxation in a 0.07 molal solution of dimethylthallium(III) nitrate in 79% glycerol/water solution (w/w). Relaxation measurements were made at ^{205}Tl frequencies of 21.96MHz and 231.6MHz as a function of temperature. A large increase in the ^{205}Tl R_1 was observed with increase in field and this suggested that the CSA mechanism was dominant at high field. The high field data showed a distinct R_1 maximum indicating that the viscosity of the solution was sufficient to render the reorientational motion of the cation outside the extreme narrowing limit. This permitted the simultaneous determination of both the shielding anisotropy, and the reorientational correlation time. The anisotropy was noted to be 5550 ± 32ppm and the reorientational correlation time at a reference temperature of 298K was given as 898 ± 39ps.

Assuming a single correlation time model the low field R_1 values were predicted by scaling the high field data, these values matched those obtained by experiment, showing a similar dominance of the CSA mechanism at this field. The models assumed in the analysis of the T_1 data were verified by analysis of the T_2 behaviour at high field.

The relaxation behaviour of the dimethylthallium(III) cation in aqueous glycerol solution suggests the cation as a useful probe for the study of molecular motion in

viscous media The work presented in this study is designed to test its application to other viscous media.

4.2.2 Measurements.

A 60% sucrose/D_2O solution (w/w) was chosen for the study. The choice of concentration was made so that the resulting solution viscosity was sufficient to slow down the motion of the cation to be in the dispersion regime at room temperature and a ^{205}Tl frequency of 231.6MHz.

To this solution, dimethylthallium(III)nitrate was added to make an overall concentration of 0.3M. The sample was then degassed by several freeze-pump-thaw cycles as outlined in section (3.2).

Spin-lattice relaxation measurements were made as a function of temperature at ^{205}Tl frequencies of 21.96MHz and 231.6MHz.

Spin-spin relaxation measurements were also made as a function of temperature at a ^{205}Tl frequency of 231.6MHz over a similar range of temperatures. The sample temperatures at high and low field were measured by sample substitution, as the broad ^{205}Tl resonance of the cation in the sucrose solution obscured the aqueous thallium resonance of the thermometric liquid.

The results are presented in tables (4 - 1) to (4 - 3). The temperature dependences of the ^{205}Tl R_1 at both high and low field are shown as plots of ln R_1 against inverse temperature in figure (4 - 2). The best fit curves to the data are generated by a fitting procedure to the

Fuoss-Kirkwood[28] distribution of correlation times model, discussed later in section (4.2.7).

The ^{205}Tl R_2 behaviour is discussed in section (4.3).

Table (4 - 1) Temperature dependence of ^{205}Tl R_1 at 21.96MHz.

Temperature	$R_1(s^{-1})$
293.2	106
298.6	85.2
306.0	59.5
312.9	43.7
320.1	32.9
327.1	30.0
336.6	16.0
354.0	10.0

Table (4 - 2) Temperature dependence of ^{205}Tl R_1 at 231.6MHz.

Temperature	$R_1(s^{-1})$
292.3	2087
296.8	2130
311.9	1956
321.6	1725
330.9	1459
338.3	1200

Table (4 - 3) Temperature dependence of ^{205}Tl R_2 at 231.6MHz

Temperature	$R_2(s^{-1})$
296.3	9226
308.2	4714
318.9	2965
328.5	1967
337.7	1534
347.3	1111

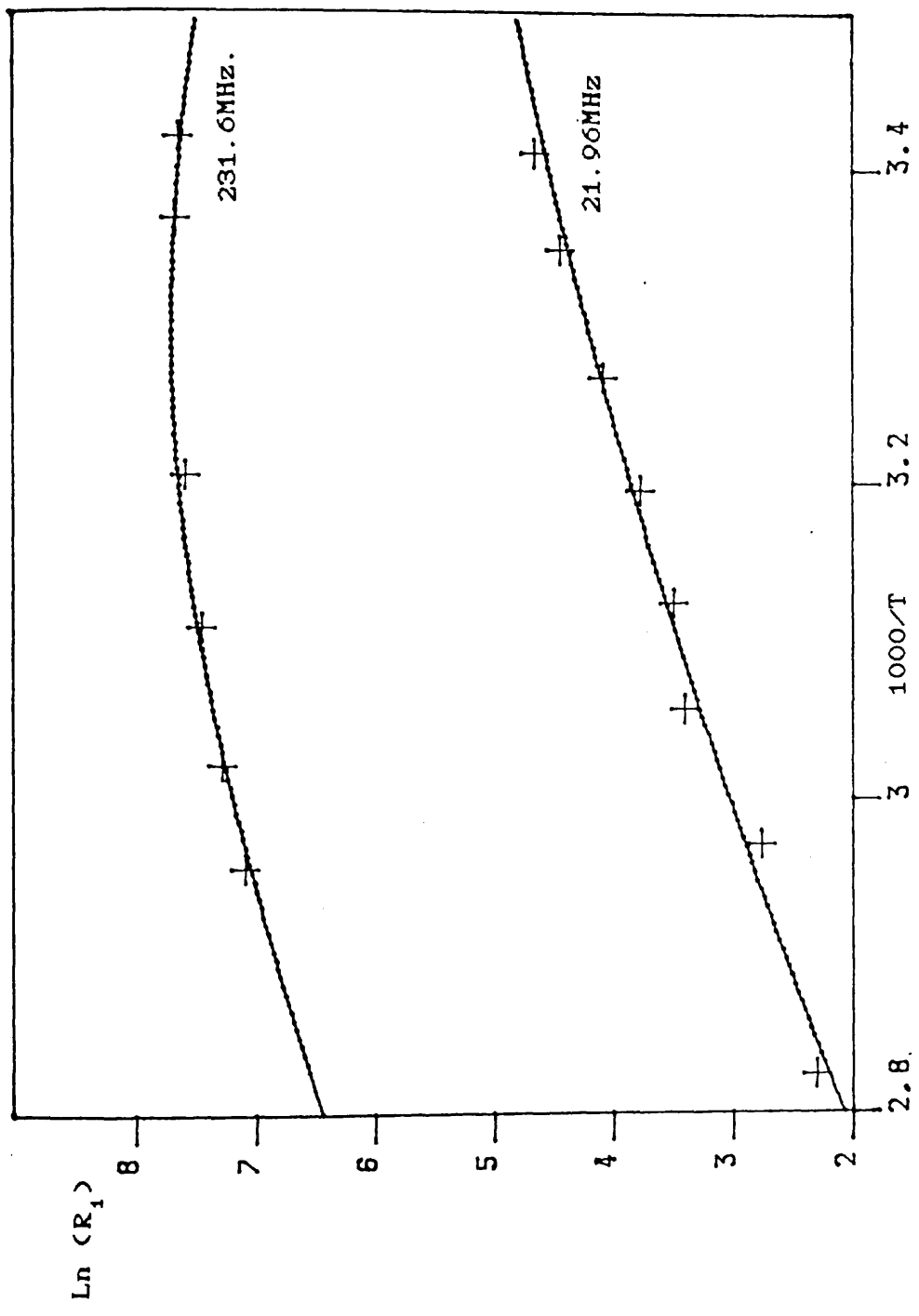

Figure (4-2) ^{205}Tl R_1 data at 21.96MHz and 231.6MHz fitted to a Fuoss-Kirkwood distribution.

4.2.3 Discussion of results and data analysis.

Considering the R_1 values given in tables (4 - 1) and (4 - 2), it is evident that the ^{205}Tl R_1 for the dimethylthallium(III) cation in aqueous sucrose solution increases dramatically with increase in field strength. This is characteristic of a significant contribution of the CSA relaxation mechanism to the overall rate and the results will be analysed by assuming a dominance of this mechanism at both field strengths of interest. This assumption will later be verified.

The ^{205}Tl R_1 shows a different temperature dependence at high and low field strength. At low field the R_1 steadily decreases as the temperature is increased, but at high field the R_1 shows an increase to a maximum value and then a steady decrease over a similar temperature range. The theoretical basis for this behaviour is best understood by recalling the rate equation for the CSA mechanism, equation (2 - 41), applied to an axially symmetric shielding tensor,

$$R_{1CSA} = \frac{1}{15} (\gamma B_0)^2 \Delta\sigma^2 \frac{2\tau_c}{1 + (\omega_0^2 \tau_c^2)} \qquad (4 - 1)$$

At low field, the value of ω_0 is such that the condition $\omega_0^2 \tau_c^2 < 1$. Thus R_{1CSA} is directly proportional to the reorientational correlation time, τ_c, and decreases linearly with increase in temperature.

At high field, the observed R_1 maximum indicates that the condition, $\omega_0^2\tau_c^2 < 1$ is not valid and thus the full form of the spectral density becomes significant. In the low temperature regime, $\omega_0^2\tau_c^2 > 1$ and hence R_{1CSA} is inversely proportional to τ_c and increases with increasing temperature. At high temperature, $\omega_0^2\tau_c^2 < 1$ and the opposite temperature dependence is observed. Between these two limits, R_{1CSA} goes through a maximum value at which $\omega_0^2\tau_c^2 = 1$.

For a full analysis of the R_1 data, it is necessary to calculate the shielding anisotropy, $\Delta\sigma$ for the dimethylthallium(III) cation in this system. Once this parameter is known, the motional activation parameters for the nucleus may also be derived. The characteristic R_1 maximum observed at high field enables one to calculate the shielding anisotropy by a number of methods. If the values of R_{1CSA} at the same temperature, at both high and low field are known, and the motion of the cation at high field is closely within or beyond the extreme narrowing limit, the ratio of the two rates directly implies τ_c and hence $\Delta\sigma$. In addition it has been noted that at the R_{1CSA} maximum the value of $(\omega_0\tau_c)^2$ is unity and so the shielding anisotropy may be calculated from a knowledge of the relaxation maximum. However, for either of these methods, there is very limited use of the relaxation data available as the R_1 at only one temperature is used in the analysis and this ultimately reduces the accuracy of the derived

parameters.

Therefore the method used in this study followed the procedure proposed by Forster[26]. Here a non linear least squares fitting procedure was applied to fit the observed data to a best fit curve using three adjustable parameters, these being the shielding anisotropy, $\Delta\sigma$ the correlation time at a temperature of 298K, $\tau_{c(298)}$ and the activation energy, E_a. This method involves the assumption that the dimethylthallium(III) cation exhibits single correlation time behaviour which varies with temperature in an exponential manner described by the following equation

$$\tau_c(T) = \tau_{c(298)} \exp\left[\frac{E_{CSA}}{R}\left(\frac{1}{T} - \frac{1}{298}\right)\right], \quad (4-2)$$

The best fit parameters obtained from the fitting procedure to the high field data alone are,

$$\Delta\sigma = 4696 \pm 23 \text{ ppm}, \quad (4-3)$$

$$\tau_{c(298)} = 715 \pm 29 \text{ ps}, \quad (4-4)$$

$$E_{CSA} = 24.8 \pm 1.3 \text{ kJ mol}^{-1}. \quad (4-5)$$

An initial inspection of these parameters shows that although the models and method of data analysis duplicated those used by Forster the calculated value for the shielding anisotropy of the dimethylthallium(III) cation in aqueous sucrose solution is significantly lower than

that found for the same cation in aqueous glycerol solution.

Therefore if the same models apply to both systems then the probe qualities of the cation would be questionable, as it appears to exhibit different physical properties in different viscous systems. The small observed ^{205}Tl chemical shift difference of ~ 1.5 ppm between solutions of dimethylthallium(III) nitrate in D_2O and in aqueous sucrose is not consistent with the formation of any long - lived complex between sucrose and dimethylthallium(III) cations and there is no obvious reason for a change in the anisotropy. This anomally may not necessarily be due to a physical change in the shape of the cation but instead, may arise as a result of applying the wrong theoretical model to rationalise the relaxation data. This approach will be tested in later sections.

4.2.4 Field dependent analysis.

Equation (4 - 2) may be used to calculate the reorientational correlation time at any given temperature using the values of E_{CSA} and $\tau_c(298)$ derived from the fitting procedure. These values may then be used in equation (4 - 1), together with the calculated shielding anisotropy to calculate the expected contribution of the CSA mechanism at a ^{205}Tl frequency of 21.96 MHz. If the ^{205}Tl relaxation behaviour of the dimethylthallium(III) cation in viscous solutions is fully characterised by the

study in aqueous glycerol solution[26], then one would expect the low field relaxation to be dominated by the CSA mechanism and hence the predicted rates from the high field data to match the observed low field rates.

Figure (4 - 3) shows the observed low field rates compared to those calculated using the best fit parameters, given by the fitting procedure to the high field data.

The observed R_1 values at each temperature are significantly higher that those predicted by the scaling procedure and there is a residual relaxation contribution. This contribution is noted to have a temperature dependence and is more significant at low temperature. Thus it becomes clear that different models apply to the study of the dimethylthallium(III) cation in aqueous sucrose systems as opposed to the aqueous glycerol system and it is necessary to discuss this difference in terms of the contribution of other relaxation mechanisms, or the application of more complex motional models.

On reaching this conclusion, the value of performing relaxation measurements at more than one field, is noted. The results obtained at 231.6 MHz alone lead one to assume a dominant contribution from the CSA mechanism but the contribution of other relaxation mechanisms or the effects of more complex motional behaviour may not be deduced. The analysis of single field R_1 measurements may therefore give rise to an oversimplified argument to account for the

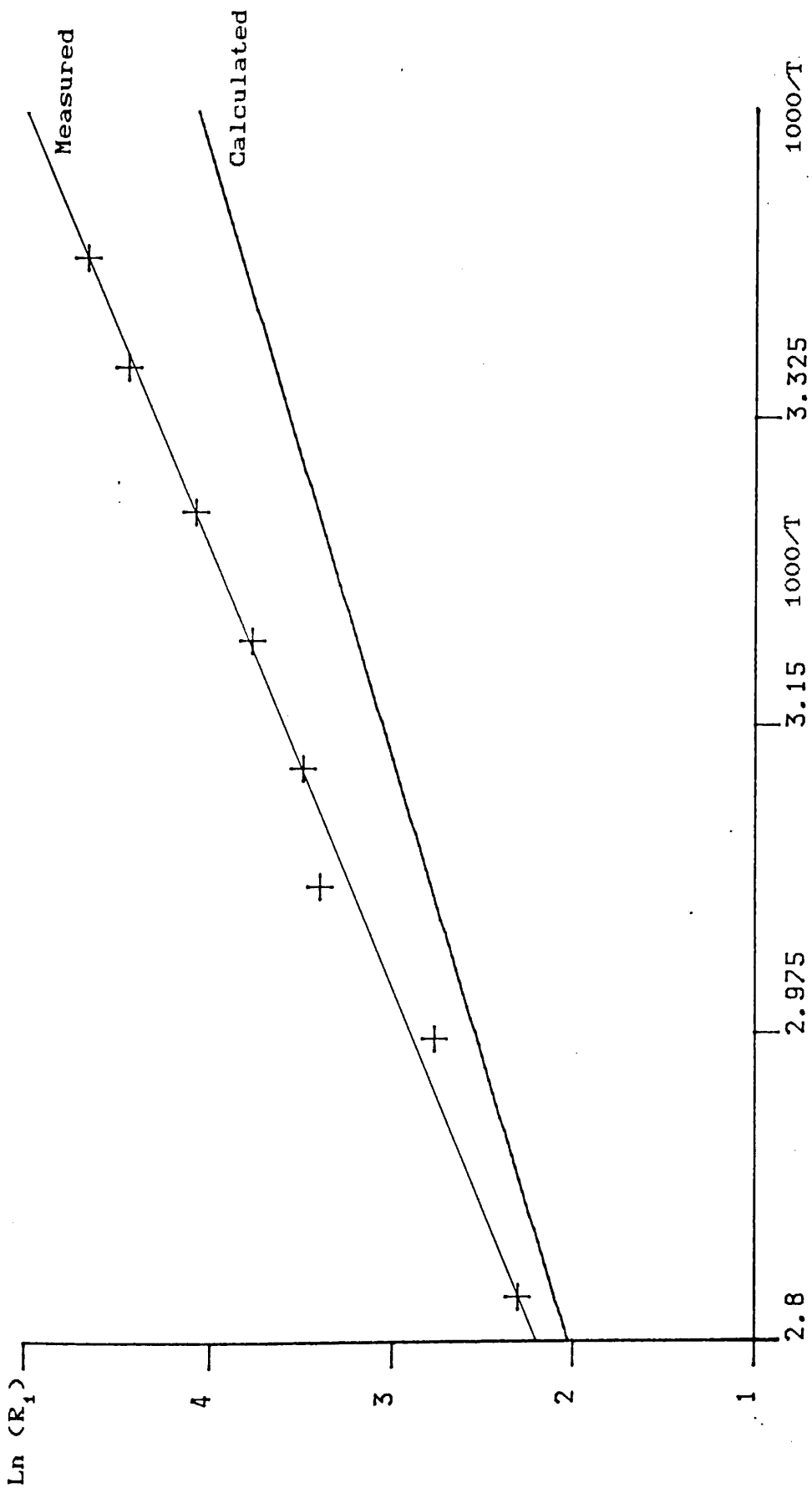

Figure(4-3) Measured ^{205}Tl R_1 at 21.96MHz. compared with calculated R_1 values assuming a single correlation time model.

relaxation behaviour of the dimethylthallium(III) cation.

4.2.5 Other relaxation mechanisms

The difference in the observed and calculated low field R_1 values may initially be considered to be due to a contribution from some other relaxation mechanism(s). Relaxation rates are additive and so we may write,

$$R_{1TOTAL} = R_{1CSA} + R_{1SR} + R_{1DD} + R_{1Sc}. \qquad (4-6)$$

Thus it is necessary to distinguish and separate the R_1 contribution from each, to the total rate.

The contribution from the spin-rotation mechanism may be immediately discounted, as it has an opposite temperature dependence to the observed residual R_1 (see section 2.3.3).

The intermolecular and intramolecular $^{205}Tl-^{1}H$ dipole-dipole contribution may be ascertained by a $^{205}Tl-\{^{1}H\}$ nOe experiment. From the full expression for the heteronuclear nOe following an A-{X} experiment, equation (3 - 22), the maximum signal enhancement factor, η for the ^{205}Tl resonance may be calculated as a function of $\omega_0\tau_c$. Selected values are given in table (4 - 4)

Table (4 -4) Calculated maximum nOe factors for the ^{205}Tl-(^{1}H) experiment as a function of ($\omega_0\tau_c$).

$\omega_0\tau_c$	η
0.01	0.867
0.1	0.834
0.25	0.687
0.5	0.390
1.0	0.035

Using the parameters given in equations (4 - 3) to (4 - 5) the correlation time at 294.1K was derived, and this in turn gave a value for $\omega_0\tau_c$ of 0.112 at a frequency of 21.96MHz. This gives a maximum possible enhancement factor of 0.824. This would be observed if the total low field relaxation rate was due to the dipole-dipole mechanism. In the observed situation, at 294.1K, the full possible contribution of the residual relaxation rate is in fact only 56% of the total measured rate and so the possible enhancement is reduced to a value of 0.457 which is low, but still discernable by experiment. However at this temperature no nOe was observed and similarly no nOe was observed at a temperature of 323K where the enhancement is predicted to be 0.354. Therefore on the basis of these results we can discount the contribution from the dipole-dipole mechanism.

Finally, we can discount the possibility of a scalar relaxation contribution to the low field residual R_1 for,

as noted in Chapter 2, the scalar mechanism does not typically give rise to R_1 contributions of this magnitude.

Therefore as the residual rate cannot be accounted for by a second relaxation mechanism we must assume that the CSA mechanism is dominant at both high and low field, and thus it is necessary to explain the anomolous behaviour in terms of a more complex model for molecular motion.

4.2.6 Models for molecular motion

To explain the apparent residual rate contribution we must study more closely the assumptions made in applying the fitting procedure to the high and low field relaxation data.

The CSA rate equation used in the three parameter fitting procedure contains a spectral density function that is based on a single exponential correlation time model. If we consider that the dimethylthallium(III) cation is probing a highly viscous system, containing a high concentration of sucrose molecules, where molecular association is apparent[15-17, 19, 21-23] then it is possible that the cation may be in an environment that does not allow it to exhibit the motional behaviour described by this simple model.

There are several models that have been formulated to describe more complex motional behaviour in liquid systems and these are founded on a variety of theoretical bases. In this study it is of interest to apply some of the models that have been suggested in situations where the

B.P.P model is inadequate in order to test the degree of application of each model to the aqueous sucrose system.

Many relaxation studies performed in associated liquids have similarly shown behaviour that cannot be rationalised by a single, exponential correlation time model. In many of these studies a distribution of correlation times model has been successfully applied. The distributions may be of two types, discrete or continuous.

A simple model leading to a discrete distribution was discussed by Woessner[9] who considered the anisotropic rotational diffusion of an ellipsoid which may give rise to two distinguishable correlation times.

However the continuous distribution has found more widespread use and is of interest in this study. In Chapter 1, the continuous distribution was noted to be either symmetrical or asymmetrical in form and so an example of each has been applied in this work.

4.2.7 Application of the The Fuoss-Kirkwood distribution of correlation times model.

The Fuoss-Kirkwood distribution[28] was formulated to account for the distribution of dielectric correlation times observed in many polar systems containing large molecules and was initially applied to the complex chain motions in the polyvinyl-chloride-diphenyl system. Fuoss and Kirkwood suggested that two types of motional behaviour may occur in this system, each of which may give rise to a distribution of correlation times. In the first

instance, the motion of a given dipole in a chain of molecules may be affected by the co-operative motions of neighbouring molecules. In the second instance, the complex configurations of the dipole chain may lead to a variation in the lengths of chain segments, and therefore the dipoles in different chain segments may exhibit a variety of motional properties.

A distribution, F(S) that is symmetrical about the central correlation time τ_o was proposed and this is given by[29],

$$F(S) = \frac{\beta}{\pi}\left[\frac{\cos(\beta\pi/2)\cosh(\beta S)}{\cos^2(\beta\pi/2)\sinh^2(\beta S)}\right], \quad (4-7)$$

where S is a constant defining the correlation times on a logarithm scale such that $S = \ln(\tau_c/\tau_o)$, and β is the distribution width parameter lying in the range $0 < \beta \leq 1$. In the limit where $\beta = 1$ the single correlation time model applies.

Connor[29] applied the distribution to the NMR relaxation case and derived an expression for the spectral density $J(\omega)$. This is given by,

$$J(\omega) = \frac{2\beta}{\omega_o}\left[\frac{(\omega_o\tau_o)^\beta}{1 + (\omega_o\tau_o)^{2\beta}}\right]. \quad (4-8)$$

This function may be inserted into the CSA spin - lattice

relaxation rate equation (4 - 1) to give the modified rate equation,

$$R_{1CSA}^{FK} = \frac{1}{15} (\gamma B_0)^2 \Delta\sigma^2 \frac{2\beta}{\omega_0} \left[\frac{(\omega_0\tau_0)^{\beta}}{1 + (\omega_0\tau_0)^{2\beta}} \right], \qquad (4 - 9)$$

The R_1 data obtained at both high and low field were rationalised simultaneously by a four parameter, non linear, least squares fitting procedure to equation (4 - 9). The adjustable parameters were: the shielding anisotropy $\Delta\sigma$, the reorientational correlation time at the centre of the distribution, at 298K $\tau_0(298)$, the distribution width parameter at 298K, β_{298} and the activation parameter, E_{CSA}. When applying this fitting procedure, the correlation time τ_0 was assumed to have an Arrhenius temperature dependence of the form given by equation (4 - 2).

A satisfactory fit to the data could only be achieved by assuming a linear increase in the β parameter with increasing temperature, and the value of this parameter at any given temperature may be calculated from the relation,

$$\beta(T) = \beta_{298} \times \frac{T}{298}, \qquad (4 - 10)$$

In this manner, β was observed to vary from 0.72 at 298K to 0.85 at 354K.

The fitting procedure gave the following best fit parameters,

$$\Delta\sigma = 5588 \pm 173 \text{ ppm}, \qquad (4 - 11)$$

$$\tau_0(298) = 802 \pm 97 \text{ ps}, \qquad (4 - 12)$$

$$E_{CSA} = 38.9 \pm 2.2 \text{ kJ mol}^{-1} \qquad (4 - 13)$$

$$\beta_{298K} = 0.72 \pm 0.03. \qquad (4 - 14)$$

The result of the fitting procedure is represented in figure (4 - 2), the points represent observed R_1 values at 231.6 MHz and 21.96 MHz, and the lines are generated by the best fit parameters given above.

The required temperature dependent distribution width needed to fit the data is not uncommon, Ghesquiere et al.[30,31] similarly used a temperature dependent Fuoss - Kirkwood distribution of correlation times to rationalise ^{13}C R_1 data at 25.14 MHz and ^{1}H R_1 data at 100 and 250 MHz in poly(4 - vinylpyridine) (P4VP)[30] and poly(4 - vinylpyridium bromide) ($P4VPD^+$)[31] in methanol solution. The β parameter was assumed to have a linear temperature dependence and this varied from 0.65 at 222K to 0.95 at 333K in the (P4VP) solution and from 0.72 at 250K to 0.98 at 350K in the ($P4VPD^+$) solution.

Read and Williams[32] studied the dielectric relaxation of poloxymethylene in the temperature range 223K - 398K and explained the results in terms of a Fuoss-Kirkwood distribution of correlation times . They found that the width parameter varied with temperature and

the values of β and τ_0 were tabulated over the full temperature range. NMR spin-lattice relaxation measurements on this compound were later made by Connor[29] in order to correlate the results from NMR relaxation measurements with those from dielectric studies. The τ_0 and β parameters tabulated by Read and Williams were used to derive NMR correlation times and thus to generate a theoretical plot of ln T_1 against 1000/T. This provided a satisfactory correlation with the NMR relaxation data measured on the high temperature side of the T_1 minimum, but data on the low temperature side were found to deviate more consistently at lower temperatures.

As shown in figure (4 - 2), the data may be adequately described by a symmetrical distribution of correlation times model. A closer look at the parameters obtained by the fitting procedure enables one to justify whether or not the model gives physically reasonable values for the dimethylthallium(III) cation in such a viscous system.

A noticeable result is that the shielding anisotropy that was initially calculated to be 4696ppm, using a single correlation time model, is now increased to

$$\Delta\sigma = 5588 \pm 173\text{ppm}. \qquad (4 - 15)$$

The higher anisotropy matches, within experimental error, the anisotropy for the same cation calculated by Forster[26] from measurements made in aqueous glycerol solution this was noted to be,

$$\Delta\sigma = 5550 \pm 32 \text{ ppm.} \qquad (4 - 16)$$

This is a particularly interesting result as it shows that although the dimethylthallium(III) cation appears to monitor a different motional character in each system, it exhibits the same physical property, its anisotropy, in both systems. This provides further support for the use of a distribution of correlation times model to describe the motional behaviour of this cation in highly concentrated aqueous sucrose solution, and in addition provides further evidence for the use of the cation as an effective probe molecule.

The anisotropy calculated in this study disagrees with the results of Hinton et al.[33] who reported values for $\Delta\sigma$ of 1976ppm and 485ppm for dimethylthallium(III) nitrate and dimethylthallium(III) bromide salts respectively. These values were obtained directly from the solid state powder patterns of these salts and are clearly lower than the value derived in this study. Possible reasons for this have been given[26,27] and very recent solid state NMR studies have indicated a value of 5960ppm[34], which is more in keeping with the value presented here.

The reorientational correlation time and activation parameter, derived from the application of the Fuoss-Kirkwood distribution are discussed in section (4.2.10), where they are used to test theories of the liquid state.

4.2.8 Application of the Cole-Davidson distribution.

The Cole-Davidson distribution[35,36] has found widespread use in the analysis of NMR relaxation measurements made in viscous liquids. Like many other distributions it was first derived to account for dielectric relaxation measurements that could not be rationalised by the simple, single correlation time theory.

The Cole-Davidson distribution function, given in Chapter 2., was applied to the NMR relaxation case by Connor[29] who derived the spectral density function,

$$J(\omega) = \frac{\tau_0 \sin\left[\arctan(\omega_0\tau_0)\right]}{\omega_0\left[1 + (\omega_0\tau_0)^2\right]^{\beta/2}}, \qquad (4 - 17)$$

where τ_0 represents the limiting correlation time, above which the distribution is assumed to be zero and β is the distribution width parameter lying in the range $0 < \beta \leq 1$.

As τ_0 does not correspond to the centre of the distribution we find that the effect of applying this model is to shift the R_1 maximum to lower temperatures as β is increased, so that it is not necessarily at $\omega_0\tau_c = 1$ for the CSA relaxation mechanism.

The spectral density given in equation (4 - 17) may be inserted into the CSA R_1 equation (4 - 1) to form a modified function that may be used in the four parameter fitting procedure applied initially to test the

Fuoss-Kirkwood distribution.

The use of the Cole-Davidson distribution with the same assumptions as before, on the temperature dependences of the limiting correlation time and distribution width parameter, could not rationalise the R_1 data obtained at high and low field. Similarly the model failed when a temperature independent β parameter was used and so this model is discounted as inappropriate.

4.2.9 Application of the scaled Lorentzian spectral density model.

It is of interest to apply a different formalism to that of a distribution of correlation times model. The model due to Levy, Karplus and McCammon[14] is discussed in detail in section 4.3.6, as it has, so far, only been used to describe the effects of the internal motions of nuclei within a ring structure and is thus appropriate to the ^{13}C relaxation in the sucrose molecule[6]. The effect of applying the model is to reduce the amplitude of the spectral density $J(\omega_0)$ at the NMR resonance frequency.

The CSA R_1 equation may be modified to include the scaled Lorentzian spectral density by simply including a fractional multiplication factor, S^2 that appears in the interaction part of the equation. Thus it is apparent that for a measured spin-lattice relaxation rate R_{1CSA}, the reduced $J(\omega_0)$ is indistinguishable from a reduced interaction term and a full $J(\omega_0)$. Hence in this manner, it is possible to account for an apparent reduction in the

observed value of $\Delta\sigma$.

The R_1 data were fitted to the modified equation by a three parameter, non linear least squares fitting procedure with the adjustable parameters being, the product $S.\Delta\sigma$, the reorientational correlation time at 298K and the activation energy. The best fit estimates for the parameters obtained by this procedure are,

$$S.\Delta\sigma = 4861 \pm 211 \text{ ppm}, \qquad (4 - 18)$$

$$\tau_{c(298)} = 1340 \pm 163 \text{ ps}, \qquad (4 - 19)$$

$$E = 38.1 \pm 3.4 \text{ kJ mol}^{-1} \qquad (4 - 20)$$

The result of the fitting procedure is shown in figure (4 - 4).

If we assume that the value of the shielding anisotropy alone is 5588 ppm, then this fitting procedure gives a value for the fractional constant S^2 equal to 0.75. Thus, to interpret this result on the theoretical basis of the original model, it appears that the amplitude of the $J(\omega_0)$ term that characterises the overall molecular reorientation of the cation, is in fact only 75% of the full theoretical value. However, a mechanism by which this type of behaviour may occur is not known.

Considering an overall view of the models used to fit the observed data, the model that appears to be the most appropriate is the Fuoss-Kirkwood distribution of correlation times. The model proposed by Cole and Davidson is not able to rationalise the data and although the scaled Lorentzian spectral density model provides a fit to

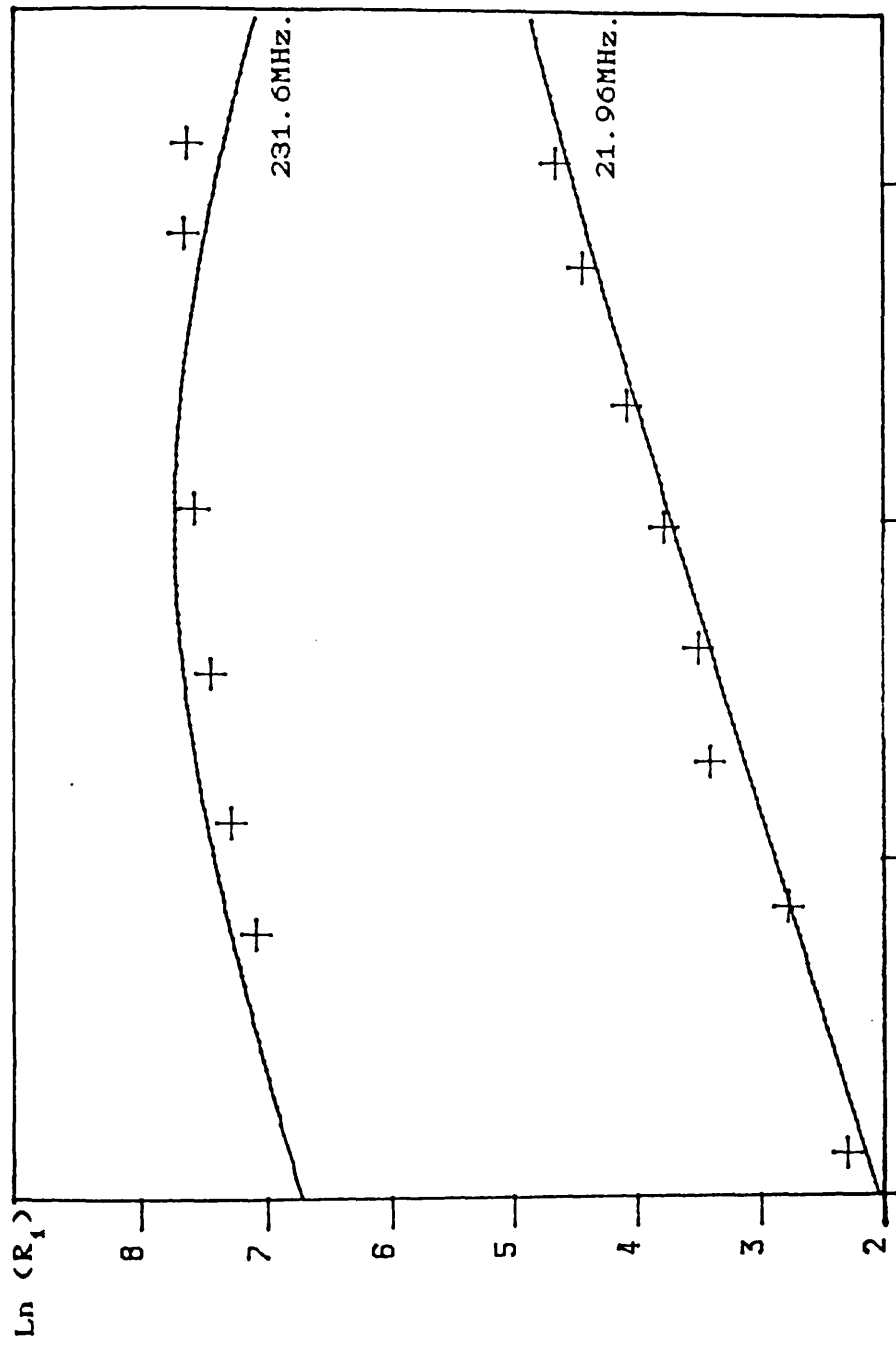

Figure (4-4) ^{205}Tl R_1 data at 21.96MHz. and 231.6MHz., fitted to a scaled Lorentzian $J(\omega)$ model.

the data, it is clear from representation of this data fitting, given in figure (4 - 4) that this model predicts the R_1 maximum to be at a higher temperature than that observed by experiment. Therefore the NMR correlation times used to test theories of the liquid state in the following section, are derived from the parameters obtained from applying the Fuoss-Kirkwood distribution.

4.2.10 Reorientational motion and theories of the liquid state.

The centre of the Fuoss-Kirkwood distribution of correlation times may be calculated at any given temperature using equation (4 - 2) and the best fit parameters given in equations (4 - 11) to (4 - 14).This parameter corresponds to the average reorientational correlation time τ_c. Table (4 - 5) gives examples of the correlation times derived by this model at selected temperatures.

Table (4 - 5) Reorientational Correlation times derived from the Fuoss-Kirkwood distribution.

Temperature (K)	τ_c (ps)
298	802
308	481
323	238
338	125
353	69

It is usual practice to relate the reorientational correlation time for the cation, obtained from NMR relaxation studies, to the viscosity of the medium that the cation is probing. The simplest relation between between these properties is given by the Debye relation[37], first discussed in section (2.1) and repeated here for convenience.

$$\tau_c = \frac{4\pi a^3 \eta}{3k_b T} \qquad (4 - 21)$$

where $\frac{4\pi a^3}{3}$ is the molecular volume in m^3, η is the shear viscosity of the surrounding continuous medium in N $m^{-2}s$, and T is the temperature in Kelvin.

From this equation it is clear that if the model holds, a plot of τ_c against η/T will yield a straight line with intercept at zero, the gradient of which is related to the volume of the reorienting species.

Bauer et al.[38] have argued that in the limit where there is no coupling of τ_c with the environment, it is physically unreasonable to suppose that τ_c has a zero value and therefore they rationalised their results in terms of the equation,

$$\tau_C = C\,\eta + \tau_{fr} \qquad (4 - 22)$$

where,

$$C = \left(\frac{4\pi a^3}{3k_b T} \right) K \qquad (4 - 23)$$

and τ_{fr} roughly estimates the correlation time for the free rotor for which

$$\tau_{fr} = \left(\frac{2\pi}{9} \right) \cdot \left(\frac{I}{k_b T} \right)^{1/2} \qquad (4 - 24)$$

where I is the moment of inertia.

The term K in the constant C represents the degree to which the observed behaviour departs from the Debye model and lies in the range $0 < K \leq 1$. Several theories have been proposed to account for the K factor and some examples of these have been presented in a review article by Dote et al.[39]. These theories include the Gierer-Wirtz microviscosity factor[40] designed to correct for the discontinuous nature of the surrounding fluid, the models of Hu and Zwanzig[41] and Youngren and Acrivos[42] to account for the deviations from the perfect spherical shape of the reorienting species leading to the introduction of slip boundary conditions, the Hill theory[43] that accounts for the transfer of spin angular momentum from the probe cation to that of the surrounding solvent molecules and the Hynes, Kapral and Weinberg theory[44,45] in which the probe cations are thought to transfer angular momenta to the nearest neighbouring solvent molecules by collisional processes.

The model most commonly used is that based on the McLung and Kivelson[46] theory of anisotropy of intermolecular potentials which represents K as a ratio of the mean square intermolecular torques on the solute

molecules to the mean square intermolecular forces on the solvent molecules. Whilst both the torques and forces on the molecule are determined by the total intermolecular potential energy, the anisotropic part of the potential is responsible for the torques only, and thus K may be interpreted as the degree of rotational-translational coupling of the motions of the species under study. In the stick limit, where K = 1, there is said to be a high degree of rotational-translational coupling, whilst in the slip limit a low degree of coupling is assumed.

It is of interest to apply the hydrodynamic models to the derived correlation times for the dimethylthallium(III) cation in the aqueous sucrose system.

The values for the shear viscosity of a 60% sucrose solution (w/w) in D_2O are unknown, however viscosity data are available for a 60% sucrose solution in H_2O (w/w) over a range of temperatures[47] and thus it is assumed that these viscosities most closely relate to the system under study. These values were used to test the validity of equation (4 - 22).

A plot of τ_c against η/T was made, and is shown in figure (4 - 5). The best fit line through the data points was given by a linear, least squares regression analysis and the slope and intercept of this line were given as,

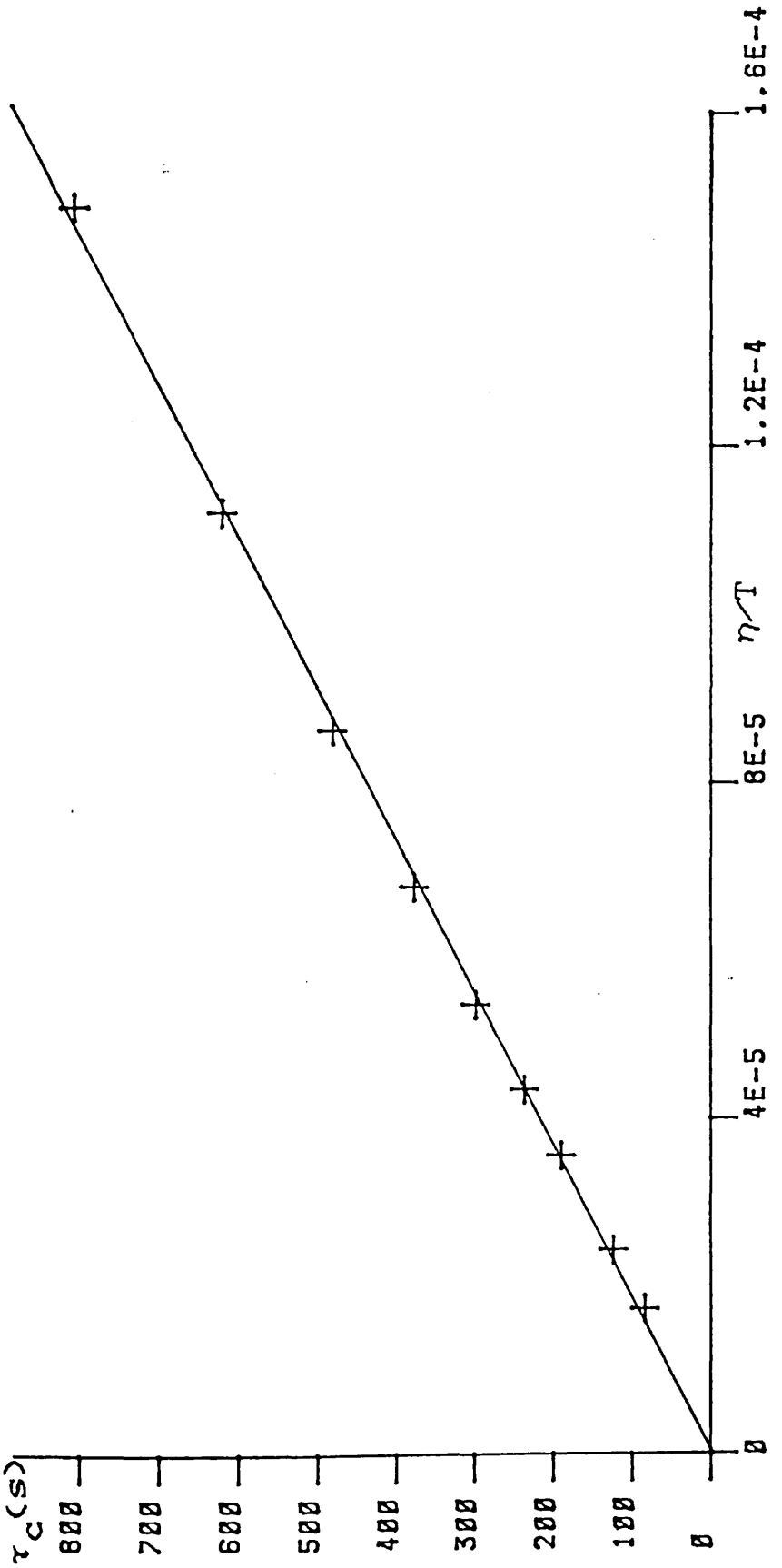

Figure (4-5) Plot of τ_c against η/T for $(CH_3)_2Tl^+$ in 60% sucrose/D_2O solution.

$$\text{Slope} = 5.57 \pm 0.06 \times 10^{-6}\ \text{N m}^{-2}\text{K}^{-1} \qquad (4-25)$$

$$\text{Intercept} = -6.5 \pm 3.7 \times 10^{-12}\text{s}. \qquad (4-26)$$

The good correlation of τ_c with $\eta/_T$ indicates that the cation appears to be monitoring the change in viscosity very efficiently thus providing further evidence of the ability of the cation to behave as an effective probe molecule.

If we apply the formalism given by equation (4 - 22), then the parameters (4 - 25) and (4 - 26) correspond to the values of C and τ_{fr} respectively. However this model treats the reorienting species as a sphere and thus has limited application in this case.

If we treat the cation as an ellipsoid in solution, then the model of Hu and Zwanzig[41] is appropriate. In this model, the molecules are regarded as being either prolate spheroids (cigar shaped, a = b < c) or oblate spheroids (pancake shaped a < b = c) which have an anisotropic reorientation. The particle does not drag along the solvent continuum during rotation, but is considered instead to be perfectly smooth, hence a symmetric top such as the dimethylthallium(III) cation is assumed to experience no torque for rotation about the symmetry axis.

The model is represented by the equation,

$$\tau_c = f \frac{4 \pi a^3 \eta}{3 k_b T} \qquad (4 - 27)$$

where f is a microviscosity factor and a is the longest semi-axis of the cation.

Hence from the slope of the plot of τ_c against η/T, we find that the effective hydrodynamic volume,

$$f \frac{4 \pi a^3}{3} = 77 \times 10^{-30} \text{ m}^3 \qquad (4 - 28)$$

Boeré and Kidd[50] have tabulated the microviscosity factor, f for both prolate and oblate spheroids in the stick and slip limit for a series of Hu and Zwanzig shape factors, ζ, where the shape factor is defined by the ratio of the minimum axis of the cation to the maximum axis.

The theory was applied by Forster[26] to the reorientation of the dimethylthallium(III) cation in D_2O. In this study the cation was defined by the dimensions (2a < 2b < 2c) of the smallest right angled box that would enclose the Van der Waals surface of the molecule and thus from the cation geometry and Van der Waals radii given in references (48) and (49), the radial semi axes of the cation (a < b < c) were calculated to be

$$a = 1.975 \times 10^{-10} \text{ m} \qquad (4 - 29)$$

$$b = 2.095 \times 10^{-10} \text{ m} \qquad (4 - 30)$$

$$c = 3.585 \times 10^{-10} \text{ m}. \qquad (4 - 31)$$

The frictional constant, which is given by

$$\zeta_{prolate} = (a + b)/2c, \qquad (4 - 32)$$

was thus calculated to be 0.567. Using this value, the microviscosity constants in both the stick and slip limits were calculated by interpolating between the values of the frictional constants and microviscosity constants given by Boeré and Kidd[50], and these were found to be,

$$f_{slip} = 0.075 \qquad (4 - 33)$$

$$f_{stick} = 0.43 \qquad (4 - 34)$$

By taking the radius of the prolate spheroid to be 3.585×10^{-10}m, and using the values of f_{SLIP} and f_{STICK}, given in equations (4 - 33) and (4 - 34), the parameter, $f\ 4\pi a^3/3$ is calculated as 83×10^{-30} m^3 in the stick limit and 15×10^{-30}m^3 in the slip limit.

Comparison of these values with that given by the plot of τ_c against η/T, (77×10^{-30}m^3), suggests that a stick type model is appropriate in this system.

4.2.11 ^{205}Tl R_2 behaviour.

Further information on the motional and relaxation behaviour of the dimethylthallium(III) cation may be obtained by an analysis of the ^{205}Tl R_2 behaviour.

The ^{205}Tl R_2, measured at 231.6MHz, is given as a function of temperature in table (4 - 3). These values

were checked by an analysis of the multiplet linewidth. The multiplet linewidths could not be singularly resolved as the ^{205}Tl resonance indicated a broad spectral envelope encompassing the ^{205}Tl septet. However individual linewidths were estimated using a computer program that simulates the bandshape of a septet of Lorentzians with a binomial intensity distribution, using a coupling constant $J(^{205}Tl - ^{1}H)$ of 403Hz.

It has been noted earlier, that at this field strength the CSA mechanism is dominant for the ^{205}Tl R_1 and is thus assumed to be dominant for the ^{205}Tl R_2. The equations for R_{1CSA} and R_{2CSA} are given in Chapter 2 as equations (2 - 41) and (2 - 42).

The proposed model for molecular motion must be consistent with both the R_1 and R_2 behaviour and therefore in this analysis, the ratio of R_2/R_1 is observed.

To calculate a theoretical curve for a Lorentzian spectral density function, the parameters obtained from the analysis of high field R_1 data using a single correlation time model were used to generate theoretical values for R_1 and R_2 as a function of temperature. The ratio R_2/R_1 is plotted against inverse temperature in figure (4 - 6), together with the ratio measured by experiment.

The ratio R_2/R_1 is observed to increase as the temperature is decreased. For the single correlation time model, this behaviour indicates that the condition

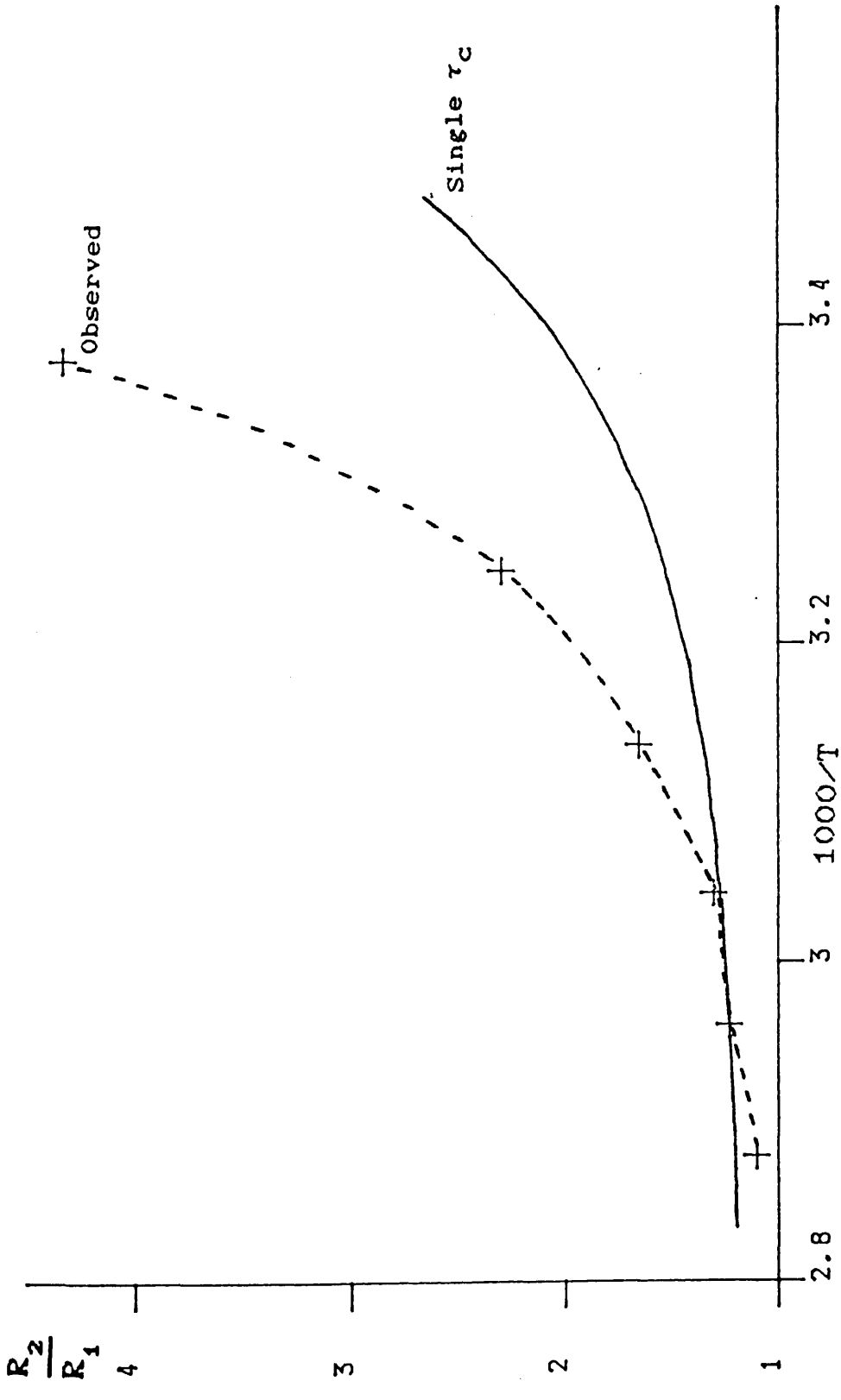

Figure (4-6) Observed R_2/R_1 temperature dependence compared with the predicted behaviour assuming a single correlation time model.

$\omega_0^2\tau_c^2 \geq 1$ holds. In this regime the R_1 becomes smaller with decreasing temperature due to a decrease in $J(\omega_0)$, whilst the R_2 becomes larger due to contributions from $J(0)$.

It is clear from figure (4 - 6) that the observed behaviour is not rationalised by the single correlation time model as R_2 appears to be much larger than expected, in comparison to R_1.

It is noted at this point that the scaled Lorentzian spectral density function discussed in section 4.2.9 gives the same R_2/R_1 ratio as the single correlation time model, and so clearly the R_2 behaviour is not consistent with this model either.

However, the observation of a significantly larger R_2 than expected is consistent with the behaviour shown by a system exhibiting a distribution of correlation times[51]. This effect is thought to arise from the inclusion of low frequency processes within the distribution.

Although we may rationalise the behaviour in a qualitative fashion, a quantitative approach is unfortunately not available to this study. This is because the spectral density given by the Fuoss-Kirkwood distribution, used to rationalise the R_1 data, contains an ω_0^{-1} term which does not allow for the calculation of the zero frequency spectral density function $J(0)$, important in the R_2 rate expression.

Section 4.3 Field dependent ^{13}C relaxation study on sucrose in 60% sucrose/D_2O solution.

4.3.1 Application of the Cole-Davidson distribution of correlation times model to other relaxation studies.

In later sections, it is noted that the Cole-Davidson distribution is successful in rationalising the ^{13}C R_1 data at both high and low field. The distribution has been applied in many other studies of solutions that show similar behaviour to the highly concentrated aqueous sucrose solution and thus it is of interest to discuss the results of these studies.

The Cole-Davidson distribution was originally formulated to account for the dielectric relaxation behaviour of glycerol and propylene glycol[36]. Glycerol was studied over the temperature range 198K to 233K and propylene glycol was studied in the range 183K to 228K. In this study the distribution width parameter was allowed to vary only slightly over the full temperature range and the limiting correlation time was assumed to vary in a manner given by the equation,

$$\tau_o = A \exp (B/(T-T\infty)). \qquad (4 - 35)$$

Where A and B are constants and $T\infty$ is a temperature near to the glass transition.

The distribution was later successfully applied to the deuteron NMR spin-lattice relaxation rates measured in liquid glycerol-d^4 over the pressure range 1bar to 8kbar from

148K to 263K[52] and the width parameter was found to be temperature and pressure independent within experimental error. The NMR correlation time was found to vary with temperature according to equation (4 - 35) and also to be in good agreement with correlation times derived from depolarised Rayleigh scattering[53] and dielectric relaxation experiments[54] on glycerol, where the Cole-Davidson distribution had also been successfully applied.

McDuffie and Litovitz[54] applied the distribution to the dielectric relaxation times measured in four associated liquids over the temperature range 253K to 283K. They found that the distribution width in glycerol, 1,3 butanediol and 2,4 methylpentanediol decreased with increase in temperature whilst the distribution width for the 1,2,6 hexanetriol was temperature independent. The NMR relaxation of these liquids was later studied by Favret and Meister[55]. In this study the T_1 and T_2 of each liquid was measured as a function of temperature between 233K and 313K at frequencies of 10 MHz and 20 MHz. These workers attempted to fit the derived correlation times in terms of a Cole-Davidson distribution but found that it was not possible without invoking a large variation in the width parameter β with temperature and concluded that the distribution was thus not appropriate.

Denney[56] applied the distribution to the dielectric relaxation of isobutyl bromide and isobutyl chloride

solutions at low temperature (100K to 273K). Hydrogen bonding is believed to be unimportant in these systems, but the anomolous relaxation behaviour was thought to occur as a result of short range intermolecular forces. Here the distribution width parameter was found to increase gradually with increasing temperature but not in a linear fashion.

The NMR spin-lattice relaxation of isoamyl bromide was studied by Roeder et al.[57] at 20 MHz and 60 MHz over the temperature range 113K to 300K and the results were explained by a Cole-Davidson distribution of correlation times with temperature dependent width parameter. The parameters obtained compared favourably with those reported by Denney[56] for the dielectric relaxation of isobutyl bromide. However the distribution provided a less satisfactory fit to the frequency dependent data in the T_1 minimum region, as the T_1 minimum was shifted by 7K to higher temperature on going from 20 MHz to 60 MHz and no explanation was offered for this behaviour.

In order to rationalise the application of the Cole-Davidson distribution, some workers have provided models for the motional behaviour that occurs in associated liquids. These are of general interest to the application of correlation time distributions and are pertinent to the aqueous sucrose system at high concentrations. Cole and Davidson[36] originally noted that the form of the distribution extends in the direction

of smaller times and cuts off the longer relaxation times at a limiting value. This would seem physically unreasonable to account for the reorientation of associated dipole groups of varying size, however this apparent anomally was rationalised by assuming that the reorientation of the dipole group is only made possible by the breaking of hydrogen bonds to the neighbouring groups, and this co-operative phenomena determines the dielectric relaxation.

McDuffie and Litovitz[54] proposed a model to account for a temperature dependent distribution of relaxation times. Here they assumed the cluster theory that was proposed by Schallamach[58] for mixtures of associated and non associated liquids, and extended this theory to the pure associated liquid. The liquid is thought to form into groups of dipoles of varying sizes dependent upon the associative forces, pressure and temperature, so that the relaxation now becomes a property of the group rather than the single dipole. These groups are continually making and breaking so that at one instant a molecule may belong to one group and at the next, another. This structural rearrangement is believed to occur as a co-operative phenomena throughout the region of association. Dielectric relaxation in these systems was explained by making the postulate that the reorientation of a dipole may only occur if the whole group, to which it is part, breaks up and that many structural break-ups occur before

the dipole becomes fully realigned. The non exponential break-up of these groups leads to a non exponential decay of polarisation which is interpreted as a distribution of relaxation times. The distribution parameters are thus a measure of the departure from exponential behaviour.

This theory was used to account for the temperature dependence of the distribution, by noting that if the distribution originates from the non exponential break-up of groups then it should be dependent on the group size. Therefore as the group size decreases with increasing temperature, the decay of polarisation will revert to a more exponential type behaviour and exhibit a smaller distribution of relaxation times.

Glarum[59] similarly rationalised observed relaxation data for isoamyl bromide by a Cole-Davidson distribution and provided an alternative model for the motional behaviour leading to a distribution of relaxation times. A defect diffusion model was proposed to explain the dielectric relaxation behaviour in this system. This model assumes that within the liquid system there are a number of defects, the motion of which is diffusional in character. When a defect reaches a dipole, the dipole relaxes completely and instantaneously. Immediately after a given dipole has relaxed the probability of a neighbouring dipole relaxing is greater than at any arbitrary time. This leads to a co-operative process in which the relaxation of a dipole is dependent on

neighbouring molecules.

The defect was interpreted in the simplest case to be a 'hole' which diffuses through the liquid structure and provides an increased volume to enable the dipole to reorient more easily.

4.3.2 Measurements.

In the preceding section, the dimethylthallium(III) cation in 60% sucrose / D_2O solution was found to exhibit motional behaviour that is very dependent upon the complex motional and associative behaviour of the sucrose molecules in the system. Thus as an extension to the work already carried out on this system, and to extend other NMR studies in aqueous sucrose solution[1,11-13] to higher sucrose concentration, it was proposed that the motion of the sucrose molecules be studied directly, as a function of temperature and NMR frequency. Thus the same sample was subjected to ^{13}C R_1 and nuclear Overhauser enhancement measurements at two frequencies (22.5 MHz and 100.6 MHz) and variable temperature. The eight ring carbons bearing single protons were studied, the assignment of which is well known[60], and the spectrum of which is shown in figure (4 - 7).

All relaxation measurements were made with full proton decoupling and nuclear Overhauser enhancements by the gated decoupling technique, described in section 3.4.6. The R_1 values for the eight carbon atoms were found to be the same within experimental error, in agreement with

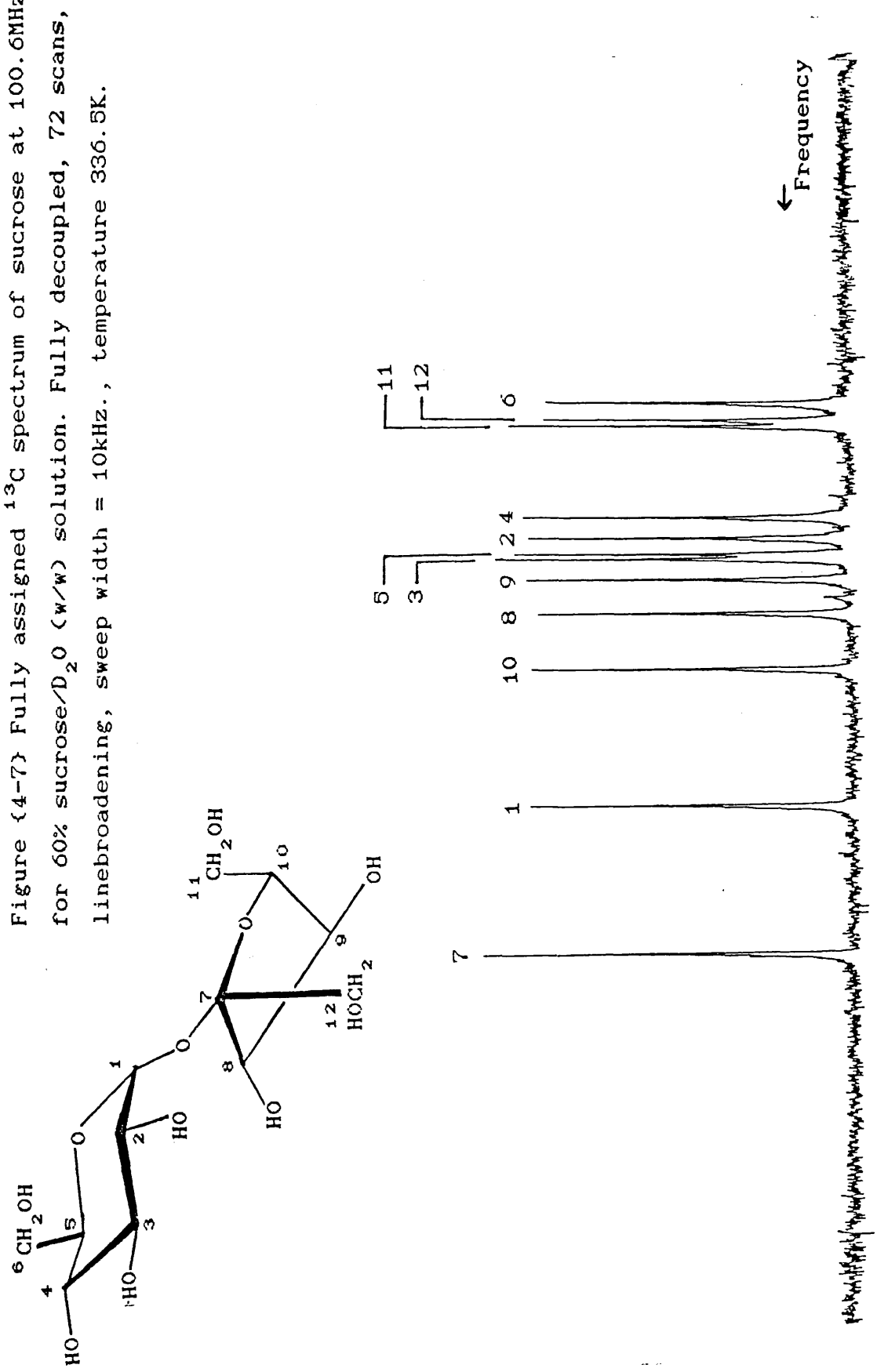

Figure (4-7) Fully assigned ^{13}C spectrum of sucrose at 100.6MHz, for 60% sucrose/D_2O (w/w) solution. Fully decoupled, 72 scans, no linebroadening, sweep width = 10kHz., temperature 336.5K.

other workers[12] and so the experimental accuracy was increased by averaging the relaxation rates for all eight carbon atoms at each temperature. The results obtained are given in tables (4 - 6) and (4 - 7).

Table (4 - 6) Temperature dependence of ^{13}C R_1 at 22.5MHz.

Temperature (K)	R_1 (s^{-1})
305.2	18.4
311.9	14.9
316.2	12.2
322.0	11.3
329.4	9.1
339.9	5.7
342.3	6.0
354.1	4.3

Table (4 - 7) Temperature dependence of ^{13}C R_1 at 100.6MHz.

Temperature (K)	R_1 (s^{-1})
304.4	4.35
308.9	4.60
315.3	4.79
321.3	4.58
327.7	4.43
336.5	3.67
344.9	3.56
356.0	2.92

The results are shown in figure (4 - 8). The points represent measured rates, and the best fit curves through the points are generated from the parameters given by the application of the Cole-Davidson distribution, discussed in section 4.3.5.

4.3.3 Discussion of results.

The temperature dependence of the ^{13}C R_1 values is non linear at high field, whilst the low field data show a linear Arrhenius behaviour. This pattern of behaviour is similar to that observed for the high and low field temperature dependence of the ^{205}Tl R_1 for the dimethylthallium(III) cation in the same system. The basis for this similarly lies in the dependence of the spectral density $J(\omega_0)$ upon the product $\omega_0^2\tau_c^2$ and is explained in section (2.2.1).

The dominant relaxation mechanism for the ring backbone ^{13}C nuclei in the sucrose molecule is thought to be the intramolecular dipole-dipole mechanism[1] and the reduced rates at high field are consistent with this and in contrast to the increased rates observed for the CSA mechanism in the ^{205}Tl relaxation.

4.3.4 Analysis of ^{13}C relaxation

To rationalise the ^{13}C relaxation rates, a similar approach to that used in the preceding section is made. Here a number of models are applied and the applicability of each model to describe the data is tested.

The general spin-lattice relaxation rate equation for

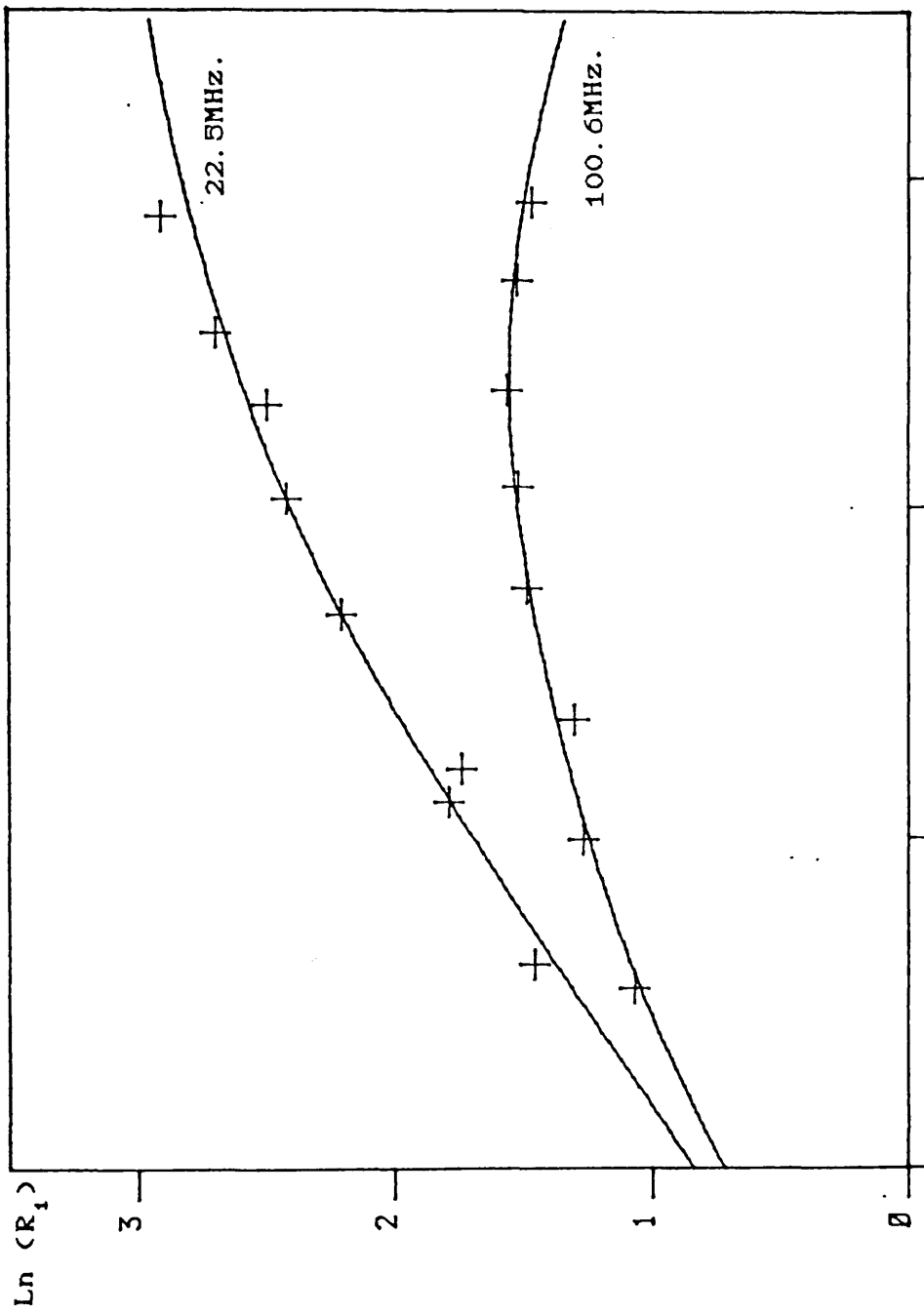

Figure (4-8) ^{13}C R_1 data at 22.5MHz. and 100.6MHz. fitted to a Cole-Davidson distribution model.

a ^{13}C nucleus coupled to N protons and solely relaxed by interaction with those protons is given by[59, 60]

$$R_{1\ DD} = \frac{N}{20}\left(\frac{\mu_0}{4\pi}\right)^2 \frac{\gamma_H^2\gamma_C^2\hbar^2}{r^6}\left[J(\omega_H-\omega_C) + 3J(\omega_C) + 6J(\omega_H+\omega_C)\right], \qquad (4-36)$$

where the symbols have their usual meaning.

The measurement of relaxation rates as a function of magnetic field strength provides a rigid test for the theoretical models we wish to test. If we assume that equation (4 - 36) correctly describes the observed behaviour, then a knowledge of the C - H bond length allows for a direct determination of the correlation time for a given relaxation rate at a specified magnetic field strength. Assuming the correlation time has an exponential temperature dependence, an Arrhenius type equation may be formulated as in equation (4 - 2). Thus a correlation time at any temperature may be calculated and a corresponding ^{13}C R_1 value at any field strength may be derived.

In the fitting procedure performed in this study the C - H bond length was fixed at 0.1110 nm which is the mean effective bond length calculated from neutron diffraction measurements[7, 8] and as used by McCain and Markley[6]. The parameters corresponding to the activation energy and correlation time at 298K were optimised in a fitting

procedure to give a simultaneous fit to the data at both fields. Figure (4 - 9) shows the fit obtained by using spectral densities calculated for the simplest model, invoking an exponential (BPP type) correlation function.

It is apparent that the simple model does not fully account for the relaxation rate behaviour at both high and low field and so it is necessary to propose a different model to account for a change in the spectral density $J(\omega_0)$.

4.3.5 The Cole-Davidson distribution of correlation times model.

The application of the Cole-Davidson distribution to the motion of sucrose molecules involves a modification of the intramolecular dipole-dipole relaxation rate equation to include the Cole-Davidson spectral density function. This function was introduced in section 4.2.8 and is given in equation (4 - 17).

The modified rate equation was used in a three parameter fitting procedure to rationalise the high and low field ^{13}C R_1 data. The three adjustable parameters used, were the limiting correlation time at 298K, $\tau_{lim(298)}$, the activation parameter E_{DD} and the distribution width parameter at 298K, $\beta_{(298)}$. The limiting correlation time was assumed to have an exponential temperature dependence and the distribution width parameter was assumed to vary with temperature according to the equation

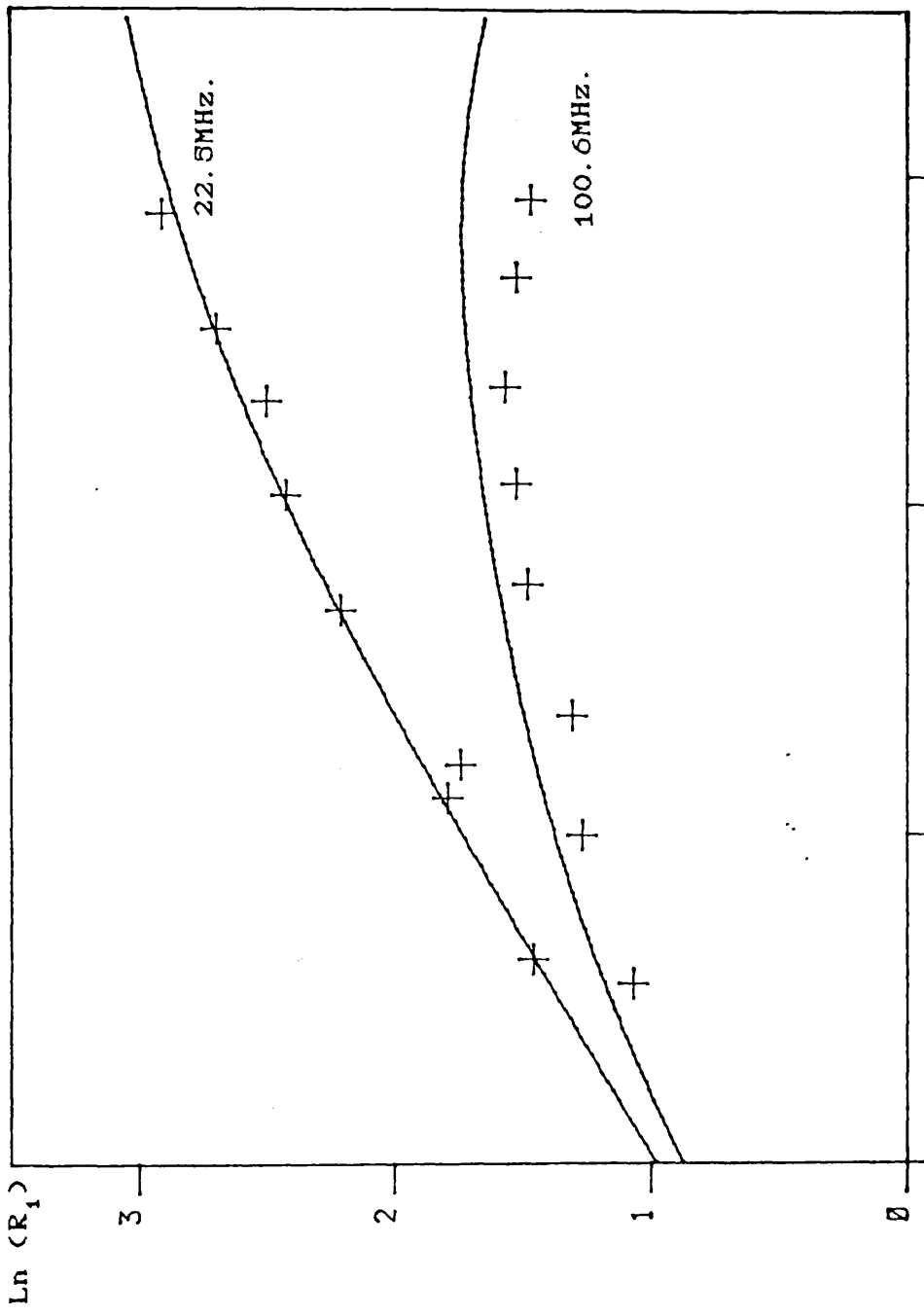

Figure (4-9) ^{13}C R_1 data at 22.5MHz. and 100.6MHz. fitted to a single correlation time model

$$\beta_{(T)} = \beta_{(298)} \times \frac{T}{298} \qquad (4 - 37)$$

The data were fitted satisfactorily by this procedure as shown in figure (4 - 8) and The best fit parameters obtained were,

$$\tau_{lim(298)} = 4189 \pm 560 \text{ ps} \qquad (4 - 38)$$

$$E_{DD} = 40.4 \pm 2.0 \text{ kJ mol}^{-1} \qquad (4 - 39)$$

$$\beta_{(298)} = 0.56 \pm 0.04 \qquad (4 - 40)$$

It is necessary to note the difference between the limiting correlation time τ_{lim} and the reorientational correlation time τ_c, which is the quantity of interest in this study. The value of τ_{lim} corresponds to the maximum correlation time exhibited by the molecule at each temperature and is not at the centre of gravity of the distribution and so the average correlation time at a given temperature T must be derived from the relation.

$$\tau_{c(T)} = \tau_{lim(T)} \times \beta_{(T)} \qquad (4 - 41)$$

Thus at 298K, $\tau_c = 2334 \pm 354$ps.

From the parameters given in equations (4 - 38) to (4 - 40), the value of the average reorientational correlation time may be derived at any temperature, and calculated values at selected temperatures are given in table (4 - 8).

Table (4 - 8) Reorientational Correlation times derived from the Cole-Davidson distribution

Temperature (K)	τ_c (ps)
293	3031
308	1419
323	715
338	384
353	217

This model will be further studied in conjunction with the ^{13}C nOe data presented in section 4.3.8.

4.3.6 Application of the scaled Lorentzian spectral density model.

Levy et al.[14] proposed a simple modification to the spectral density function that may be applicable in this situation. They noted by using molecular dynamics simulations that the correlation functions for the carbon atoms in proteins decayed initially by rapid atomic fluctuations, before the much slower, yet more significant, decay due to overall molecular tumbling. These fluctuations occur typically on a picosecond timescale and are caused by vibrations and other slight internal motions of atoms.

These motions alone cannot effect the complete decay of the correlation function and so they result in a reduction of the amplitude of $J(\omega)$ at the larmor frequency

ω_o.

The spectral density function is thus given by[14],

$$J(\omega_o) = \langle A(0)\ A(t_p)\rangle \frac{\tau_c}{(1 + \omega_o^2 \tau_c^2)} \quad (4 - 42)$$

where $\langle A(0)\ A(t_p)\rangle$ is the plateau amplitude of the correlation function after t_p seconds when the initial loss of correlation is complete. $\langle\ \rangle$ signifies a correlation time function.

This function may be thought of as the rigid molecule spectral density function multiplied by a constant S^2 that reflects the effects of vibrational averaging. The value of S^2 lies in the range 0 to 1 and as the averaging becomes more efficient, S^2 decreases.

This model was applied to modify equation (4 - 36) to include the constant S^2, and using this modified rate equation the ^{13}C R_1 values at both high and low field were simultaneously rationalised by a three parameter fitting procedure. The C - H bond length was fixed at 0.1110 nm. and the three adjustable parameters were the constant S^2, the activation energy E_{DD} and the correlation time at 298K, $\tau_c(298)$. The result of the fitting procedure is shown in figure (4 - 10) and the best fit parameters obtained are

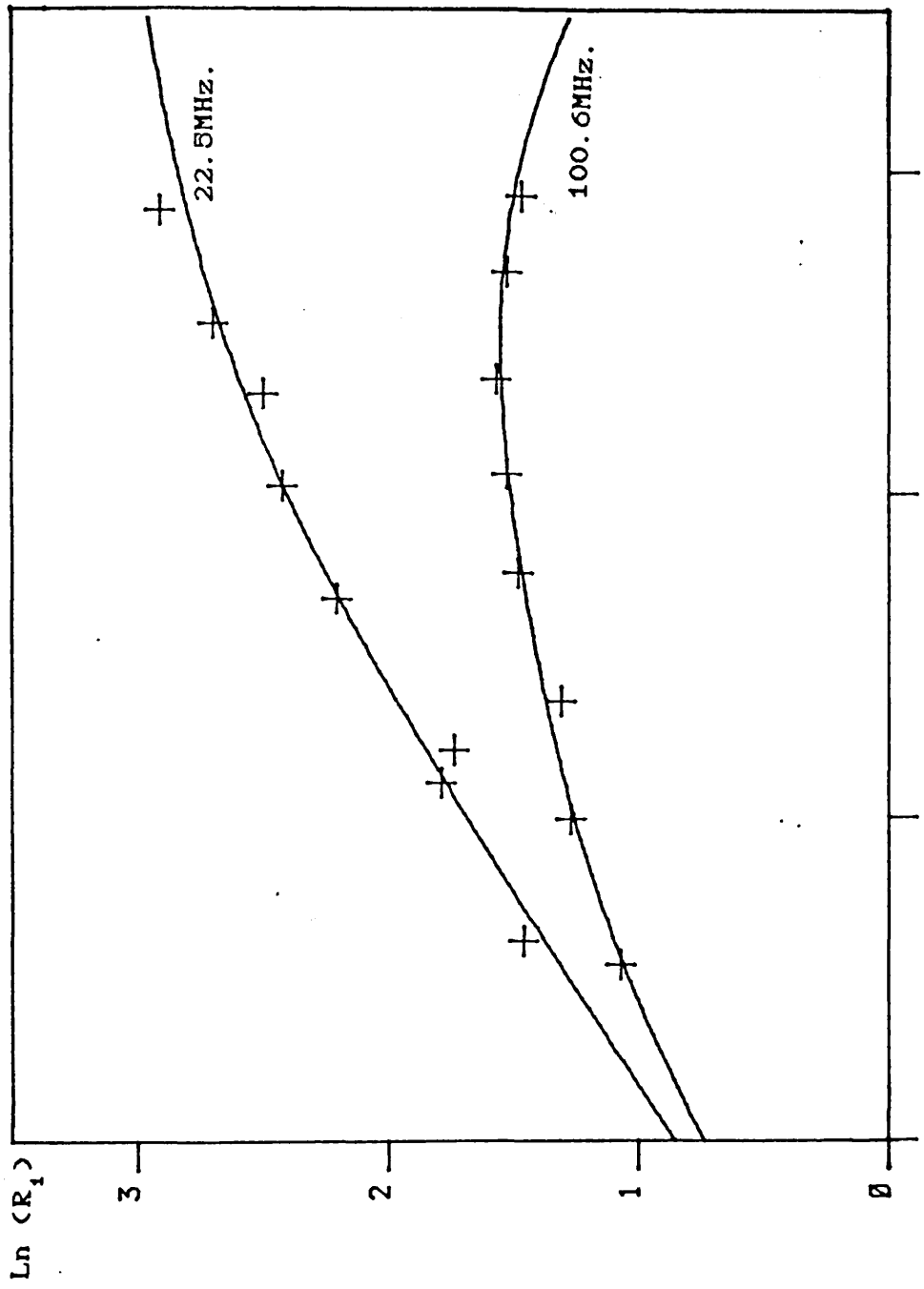

Figure (4-10) ^{13}C R_1 data at 22.5MHz. and 100.6MHz. fitted to a scaled Lorentzian spectral density model.

$$\tau_c(298) = 2524 \pm 225 \text{ ps} \qquad (4 - 43)$$

$$E_{DD} = 36.0 \pm 1.7 \text{ kJ mol}^{-1} \qquad (4 - 44)$$

$$S^2 = 0.83 \pm 0.02. \qquad (4 - 45)$$

It is noteworthy that the value of S^2 (0.83 ± 0.02) is in excellent agreement with that found by McCain and Markley[6] (0.89 ± 0.05) who as described earlier in section 4.1.1, studied a lower range of concentrations over a wider range of frequencies and similar range of temperatures. The model therefore appears to be applicable over a large range of concentrations and viscosities.

The literature suggests that whilst the sucrose molecules behave as single hydrates at ~ 26% concentration the behaviour in the 60% solution is considerably different and molecular association is apparent. Therefore the differing behaviour of the sucrose molecules over the concentration range provides a very exacting test of the applicability of the model and hence this model suggests that the effects of molecular association do not alter the ^{13}C relaxation behaviour.

It is of interest to note that the best fit parameters given by this model compare closely with those given by the fitting procedure using the Cole-Davidson distribution of correlation times model. Thus it would appear that although the models are founded upon vastly different theoretical bases, the information they give on the system is consistent.

The activation energy for the reorientation of the

sucrose molecule is similar to that observed for the reorientation of the dimethylthallium(III) cation in the same system and is also similar to the activation energy for η/T (36.8 ± 0.6kJ mol^{-1}). It would appear that the processes that are necessary to allow for the reorientation of the dimethylthallium(III) cation provide similar constraints for the sucrose reorientation. However, comparison of the respective reorientational correlation times at 298K clearly show that the larger, bulkier, sucrose molecule reorients at a rate that is ~ three times slower than that of the dimethylthallium(III) cation. This provides further evidence to suggest that no stable, long-lived thallium-sucrose complex is formed in this system.

From the parameters given in equations (4 -43) to (4 - 45), the reorientational correlation time given by this model may be calculated at any temperature and examples of these are given at selected temperatures in table (4 - 9)

Table (4- 9) Reorientational Correlation times derived from the scaled Lorentzian spectral density model.

Temperature (K)	τ_c (ps)
293	3232
308	1576
323	821
338	453
353	263

4.3.7 Application of the Fuoss-Kirkwood distribution of correlation times model.

In section (4.2.7), the Fuoss-Kirkwood distribution of correlation times was found to be a suitable model to fit the field dependent ^{205}Tl R_1 data for the dimethylthallium(III) cation in 60% sucrose / D_2O solution. It is therefore of interest to test the application of this model to describe the motional behaviour of the sucrose molecule in the same system.

The intramolecular dipole-dipole R_1 equation modified to include the distribution is given by[30],

$$R_{1\ DD} = \frac{N}{10}\left(\frac{\mu_o}{4\pi}\right)^2 \frac{\gamma_H^2\gamma_C^2\ h^2\ \beta\ \tau_R^{\beta}}{r^6}\left[\frac{(\omega_H - \omega_C)^{\beta-1}}{1 + (\omega_H - \omega_C)^{2\beta}\ \tau_R^{2\beta}}\right.$$

$$\left. + \frac{3\ \omega_c^{\beta-1}}{1 + (\omega_C\tau_R)^{2\beta}} + \frac{6(\omega_C + \omega_H)^{\beta-1}}{1 + (\omega_C + \omega_H)^{2\beta}\ \tau_R^{2\beta}}\right], \qquad (4 - 46)$$

where τ_R is the reorientational correlation time, and all other symbols have their usual meaning.

A non linear least squares fitting procedure was applied and assuming that the correlation time, τ_R has an exponential temperature dependence, the distribution could not account for the relaxation behaviour by assuming a single distribution width parameter or by assuming that the width parameter increased linearly with increase in temperature. Therefore, in contrast to the ^{205}Tl study, the symmetrical distribution of correlation times model was found to be inappropiate

4.3.8 Analysis of nOe data.

As mentioned earlier, additional nOe measurements were made as a function of temperature at two field strengths. The analysis of these results may give a further indication of the applicability of the models so far proposed to fit the field dependent ^{13}C R_1 data.

The analysis of nOe data for a single correlation time model has been discussed in section (3.4.7). In addition, the nOe is often a good indicator of the presence of a

distribution of correlation times[51], for example, in systems where a distribution is prevalent, the nOe may be considerably less than the maximum even though the condition $(\omega_0\tau_c)^2 << 1$ holds. Conversely, in situations where $(\omega_0\tau_c)^2 > 1$, a distribution of correlation times may result in a residual nOe of any value up to 50% of the maximum. However nOe factors close to the maximum may be observed, regardless of the distribution width, if the majority of the correlation times are within the extreme narrowing limit and therefore the observation of an nOe close to the maximum does not necessarily provide evidence for isotropic, single correlation time behaviour.

The expected nOe was calculated at frequencies of 22.5MHz and 100.6MHz at selected temperatures by applying the Cole-Davidson distribution to the full nOe expression given by equation (3 - 22) and using the parameters obtained from the R_1 analysis. The nOe values were also calculated at the same temperatures and frequencies using the scaled Lorentzian spectral density model (single correlation time), and similarly using the parameters obtained in the R_1 analysis. These values are compared to those observed by experiment, in tables (4 - 10) and (4 -11).

Table (4 - 10) Comparison of the nOe measured at 100.6MHz with the values predicted by the Cole-Davidson, and Lorentzian J(ω) models.

Temperature (K)	nOe Observed	nOe Cole-Davidson	nOe Lorentzian J(ω)
304	1.4	1.4	1.2
309	1.4	1.5	1.3
315	1.5	1.5	1.3
321	1.6	1.6	1.4
328	1.7	1.7	1.6
337	2.0	2.0	1.8
345	2.2	2.3	2.1

Table (4 - 11) Comparison of the nOe measured at 22.5MHz with the values predicted by the Cole-Davidson, and Lorentzian models.

Temperature (K)	nOe Observed	nOe Cole-Davidson	nOe Lorentzian J(ω)
304	2.1	2.0	1.9
308	2.0	2.2	2.1
316	2.3	2.5	2.4
321	2.7	2.6	2.6
327	2.9	2.7	2.7
335	2.8	2.8	2.8
354	2.9	2.9	2.9

The results suggest that both the Cole-Davidson and Lorentzian $J(\omega)$ models adequately describe the nOe data over the full range of $\omega_o\tau_c$ values and do not allow one to further differentiate between the two proposed models.

Section 4.4 ^{205}Tl relaxation studies on diethylthallium(III) nitrate in DMSO-d^6 and sucrose/DMSO-d^6 solutions.

4.4.1 Introduction

The studies on the dimethylthallium(III) cation as a probe for its molecular environment, described in the present work and in previous work,[26,27] have all involved aqueous solutions. Therefore it follows that it is of interest to study the ability of the higher alkylthallium cations to act as molecular probes for the study of less polar solvents in both low and highly viscous systems. The system chosen for study was the diethylthallium(III) nitrate in DMSO-d^6 system including a variation in sucrose concentration.

The addition of sucrose to DMSO-d^6 has the effect of raising the viscosity of the resulting solution and this increase is far greater than that resulting from the addition of sucrose to water. A comparison of the viscosities of sucrose/H_2O and sucrose/DMSO-d^6 solutions[61] given in table (4 - 12) clearly shows this difference.

Table (4 - 12) Viscosities of selected sucrose/H_2O and sucrose/DMSO solutions.

% sucrose in H_2O (w/w)	viscosity (x 10^3 N $m^{-2}s$)	% sucrose in DMSO (w/w)	Viscosity (x 10^3 N $m^{-2}s$)
20.00	1.695	20.57	12.08
39.00	4.803	38.78	211.40

Data taken from references (47) and (61)

Thus it is noticeable that if the molecular reorientational motion is slowed down in proportion to the macroscopic shear viscosity then the addition of a significantly smaller mass of sucrose to DMSO is required to slow down the motion of the cation to render it outside the extreme narrowing limit. Therefore on this basis the ^{205}Tl R_1 maxima are predicted to appear at lower concentrations of sucrose.

Thus there was the prospect of achieving R_1 maxima which would enable the analysis discussed in section (4 - 2) to initially test the applicability of the distribution of correlation times model in this system, and further to test the model over a range of sucrose concentrations.

4.4.2 Measurements.

Six solutions were prepared by adding weighed amounts of sucrose to weighed amounts of DMSO-d^6. A weighed amount of diethylthallium(III) nitrate was added to a $1cm^3$ sample of each solution so that the concentration was 0.3M in the

thallium salt (ie. assuming negligible volume change). The sucrose/DMSO-d^6 compositions were 0, 10%, 20%, 30%, 40% and 43% sucrose (w/w). The samples were degassed as described in section (3.2) and placed in 8mm sample tubes containing a capillary of 0.8M dimethylthallium(III) nitrate in D_2O for the purpose of temperature measurement.

^{205}Tl R_1 measurements were performed as a function of temperature at ^{205}Tl frequencies of 231.6 MHz and 21.96 MHz in the usual way. The results are given in table (4 - 13).

Table (4 - 13) ^{205}Tl R_1 Values for Diethylthallium(III) Nitrate in Sucrose/DMSO-d^6 Solutions (w/w%) at 21.96MHz and 231.6MHz.

a) Pure DMSO-d^6 Solution

Temperature (K)	$R_1^{(21.96)}$ (s^{-1})	Temperature (K)	$R_1^{(231.6)}$ (s^{-1})
302.9	7.5	303.3	743
313.1	6.4	312.7	607
323.6	4.6	321.9	469
333.7	4.0	330.2	393
344.1	3.6	338.9	335
		346.9	292

b) 10% Sucrose/DMSO-d^6 Solution

Temperature (K)	$R_1^{(21.96)}$ (s^{-1})	Temperature (K)	$R_1^{(231.6)}$ (s^{-1})
303.7	12.7	305.2	1133
312.2	10.3	313.8	913
323.0	8.0	322.4	746
333.8	7.0	330.4	621
344.1	5.8	338.3	522
354.4	4.6	346.1	440

c) 20% Sucrose/DMSO-d^6 Solution.

Temperature (K)	$R_1^{(21.96)}$ (s^{-1})	Temperature (K)	$R_1^{(231.6)}$ (s^{-1})
296.6	34.4	281.8	2091
301.4	29.0	285.9	2099
306.1	22.2	289.0	2072
312.4	17.2	291.8	2046
323.4	13.1	297.2	1901
334.5	10.2	313.5	1436
345.3	8.1	322.4	1185
355.5	5.8	331.1	958
		339.0	799

d) 30% Sucrose/DMSO-d^6 Solution.

Temperature (K)	$R_1^{(21.96)}$ (s^{-1})	Temperature (K)	$R_1^{(231.6)}$ (s^{-1})
300.0	67.5	291.9	1883
310.0	43.5	299.3	2045
321.3	28.3	300.7	2055
331.4	19.5	308.4	1990
341.7	13.6	317.2	1833
352.7	7.2	339.2	1344
		348.5	1101

e) 40% Sucrose/DMSO-d^6 Solution.

Temperature (K)	$R_1^{(21.96)}$ (s^{-1})	Temperature (K)	$R_1^{(231.6)}$ (s^{-1})
301.4	135	302.0	1292
311.5	102	310.4	1652
322.4	61.6	319.4	1909
		327.8	2021
		336.5	1979
		345.0	1816

f) 43% Sucrose/DMSO-d^6 Solution.

Temperature (K)	$R_1^{(21.96)}$ (s^{-1})	Temperature (K)	$R_1^{(231.6)}$ (s^{-1})
300.9	7.5	310.3	1893
312.1	6.4	318.3	1999
322.4	4.6	327.0	2161
333.4	4.0	336.0	2056
345.4	3.6	344.7	1888

These results are shown in figures (4 - 11) to (4 - 14). The points represent measured rates, and the lines in figures (4 - 13) and (4 - 14) are generated from the parameters given by applying a fitting procedure to the Fuoss-Kirkwood distribution of correlation times model, discussed later.

As before, the results obtained in each solution show a strong increase in ^{205}Tl R_1 as the frequency is increased from 21.96 MHz to 231.6 MHz. This indicates that the CSA mechanism is again important.

At ambient temperature, the ^{205}Tl R_1 at a frequency of 231.6 MHz is observed to increase with each successive increase in sucrose concentration up to the 40% solution, where a decrease is evident. There is further decrease in the 43% solution. This behaviour is consistent with the idea that the cation is monitoring the increase in viscosity in all solutions by a slowing down of the reorientational motion such that the R_1 maximum has been reached in this range of concentrations. The further reduction in rate confirms this assumption.

The temperature dependence of the R_1 at each sucrose concentration, shown in figures (4 - 13) and (4 - 14), reflects similar behaviour, where the viscosity change is caused by temperature variation.

At a ^{205}Tl frequency of 21.96 MHz, a linear Arrhenius temperature dependence of the ^{205}Tl R_1 is observed in solutions up to and including the 20% solution, indicating

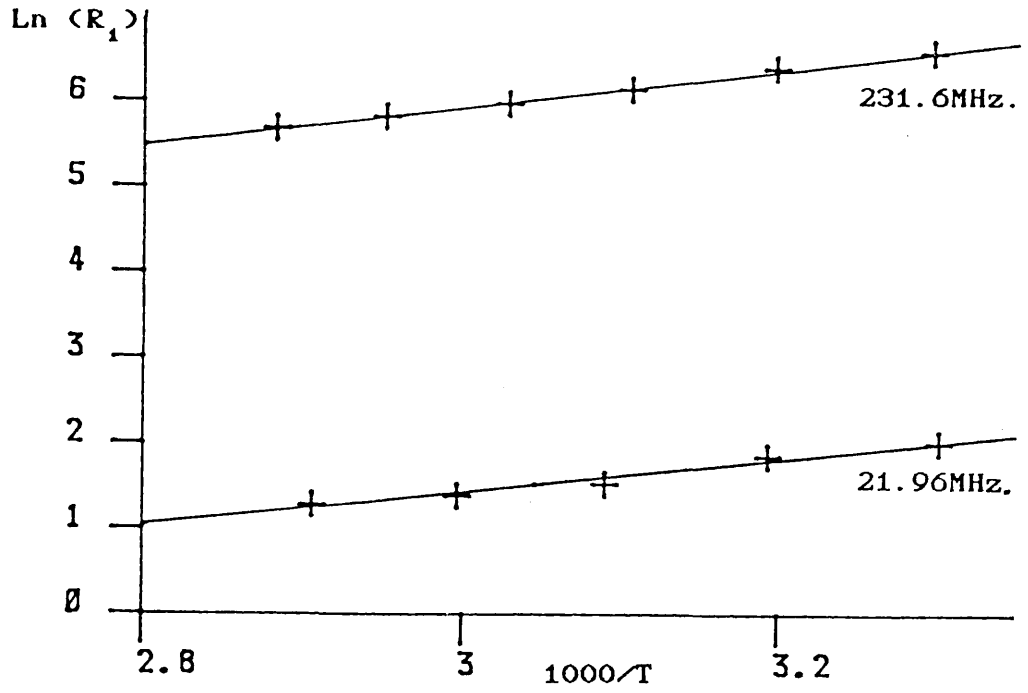

Figure (4-11) Temperature dependence of ^{205}Tl R_1 for $(C_2H_5)_2Tl^+$ in DMSO-d^6 at 21.96MHz. and 231.6MHz.

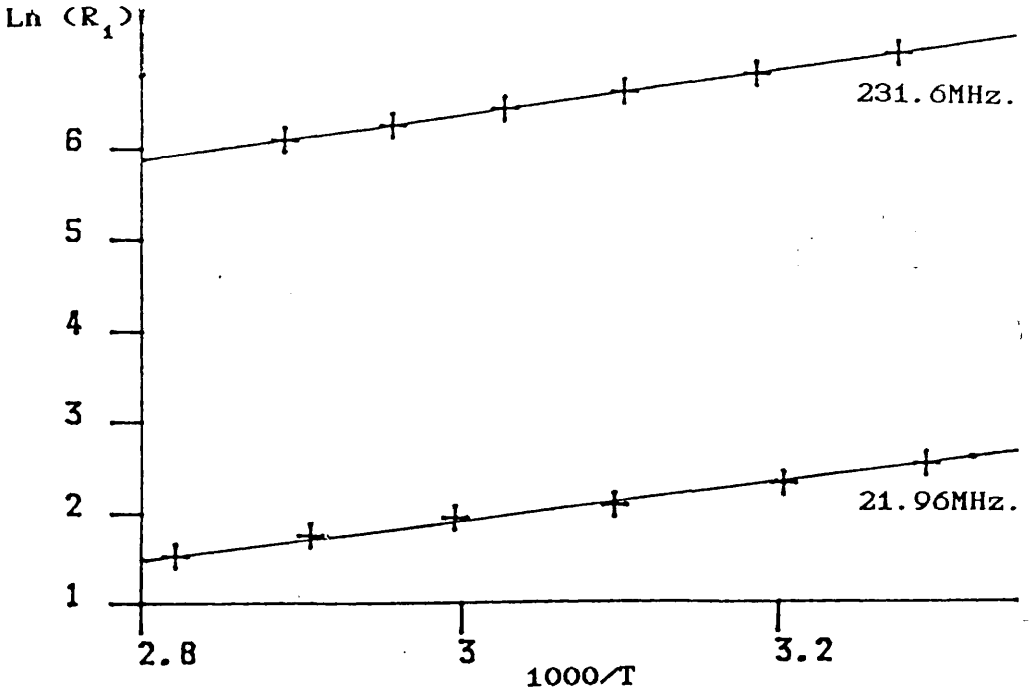

Figure (4-12) Temperature dependence of ^{205}Tl R_1 for $(C_2H_5)_2Tl^+$ in 10% sucrose/DMSO-d^6 solution at 21.96MHz. and 231.6MHz.

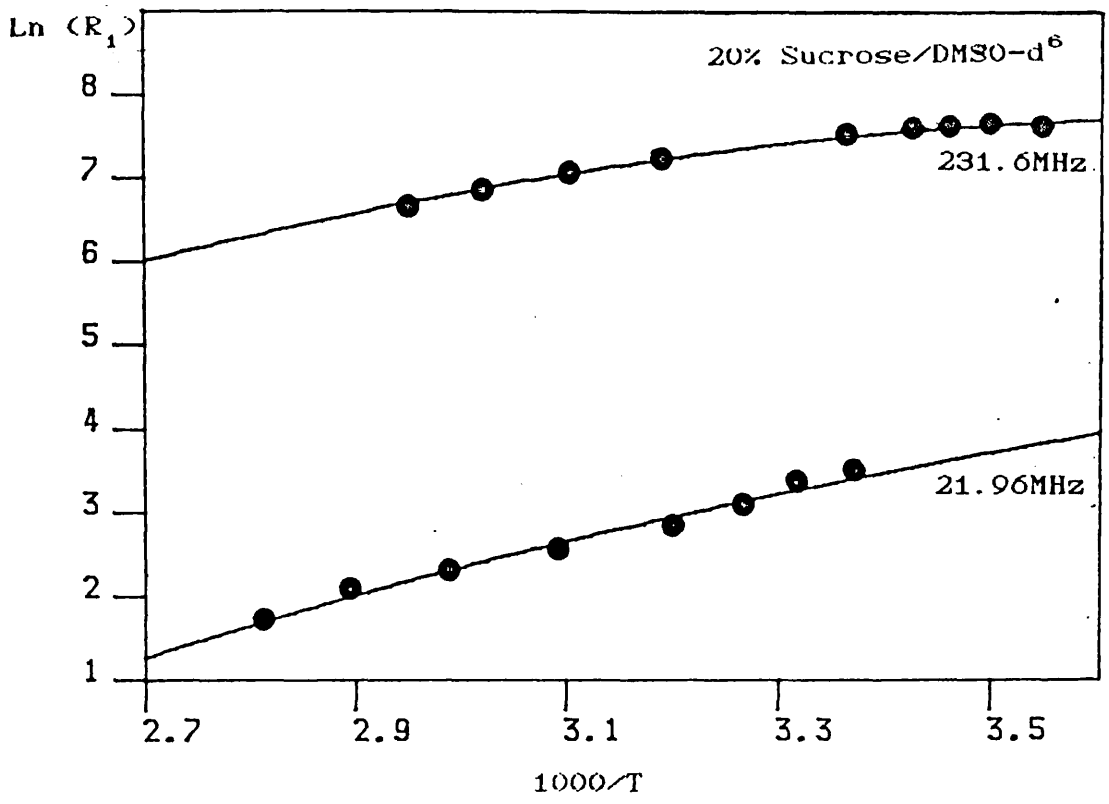

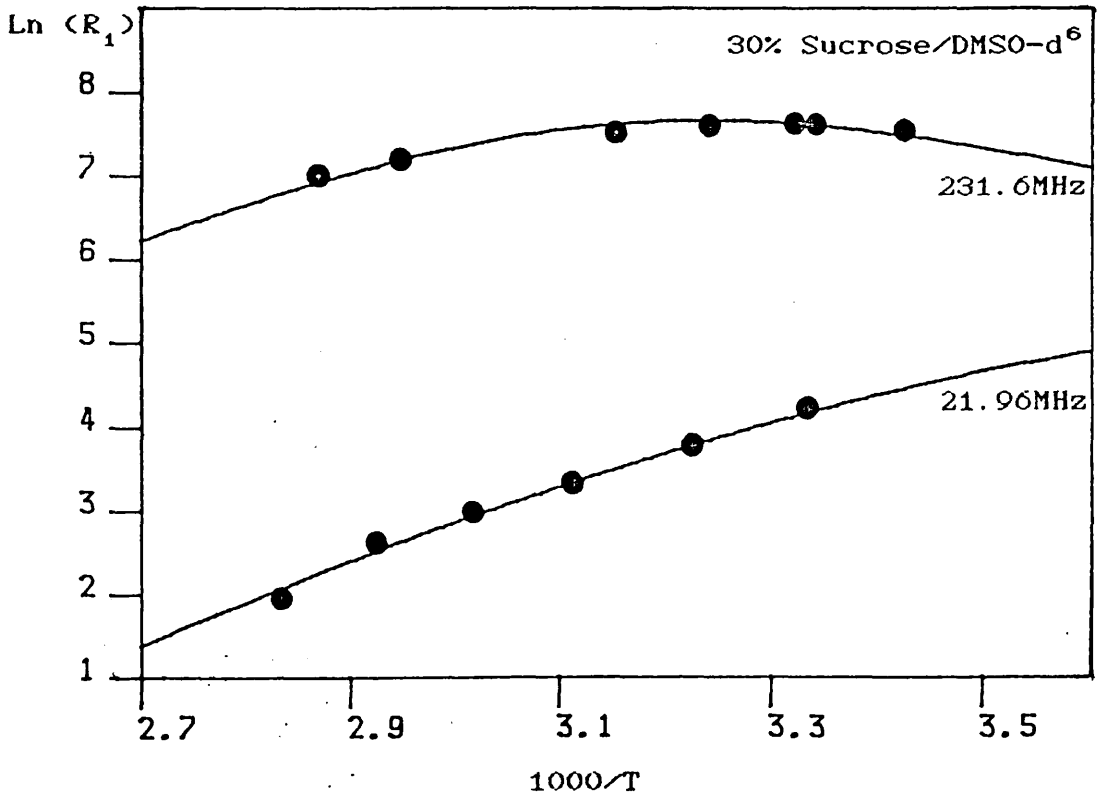

Figure (4-13) Fuoss-Kirkwood data fit to ^{205}Tl R_1 data for $(C_2H_5)_2Tl^+$ in 20% and 30% sucrose/DMSO-d^6 solution.

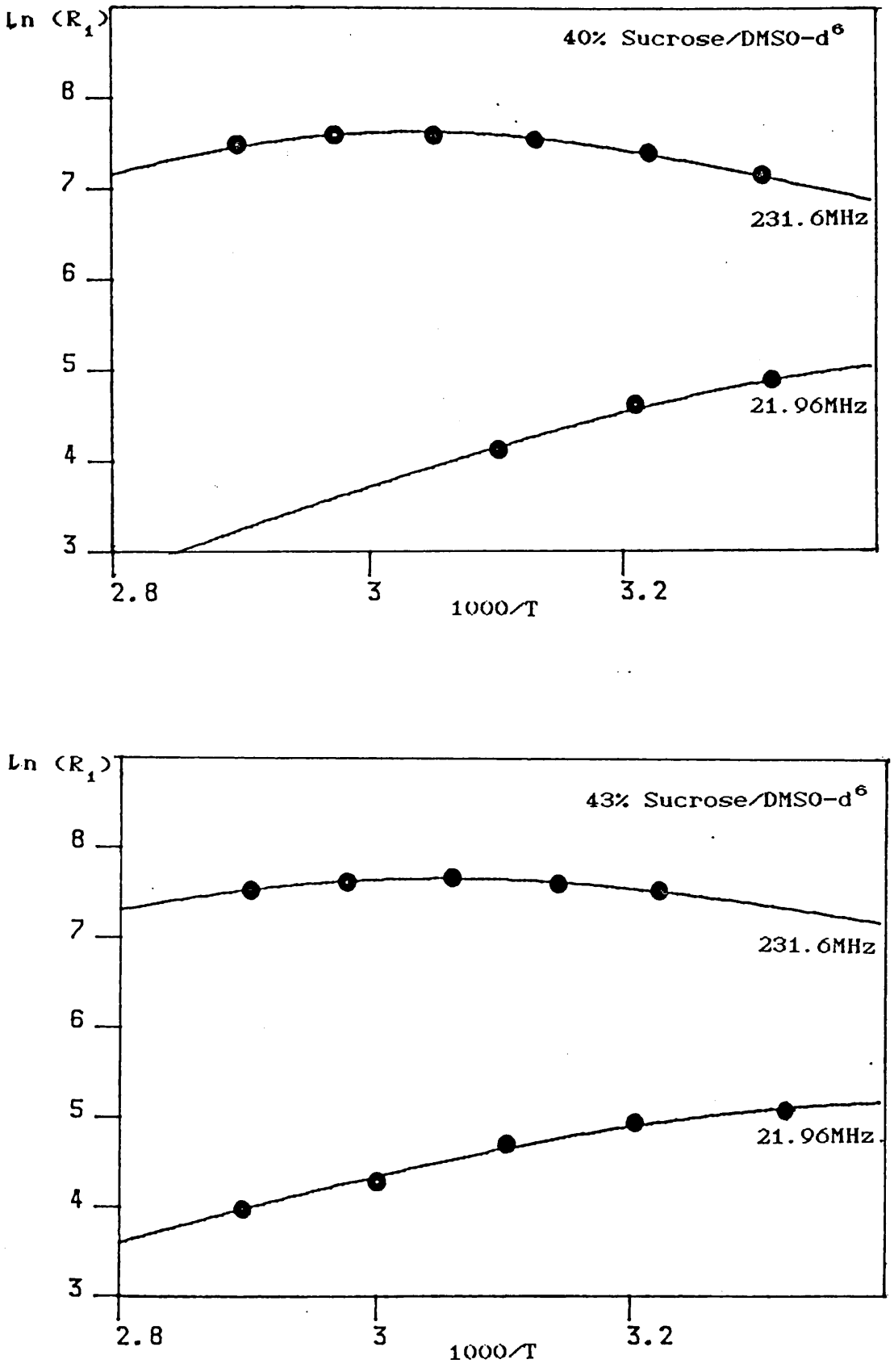

Figure (4-14) Fuoss-Kirkwood data fit to ^{205}Tl R_1 data for $(C_2H_5)_2Tl^+$ in 40% and 43% sucrose/DMSO-d^6 solution.

that the molecular motion is within the extreme narrowing limit. However, in the 30%, 40% and 43% solutions, slight curvature is observed in the plots at lower temperatures suggesting that, even at this low field strength, relaxation is in the dispersion regime in these solutions. At 231.6 MHz the increase in resonance frequency results in a larger value for $\omega_o^2\tau_c^2$ and hence an R_1 maximum is observed in each of these solutions. In the 20% solution at 231.6 MHz it was necessary to cool the sample to a lower temperature to observe an R_1 maximum.

4.4.3 Field dependent analysis of R_1 data.

The observation of ^{205}Tl R_1 maxima for the diethylthallium(III) cation in the 20%, 30%, 40%, and 43% solutions enables one to apply the analysis discussed in section 4.2.3, to the high field data, to calculate an anisotropy, correlation time at 298K and an activation parameter for the cation in each solution.

Starting with a single correlation time model the best fit parameters calculated are presented in table (4 - 14).

Table (4 - 14) Best fit parameters derived from the single correlation time model fit to the ^{205}Tl R_1 data measured in sucrose/DMSO-d^6 solutions

	0*	10%*
τ_{298}(ps)	106 ± 2	178 ± 1
E_a (kJ mol^{-1})	19.3 ± 0.6	20.1 ± 0.1

* See Section (4.4.5)

Table (4 - 14) Continued.

	20%	30%	40%	43%
$\Delta\sigma$ (ppm)	4653 ± 7	4574 ± 21	4576 ± 13	4678 ± 56
τ_{298}(ps)	434 ± 4	799 ± 33	2220 ± 48	1738 ± 27
E_a (kJ mol^{-1})	23.7 ±0.3	23.0 ±0.9	30.0 ±0.7	26 ± 4

The anisotropy of the diethylthallium(III) cation in each solution is noticeably lower than the anisotropy of the dimethylthallium(III) cation (5588 ± 173 ppm). The basic expectation is that the anisotropy for these two cations will be very similar and it is noted that the isotropic shifts differ by only 302ppm[61]. This gives an initial indication that the ^{205}Tl relaxation behaviour for the two organothallium cations in different sucrose/solvent systems may be similar even though the sucrose concentration in the DMSO-d^6 solvent is considerably lower.

Using the best fit parameters obtained for the diethylthallium(III) cation in each solution at high field, we can apply the scaling procedure outlined in section 4.2.4 to calculate the CSA contribution at low field. The results of this procedure apparently suggest that the CSA mechanism is not dominant at low field, and a residual rate is observed

A Tl-{^1H} nuclear Overhauser enhancement experiment at 21.96 MHz was performed on each solution at 294.6K and at 332.8K. This showed no enhancement of the thallium resonance and thus discounted any contribution from the dipole-dipole mechanism. The contribution of the scalar and spin-rotation mechanisms were similarly discounted by the arguments presented in section 4.2.5. Thus it appears that, in a similar fashion to the ^{205}Tl relaxation study on the dimethylthallium(III) cation in aqueous sucrose

solution, the relaxation behaviour must be accounted for by applying a more complex model for molecular reorientation. This is further evidence that the motional properties of organothallium cations in sucrose/solvent systems are strongly dependent on the properties of the sucrose, and of the solvent, rather than any intrinsic property of the cation itself.

4.4.4 Application of the Fuoss-Kirkwood distribution.

The success of applying the Fuoss-Kirkwood distribution of correlation times model to rationalise the frequency dependence of the ^{205}Tl relaxation rates for the dimethylthallium(III) cation in concentrated aqueous sucrose solution suggests that its use may be appropriate here.

The ^{205}Tl R_1 data obtained at both 231.6MHz and 21.96 MHz was therefore analysed using the procedure described earlier in section 4.2.7, based on equation (4 - 9) and using the same assumptions. The best fit parameters obtained are given in table (4 - 15).

Table (4 - 15) Best fit parameters derived from the application of the Fuoss-Kirkwood distribution to the ^{205}Tl R_1 data measured in the 20,30,40 and 43% solutions.

	20%	30%	40%	43%
$\Delta\sigma$ (ppm)	5685 ± 344	4980 ± 105	5057 ± 67	6231 ± 146
τ_{298} (ps)	235 ± 48	993 ± 85	3003 ± 171	3390 ± 391
E_a (kJ mol^{-1})	21 ± 1	32 ± 2	41 ± 2	49 ± 4
β_{298}	0.82 ±0.02	0.86 ±0.03	0.77 ±0.03	0.52 ±0.02

The range of sucrose concentrations studied allows one to observe the concentration effect on the distribution of correlation times model. If the complex motion of the diethylthallium(III) cation arises from the effects of molecular association or other effects associated with the high concentrations of sucrose molecules, then one would expect the deviation from the single correlation time model to be greater as the concentration is increased. This deviation is monitored by the β parameter corresponding to the width of the distribution. The prediction is that a larger β parameter (smaller distribution width) would be appropriate at lower sucrose concentrations. This behaviour is shown to an extent in table (4 - 15).

The anisotropies given by the fitting procedure are

all in turn increased to larger values than those predicted by a single correlation time model. However there are inconsistencies in the values reported for each solution, and so a single anisotropy may not be presumed.

The activation energy and reorientational correlation times reported in table (4 - 15) now appear to change progressively with increase in viscosity, in contrast to the erratic behaviour suggested in table (4 - 14). Thus the distribution of correlation times model provides a more satisfactory overall explanation of both the motional and relaxation behaviour in these systems.

4.4.5 ^{205}Tl relaxation in pure DMSO-d^6 solution and 10% sucrose solution.

To rationalise the ^{205}Tl R_1 data obtained in solutions that do not exhibit an R_1 maximum, it is necessary to estimate a value for the anisotropy of the cation. From the relaxation studies performed in sucrose/DMSO-d^6 solutions, several values for the anisotropy were determined and for the purpose of this study the average value of 5400ppm was taken.

With the CSA mechanism as the dominant contributor to the ^{205}Tl R_1 at high field, equation (4 - 1) may be used to derive reorientational correlation times for the cation from the measured ^{205}Tl R_1 at each temperature. Hence the correlation time at a reference temperature of 298K was found to be 106 ± 2ps for the pure DMSO-d^6 solution and 178 ± 1ps for the 10% sucrose solution.

The correlation time in pure DMSO-d^6 solution is significantly longer than that observed for the dimethylthallium(III) cation in pure D_2O solution, which was reported[26] to be 39ps. This difference may arise from the difference in solvent viscosity and also from the larger cation size.

Scaling these data to 21.96MHz shows agreement with the observed rates, in both solutions. Hence it appears that CSA provides the only significant relaxation mechanism and the single correlation time model is appropriate.

Section 4.5 ^{205}Tl relaxation studies on $Tl(I)^+$ ion in sucrose/D_2O solutions.

4.5.1 Introduction.

In the self-diffusion study presented in Chapter 5 it is noted that the ^{205}Tl nucleus has favourable spin properties that make it readily accessible to the study of self-diffusion by the pulsed field gradient spin-echo technique. As part of this work, the ^{205}Tl self-diffusion measurements are performed in aqueous sucrose solutions in order to study the application of ^{205}Tl cations to probe translational motion in viscous systems. The $Tl(I)^+$ ion is proposed as a probe cation for such work as it is a spherical species with favourably long relaxation times in aqueous solution. However the relaxation behaviour of the cation in aqueous sucrose solutions was unknown and therefore it was necessary to extend the study of thallium containing probe cations in sucrose/solvent systems to include $Tl(I)^+$ ion.

4.5.2 Measurements.

For the relaxation study, 0.246M solutions of $TlNO_3$ were made up in 10%, 30%, 45% and 60% sucrose/D_2O (w/w), degassed and sealed in 5mm NMR tubes. ^{205}Tl R_1 measurements were made as a function of temperature at a ^{205}Tl frequency of 21.89 MHz and temperatures were measured by observation of the ^{205}Tl chemical shift of a sample of dimethylthallium(III) nitrate (0.8M) in D_2O held in a concentric 8mm NMR tube. The results are presented in table (4 - 16).

Table (4 - 16) Temperature dependence of ^{205}Tl R_1 for $Tl(I)^+$ in sucrose/D_2O solutions at 21.89MHz.

a) No added sucrose

Temperature (K)	R_1 (s^{-1})
294.1	0.47
297.4	0.50
303.3	0.52
310.9	0.59
320.7	0.59
330.1	0.64
339.4	0.67

b) 10% sucrose/D_2O solution.

Temperature (K)	R_1 (s^{-1})
294.9	0.91
306.4	0.96
314.8	1.00
326.4	1.11

c) 30% sucrose/D_2O solution.

Temperature (K)	R_1 (s^{-1})
292.9	0.95
302.2	0.98
320.9	0.96
331.7	0.98

d) 45% sucrose/D_2O (w/w) solution.

Temperature (K)	R_1 (s^{-1})
294.1	0.83
308.4	0.74
316.2	0.70
324.9	0.63
333.5	0.61
346.1	0.54

e) 60% sucrose/D_2O (w/w) solution.

Temperature (K)	R_1 (s^{-1})
294.1	1.22
304.6	0.80
319.7	1.06
331.2	1.12
342.4	0.82

In addition to these results, preliminary studies on low concentrations of $TlNO_3$ (ca. 0.246M) in 45% and 60% sucrose/D_2O solutions indicated that the ^{205}Tl R_1 increases with decreasing $Tl(I)^+$ ion concentration. Furthermore, R_1 measurements performed at 21.89MHz and 230.8MHz on these solutions indicated an inverse field dependence in R_1. These results are presented in tables (4 - 17) and (4 -18)

Table (4 - 17) ^{205}Tl R_1 as a function of temperature for $Tl(I)^+$ (ca.0.246M) in 45% sucrose/D_2O (w/w) solution.

Temp. (K)	R_1 (21.89) (s^{-1})	Temp. (K)	R_1 (230.8) (s^{-1})
293.0	5.60	301.0	1.44
303.3	5.35	310.6	1.27
316.9	5.04	320.1	1.16
329.3	4.44	329.2	1.06
339.3	3.54	338.7	0.99

Table (4 - 18) ^{205}Tl R_1 as a function of temperature for $Tl(I)^+$ (ca.0.246M) in 60% sucrose/D_2O solution.

Temp. (K)	R_1 (21.89) (s^{-1})	Temp. (K)	R_1 (230.8) (s^{-1})
293.0	4.86	301.2	1.98
298.4	4.24	310.3	1.53
312.7	3.18	319.8	1.17
321.1	2.03	329.0	0.99
335.0	1.31	338.0	0.81

4.5.3 Discussion of results.

The results presented in table (4 - 16) show that after an initial increase in rate with the addition of sucrose, further addition has little effect on the observed total rate, but the temperature dependence of R_1 shows that there is a steady changeover from the spin-rotation mechanism to another mechanism. The ^{205}Tl R_1 in the pure aqueous $TlNO_3$ sample has a positive

temperature dependence and this behaviour is consistent with the dominance of the spin rotation mechanism.

The ^{205}Tl R_1 values measured in the aqueous sucrose solutions may be considered to comprise of additive rate contributions from each of the possible relaxation mechanisms. Each mechanism may contribute in varying degrees towards the residual non spin-rotation rate.

The temperature dependence of the spin-rotation mechanism is noted to be opposite to that of the other mechanisms and hence at high temperature the total rate will be dominated by spin-rotation whilst at low temperature the residual mechanism will provide the dominant contribution.

For a complete analysis of the ^{205}Tl relaxation behaviour, it is necessary to separate the contributions from each mechanism. This procedure is difficult as the contribution of the spin-rotation mechanism may not be assumed to be constant in each sucrose solution. This is because the increase in viscosity may result in a decrease in τ_{SR}, the spin-rotation correlation time and therefore reduce the efficiency of the mechanism. In addition the increase in sucrose concentration may increase the contribution of the residual rate mechanism so as to make it the dominant contributor to the total rate. However, it is possible to make some observations on the general nature of the mechanism(s) contributing to the total R_1.

The contribution of the Tl-H dipole-dipole mechanism

may be ascertained by a Tl-{^{1}H} nuclear Overhauser enhancement experiment. The nOe measurements were made on all samples at a ^{205}Tl frequency of 21.89 MHz and a temperature of 294.6K, the results are shown in table {4 - 19}.

Table {4 - 19} ^{205}Tl nOe factors at 21.89MHz for $TlNO_3$ in sucrose/D_2O solutions.

Sucrose concentration (% w/w)	Noe (η)
10%	0
30%	0
45%	0.09
60%	0.14

From the equation for the full possible nOe given by a A-{X} double resonance experiment, equation {3 - 22}, (Chapter 3), the maximum value for η may be calculated by assuming that the motional extreme narrowing limit applies, thus,

$$\eta_{MAX} = 0.8696 \qquad \{4 - 47\}$$

Therefore, if we assume at first, that this motional limit applies in the 45% and 60% sucrose solutions, then the contributions to the overall relaxation from the dipole-dipole mechanism are 10% and 16% in each solution respectively.

Outside the extreme narrowing limit, equation {3 - 22} predicts a lower nOe factor and so the calculated

contribution of the Tl-H dipole-dipole mechanism in each solution will be increased. The inverse field dependence quoted from the preliminary results mentioned earlier may suggest that the molecular motion is outside the extreme narrowing limit at high field. Additional approximate ^{205}Tl R_1 values for the $Tl(I)^+$ ion (0.246M) in all sucrose/D_2O solutions were measured by the T_1 null method at 51.7 MHz. Again an inverse field dependence was observed. Thus it would appear that at a frequency of 21.89 MHz the extreme narrowing condition may not apply, and on this assumption the contribution of the Tl-H dipolar mechanism is predicted to be higher than the 10% and 16% noted above.

However, as the correlation time for the reorientation of the $Tl(I)^+$ ion in either solution is unknown, quantitative values for the dipolar contribution may not be derived from equation (3-22).

Furthermore the Tl-H dipole-dipole contribution may not be separated into contributions from the inter and intramolecular mechanisms by the relaxation measurements performed in this study, and so the nature of the Tl-H dipolar interaction is similarly unknown.

The contribution from the scalar mechanism arising from chemical exchange, may be discounted as this would give rise to a temperature dependence in the ^{205}Tl linewidth, which was not observed.

The CSA contribution may also be discounted due to the

observed inverse field dependence of R_1.

Therefore the results suggest that the total R_1 is comprised of contributions from the spin-rotation and Tl-H dipolar mechanisms, though the extent of the contribution of each is unknown.

4.5.4 Estimate of ^{205}Tl spin-spin relaxation behaviour.

It is necessary to have an indication of any adverse spin-spin relaxation behaviour in these solutions, that may inhibit the use of the PGSE self-diffusion experiment in the study of $Tl(I)^+$ ions in the sucrose/D_2O system. An estimate of this behaviour is afforded by the observation of the ^{205}Tl linewidth which is inversely proportional to the ^{205}Tl T_2.

For the solutions studied in this section the linewidth was observed to be insensitive to changes in sucrose concentration and temperature and though not a true measure of the T_2, because of the additional broadening effects of temperature gradients and magnetic inhomogeneity, the invariant linewidth was consistent with the idea that the sucrose did not have a strong effect on the T_2 as predicted by the T_1 behaviour in these solutions. Thus on the basis of this observation the $Tl(I)^+$ ion appears to be a very appropriate probe molecule for the PGSE study of viscous sucrose solutions, and this property will be tested in practice in Chapter 5.

References for CHAPTER FOUR

1. A.Allerhand, D.Doddrell, and R.Komoroski, J.Chem.Phys., 55, 189 (1971).
2. A.Suggett and A.H.Clark, J.Solution Chem., 5, 1 (1976)
3. A.Suggett, S.Ablett and P.J.Lillford, J.Solution Chem., 5, 17 (1976)
4. A.Suggett, J.Solution Chem., 5, 33 (1976)
5. K.S.Cole and R.H.Cole, J.Chem.Phys., 9, 341 (1941)
6. D.C.McCain and J.L.Markley, J.Amer.Chem.Soc., 108, 4259 (1986)
7. G.M.Brown and H.A.Levy, Science, 141, 921 (1963)
8. G.M.Brown and H.A.Levy, Acta.Crystallogr.Sect B, 29, 790 (1973)
9. D.E.Woessner, J.Chem.Phys., 37, 647 (1962)
10. W.T.Huntress Jr., J.Chem.Phys., 48, 3524 (1968)
11. K.Bock and R.U.Lemieux, Carbohydr.Res., 100, 63 (1982)
12. D.C.McCain and J.L.Markley, Carbohydr.Res.,152, 73 (1986)
13. K.Bock, B.Meyer and M.Vignon, J.Magn.Reson., 38, 545, (1980)
14. R.M.Levy, M.Karplus and J.A.McCammon, J.Amer.Chem.Soc., 103, 994 (1981)
15. F.S.Schneider, D.Schliephake and A.Klimmek, Zucker, 17, 465 (1963)
16. L.A.Sapronova, A.B.Luk'yanov, V.S.Shterman, V.F.Andronov and G.I.Burkov, Sakh.Promst., 12, 24 (1983)
17. N.Tikhomiroff, Ind.Aliment.Agric.(Paris), 82, 755 (1965)
18. G.E.Walrafen, J.Chem.Phys., 44, 3726 (1966)
19. M.Mathlouthi, C.Luu and D.V.Luu, C.R. Acad.Sci.,

289, 81 (1979)

20. R.U.Lemieux and K.Bock, Jpn.J.Antibiot., xxxii suppl., S-163 (1979)
21. M.Mathlouthi and D.V.Luu, Carbohydr.Res., 81, 203 (1980)
22. M.Mathlouthi, C.Luu, D.V.Luu and A.M.Meffroy-Biget, Carbohydr.Res., 81, 213 (1980)
23. M.Mathlouthi, Carbohydr.Res., 91, 113 (1981)
24. P.J.Burke, R.W.Matthews, I.D.Cresshull and D.G.Gillies, J.C.S. Dalton, 132 (1981)
25. G.B.Deacon, J.H.S.Green and R.S.Nyholm, J.Chem.Soc., 3411 (1965)
26. M.Forster, Ph.D.Thesis, University of London (1984)
27. M.J.Forster and D.G.Gillies, Mol. Phys., in press.
28. R.M.Fuoss and J.G.Kirkwood, J.Amer.Chem.Soc., 63, 385 (1941)
29. T.M.Connor, Trans.Faraday.Soc., 60, 1574 (1964)
30. D.Ghesquiere, B.Ban and C.Chachaty, Macromolecules, 10, 743 (1977)
31. D.Ghesquiere and C.Chachaty, Macromolecules, 11, 246 (1978)
32. B.E.Read and G.Williams, Polymer, 2, 239 (1961).
33. K.R.Metz and J.F.Hinton, J.Magn.Reson., 53, 131 (1983)
34. D.G.Gillies, Unpublished Results.
35. D.W.Davidson and R.H.Cole, J.Chem.Phys., 18, 1417 (1950)
36. D.W.Davidson and R.H.Cole, J.Chem.Phys., 19, 1484 (1951)
37. P.Debye, Polar Molecules, Dover Publications
38. D.R.Bauer, J.I.Brauman and R.Pecora, J.Amer.Chem.Soc., 96, 6840 (1974)
39. J.Dote, D.Kivelson and R.N.Shwartz, J.Phys.Chem., 85, 2169 (1981)

40. A.Gierer and K.Wirtz, Z.Naturforch A, 8, 532 (1953)

41. C.Hu and R.Zwanzig, J.Chem.Phys., 60, 4354 (1974)

42. G.K.Youngren and A.Acrivos, J.Chem.Phys., 63, 3846 (1975)

43. N.Hill, Proc. R. Soc. London ser.B, 67, 149 (1954)

44. J.T.Hynes, R.Kapral and M.Weinberg, J.Chem.Phys., 61, 3256 (1977)

45. J.T.Hynes, R.Kapral and M.Weinberg, J.Chem.Phys., 69, 2725 (1978)

46. R.E.D.McClung and D.Kivelson, J.Chem.Phys., 49, 3380 (1968)

47. J.F.Swindells, C.F.Snyder, R.C.Hardy and P.E.Golden, Natn. Bur. Stand. Supp. to Circ. No. C440

48. Y.Lee and L.W.Reeves, Can. J. Chem., 53, 161 (1975).

49. A.Bondi, J. Chem. Phys., 68, 441 (1964).

50. R.J.Boeré and R.G.Kidd, Ann. Rep. NMR. Spectry., 13, 319 (1982).

51. F.Heatley, Prog. Nucl. Magn. Reson. Spectrosc., 13, 47 (1979).

52. M.Wolfe and J.Jonas, J. Chem. Phys., 71, 3252 (1979).

53. H.A.Posch, H.D.Darby and T.A.Litovitz, Ber. Bunsenges. Phys. Chem., 81, 744 (1977).

54. G.E.McDuffie and T.A.Litovitz, J. Chem. Phys., 37, 1699 (1962).

55. A.G.Favret and R.Meister, J. Chem. Phys., 41, 1011 (1964).

56. D.J.Denney, J. Chem. Phys., 27, 259 (1957).

57. S.B.W.Roeder, E.O.Stejskal and W.E.Vaughan, J. Chem. Phys., 43, 1317 (1965).

58. A.Schallamach, Trans. Faraday. Soc., 42, 180 (1946).

59. S.Glarum, J. Chem. Phys., 33, 639 (1960).

60. P.E.Pfeffer, K.M.Valentine and F.W.Parrish, J. Amer. Chem. Soc., 101, 1265 (1979).

61. P.G.Sears, W.P.Siegfried and D.E.Sands, J. Chem. Engng. Data, 9, 263 (1964).

CHAPTER FIVE SELF-DIFFUSION STUDIES OF THALLIUM CATIONS IN D_2O AND SUCROSE/ D_2O SOLUTIONS.

Section 5.1 Measurement of diffusion by NMR techniques.

Hahn[1] noted, as early as 1950 a shortening of the nuclear spin-spin relaxation time T_2 caused by magnetic field inhomogeneity. This effect was also noted by Carr and Purcell[2] and their subsequent analysis formed the basis of NMR field gradient spin-echo methods for measuring self-diffusion coefficients.

There are two basic experiments, the Steady Gradient Spin Echo(SGSE) and the pulsed field gradient variation of this (PGSE). The experimental implementation of the latter has already been discussed in section (3 - 5) and for convenience the equation for the echo attenuation, is reproduced here.

$$M_y(2\Delta) = M_y(0) \exp\left[- \frac{2\Delta}{T_2} - \gamma^2 G^2 D \delta^2 (\Delta - \frac{\delta}{3}) \right], \quad (5 - 1)$$

where all the symbols have their usual meaning.

The limiting factor of any field gradient spin echo experiment is the T_2 of the nucleus under study. The echo attenuation due to natural T_2 processes, always competes with the echo attenuation due to diffusion in the presence of a field gradient. The measurement of self-diffusion coefficients becomes increasingly difficult in highly

viscous solutions where diffusional motion is slow, the T_2 is often short and the echo attenuation due to diffusion is very small. Therefore many variations of the PGSE sequence have been suggested to extend the self-diffusion experiment to these systems. In addition the PGSE experiment has also been modified to provide self-diffusion measurements in systems where particular experimental problems apply.

The use of three-pulse sequences offers particular advantages in specialised cases. Boss et al.[3] described a sequence in which the the usual PGSE sequence is preceded by a 180^{o} pulse. This has application in multicomponent systems where each component may not be singularly resolved. The 180^{o} pulse inverts the populations before the application of the PGSE sequence. This has a different effect on the components with different T_1 values. If the 180^{o} pulse is applied at a time, t before the first 90^{o} pulse, it can be arranged that $t = T_1 \ln 2$ for one component of the mixture and hence the signal from that component will be suppressed completely and self-diffusion experiments may then be performed on the remaining components of the mixture. This technique was successfully used[3] to measure the self-diffusion coefficient of benzene in a mixture with polyisobutylene by suppressing the contribution of the polymer to the echo.

The stimulated echoes arising from a simple three pulse sequence have also found specialised application in

the measurement of self-diffusion coefficients. The stimulated echo was first identified by Hahn[1] and later quantified by Woessner[4] for echo attenuation in a steady field gradient experiment. This was then extended to the pulsed field gradient technique by Tanner[5,6].

Observation of the stimulated echo rather than the normal spin echo makes the echo attenuation dependent upon T_1 rather than T_2. The advantage this offers is apparent in systems where $T_1 >> T_2$. This situation may arise in various different ways[6]. In highly viscous liquids, where the motion associated with spin relaxation is outside the the extreme narrowing limit, the T_1 passes through a minimum and becomes longer as T_2 is progressively shortened. Similar differences in T_1 and T_2 may also occur when chemical exchange is prevalent, or when the T_2 is shortened by a scalar coupling to a fast relaxing quadrupolar nucleus.

In addition to the advantages the technique affords in the above systems it also has application in situations where the diffusion is dependent on the length of time that the nucleus is left to diffuse, since by the use of this technique, the diffusion timescale may be extended to longer times.

The sequence involves a $90^{o}-\tau_1-90^{o}-\tau_2-90^{o}-\tau_3$ pulse train. The first pulse allows the spins to precess in the x'y' plane of the rotating frame in the presence of a field gradient. The spins are then turned through 90^{o} to

the longitudinal axis where the spin phase memory is stored. Here the spins are unaffected by the field gradient and relax via T_1 processes. Finally a third, read pulse is then applied and the spins converge to form an echo at a time $\tau_3 = \tau_1 + \tau_2$. If a pulsed field gradient G is applied between the first and third 90^o radiofrequency pulses, then according to Tanner[5,6].

$$\ln\left[\frac{M(\tau_3)}{M(0)}\right] = -\frac{(\tau_2-\tau_1)}{T_1} - 2\frac{\tau_1}{T_2} - \ln 2 - (\gamma G\delta)^2 D\,(\Delta - \delta/3), \qquad (5-2)$$

where $M(\tau_3)$ is the intensity of the stimulated echo and $M(0)$ is the intensity of the initial magnetisation. All other terms have their usual meaning.

The properties of multiple quantum spin echoes have also found relevant application to the measurement of self-diffusion coefficients for special cases. Several groups have noted[7,8,9] that in the rotating frame, the precession rates of nuclear magnetic multiple quantum coherences increase linearly with the order of the coherence. Hence for an N quantum coherence, the effective field gradient at the nucleus is multiplied by N times. This allows for the use of smaller field gradients in the study of systems characterised by very short T_2 values and slow diffusional motion. In addition, for N coupled protons the N^{th} quantum coherence is free from dipolar

couplings and hence the spectra are simpler and better resolved than the single quantum spectra. This offers particular advantages to the study of oriented molecules.

The application of multiple quantum spin echoes to the measurement of self-diffusion coefficients was first suggested by Bodenhausen et al.[10] and used in later studies to determine self diffusion coefficients in liquid crystals[11,12], where a simple modification to the Stejskal-Tanner pulsed field gradient experiment allowed for the generation and detection of multiple quantum spin echoes. At present the method has only been tested and no routine application has been made.

5.1.1 Diffusion coefficients from NMR relaxation times.

In many systems diffusion coefficients may be derived from the measurement of T_1 and T_2. For this method it is necessary that the total relaxation rate receives a contribution from the intermolecular dipole-dipole relaxation mechanism. The mechanism arises in part from the modulation of the dipole-dipole interaction by translational diffusion and a quantitative treatment of this process has been discussed by Torrey[13] and Abragam[14].

In the simplest form the intermolecular dipole-dipole relaxation rate R_{1DD}, for heteronuclear spins in the motional extreme narrowing limit is given by the relation,

$$R_{1DD} = \left(\frac{\mu_0}{4\pi} \right)^2 \frac{2}{15} \frac{N_x \gamma_A^2 \gamma_x^2 h^2}{D a} \qquad (5 - 3)$$

where, N_x is the concentration of x spins, a is the distance of closest approach and D is the mutual diffusion coefficient of molecules containing spins A and X.

Clearly the diffusion coefficient measured by this technique is not the self-diffusion coefficient of a single molecule but rather a mutual diffusion coefficient reflecting the translational motion of the two interacting spins. However as NMR relaxation measurements are the subject of detailed discussion in this thesis it is of interest to note this relationship.

The intermolecular dipole-dipole mechanism often contributes to the relaxation of protons in solution and is also relevant in paramagnetic systems, where it contributes to the electron-nuclear dipole-dipole relaxation that is often efficient in such systems.

However the method is based upon theoretical models and before the diffusion coefficient may be calculated, the mechanism of interest must be separated from all other contributions to the total relaxation rate. In addition it is often very difficult to separate contributions from each species in a multicomponent system. In contrast, field gradient techniques give direct measurement of the self-diffusion coefficient without assuming a theoretical framework.

The diffusion coefficient derived from nuclear spin

relaxation times relates to the measurement of diffusion on a much shorter timescale than the coefficients derived from PGSE techniques. For nuclear spin relaxation, the molecular motion is monitored on the timescale of the reorientational correlation time, which is typically in the order of several picoseconds in non viscous liquids. This is compared with the millisecond/second timescale over which the typical PGSE experiment monitors diffusion. This difference in timescale is not negligible in studies of the diffusion of large macromolecules and the errors arising from the measurement of self-diffusion coefficients over inadequate timescales are discussed in Chapter2.

Section 5.2 ^{1}H self-diffusion measurements on the dimethylthallium(III) cation in D_2O

5.2.1 Measurements.

Self-diffusion measurements were made on a sample of 0.8M dimethylthallium(III) nitrate in D_2O which had been sealed in a 5mm NMR tube. The measurements were made as a function of temperature using the PGSE technique and temperature measurement was made by substituting a sample of methanol or ethylene glycol as described in section (3.3.5). The measured self-diffusion coefficients for the dimethylthallium(III) cation in liquid D_2O are presented in table (5 - 1).

Table (5 - 1) D as a function of temperature for $(CH_3)_2Tl^+$ in D_2O

Temperature (K)	D x $10^{10} m^2 s^{-1}$
300.9	6.13
306.1	6.55
313.1	8.20
321.6	10.5
330.4	11.1
335.9	13.4
347.5	16.9
353.5	18.3

Overall error in the measured value of D is ± 3.8%

A plot of ln(D) against 1/T is shown in figure (5 - 1). The linear plot indicates that the behaviour may be described by the following equation,

$$D(T) = D_{298} \exp\left[\frac{E_a}{R}\left(\frac{1}{298} - \frac{1}{T}\right)\right] \qquad (5 - 4)$$

where D_{298} is the self-diffusion coefficient at 298K in $m^2 s^{-1}$, E_a is the activation energy for the diffusion process in kJ mol^{-1}, and T is the temperature in Kelvin.

A non-linear, least squares fitting procedure was applied to fit the data to equation (5 - 4) and this gave the best fit estimates for the parameters,

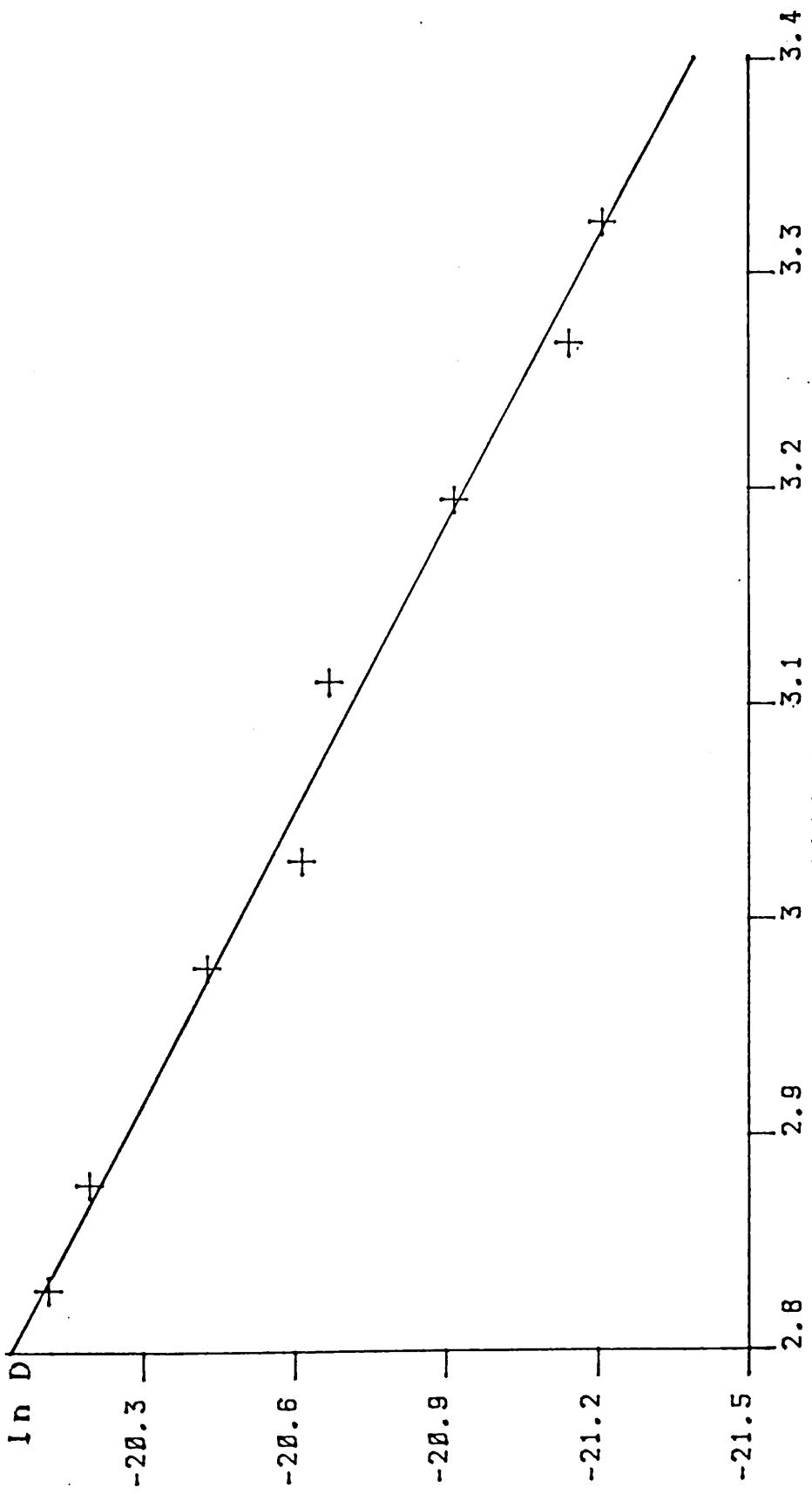

Figure (5-1) Plot of Ln D against 1000/T for $(CH_3)_2Tl^+$ in D_2O.

$$D_{298} = 5.6 \pm 0.2 \times 10^{-10} m^2 s^{-1} \qquad (5-5)$$

$$E_a = 18.8 \pm 0.8 \text{ kJ mol}^{-1}. \qquad (5-6)$$

5.2.2 Diffusion and molecular motion.

The activation energy for the self-diffusion of the dimethylthallium(III) cation in D_2O is the same, within experimental error, as the energy for the reorientational motion of the cation derived from ^{205}Tl spin-lattice relaxation measurements[15], reported to be 19.6 ± 0.6 kJ mol^{-1}. Similarly from the reported viscosity data for D_2O over the temperature range 278K to 398K [16] the activation energy for η/T is calculated to be 18.7 kJ mol^{-1}. Thus on the basis of this evidence it appears that each of these properties is controlled by a common kinetic process.

Forster[15] discussed the reorientational motion of the dimethylthallium(III) cation in D_2O in terms of a structure limited model. In this model the reorientation was assumed to proceed through a series of large angle jumps that are initiated by the break up of the solvent hydrogen bonded structure. This model is consistent in its interpretation with other models proposed to account for molecular transport processes in liquid H_2O and D_2O.

O Reilly[17] used a structure limited large angle jump model to discuss the temperature dependence of the viscosity, self-diffusion coefficient and relaxation times in H_2O and D_2O.

Other workers[18,19] have rationalised similar data by invoking a theory to suggest that each of these processes involves the break up of clusters of hydrogen bonded molecules of water. Similarly molecular dynamics studies[20,21,22] on the self-diffusion and reorientation of water molecules in liquid H_2O have been discussed on the basis of this type of model.

In the molecular dynamics study reported by Rahman and Stillinger[21] the occasional large angle jump model was not found to be appropriate, but instead, the self-diffusion of water molecules was thought to proceed in a random manner through a force field arising from a constantly changing network of hydrogen bonds.

The overall interpretation of molecular transport as being controlled by the break up of hydrogen bonds is a consistent theme in all work and thus on the basis of this evidence it is assumed that the self-diffusion of the dimethylthallium(III) cation in D_2O proceeds via this mechanism.

5.2.3 Application of hydrodynamic theory.

The magnitude of the self-diffusion coefficient is given by the Einstein equation,

$$D = \frac{k_b T}{f} \quad , \qquad (5-7)$$

where f is a frictional constant.

For a sphere of radius a moving in a continuous medium of shear viscosity η, the value of f is given by the

Stokes equation in both the stick and slip limits. For the stick limit, $f = 6\pi\eta a$, whilst for the slip limit, $f = 4\pi\eta a$. By inserting these frictional factors into equation (5 - 7) it is noticeable that the quantity $D\eta/T$ is a constant provided the molecular radius a does not change with temperature. Hence the measurement of self-diffusion coefficients for a molecular species over a range of temperatures provides, in the first instance a test of the application of the Stokes-Einstein model to the system of interest and in the second, allows one to differentiate between the two limits.

However, in the original formulation of equation (5 - 7) the motion of a single particle is considered and the interaction of the particle with others is assumed to be negligible. Thus the relationship can strictly only apply in the limit of infinite dilution. The Stokes equation similarly imposes a restriction that the species must be perfectly spherical. Therefore the self-diffusion study of the linear dimethylthallium(III) cation in D_2O at 0.8M concentration clearly does not meet either of these criteria to provide an efficient test of the model in its original formulation. However, it is of interest in this work to apply the model and treat the cation as a species that takes up the volume of a sphere with radius equal to half the longest axis of the cation. By this method, the degree of application of the Stokes-Einstein model to non ideal systems may be tested.

If the hydrodynamic theory is applicable here, a plot of the self-diffusion coefficient D against T/η will give a straight line passing through the origin, with a gradient,

$$M = \frac{k_b}{C\pi a}, \qquad (5-8)$$

where the constant C represents the degree of stick or slip nature.

A plot of D against T/η is shown in figure (5 - 2) and a linear least squares regression analysis yields the best fit parameters,

$$\text{Slope} = 2.20 \pm 0.4 \times 10^{-15}\ NK^{-1}, \qquad (5-9)$$

$$\text{Intercept} = -5.5 \pm 2.3 \times 10^{-11}\ s. \qquad (5-10)$$

From the slope of the plot the effective radius of the cation may be calculated for both stick and slip limits. Thus

$a = 3.33 \times 10^{-10} m$ in the stick limit, and

$a = 5.00 \times 10^{-10} m$ in the slip limit.

The value for a calculated from molecular geometry was given in section (4.2.10) as,

$$a = 3.585 \times 10^{-10} m. \qquad (5-11)$$

Thus, if there is no appreciable hydration sphere of the solvent around the cation the model predicts that the

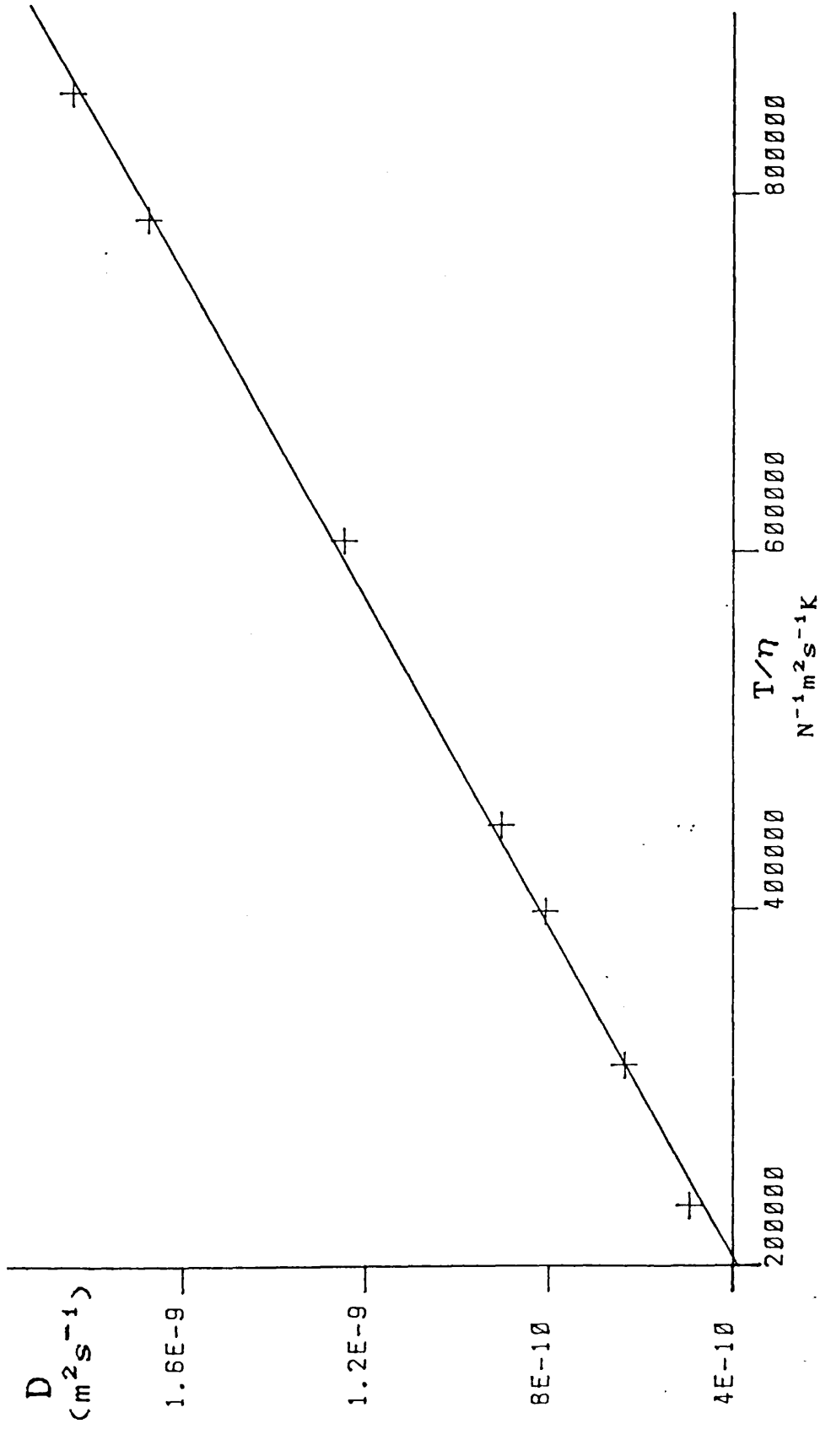

Figure (5-2) plot of D against T/η for $(CH_3)_2Tl^+$ in D_2O.

stick limit best describes the physical interaction of the solvent with the cation. However, the model will predict a more slip type behaviour if the cation radius is increased by a large solvation sphere.

A more extensive treatment has been applied to the translational motion of molecules that are non spherical in shape. Perrin[23] has shown that it is necessary to introduce three frictional coefficients to describe this situation, hence equation (5 - 7) becomes,

$$D = \frac{k_b T}{3} \left(\frac{1}{f_1} + \frac{1}{f_2} + \frac{1}{f_3} \right), \qquad (5 - 12)$$

where f_1, f_2 and f_3 describe the frictional coefficient about each axis. For an ellipsoidal molecule the diffusion coefficient about the two perpendicular axes are equal, thus $f_2 = f_3$ and the effective frictional coefficient is given by,

$$\frac{1}{f_{eff}} = \frac{1}{3} \left(\frac{1}{f_1} + \frac{2}{f_2} \right). \qquad (5 - 13)$$

This suggests that the effective radius of the diffusing ellipsoid is given by an equation of the same form.

Using the dimensions given in section (4.2.10), the effective cation radius was calculated to be

$$a_{eff} = 2.38 \times 10^{-10} \text{ m} , \qquad (5 - 14)$$

and the stick or slip parameter, C thus has a value of

8.4. This lies outside the limiting values of C and thus the model appears to be inappropriate for describing the diffusional motion of the cation.

Section 5.3 Application of the Dimethylthallium(III) cation to self-diffusion studies in viscous solutions.

5.3.1 Measurements

For this study a 10% and a 30% sucrose solution in D_2O were prepared. To each solution, dimethylthallium(III) nitrate was added to yield a 0.8M solution.

In the ^1H spectra of both solutions, both components of the methyl doublet were observable to low frequency of the sucrose resonances. The self-diffusion experiment was initially performed in the 10% sucrose/D_2O solution and the results of this study are given in table (5 - 2)

Table (5 - 2) D as a function of temperature for $(CH_3)_2Tl^+$ in 10% sucrose/D_2O (w/w) solution.

Temperature (K)	D x $10^{10} m^2 s^{-1}$
308.9	4.63
315.2	5.89
321.2	7.59
330.4	9.44
338.4	11.0
344.9	13.7
348.8	13.9
357.6	16.8

Overall error in the measured value of D is ± 4.0%

5.3.2 Discussion of results.

These results gave a linear plot for ln D against inverse temperature and this is shown in figure (5 - 3).

The linear plot indicates that the temperature dependence may be described by equation (5 - 4). A non linear least squares fitting procedure was applied to fit the data to this equation and this yielded the best fit estimates for the parameters,

$$D_{298} = 3.75 \pm 0.24 \times 10^{-10} \ m^2 s^{-1} \qquad (5 - 15)$$

$$E_a = 22.6 \pm 1.2 \ kJ \ mol^{-1} \qquad (5 - 16)$$

The self-diffusion of the dimethylthallium cation appears to reflect the increase in viscosity of the solvent in the 10% sucrose/D_2O solution by a reduction in

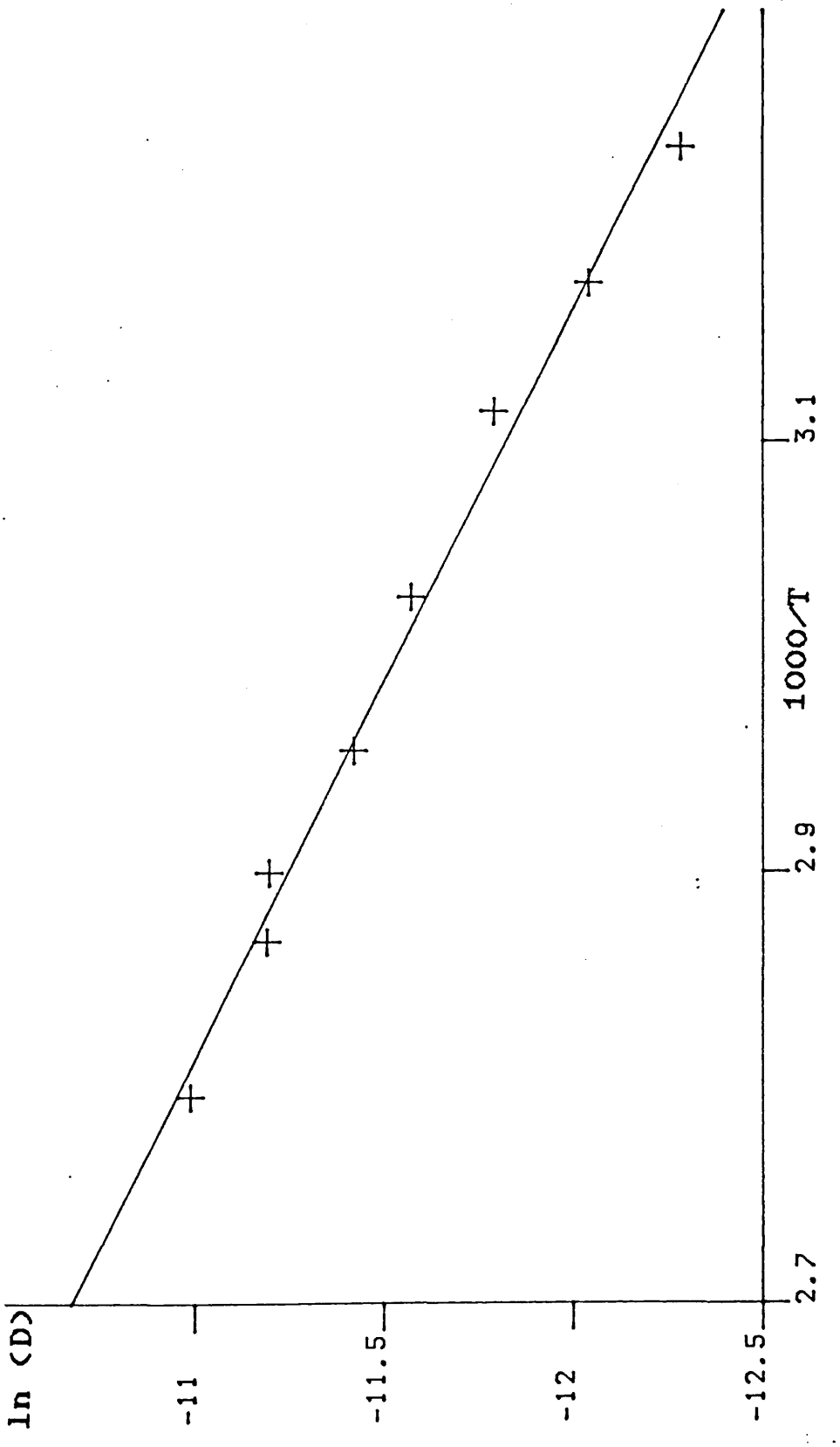

Figure (5-3) Plot of ln (D) against 1000/T for $(CH_3)_2Tl^+$ in 10% sucrose/D_2O (w/w) solution.

the diffusion coefficient and an increase in the activation energy for the diffusional process.

For a more extensive study on the self-diffusion of the dimethylthallium(III) cation as a function of viscosity it is necessary to study a significantly larger range of sucrose concentrations. Unfortunately, self-diffusion measurements could not be made in the 30% solution on existing equipment because of the spin-echo attenuation due to the increased rate of natural T_2 decay processes in this more viscous solution. This means that the time delay, Δ in the PGSE experiment needs to be shortened, which is in conflict with the need to allow the slower diffusing molecule more time to diffuse to effect a measurable echo attenuation.

It is possible that the ^1H self-diffusion of the dimethylthallium(III) cation in 30% sucrose/D_2O solution may be studied simply by increasing the magnitude of the applied linear field gradient. For a large value of G the change in resonance frequency and hence the echo attenuation, will be more sensitive to small displacements of the ^1H nuclei along the field gradient axis. To increase the applied field gradient it is necessary to apply larger D C currents to the homospoil coil arrangement of the Jeol FX90Q spectrometer and this is limited by the power handling capabilities of the coils. In addition the rapid switching of large currents through the coils may give rise to mechanical vibrations in the

probe which may lead to a slight displacement of the sample during the experiment. Further errors may arise from the generation of eddy currents in the walls of the probe which have their own associated magnetic field.

The modified PGSE techniques discussed in section (5.1.1) may also provide a method to study diffusion in this system. It has been noted that the stimulated echo technique is relevant to the study of self-diffusion in systems where $T_1 >> T_2$. The relaxation of the protons in the dimethylthallium(III) cation in aqueous solution has been noted[24] to be such a case. The proton linewidths are broadened by a scalar mechanism involving coupling to the fast relaxing ^{205}Tl nucleus. The broadening is larger at high field where the CSA mechanism is more efficient. This additional broadening has been calculated to be, $(2\pi T_{1(Tl)})^{-1}$ and thus the natural proton linewidth $\upsilon_{1/2}$ is given by,

$$\upsilon_{1/2} = \frac{1}{\pi T_2^{eff}} = \frac{1}{\pi T^*_{2(H)}} + \frac{1}{2 \pi T_{1\ (Tl)}}, \quad (5 - 17)$$

where $(\pi T^*_{2\ (H)})^{-1}$ corresponds to the sum of the natural linebroadening and the effects of magnetic field inhomogeneity. This additional contribution results in the ^1H T_2 being shorter than the ^1H T_1. In addition, this difference is accentuated when the molecular motion of the cation is outside the extreme narrowing limit.

In the 30% sucrose solution, at ambient temperature the ^1H T_1 was observed to be in the order of 1 s whilst the ^1H T_2 was measured to be 0.049 s. The stimulated echo technique requires a large T_1/T_2 ratio and is often limited to cases where the initial magnetisation is strong. Therefore, for the measurement of ^1H self-diffusion coefficients for the dimethylthallium(III) cation it is clear that both of these conditions are met.

A further problem that arises in the measurement of ^1H self-diffusion coefficients in the presence of large concentrations of sucrose, is that of signal dynamic range. The small broadened peaks due to the methyl protons of the cation are difficult to observe in the presence of large ^1H signals from the sucrose solute. This problem may be alleviated if the T_1 values of the sucrose protons are different from that of the dimethylthallium(III) protons. In this case the three pulse sequence due to Boss[3] may be used.

Although these techniques may extend the range of study to solutions with slightly greater viscosity than the 30% solution it is concluded that the dimethylthallium(III) cation has only very limited use as a probe cation to monitor translational motion in viscous liquids. It is therefore necessary to consider how, by the appropriate choice of nucleus and probe cation, one may study the self-diffusion of cations in highly viscous sucrose solution.

Section 5.4 ^{205}Tl self-diffusion studies.

5.4.1 Accessible nuclei for the PGSE experiment.

Of the nuclei available for study, clearly those with high receptivity are in principle more favourable. The value of the magnetogyric ratio, γ of course plays a direct role in the experiment since it appears (as $(\gamma G)^2$) in the equation for the spin echo attenuation,(equation (5 - 1)). Nuclei with high magnetogyric ratios will exhibit significant spin echo attenuation due to diffusion along a linear field gradient and clearly those nuclei with lower magnetogyric ratios have to diffuse much further in a given field gradient to cause the same degradation of the spin echo.

If we compare, for example, the ^{13}C and ^{1}H PGSE experiments, since γ (^{1}H) / γ (^{13}C) is equal to 3.98, the field gradient must be ~ 4 times larger for ^{13}C nuclei in order to observe the same echo attenuation. Alternatively the ^{13}C nucleus needs to diffuse 16 times as long as the ^{1}H nucleus to achieve the same echo attenuation for a given field gradient. Thus the lowest limit of the measurable self-diffusion coefficient by the ^{13}C technique is 16 times larger than that measured by the ^{1}H technique.

For this reason, nuclei such as ^{1}H, ^{19}F[25-28], ^{205}Tl, ^{31}P and ^{7}Li[29] that possess relatively high magnetogyric ratios' are favourable for these studies.

A further important quality for probe nuclei is that

they possess a long T_2 as discussed earlier. Many quadrupolar nuclei exhibit very short T_2 values and are therefore inaccessible to the PGSE technique. However some hydrated ions in aqueous solution may have a small quadrupole moment and a symmetrical electronic environment and therefore the quadrupolar relaxation mechanism is not as effective and the nuclei may be accessible to the experiment. Such examples are the $^{7}Li^{+}$, $^{9}Be^{2+}$, $^{33}Cs^{+}$ and $^{35}ClO_4^{-}$ ions that all have typical T_2 values ranging from 0.1 second to the order of several seconds.

Despite the clear advantage of the ^{1}H nucleus for these experiments, they are often made difficult by the presence of complex spectra (overlapping and strongly coupled) and by the effect of J modulation effects on the spin echoes. The use of proton decoupled ^{13}C spectra which are free from such difficulties has been demonstrated.[30] Up to the present the ^{205}Tl nucleus has not been suggested as a probe for NMR PGSE techniques. This is surprising in view of its favourable spin properties; the nucleus has a high magnetogyric ratio and natural abundance and the typical nuclear spin relaxation times for the $Tl(I)^{+}$ ion in aqueous solution are in the order of 2 seconds[31]. The work presented in later sections utilises these properties to study systems in which ^{1}H self-diffusion measurements are impractical.

5.4.2 ^{205}Tl Probe cations for PGSE studies.

The self-diffusion studies reported in sections (5.2)

and (5.3) for the dimethylthallium(III) cation might in principle be performed by observation of the ^{205}Tl nucleus. However the slower molecular motion in more viscous solution means that the CSA relaxation mechanism is more efficient and this causes the T_2 to get unacceptably small and therefore no advantage is offered to the study of dimethylthallium(III) cations in sucrose solutions.

The work presented in section (4.5) has shown the $Tl(I)^+$ ion to be in principle an excellent diffusional probe. This assessment is based on the rather long T_1 values (shortest ~1 s) and the relative insensitivity of the T_1 values and linewidths to changes in temperature and sucrose concentration. Furthermore, the relaxation rates are typically lower at high fields and therefore the ^{205}Tl self-diffusion experiment is not just limited to NMR spectrometers working at low field strengths.

5.4.3 Self-diffusion of $Tl(I)^+$ in D_2O.

An initial study of the self-diffusion of the thallium(I) ion in aqueous solution was performed in order to characterise the translational motion of the cation and to test its suitability for the PGSE experiment.

The self-diffusion coefficients were measured as a function of temperature on a sample of $TlNO_3$ in D_2O (0.246M) that had been degassed in the usual manner and sealed in a 5mm NMR tube.

The magnetic field gradient calibration and

temperature measurement was achieved in a similar manner as for the ^{1}H PGSE experiment. Thus it was assumed that the tuning of the multinuclear probe to the ^{1}H frequency between experiments did not alter the sample temperature or the magnitude of the field gradient.

The validity of the ^{1}H field gradient calibration to the ^{205}Tl PGSE experiment was tested by measuring the self-diffusion of the dimethylthallium(III) cation in D_2O by both ^{1}H and ^{205}Tl PGSE experiments and both results were found to be in accordance within experimental error.

An example of the series of ^{205}Tl spectra for $Tl(I)^{+}$ ion in D_2O given by the application of the PGSE sequence, for different pulsed field gradient duration times (δ) is shown in figure (5 - 4). The spectra were recorded at a temperature of 330.2K using a pulse sequence that maintained a constant time period between 90^{o} and 180^{o} pulses (method (b) in section 3.5.2). The applied pulsed field gradient was 2.13G cm^{-1}.

The measured self-diffusion coefficient for the $Tl(I)^{+}$ ion in D_2O, over a range of temperatures is presented in table (5 - 3)

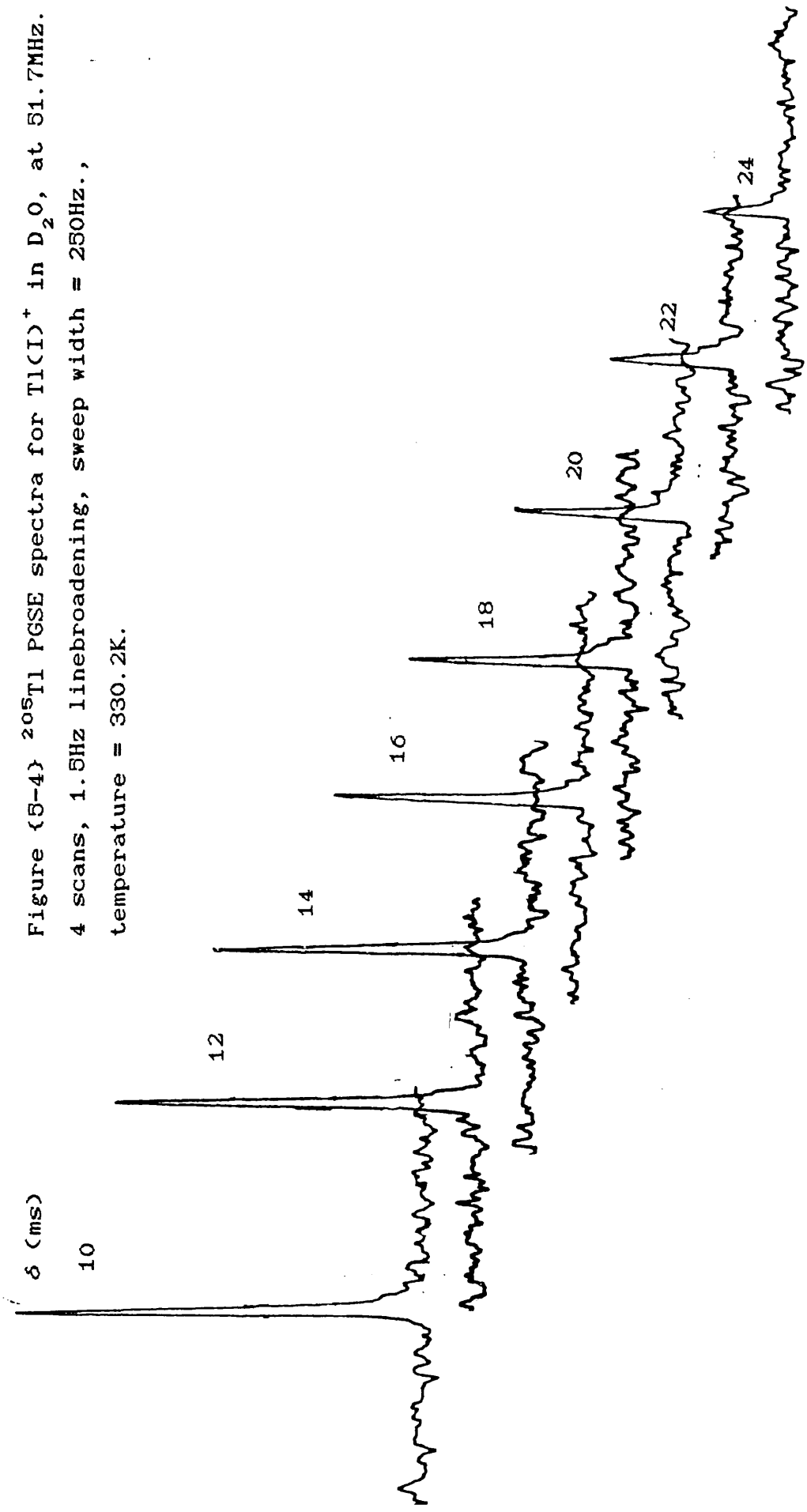

Figure (5-4) ^{205}Tl PGSE spectra for $Tl(I)^{+}$ in D_2O, at 51.7MHz. 4 scans, 1.5Hz linebroadening, sweep width = 250Hz., temperature = 330.2K.

Table (5 - 3) D as a function of temperature for $Tl(I)^+$ ion in D_2O.

Temperature (K)	D x 10^9 ms^{-1}
301.9	2.06
310.8	2.22
317.4	2.59
324.8	2.83
328.5	2.96
330.2	2.97
335.5	3.22
344.4	3.85

Overall error in the measured value of D is ± 3.8%

A plot of ln D against inverse temperature is given in figure (5 - 5) and shows a linear relationship. The temperature dependence may be represented by equation (5 - 4) and a non linear least squares fitting procedure to fit the data to this equation yielded the best fit estimates for the parameters,

$$D_{298} = (1.84 \pm 0.06) \times 10^{-9} \text{ m}^2 \text{ s}^{-1} \quad (5 - 18)$$

$$E_a = 13.0 \pm 0.8 \text{ kJ mol}^{-1} \quad (5 - 19)$$

5.4.4 Comparison with other work.

Limited $Tl(I)^+$ self-diffusion studies have been performed by other workers using tracer techniques. Patil and Potdar[32] measured the self-diffusion and tracer

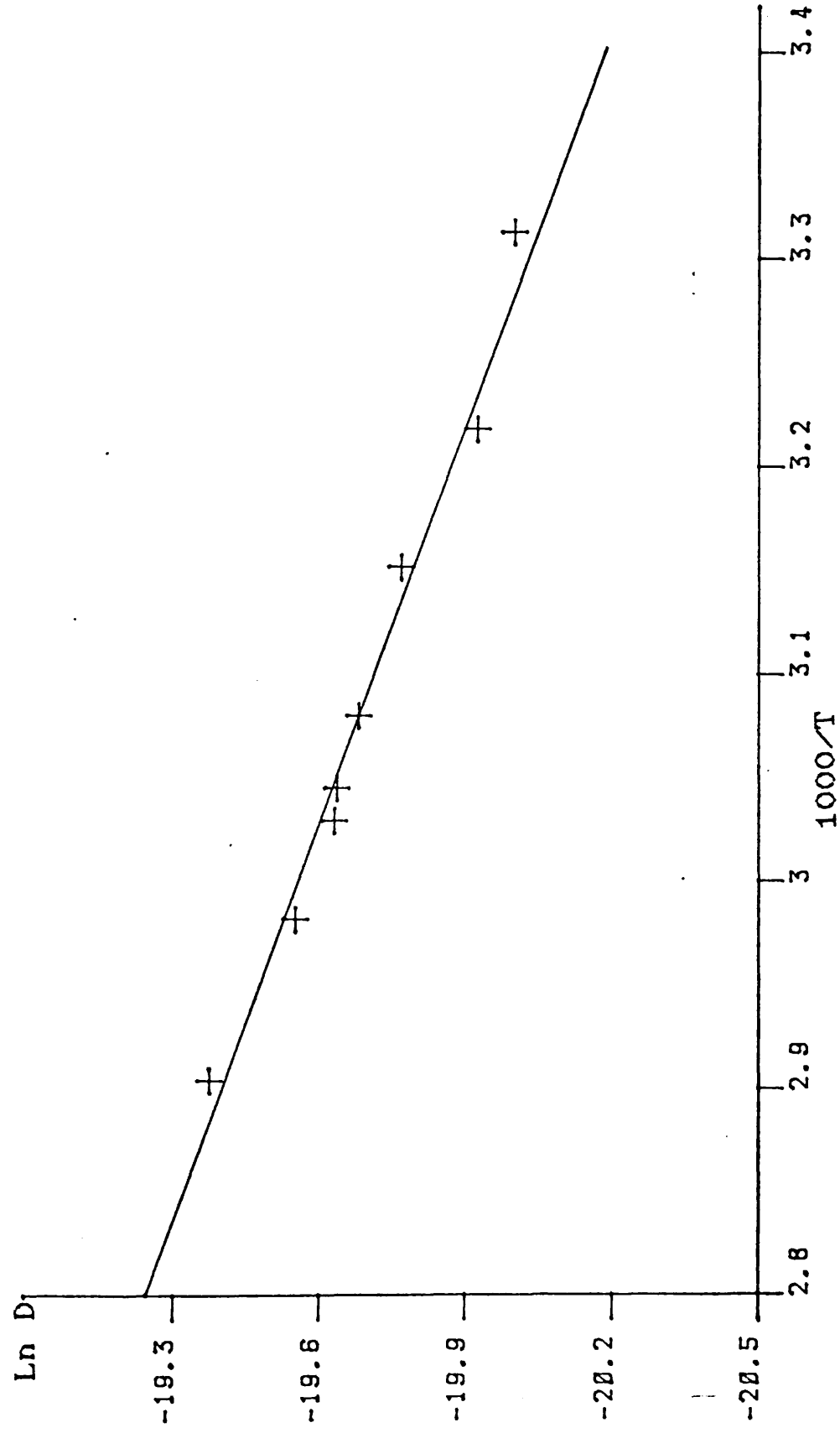

Figure (5-5) Plot of ln D against 1000/T for Tl^+ in D_2O.

interdiffusion coefficients for the $Tl(I)^+$ ion labelled with ^{204}Tl in an aqueous solution of Tl_2SO_4 (0.01M) with 1% agar gel. The distinction between the two diffusion coefficients in this case arises in the experimental method of measurement. For self-diffusion, the agar gel containing the labelled Tl_2SO_4 was added to gel containing Tl_2SO_4 at the same concentration, whereas for tracer interdiffusion the labelled species in gel was added to a pure aqueous solution of the gel. The self diffusion coefficient extrapolated to zero agar gel content at a temperature of 298K, was reported to be 2.065×10^{-9} m^2 s^{-1}.

Over the temperature range of 25^oc to 50^oc a linear plot was observed for ln D against inverse temperature with an activation energy of 17.2 kJ mol^{-1}.

The tracer interdiffusion coefficient was reported to be 1.75×10^{-9} m^2 s^{-1}. The difference in values may be rationalised by assuming that each coefficient pertains to a different mechanism for diffusion. For the tracer interdiffusion coefficient one is measuring the diffusion of ions under the influence of a concentration gradient, in this system the $Tl(I)^+$ ions must diffuse at the same rate as the SO_4^{2-} ions in order to maintain neutrality in solution and thus the rates of diffusion are influenced by the motion of the partner ion. For self-diffusion the motion is an intrinsic property of the ion itself and is independent of the motion of the partner ions.

The reported self-diffusion coefficient is higher than that noted in this study. This is to be expected as the values presented in this thesis pertain to the solvent D_2O which is more viscous than H_2O. From the results of Longsworth's[33] study on the self diffusion of HDO in both H_2O and D_2O the solvent isotope effect was observed to reduce the self-diffusion coefficient at 298K, by 16%. In the study made by Biondi and Bellugi[34] the effects of H_2O and D_2O solvents on the interdiffusion coefficients of $Tl(I)^+$ ion were compared and from the results reported, the solvent isotope effect is noted to reduce the diffusion coefficient by 18.5% at a temperature of 298K. Therefore the difference in self-diffusion coefficients in H_2O and in D_2O reported in the present work appears to be within the range reported by other workers.

An additional reported value for the self-diffusion coefficient of the $Tl(I)^+$ ion in H_2O was provided by Wakeham[35] in an exploratory study to apply the chromatographic tracer technique to the measurement of self diffusion coefficients in electrolyte solutions. An aqueous solution of Tl_2SO_4 labelled with radioactive ^{204}Tl was injected into a flowing stream of aqueous Tl_2SO_4 of the same concentration to observe ^{204}Tl self-diffusion. The self-diffusion coefficient for $Tl(I)^+$ at infinite dilution at 303K was reported to be $(1.39 \pm 0.09) \times 10^{-9}$ $m^2\ s^{-1}$.

This result is significantly lower than the value

given by Patil and Potdar and also lower than that reported in this thesis. Further disagreement with the reported value of Wakeham, is found in the work of Cuddeback and Drickamer[36] who studied the pressure dependence of the self-diffusion coefficient of the $Tl(I)^+$ ion in an aqueous solution of $TlNO_3$ (0.1M) up to a pressure of 9000 atms. At a minimum pressure of 20 atms and a temperature of 298K, the value was reported to be $(2.07 \pm 0.1) \times 10^{-9}$ $m^2 s^{-1}$ and an increase in pressure up to 250 atms was required to reduce this to a value of 1.35×10^{-9} m^2 s^{-1}.

As pointed out by Hinton et al.[37], the $Tl(I)^+$ ion has a similar ionic radius to the $K(I)^+$ ion and this was the basis for the use of the $Tl(I)^+$ ion as a replacement for $K(I)^+$ to enable NMR to be used as an aid in the study of the function of $K(I)^+$ ions in biological systems. The self-diffusion coefficient of the $K(I)^+$ ion in aqueous KI has been measured by ^{42}K tracer techniques and for a 0.29M concentration at 298K the coefficient is reported[38] to be $(2.06 \pm 0.04) \times 10^{-9}$ m^2 s^{-1}. Thus it appears that the $K(I)^+$ and $Tl(I)^+$ ions show comparable self-diffusion behaviour in aqueous solution and this provides evidence to suggest that the ^{205}Tl PGSE experiment on $Tl(I)^+$ probe cations may be used to simulate the translational motion of $K(I)^+$ ions and indeed may have further application in studies on biological systems.

As yet the PGSE experiment has not been proposed to

study these cations in biological systems and motional studies have been limited to the reorientational behaviour of the thallium species. The information derived from self-diffusion coefficients in these systems is often more appropriate than the reorientational motional parameters derived from T_1 measurements. This is because the measurement of self-diffusion coefficients gives a direct measure of the motional property of interest, whilst the reorientational motion may only be derived from T_1 measurements by invoking a theoretical model framework involving nuclear spin relaxation mechanisms. In addition, the T_1 study on the $Tl(I)^+$ ion in aqueous sucrose solutions presented in Chapter 4 has shown that no information on molecular reorientation may be obtained by this method.

Finally, the value of 13.0 ± 0.8 kJ mol^{-1} found for the activation energy for the self-diffusion of the $Tl(I)^+$ ion in D_2O, is significantly lower than the value of 17.2 kJ mol^{-1} reported by Patil and Potdar from their tracer studies and also lower than the value of 18.8 kJ mol^{-1} found for the dimethylthallium(III) cation in D_2O. The present conclusion is that the value reported here seems rather low and there may be significant experimental error.

5.4.5 Hydrodynamic theory.

A plot of D versus T/η is shown in figure (5 - 6), where η is the viscosity of D_2O. The linear behaviour

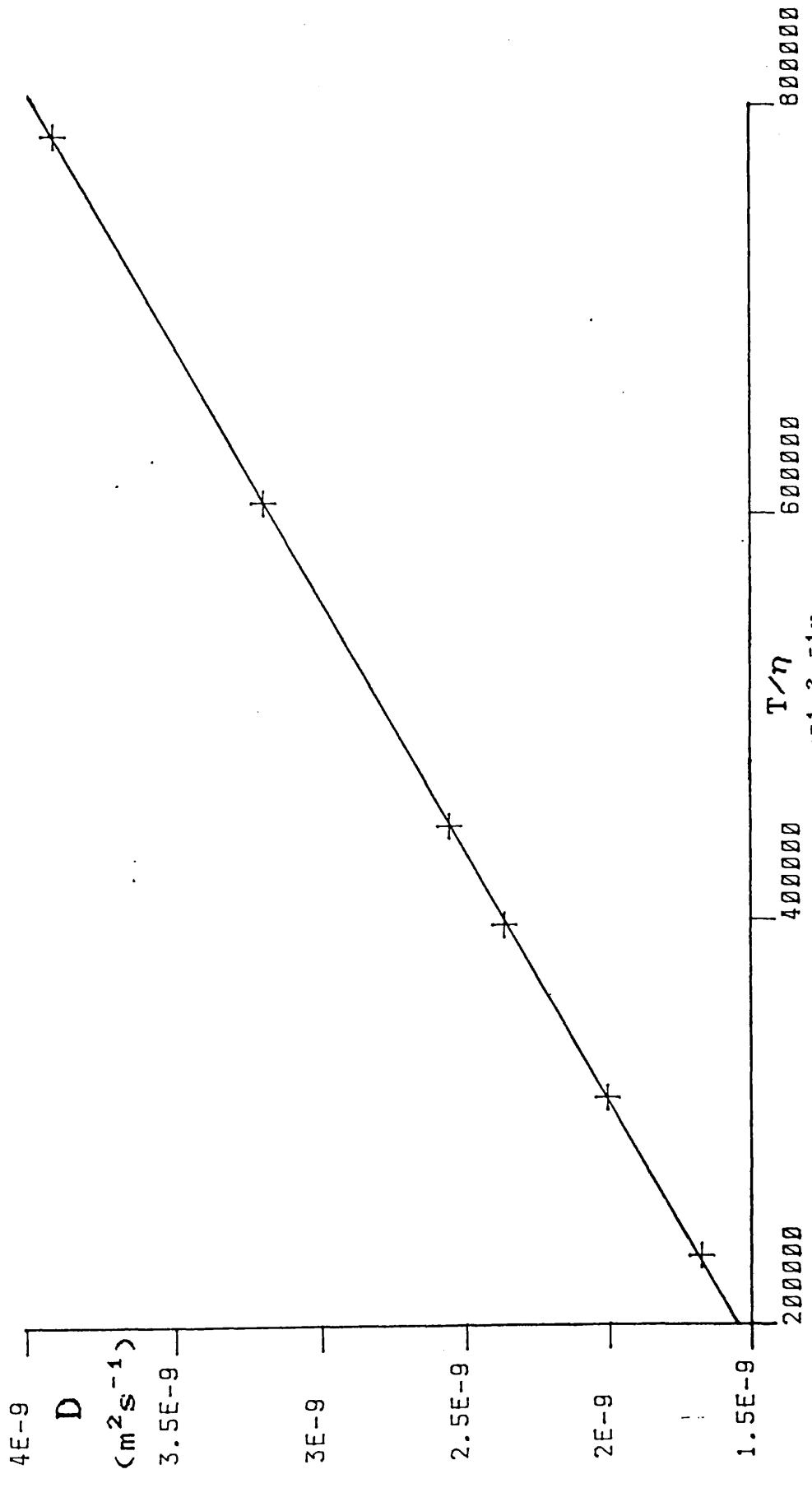

Figure (5-6) Plot of D against T/η for $Tl(I)^+$ in D_2O.

allowed for a least squares linear regression analysis to be applied which yielded the following results,

$$\text{Slope} = 3.91 \pm 0.03 \times 10^{-15}\ \text{N}\ \text{K}_j^{-1} \quad (5-20)$$

$$\text{Intercept} = 8.13 \pm 0.14 \times 10^{-10}\ \text{m}^2\text{s}_o^{-1} \quad (5-21)$$

The linear plot of D versus T/η suggests that $D\eta/T$ is a constant over the temperature range and therefore that D correlates well with viscosity.

From the slope, the effective radius a, of the cation in solution may be calculated by use of equation (5 - 8). The values obtained are,

$a = 1.80 \pm 0.01 \times 10^{-10}$ m for the stick limit and

$a = 2.81 \pm 0.01 \times 10^{-10}$ m for the slip limit.

The ionic radius of the unsolvated $Tl(I)^+$ ion is known to be 1.40×10^{-10} m which is outside the limits given by the Stokes-Einstein equation.

From the values of D given for a series of monovalent ions in aqueous solution[39], the application of hydrodynamic theory repeatedly gives a calculated, effective ionic radius that is larger than the known, unsolvated ionic radius, in line with the findings of this study. It was suggested[39] that the increase in radius in solution was consistent with a small degree of ion solvation.

5.4.6 Self-diffusion of $Tl(I)^+$ in sucrose/D_2O solutions.

The preparation of samples used in this study is given in section (4.5.2). The self-diffusion coefficients for the $Tl(I)^+$ ion in 10%, 30% and 45% sucrose solution were measured as a function of temperature in the usual manner and the results of these studies are shown in table (5 - 4).

Table (5 - 4) D as a function of temperature for $Tl(I)^+$ ion in sucrose / D_2O solutions.

a) 10% sucrose/D_2O solution

Temperature (K)	D x 10^9 m^2s^{-1}
301.9	1.52
310.8	1.83
317.4	1.84
313.0	2.04
317.4	2.18
326.0	2.61
332.7	2.97
336.8	3.00

Overall error in the measured value of D is ± 4.2%

b) 30% sucrose/D_2O solution.

Temperature (K)	D x 10^9 m^2s^{-1}
298.6	0.74
303.6	0.77
311.3	0.99
317.2	1.21
320.7	1.16
326.5	1.34
331.5	1.51
337.3	1.56
343.4	1.88

Overall error in the measured value of D is ± 3.8%

c) 45% sucrose/D_2O solution.

Temperature (K)	D x 10^9 m^2s^{-1}
298.6	0.39
303.6	0.41
311.3	0.48
317.2	0.54
320.7	0.68
326.5	0.83
331.5	0.81
335.3	0.87

Overall error in the measured value of D is $\pm$ 3.9%

In all sucrose/D_2O solutions studied, the temperature dependence of the self-diffusion coefficient may be described by equation (5 - 4) and plots of ln D against inverse temperature are presented in figure (5 - 7). A non linear least squares fitting procedure to equation (5 - 4) gave the best fit estimates for D_{298} and E_a for each solution and these are presented with the results obtained for the pure D_2O solution, in table (5 - 5).

Table (5 - 5) Best fit estimates for D_{298} and E_a for $Tl(I)^+$ in D_2O and sucrose / D_2O solutions.

Concentration sucrose/D_2O (w/w)	D_{298} ($\times 10^9 m^2 s^{-1}$)	E_a kJ mol^{-1}
0	1.84 ± 0.06	13.0 ± 0.8
10	1.48 ± 0.06	15.9 ± 1.3
30	0.73 ± 0.03	17.4 ± 1.2
45	0.36 ± 0.03	20.3 ± 2.5

5.4.7 Hydrodynamic theory.

In a similar manner to the study in D_2O, the self-diffusion data may be used to calculate an effective radius of the cation in each sucrose solution by the application of the Stokes-Einstein theory discussed in section (2.1.2) In this analysis it is necessary to have a

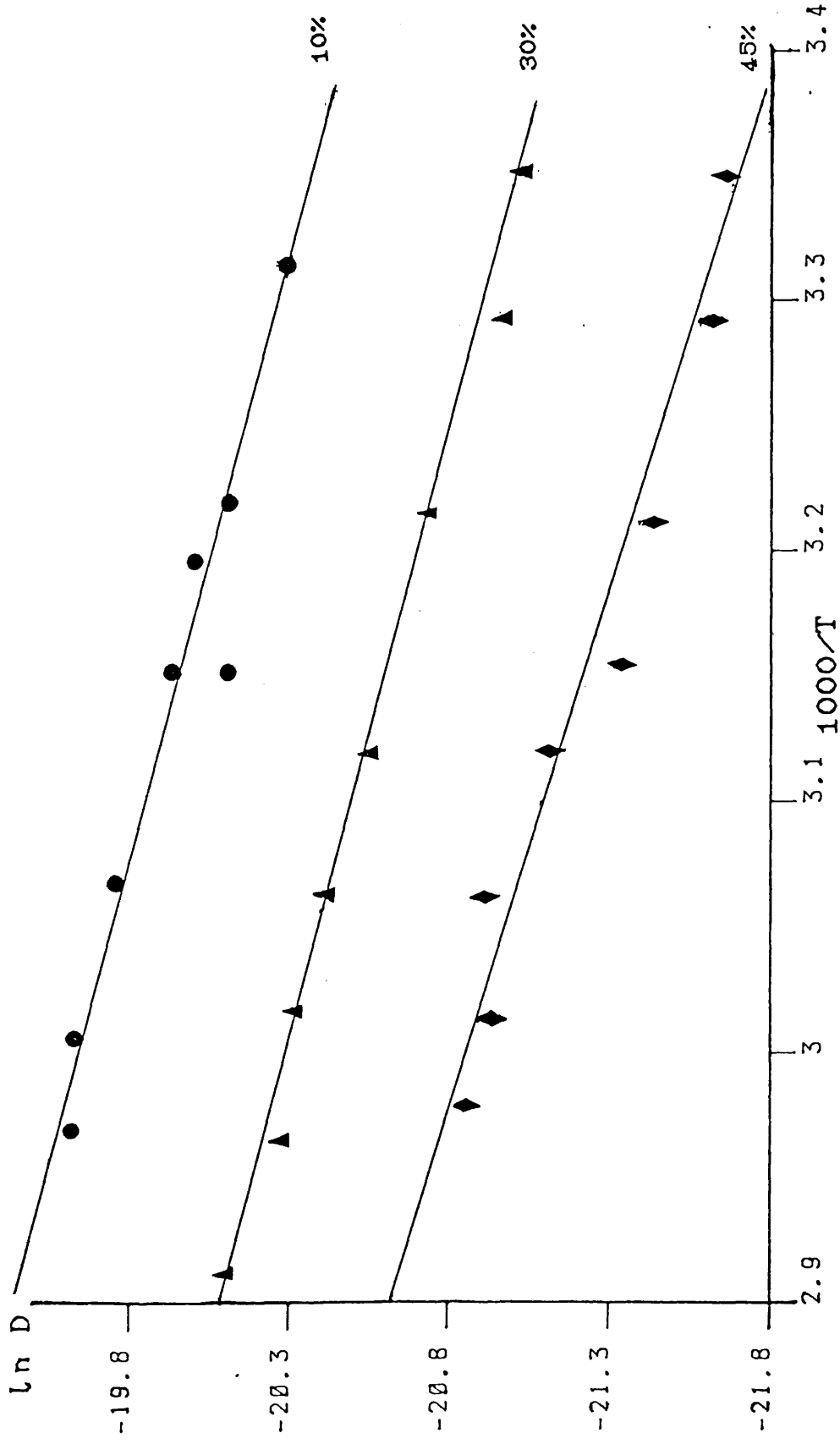

Figure (5-7) Plot of Ln (D) against 1000/T for $Tl(I)^+$ in 10%, 30% and 45% Sucrose/D_2O solutions.

knowledge of the viscosity of each solution as a function of temperature. Surprisingly, viscosity data for sucrose/D_2O solutions do not appear to have been reported in the literature and so the closest approximation for these values, available to this study are those data reported by Swindells et al.[40] for sucrose in H_2O (w/w%). Clearly the assumptions made regarding viscosities do not permit accurate analysis, but a general view of the cation behaviour in sucrose solution may be taken and any obvious error in the assumptions made should appear as inconsistencies in the final derived parameters.

For the 30% and 45% solutions, for which there is viscosity data available, plots of D against T/η were made and these are represented in figure (5 - 8).

A least squares regression analysis was applied to the resulting linear plots and this gave the best fit parameters for the slope and intercept. These values are presented in table (5 - 6).

Table (5 - 6) Slope and intercept of the plot of D against T/η in 30% and 45% sucrose/D_2O (w/w) solutions.

Concentration of sucrose in D_2O (w/w%)	Slope ($\times 10^{15}$ NK^{-1})	Intercept ($\times 10^{-10} m^2 s^{-1}$)
30	4.70 ± 0.01	0.215 ± 0.002
45	5.63 ± 0.04	0.150 ± 0.004

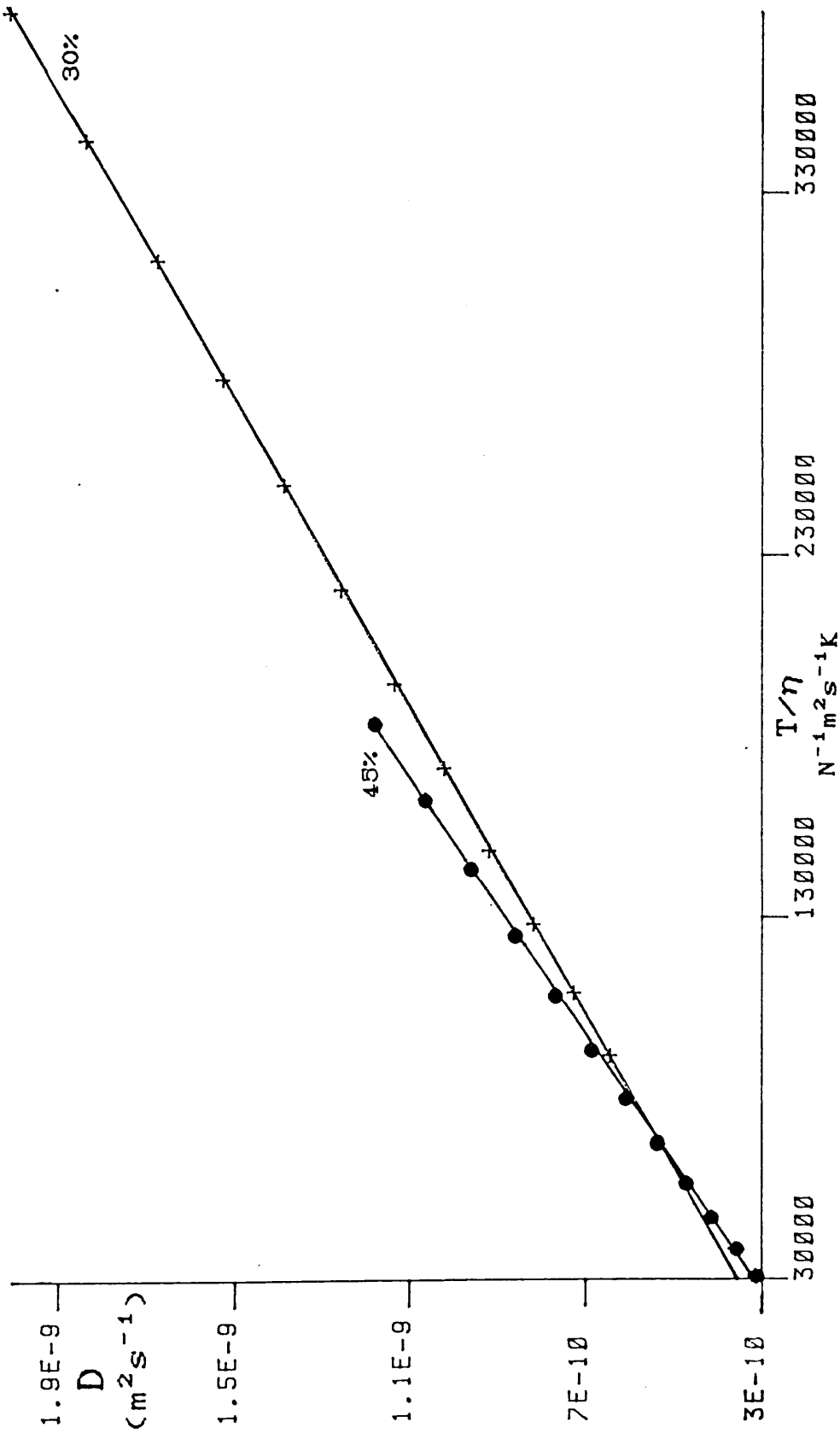

Figure (5-8) Plot of D against T/η for $Tl(I)^+$ in 30% and 45% Sucrose/D_2O solutions.

From the slope of the plots the effective hydrodynamic radii of the cation may be calculated in both the stick and slip limits. Thus for the 30% solution,

$$a_{STICK} = 1.556 \pm 0.003 \times 10^{-10}m \qquad (5 - 22)$$

$$a_{SLIP} = 2.336 \pm 0.004 \times 10^{-10}m \qquad (5 - 23)$$

whilst for the 45% solution,

$$a_{STICK} = 1.30 \pm 0.01 \times 10^{-10}m \qquad (5 - 24)$$

$$a_{SLIP} = 1.95 \pm 0.01 \times 10^{-10}m \; . \qquad (5 - 25)$$

The effective radii calculated by this model show that the cation does not appear to alter radically in size in the sucrose solutions studied. These radii bear close relation to those derived in the pure D_2O solution and thus the results suggest that the formation of a long lived sucrose-thallium complex is unlikely.

Confirmatory evidence of this result is provided by the ^{205}Tl chemical shift behaviour in aqueous sucrose solutions that shows a shift of 13ppm to low frequency on addition of sucrose to 30% (w/w) concentration and a further shift of 17ppm on addition to 60% concentration. These shifts are relatively small in comparison to those observed in $Tl(I)^+$ systems that exhibit ligand complexing behaviour[41-45] and are suggested to arise from the change in solvation of the $Tl(I)^+$ ion rather than the formation of a sucrose-thallium complex.

For the diffusion rate to be affected by the formation

of such a complex, the lifetime must be longer than the timescale over which the self-diffusion coefficient is measured. In this system, the term 'long lived' refers to the millisecond timescale. Further experiments involving measurements over different timescales of diffusion may identify any interaction on a shorter timescale and may, further provide information on possible restricted diffusion processes[46] occuring in highly concentrated aqueous sucrose solutions.

The present results are of an exploratory nature and do not reflect the limit of measurement of the self-diffusion coefficient for $Tl(I)^+$ ion in sucrose/D_2O solutions. The limitation to the measurements in this study was caused by instability in the spectrometer which prevented the measurement of the 60% solution, although it is perfectly feasible to measure D values at this concentration.

In conclusion it is proposed that the $Tl(I)^+$ ion is a very useful probe for the study of the translational motion of ions in highly viscous liquids. The cation appears to monitor its environment very efficiently over a range of viscosities and this is in contrast to its apparent poor probe qualities for the study of reorientational motion, as discussed in Chapter 4.

The other cation in this study, the dimethylthallium(III) cation, has been shown to have limited probe qualities for the study of translational

motion in viscous liquids, but provides a very sensitive monitor of its physical surroundings in solutions of relatively low viscosity. The limited use of this cation in self-diffusion studies, must however be contrasted with its apparent usefulness as a probe molecule for reorientational motion in different viscous solutions, where it has proved to be very successful.

References for CHAPTER FIVE.

1. E.L.Hahn, Phys. Rev., 80, 580 (1950).
2. H.Carr and E.M.Purcell, Phys. Rev., 94, 630 (1954).
3. B.D.Boss, E.O.Stejskal and J.D.Ferry, J. Phys. Chem., 71, 1501 (1967).
4. D.E.Woessner, J. Chem. Phys., 34, 2057 (1961).
5. J.E.Tanner, Ph.D. Thesis, University of Wisconsin (1966).
6. J.E.Tanner, J. Chem. Phys., 52, 2523 (1970).
7. S.Vega and A.Pines, J. Chem. Phys., 66, 5624 (1977).
8. A.Bax, P.G.Deyoung, A.F.Mehlkopf and J.Smidt, Chem. Phys. Lett., 69, 567 (1980).
9. A.Wokaun and R.R.Ernst, Mol. Phys., 36, 317 (1978).
10. G.Bodenhausen, R.L.Vold and R.R.Vold, J. Magn. Reson., 37, 93 (1980).
11. J.F.Martin, L.S.Selwyn, R.R.Vold and R.L.Vold, J. Chem. Phys., 76, 2632 (1982).
12. D.Zax and A.Pines, J. Chem. Phys., 78, 6333 (1983).
13. H.C.Torrey, Phys. Rev., 92, 962 (1953).
14. A.Abragam, "The Principles of Nuclear Magnetism", O. U. P. (1961).
15. M.J.Forster, Ph.D. Thesis, University of London (1984).
16. R.C.Hardy and R.L.Cottingham, J. Chem. Phys., 17, 509 (1949).
17. D.E.O'Reilly, J. Chem. Phys., 60, 1607 (1974).
18. J.C.Hindman, J.Zielen, A.Svirmickas and M.Wood, J. Chem. Phys., 54, 621 (1971).
19. J.C.Hindman, J. Chem. Phys., 60, 4488, (1974).
20. F.H.Stillinger and A.Rahman, J. Chem. Phys., 55, 3336 (1971).
21. F.H.Stillinger and A.Rahman, J. Chem. Phys., 57, 1281 (1972).

22. R.W.Impey, P.A.Madden and I.R.McDonald, Mol. Phys., 46, 513 (1982).

23. F.Perrin, J. Phys. Rad., 7, 1, (1936).

24. F.Brady, R.W.Matthews, M.J.Forster and D.G.Gillies, J. Chem. Soc. Chem. Comm., 911 (1981).

25. R.D.Ferguson and E.Von Meerwall, Bull. Am. Phys. Soc., 24, 799 (1979).

26. E. Von Meerwall and R.D.Ferguson, J. Chem. Phys., 72, 2861 (1980).

27. R.D.Ferguson and E.Von Meerwall, J. Polym. Sci. Polym. Phys. Ed. 18, 1285 (1980).

28. E.Von Meerwall, Adv. Polym. Sci., 54, 1 (1983).

29. A.Weiss and K.H.Nothnagel, Ber. Der. Bunsenges., 75, 216 (1971).

30. M.E.Moseley and P.Stilbs, Chemica Scripta, 16, 114 (1980).

31. M.Bacon and L.W.Reeves, J. Amer. Chem. Soc., 95, 272 (1973).

32. S.F.Patil and J.K.Potdar, Proc. Nucl. Chem. Symp., 229 (1980).

33. L.G.Longsworth, J. Phys. Chem., 64, 1914 (1960).

34. C.Biondi and L.Bellugi, Chemical Physics, 62, 145 (1981).

35. W.A.Wakeham, Farad. Symp. Chem. Soc., 15, 145 (1981).

36. R.B.Cuddeback and H.G.Drickamer, J. Chem. Phys., 21, 597 (1953).

37 J.F.Hinton, K.R.Metz and R.W.Briggs, Ann. Rep. NMR Spectry., 13, 211 (1982).

38. R.Mills and J.W.Kennedy, J. Amer. Chem. Soc., 75, 5696 (1953).

39. P.W.Atkins, "Physical Chemistry", O.U.P (1977).

40. J.F.Swindells, C.F.Snyder, R.C.Hardy and P.E.Golden, Natn. Bur. Stand. Supp. to Circ. No.C440.

41. C.Srivanavit, J.I.Zink and J.J.Dechter, J. Amer. Chem. Soc, 99, 5876 (1977).

42 D.Gudlin and H.Schneider, Inorganica Chimica Acta, 33, 205 (1979).

43. S.O.Chan and L.W.Reeves, J. Amer. Chem. Soc. 96, 404 (1974).

44. R.W.Briggs, F.A.Etzkorn and J.F.Hinton, J. Magn. Reson., 37, 523 (1980).

45. J.F.Hinton, G.L.Turner and F.S.Millet, J. Magn. Reson., 45, 42 (1981).

46. J.E.Tanner, J.Chem. Phys., 69, 1748 (1978).

CHAPTER SIX - ^{205}Tl RELAXATION STUDIES ON THALLOUS ION IN THE PRESENCE OF TANOL

Section 6.1 Introduction.

6.1.1 Previous ^{205}Tl relaxation studies.

^{205}Tl relaxation studies have been performed in the presence of added paramagnetic ions in both aqueous and non aqueous solution. The studies pertain more to the effect of oxygen on the relaxation of the ^{205}Tl nucleus than the TANOL species of interest, but both species are thought to behave in a similar manner[1] and therefore the results and conclusions of these studies are of interest.

The first study of aqueous $Tl(I)^+$ ion / paramagnetic systems was reported in 1959 by Gasser and Richards[2] who studied the effects of added paramagnetic $Fe(CN)_6^{3-}$ ion on the ^{205}Tl R_1. The rate was observed to increase linearly by over an order of magnitude as the paramagnetic ion concentration was increased up to a concentration of 0.01M. They concluded that the relaxation mechanism was similar to that proposed for the relaxation of water protons in the Cu^{2+}/ H_2O system [3] which was explained in terms of an electron-nuclear dipolar interaction modulated by translational motion.

The effect of dissolved molecular oxygen on the ^{205}Tl R_1 and R_2 was studied by Bacon and Reeves[4]. They found that both rates increased significantly in the presence of dissolved oxygen and that the R_2 was not appreciably

greater than the R_1. This suggested that a contact hyperfine interaction was unlikely, and therefore the electron-nuclear dipole-dipole mechanism was thought to dominate the relaxation. A more detailed study was presented later by Chan and Reeves[5] who noted that at a ^{205}Tl frequency of 15.1 MHz the ^{205}Tl R_1 and R_2 in aqueous solution increased linearly with increasing oxygen pressure up to 5 atmospheres. In addition R_1 and R_2 were found to be equal, within experimental error, over the full range of oxygen pressures and this confirmed the conclusions of the previous study. In both studies it was noted that in the absence of dissolved oxygen the relaxation rates were independent of the resonance frequency (7.95 MHz and 15.1 MHz), thallium salt concentration (0.3 M - 3.5 M), resonant spin (^{205}Tl or ^{203}Tl) and anion and the spin-rotation mechanism was thought to provide the dominant contribution to the relaxation.

In methanol solution[5] the ^{205}Tl R_1 and R_2 were equal but the effect of oxygen was about 3.8 times greater than in water. This was explained by the greater solubility of oxygen in methanol.

Forster[6] undertook a field dependent study on the effect of oxygen on the ^{205}Tl relaxation of the $Tl(I)^+$ ion in aqueous solution which resulted in a different interpretation. The ^{205}Tl R_1 was measured as a function of temperature at ^{205}Tl frequencies of 21.89 MHz and

230.8 MHz and these were complemented by $R_{1\rho}$ measurements. In addition ^{205}Tl R_2 measurements were made at a ^{205}Tl frequency of 230.8 MHz. The ^{205}Tl R_1 was observed to decrease with increasing field strength and was independent of temperature within experimental error. The results were rationalised by assuming that both R_1 and R_2 were dominated by the scalar relaxation mechanism of the second kind.

The nitroxide free radical, TANOL (4-hydroxy-2,2,2,6 tetramethylpiperidine-1-oxyl) is, like oxygen, an uncharged, paramagnetic species and its effect on the ^{205}Tl relaxation rates R_1 and R_2 of the $Tl(I)^+$ ion in aqueous solution was studied by Bangerter and Schwartz[7]. These workers found that at a ^{205}Tl frequency of 51.75 MHz both the ^{205}Tl R_1 and R_2 were enhanced by, and strongly dependent on the concentration of TANOL in solution. In addition R_2 was found to be significantly greater than R_1, suggesting a strong scalar coupling between the unpaired electron spin of TANOL and the ^{205}Tl nucleus. The modulation of the scalar hyperfine interaction was thought to dominate R_2 but was not considered to make a significant contribution to R_1, where the electron-nuclear dipole-dipole mechanism was thought to dominate. The R_1 was shown to be temperature independent within experimental error, whilst the R_2 showed a marked decrease with increasing temperature.

In the light of the information gained from the

studies with TANOL, Bangerter[1] reinvestigated the effects of dissolved oxygen on the ^{205}Tl R_1 and R_2 for the $Tl(I)^+$ ion in aqueous solution. In this study it was found that as the partial pressure of oxygen was increased, the R_2 was increased by a significantly greater amount than the R_1, in conflict with the observations of Reeves and co-workers[4,5] and thus it was assumed that oxygen behaved in a similar manner to TANOL.

6.1.2 Relevant relaxation mechanisms for ion/paramagnetic systems.

In the course of the study presented in the following sections, the observed ^{205}Tl relaxation rates obtained for the $Tl(I)^+$ ion in aqueous solutions containing TANOL free radicals, are explained in terms of the possible contributions of nuclear spin relaxation mechanisms and also of the electron-nuclear spin relaxation contributions of the dipolar and scalar types.

The general descriptions of the dipole-dipole and scalar relaxation mechanisms are discussed in Chapter 2. However, these apply to the effects of nuclear-nuclear interactions. The electron-nuclear interaction is a special case for both scalar and dipolar mechanisms and thus warrants an additional discussion.

6.1.2.1 Electron-nuclear dipolar mechanism.

This mechanism arises from a modulation of the interaction between the electron and nuclear magnetic dipoles. The modulation may arise from translational and

reorientational motions, or by electron spin relaxation. Thus the effective correlation time is given by the differing contributions of each of these processes, such that

$$\frac{1}{\tau_c} = \frac{1}{\tau_{rot}} + \frac{1}{\tau_e} + \frac{1}{\tau_N} + \frac{1}{\tau_S}. \qquad (6-1)$$

Where $\tau_{rot.}$ is the correlation time for the rotational motion of the Tl(I) ion-paramagnetic complex, τ_e and τ_N are the exchange times for the electron and the nucleus respectively and τ_S is the electronic relaxation time.

If we assume that in the solution under study, the TANOL radical forms a complex with the $Tl(I)^+$ ion, and there is rapid chemical exchange between bound and free environments, then the ^{205}Tl relaxation rates may be interpreted in terms of the Solomon - Bloembergen equations[8,9]. These equations in turn may be simplified by assuming that, at a typical NMR spectrometer frequency of 230.8 MHz, the ^{205}Tl and electron resonance frequencies are of the order of 10^9 and 10^{12} Hz respectively such that $\omega_I \pm \omega_S \sim \omega_S$ and $\omega_I^2\tau_c^2 << 1$. Thus we have,

$$R_{1DD} = \frac{2}{15}\left[\frac{\mu_0}{4\pi}\right]^2 \frac{S(S+1)\,\gamma_I^2\,\gamma_S^2\,\hbar^2\,x}{r_{IS}^6}\left[3\tau_c + \frac{7\tau_c}{1+\omega_S^2\,\tau_c^2}\right]$$

$$(6-2)$$

$$R_{2DD} = \frac{1}{15}\left[\frac{\mu_0}{4\pi}\right]^2 \frac{S(S+1)\,\gamma_I^2\,\gamma_S^2\,h^2\,x}{r_{IS}^6}\left[7\tau_c + \frac{13\tau_c}{1+\omega_S^2\tau_c^2}\right]. \qquad (6-3)$$

Where S is the spin quantum number of the paramagnetic species, r_{IS} is the mean electron-nuclear distance, γ_I and γ_S are the magnetogyric ratios of the nucleus and electron respectively and the quantity x reflects the degree of complexing of the species. All other terms have their usual meaning. Two limiting forms of equations (6 - 2) and (6 - 3) are of interest. In the limit where $\omega_S^2\tau_c^2 \gg 1$, then $R_2 = \frac{7}{6} R_1$, whilst in the limit where the correlation time is sufficiently short that $\omega_s^2\tau_C^2 \ll 1$, then the ratio R_2/R_1 is unity.

The possibility of complex formation in aqueous thallium(I) nitrate / TANOL solution was discussed by Bangerter and Schwartz[7]. In their study TANOL was observed to enhance the relaxation of the ^{205}Tl nucleus by two orders of magnitude greater than the Mn^{2+} ion at the same concentration and this suggests the formation of a Tl(I)-TANOL complex. However EPR studies do not indicate any strong interaction between the species in aqueous solution.

Electron-nuclear dipolar relaxation may occur without the formation of a long-lived Tl(I) - TANOL complex but rather by an intermolecular mechanism arising from the

interaction between electron and nuclear dipoles of different species. The theoretical basis of this mechanism has been discussed by Abragam[11] and expressions for the relaxation rates R_{1DD} and R_{2DD} have been given by Berner and Kivelson[12]. The full spectral density functions contained within these expressions have been derived by Pfeiffer[13].

An important feature of the rate expressions is that they contain terms related to the electronic spin-lattice relaxation time, the relative diffusion of the nuclear spin I and the electron S and the concentration of the paramagnetic species.

Thus relaxation by the intermolecular electron-nuclear dipolar mechanism may arise from a modulation of the dipolar interaction by either the relative diffusion of I and S or by rapid electron spin relaxation.

6.1.2.2 Electron-nuclear scalar mechanism

The Fermi contact interaction that results in a nuclear-electron magnetic coupling may lead to relaxation of the ^{205}Tl nucleus via a scalar relaxation mechanism. The mechanism has been discussed in detail by Bloembergen[9] and Abragam[11] and the relaxation rates were given by,

$$R_{1\ SC} = \frac{2}{3}\ S(S+1)A^2 \times \left[\frac{\tau_{SC2}}{1 + (\omega_I - \omega_S)^2 \tau_{SC2}^2} \right] \qquad (6-4)$$

$$R_{2\,sc} = \frac{1}{3}\, S(S+1)A^2 \times \left[\tau_{sc1} + \frac{\tau_{sc2}}{1 + (\omega_I - \omega_S)^2 \tau_{sc2}^2} \right], \qquad (6-5)$$

where A is the scalar coupling constant and x is the fraction of the observed nuclear spins that experience a scalar interaction.

In this system the scalar correlation times τ_{sc1} and τ_{sc2} may correspond to the electronic relaxation times T_{1e}, T_{2e} respectively or a chemical exchange time τ_e. The shorter time dominates each scalar correlation time and if the condition

$$\frac{1}{T_{1e}}, \frac{1}{\tau_e} \gg A, \qquad (6-6)$$

holds then the scalar mechanism may contribute to the relaxation of the nuclear spin. If $\tau_e \ll T_{1e}, T_{2e}$ the mechanism will be that of scalar relaxation of the first kind whilst if the converse holds the scalar relaxation of the second kind will dominate. For the former mechanism the simplest model assumes that the scalar coupling constant A, between spins I and S may take on the full value when the spins are on the same molecule[14] but this immediately becomes zero when the spins are apart. Thus chemical exchange will lead to a time variance in the value of A and this gives rise to relaxation mechanism. For the scalar mechanism of the second kind it is assumed

that the relaxation of the electron spin is rapid and thus the local magnetic field produced by the electron spin, and experienced by the scalar coupled nuclear spin fluctuates in time and hence provides a pathway for relaxation to occur.

The study presented later will provide evidence to suggest that the scalar mechanism provides the dominant contribution to both the ^{205}Tl R_1 and R_2 of the $Tl(I)^+$ ion in aqueous TANOL solution.

Section 6.2 ^{205}Tl Nuclear spin relaxation.

6.2.1 Introduction.

It is clear from the literature that the ^{205}Tl relaxation in $Tl(I)^+$ ion/paramagnetic systems is strongly dependent on the concentration of the dissolved paramagnetic species. In studies performed in the presence of oxygen, it is necessary to express this concentration in terms of the partial pressure of oxygen above the aqueous $Tl(I)^+$ ion solution and the exact concentration of the dissolved species at a given temperature may not be monitored. The problem is complicated when the sample temperature is increased, for at higher temperatures the amount of oxygen in the water is reduced.

The addition of known amounts of TANOL to aqueous solution allows for a more accurate knowledge of the concentration of dissolved paramagnetic species and this concentration is temperature invariant.

The practical aspects of using TANOL are also favourable. The samples may be sealed in the usual way and easily transported between different spectrometers and do not require the experimental arrangement needed to maintain a constant oxygen partial pressure above the aqueous solution.

Thus the aqueous TANOL system was proposed for the study of the effects of paramagnetics on the ^{205}Tl relaxation in $Tl(I)^{+}$ ion and the initial work[7] on these systems was extended to explore the field dependence of the ^{205}Tl relaxation.

6.2.2 Measurements.

For the study, four aqueous thallium(I) nitrate / TANOL solutions and a reference aqueous thallium(I) nitrate solution were prepared. Each TANOL concentration was made by dilution of a parent stock solution of TANOL in H_2O (1×10^{-2} M) to minimise concentration errors. Thallium(I) nitrate was added to make up a 0.2M concentration in each TANOL solution and each sample was degassed in the usual way. The ^{205}Tl R_1 was measured in all five samples containing; 1×10^{-3} M, 1×10^{-4} M, 5×10^{-5}M, 1×10^{-5} M and no TANOL at ^{205}Tl frequencies of 21.89 MHz and 230.8 MHz. In addition, $R_{1\rho}$ measurements were performed on the 5×10^{-5} M, 1×10^{-5} M and no TANOL samples using the DANTE sequence discussed in section (3.4.5). The ^{205}Tl R_2 values were measured for all solutions at 230.8 MHz. All measurements at 21.89 MHz were made at ambient

temperature (296K) and measurements at 230.8 MHz were made at a set temperature of 296K on the variable temperature control unit of the Bruker WH-400 spectrometer.

The results are given in tables (6 - 1) and (6 - 2), together with the values for the ^{205}Tl R_1 and R_2 reported by Bangerter and Schwartz[7] in a study made at a ^{205}Tl frequency of 51.75 MHz

Table (6 - 1) Field dependence of ^{205}Tl R_1 and $R_{1\rho}$ as a function of TANOL concentration

Concentration TANOL (M)	$R_1(s^{-1})$ (230.8 MHz)	$R_1(s^{-1})$ (51.75 MHz)
0	0.61	0.57
1×10^{-5}	1.54	1.39
5×10^{-5}	1.89	5.3
1×10^{-4}	3.36	10.4
1×10^{-3}	31.0	106

Table (6 - 1) continued.

Concentration TANOL (M)	$R_1(s^{-1})$ (21.96 MHz)	$R_{1\rho}(s^{-1})$
0	0.61	0.81
1×10^{-5}	2.82	17.6
5×10^{-5}	13.9	99
1×10^{-4}	26.3	——
1×10^{-3}	——	——

Table (6 - 2) Field dependence of ^{205}Tl R_2 as a function of TANOL concentration.

Concentration TANOL (M)	$R_2(s^{-1})$ (230.8 MHz)	$R_2(s^{-1})$ (51.75 MHz)
0	1.17	0.75
1×10^{-5}	15.7	15.3
5×10^{-5}	86	88
1×10^{-4}	161	185
1×10^{-3}	1530	2240

No ^{205}Tl R_1 measurement is reported at 21.89MHz for the 1 x 10^{-3}M TANOL solution as the line is too broad to be measured using the maximum sweep width of 5000 Hz.. Similarly no $R_{1\rho}$ data are reported for the 1 x 10^{-4}M and 1 x 10^{-3}M solutions since the lines were too broad to satisfy the spin-locking condition necessary to perform this experiment.

6.2.3 Discussion of results.

The results show that an increase in TANOL concentration gives rise to an increase in the ^{205}Tl R_1 at both frequencies, and also the R_2 and the $R_{1\rho}$. It is also noted that the effect on R_1 is much greater at 21.89 MHz than at 230.8 MHz. Overall, this behaviour is consistent with the observed effects on R_1 and R_2 at 51.75MHz noted by Bangerter and Schwartz[7].

The $R_{1\rho}$ and R_2 values should be equal to the R_1 in the pure aqueous solution and so these results appear to be marginally in error. It is noted that any imperfections in the $R_{1\rho}$ and R_2 measurements tend to give results that are larger than the true values and this is consistent with the differences observed.

6.2.4 Separation of relaxation contributions.

The ^{205}Tl relaxation rates of the $Tl(I)^+$ ion in a paramagnetic free, aqueous solution are dominated by the spin-rotation mechanism[5]. It is clear that the addition of TANOL leads to an interaction between the unpaired

electron spin of the radical and the ^{205}Tl nucleus which enhances the nuclear spin relaxation. This interaction may be scalar and/or dipolar.

The total observed rate is thus comprised of the contribution from the electron-nuclear mechanism and the spin-rotation mechanism. The latter is equal to the relaxation rate in the TANOL free solution and therefore may be subtracted from the total rate observed in the TANOL solutions. The electron-nuclear relaxation rate contribution R_{1E-N} arising from the addition of TANOL is given in table (6 - 3)

Table (6 - 3) Field dependence of R_{1E-N} as a function of TANOL concentration.

Concentration TANOL (M)	R_{1E-N} (s^{-1}) (230.8 MHz)	$^{*}R_{1E-N}$ (s^{-1}) (51.75 MHz.)
1×10^{-5}	0.9	0.8
5×10^{-5}	1.3	4.7
1×10^{-4}	2.8	9.8
1×10^{-3}	30	105

* Derived from the results of Bangerter and Schwartz[7]

...Continued Overleaf

Table (6 - 3) Continued.

Concentration TANOL (M)	R_{1E-N} (s^{-1}) (21.89 MHz)	$R_{1\rho\ E-N}$ (s^{-1})
1×10^{-5}	2.2	17
5×10^{-5}	13	98
1×10^{-4}	26	—
1×10^{-3}	—	—

6.2.5 Analysis of the electron-nuclear R_1 contribution.

Considering the ^{205}Tl relaxation data presented in this work and in the work of Bangerter and Schwartz[7], there are a number of observations that arise, which must be accounted for in the analysis. These are:

a) The observed field dependence of the mechanism(s) that results in a decrease in the ^{205}Tl R_1 and R_2 with increase in field strength.

b) The significantly larger ^{205}Tl R_2 compared with the R_1 at the same field strength for each concentration of TANOL

c) The different temperature dependences[7] of R_1 and R_2 that show a decrease in R_2 with increasing temperature and a temperature invariant R_1

In each TANOL solution the R_2 measured at 230.8 MHz was observed to be significantly greater than the R_1 measured at the same frequency. For the higher

concentrations of TANOL, the ratio of R_2/R_1 is in the order of 60 and therefore this suggests that the spin-spin relaxation is dominated by the electron-nuclear scalar mechanism.

If we assume at this point, that a dominant scalar relaxation mechanism applies to both spin-spin and spin-lattice relaxation, the field dependence of the relaxation rates should be described by equations (6 - 4) and (6 - 5). By close inspection of these equations the apparent decrease in R_1 with increasing field strength may be explained by assuming that at low field the condition $\Delta\omega^2\tau_{SC2}^2 < 1$ holds, allowing for an efficient scalar mechanism to operate. At high field the condition $\Delta\omega^2\tau^2_{SC2} > 1$ applies, and thus the efficiency of the scalar mechanism is diminished and consequently the ^{205}Tl R_1 is reduced. In turn it is noted from equation (6 - 5) that for spin-spin relaxation by the scalar mechanism, the scalar correlation time τ_{SC1} accounts for J(0), the frequency independent spectral density, and this is not diminished by the matching condition $\Delta\omega^2\tau_{SC2}^2$. This provides an explanation for the significantly large R_2/R_1 ratios observed.

It is of interest to note at this point, that for the condition $\Delta\omega^2\tau_{SC}^2 \leq 1$ to hold at a ^{205}Tl frequency of 21.89 MHz, the electron-nuclear scalar correlation time τ_{SC2} must be in the order of 10^{-12}s whereas for the nuclear-nuclear scalar mechanism discussed in Chapter 2,

the correlation time must be in the order of 10^{-8}s. Thus the nuclear-nuclear mechanism does not often contribute to the nuclear R_1 since often $\Delta\omega^2\tau_{SC}^2 >> 1$ which reduces the efficiency of the mechanism to a negligible contribution. However the timescale of molecular motion is often in the order of 10^{-11}/ 10^{-12}s and this gives rise to an efficient electron-nuclear mechanism. In addition the efficiency of the mechanism is increased by the large scalar coupling constant associated with thallium/free radical systems[15, 16] which is often significantly greater than the nuclear-nuclear coupling constant.

To explain the different temperature dependences of R_1 and R_2 in terms of equations (6 - 4) and (6 - 5) it is necessary to invoke the theory that the scalar correlation time τ_{SC1} has a different temperature dependence from the correlation time τ_{SC2}. It is noticeable by inspection of the rate equations, that whilst R_2 receives a contribution from both τ_{SC1} and τ_{SC2} the R_1 is only affected by the behaviour of τ_{SC2} and the difference in temperature dependence may lie in this fact.

To account for a difference in τ_{SC1} and τ_{SC2} it must be assumed that the electronic relaxation times, T_{1e} and T_{2e} are significantly short compared to the lifetime of any TANOL-Tl(I) complex formed and thus the scalar correlation times τ_{SC1} and τ_{SC2} will be dominated by the spin-lattice and spin-spin relaxation times of the electron respectively. If the T_{1e} of the electron is

temperature dependent such that it decreases with increasing temperature then this may lead to a decrease in the scalar relaxation rate R_{2SC}. If the T_{2e} of the electron is insensitive to temperature change then this may in turn lead to a temperature independent R_{1SC}.

The electron T_1 of TANOL in sec-butyl benzene at 8.62GHz. has been studied by Percival and Hyde[17]. At a temperature of 31°c the T_1 was found to be 0.35×10^{-6}s and was dominated by the spin-rotation mechanism. This order of T_1 does not appear to be short enough to give rise to a significant electron-nuclear scalar relaxation contribution and thus no experimental corroboration of the above theory has been given.

6.2.6 Discussion on the scalar correlation time, τ_{SC2} and scalar interaction term.

To calculate the scalar correlation time pertinent to the ^{205}Tl R_1 values obtained as a function of frequency, equation (6 - 4) was used in a non-linear least squares fitting procedure to the R_1 data measured in the solutions containing TANOL at 1×10^{-5} M and 5×10^{-5} M concentrations. To improve the accuracy of the fitting procedure the results in this study were used in conjunction with those obtained in the same systems at 51.75 MHz by Bangerter and Schwartz. The fitting procedure used two adjustable parameters, these being the scalar interaction term, $\frac{2}{3} S(S+1)A^2x$, denoted K_{int} and the scalar correlation time τ_{SC2}. The best fit estimates of these

parameters are presented in table (6 - 4) and the fit to the observed rates is shown in figure (6 - 1).

Table (6 - 4) Best fit estimates for τ_{sc2} and K_{int} in 1 x 10^{-5}M and 5 x 10^{-5}M TANOL solutions.

Concentration of TANOL (M)	K_{int} ($rads^2s^{-2}$)	τ_{sc2}(ps)
1 x 10^{-5}	1.0 ± 0.3	16 ± 4
5 x 10^{-5}	6.2 ± 0.6	16 ± 1

The consistency of the scalar correlation time τ_{sc2} is as expected in these solutions as the only parameter in equation (6 - 4) directly affected by the change in concentration is the parameter x, which is the mole fraction of $Tl(I)^+$ ions that are complexed with the TANOL species at any one instant.

The dependence of the x parameter on TANOL concentration may simply be ascertained from the ratio of the interaction terms in each solution.

For this procedure the values of the interaction term for the 1 x 10^{-5}M and 5 x 10^{-5}M TANOL solutions were taken from table (6 - 4) and the value for this term for the 1 x 10^{-4}M TANOL solution was calculated by assuming a scalar

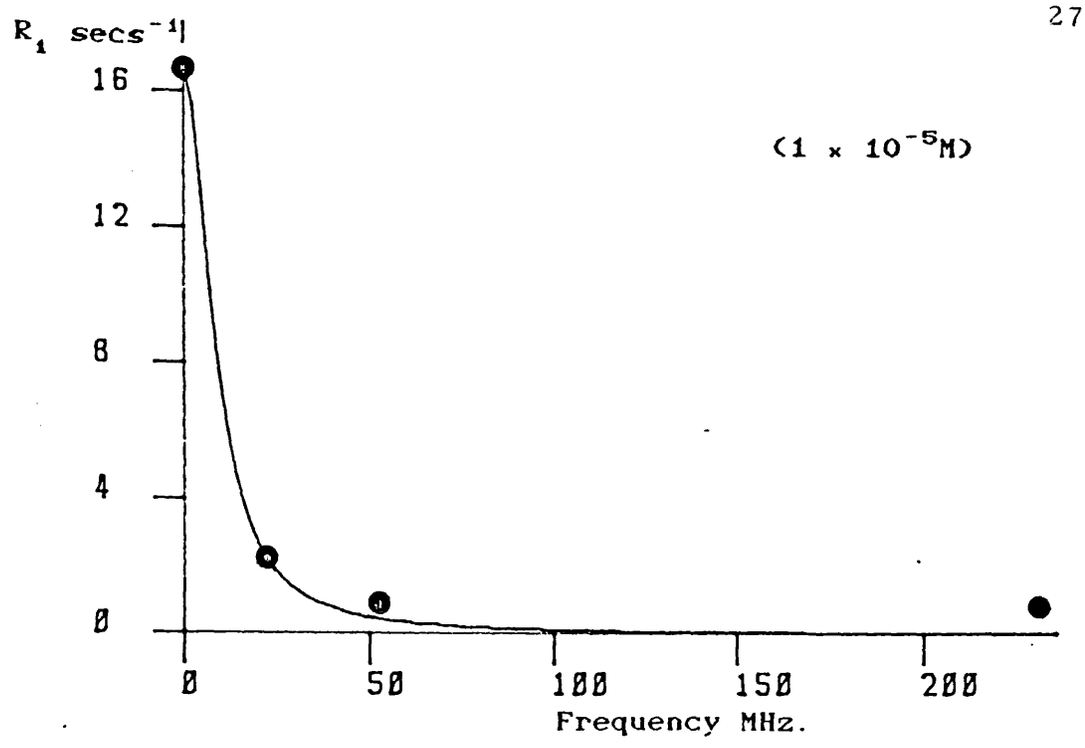

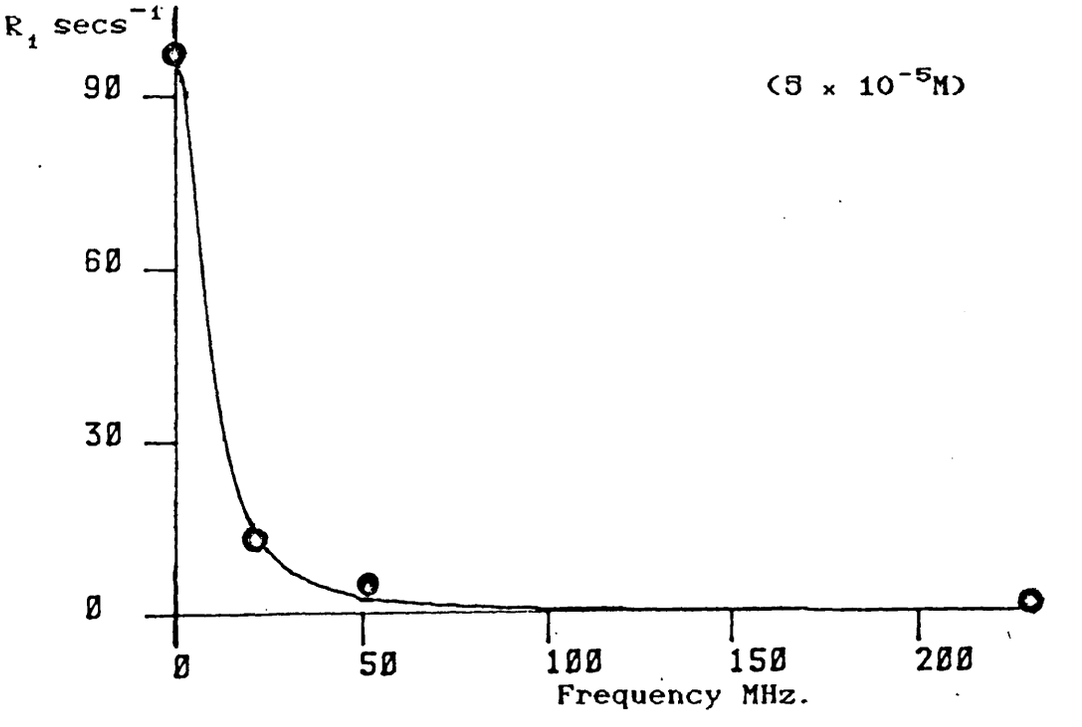

Figure (6-1) Frequency dependence of ^{205}Tl R_1 in (1 x 10^{-5}M) and (5 x 10^{-5}M) aqueous TANOL solutions, fitted to the Scalar R_1 equation.

correlation time of 16ps and calculating the necessary value for this term to yield the observed ^{205}Tl R_1 at 21.89 MHz. From this procedure we find that for a five fold increase in concentration of TANOL, from $1 \times 10^{-5}M$ to $5 \times 10^{-5}M$, the ratio of the interaction terms,

$$\frac{k_{int}(5 \times 10^{-5}M)}{k_{int}(1 \times 10^{-5}M)} = 6.2 \quad , \qquad (6-7)$$

whilst for a twofold increase from $5 \times 10^{-5}M$ to 1×10^{-4} M the ratio is

$$\frac{k_{int}(1 \times 10^{-4}M)}{k_{int}(5 \times 10^{-5}M)} = 1.88. \qquad (6-8)$$

This shows that the interaction term containing the parameter x increases linearly with increased TANOL concentration, and this provides further evidence that the scalar relaxation mechanism is the dominant contributor to the ^{205}Tl R_1.

If it is assumed that, at 230.8 MHz, the other relaxation mechanisms make a negligible contribution to the total ^{205}Tl R_1 then the parameters in table (6 - 4) would predict ^{205}Tl R_1 values, for the $1 \times 10^{-5}M$ and $5 \times 10^{-5}M$ solutions, to be $0.024s^{-1}$ and $0.142s^{-1}$ respectively. The observed ^{205}Tl R_1 in each solution is significantly greater and this suggests that there is a

possible additional contribution from the intermolecular electron-nuclear dipolar relaxation mechanism.

Assuming this model, it is necessary to give a physical relevance to the scalar correlation time observed in these systems. Previously, τ_{sc2} was assumed to be a temperature invariant electron spin-spin relaxation time, to account for the lack of temperature dependence for the scalar R_1. However, an electron T_2 of 16ps is unreasonable as this would give rise to an EPR linewidth of 2×10^{10} Hz which could not be observed. Bangerter and Schwartz[7] have studied the EPR spectrum of TANOL at 1×10^{-3}M concentration and observed three well resolved lines resulting from the hyperfine coupling of the unpaired electron with ^{14}N (S = 1) and so this negates the possibility of a very short electron T_2.

If the electron T_2 is greater than 16ps, then it appears that the modulating process that dominates the scalar correlation time must be that due to an exchange process and thus the 16ps timescale must relate to the lifetime of the $Tl(I)^+$ - TANOL complex formed. This assumption is in agreement with EPR and optical studies[7] that suggest that no long-lived $Tl(I)^+$ - TANOL complex is formed in solution. If this is indeed the case then it is necessary to consider how the chemical exchange may lead to a transmittance of unpaired electron spin density from the free radical to the $Tl(I)^+$ ion. Glazer and Poindexter[18] dicussed the scalar coupling between

radical and receptor ion via a transient complexation process resulting from ion/radical collisions. They noted that there are two plausible mechanisms for the creation of free electron spin density at the receptor nucleus; firstly, by a charge transfer process that may occur when the unpaired electron is in an orbital whose energy is higher than the unoccupied orbital in the receptor, and secondly by an exchange polarisation process which occurs through the reverse transfer of an electron from the receptor atom to the radical as it attempts to pair with the lone radical electron.

Bangerter[1] similarly discussed a collisional model to account for the scalar hyperfine interaction between the $Tl(I)^+$ ion and the paramagnetic species, TANOL and oxygen. The unpaired electron spin density is thought to be transmitted to the ^{205}Tl nucleus via the $6S^2$ orbital electrons, as this orbital has a non-vanishing integral at the nucleus. The collisional process between the ion and paramagnetic species results in the $6S^2$ electron pair interacting with the paramagnetic species and creating sufficient unpaired electron spin density at the ^{205}Tl nucleus to result in a large scalar coupling constant.

Further evidence for this theory is provided by Dwek et al.[15,16]. In their study the electron spin density induced at the thallium nucleus by the intermolecular coupling with free radicals was calculated by perturbation theory. The value obtained was 575 times greater than that

of hydrogen, suggesting that the intermolecular scalar coupling between the ^{205}Tl nucleus and the unpaired electron of the free radical is likely to be very large.

6.2.7 ENDOR experiments.

To further the study of the effect of TANOL on the relaxation of the $Tl(I)^{+}$ ion in aqueous solution, and to define the mechanism(s) responsible for relaxation in these systems, it is of interest to apply the Electron Nuclear Double Resonance (ENDOR) experiment to this system. The theoretical basis behind the experiment has been described by Dwek et al.[19] and readers are referred to this text for a more detailed discussion.

In this experiment, the intensity of the thallium signal is observed whilst the electron spin resonance is completely saturated. The enhancement of the thallium signal and its sign enable one to differentiate between the dipolar and scalar mechanisms[11]. In the extreme narrowing limit the maximum observed enhancement factor, η for each mechanism is given by,

$$\eta_{DIPOLAR} = -\frac{1}{2}\left|\frac{\gamma_S}{\gamma_I}\right| \qquad (6-9)$$

$$\eta_{SCALAR} = +\left|\frac{\gamma_S}{\gamma_I}\right| . \qquad (6-11)$$

If both scalar and dipolar interactions are present, the observed enhancement will lie between these two limits.

The electron magnetogyric ratio is three orders of magnitude larger than that of the ^{205}Tl nucleus and thus from these equations it is clearly apparent that the ENDOR experiment will give very large enhancements in the thallium signal if either the dipole-dipole or scalar mechanism contributes. The signal will be negative for a dominant dipolar contribution and positive for a dominant scalar contribution, and thus the experiment provides a clear indication of the contributing mechanisms within the $Tl(I)^{+}$ - paramagnetic system.

Initial ENDOR studies on thallium compounds in non aqueous solutions containing free radicals, were presented in the review article by Dwek et al.[15]. The thallium salts studied in this work were thallium(I) acetate in methanol, thallium(I) nitrate in acetone and diethylthallium(III) chloride in pyridine. Each solution was studied in the presence of tritertiarybutylphenoxyl (TTBP) radicals and also in the presence of galvanoxyl radicals. The presence of either radical resulted in a positive enhancement for all the thallium compounds, but this was observed to be much larger in the thallium(I) compounds compared to the thallium(III) compounds. In addition, the broadening of the ^{205}Tl resonance was observed to be greater for the the thallium(I) compounds These results suggest that the scalar mechanism is dominant in all solutions and has a greater effect on thallium(I) rather than thallium(III). This behaviour was

rationalised by noting that the $6S^2$ orbital is present in the thallium(I) species yet absent in the thallium(III) species. Thus, when these orbitals are absent the transmittance of unpaired electron spin density occurs via orbitals which are assumed to be less efficient.

It is of interest to note at this point that for the dimethylthallium(III) cation in aqueous solution, paramagnetic oxygen is noted[6] to have little effect on the ^{205}Tl R_1, this may similarly be rationalised by considering that the $6S^2$ orbital is absent in this species.

In conclusion, it is apparent that the interaction between TANOL and aqueous $Tl(I)^+$ ion is dominated by the large intermolecular scalar coupling in which unpaired electron spin density is transmitted through the $6S^2$ orbital of the $Tl(I)^+$ ion to the ^{205}Tl nucleus. Diffusional encounters between ion and free radical allow for very short lived complexes to be formed which induces a very high electron spin density on the ^{205}Tl nucleus and thus the complex exhibits a very large scalar coupling constant. It is the modulation of this coupling constant by intermolecular diffusion that leads to both ^{205}Tl spin-lattice and spin-spin relaxation. The mechanism becomes more efficient as the concentration of TANOL increases, due to a linear increase in the mole fraction of $Tl(I)^+$ ions that are complexed with the TANOL species.

References for CHAPTER SIX.

1. B.W.Bangerter, J. Magn. Reson., 28, 141 (1977).
2. R.P.H.Gasser and R.E.Richards, Mol. Phys., 2, 357 (1959).
3. N.Bloembergen, E.Purcell and R.V.Pound, Phys. Rev., 73, 679 (1948).
4. M.Bacon and L.W.Reeves, J. Amer. Chem. Soc., 95, 272 (1973).
5. S.O.Chan and L.W.Reeves, J. Amer. Chem. Soc., 96, 404 (1974).
6. M.J.Forster, Ph.D. Thesis, University of London (1984).
7. B.W.Bangerter and R.N.Shwartz, J. Chem. Phys., 60, 333 (1974).
8. I.Solomon, Phys. Rev., 99, 559 (1955).
9. N.Bloembergen, J. Chem. Phys., 27, 272 (1957).
10. A.S.Mildvan and M.Cohn, Advan. Enzymol., 33, 1 (1970).
11. A.Abragam, "The Principles of Nuclear Magnetism", O. U. P., (1961).
12. B.Berner and D.Kivelson, J. Phys. Chem., 83, 1401 (1979)
13. H.Pfeiffer, Ann. Phys., Leipzig 8, 1 (1961).
14. P.S.Hubbard, Proc. Roy. Soc., A291, 537 (1966).
15. R.A.Dwek, Adv. Mol. Relax. Processes, 4, 1 (1972).
16. R.A.Dwek, R.E.Richards, D.Taylor and R.A.Shaw, J. Chem. Soc., A, 244 (1970).
17. P.W.Percival and J.S.Hyde, J. Magn. Reson., 23, 249 (1976).
18. R.L.Glazer and E.H.Poindexter, J. Chem. Phys., 55, 4548 (1971).
19. R.A.Dwek, R.E.Richards and D.Taylor, Ann. Rev. NMR Spectry., 2, 293 (1969).

CHAPTER SEVEN THALLIUM(I) ETHOXIDE.

Section 7.1 Previous studies on thallium(I) alkoxides.

7.1.1 Structural studies.

The structure of thallium(I) alkoxides has been studied extensively by many varied techniques. Sidgwick and Sutton[1] applied the ebullioscopic and cryoscopic methods for relative molecular mass determination to the study, and noted that for Tl(OR) (R = CH_3,C_2H_5,$C_6H_5CH_2$) in benzene solution and for thallium(I) ethoxide in ethanol solution the molecules form tetrameric associates, $\{Tl(OR)\}_4$. However measurements made on thallium(I) cyclohexyloxide in benzene and thallium(I) methoxide in methanol indicated that the species present were trimeric and monomeric respectively. The ebullioscopic technique was later used by Bradley[2] to show that thallium 1,1 dimethylpropoxide was also tetrameric in benzene solution.

The tetramer was thought, by Sidgwick and Sutton[1], to form a cubic structure in which the thallium and oxygen atoms occupy the corners of the cube. Hence in each tetramer the group of four oxygen atoms and the four thallium atoms form two regular interpenetrating tetrahedra. The cubic structure was later modified by Dahl *et al.*[3] following a single crystal X-ray study of thallium(I) methoxide. They concluded that this compound, in the solid state, forms tetramers in which the thallium

and methoxide groups occupy the corners of two interpenetrating tetrahedra of differing size. This gives rise to a distorted cubic structure in which the Tl-O-Tl angle is greater than 90^{o} and the O-Tl-O angle is less than 90^{o}. In addition the average Tl-Tl distance was noted to be 3.84×10^{-10}m.

Maroni and Spiro[4] reported Raman and infra-red spectra of liquid thallium(I) ethoxide and low frequency Raman and infra-red spectra of solid thallium(I)-n-propoxide. The analysis assumed tetramer formation and the assignment of the bands were consistent with this assumption. In addition the spectra suggested strong Tl-Tl interactions.

7.1.2 Previous NMR studies.

Schneider and Buckingham[5] have studied the structure of pure liquid thallium(I) ethoxide by ^{205}Tl and ^{203}Tl NMR spectroscopy. The thallium nuclei were observed at frequencies of 15.91MHz and 15.75MHz respectively by the CW frequency sweep technique. The ^{205}Tl spectrum exhibited a symmetric five line multiplet whilst the ^{203}Tl spectrum exhibited a symmetric seven line multiplet. The multiplicities and the relative intensities in the multiplets indicated tetrameric species and ^{205}Tl $-^{203}$Tl spin coupling, with a coupling constant of 2560Hz. The analysis of these spectra is discussed in more detail later.

The observation of the ^{1}H resonance spectrum gave the

characteristic multiplet pattern for an ethyl group that showed no coupling to the Tl nuclei over a temperature range of $-70^{o}c$ to $+20^{o}c$.

The system was studied further by diluting the pure sample to 20 mole% with cyclohexane. It was found that the dilution made no difference to the two spectra, other than a reduction in the signal intensities. It was concluded that the observations were consistent with thallium(I) ethoxide in both pure and diluted samples, having the symmetrical tetrameric structure proposed by Sidgwick and Sutton

Gillies et al.[6] have studied the ^{205}Tl NMR spectra of a series of eleven thallium(I) alkoxides in toluene (1M). The spectra were obtained by CW frequency sweep and pulsed Fourier transform techniques at a ^{205}Tl frequency of 34.7MHz. The spectra spanned a chemical shift range of 434ppm and the ^{205}Tl - ^{203}Tl coupling constants were observed to be particularly large, lying in the range, $2170Hz \leq J \leq 2575Hz$.

The intensities of the signals making up the multiplet pattern of the ^{205}Tl NMR spectra of Tl(OR) [R = C_2H_5, n-C_4H_9, n- C_5H_{11}, n- C_6H_{13}, $CHCH_3(CH)_2CH_3$, $CHCH_3(CH_2)_3CH_3$ or $CH_2C_6H_5$] are consistent with a predominately tetrameric structure in solution. However they noted that, due to the lack of sufficient accuracy in the determination of relative peak areas, the presence of significant proportions of trimeric and/or hexameric species in the

solutions could not be discounted.

Recently, Forster[7] has made a ^{205}Tl R_1 study in pure thallium(I) ethoxide. Measurements were made as a function of temperature at ^{205}Tl resonance frequencies of 21.95MHz and 231.5MHz. It was observed that the ^{205}Tl R_1 increased considerably at high field, implying a significant CSA relaxation contribution. A linear plot of ln R_1 against inverse temperature at both high and low field showed the reorientational motion to be within the extreme narrowing limit at both field strengths. Assuming a dominant CSA relaxation mechanism applied at high field, a scaling procedure was performed on the high field data to show that the CSA mechanism was not dominant at low field. A scalar mechanism arising from interaction between ^{205}Tl and ^{203}Tl nuclei was suggested to be the dominant low field relaxation mechanism.

The discussion was extended to note the lineshape behaviour of the ^{205}Tl resonance. As the temperature was increased, at low field, the ^{205}Tl lines were observed to broaden, coalesce and then collapse in a manner characteristic of a chemical exchange process. However, at high field the linewidths of the ^{205}Tl multiplet were so broad that the ^{205}Tl - ^{203}Tl coupling was not resolved. The large increase in linewidth at high field was noted to be due to a CSA contribution to R_2 but the overall linewidth at high and low field could not be rationalised on the basis of a contribution of a CSA, scalar or other

mechanism.

7.1.3 Spectral analysis.

The work of Schneider and Buckingham[5] provided useful information on the composition of thallium(I) ethoxide tetramers in neat and dilute solution and thus accounted for the seven and five line spectra observed for the ^{205}Tl and ^{203}Tl nuclei respectively. The assumption made was that spin coupling occured between the ^{205}Tl and ^{203}Tl nuclei within the tetrameric species and that all nuclei of the same isotopic species were magnetically equivalent.

The neat liquid is composed of tetramers of all the possible configurations of ^{205}Tl and ^{203}Tl species and each multiplet spectrum is therefore a superimposition of the spectra arising from each of the possible tetramer configurations. The probability of selecting either a ^{205}Tl or a ^{203}Tl species to form part of a tetramer is calculated from the natural abundances of the respective isotopes. Thus if the symbol (a) corresponds to the probability of a ^{205}Tl species forming a tetramer and (b) corresponds to the probability for the ^{203}Tl isotope, then the abundances of the possible tetramer compositions are given by the binomial expansion,

$$(a+b)^4 = a^4 + 4a^3b + 6a^2b^2 + 4ab^3 + b^4. \quad (7-1)$$

From the known natural abundances for each isotope, a = 0.7048 and b = 0.2952. Therefore the relative abundance of each of the five possible tetrameric structures may be

calculated and the corresponding resonance spectra for both ^{205}Tl and ^{203}Tl nuclei may be predicted. These are given in table (7 - 1).

Table (7 - 1) Normalised abundances and spectral multiplicities of possible tetramer configurations for thallium(I) alkoxide tetramers.

Tetramer	Normalised abundance	SPECTRUM ^{205}Tl	SPECTRUM ^{203}Tl
5-5-5-5	0.2468	Singlet	———
5-5-5-3	0.4134	Doublet	Quartet
5-5-3-3	0.2597	Triplet	Triplet
5-3-3-3	0.0725	Quartet	Doublet
3-3-3-3	0.0076	———	Singlet

The figures 5 and 3 represent the ^{205}Tl and ^{203}Tl species respectively.

From the relative abundance figures given in table (7 - 1), it is possible to calculate the theoretical intensities of the components of the multiplet in both ^{205}Tl and ^{203}Tl spectra. These are found to be in accordance with the observed intensities[5,7], thus providing evidence to support this model. Examples of typical ^{205}Tl and ^{203}Tl spectra for thallium(I) ethoxide are shown in figure (7 - 1).

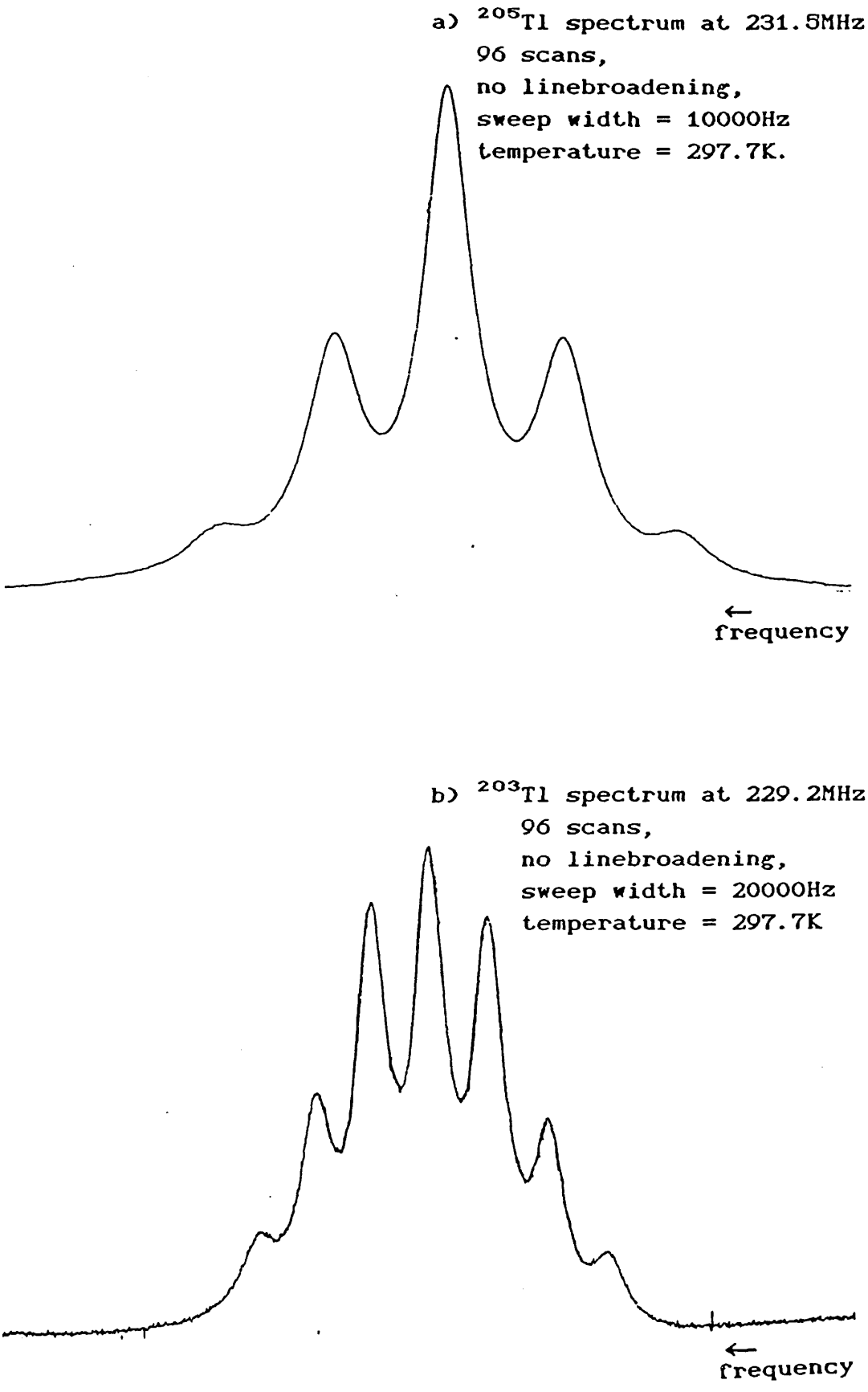

Figure (7-1) ^{205}Tl and ^{203}Tl spectra for thallium(I) ethoxide.

Section 7.2 ^{205}Tl and ^{203}Tl relaxation studies on neat thallium(I) ethoxide.

7.2.1 Introduction.

Previous NMR studies have shown that there is a strong interaction between ^{205}Tl and ^{203}Tl nuclei, and this interaction gives rise to an important contribution to the ^{205}Tl nuclear spin relaxation. However, the true nature of this contribution was not fully characterised, and so it was proposed that an additional ^{203}Tl R_1 study would provide a further insight into the relaxation properties of both thallium nuclei in the thallium(I) ethoxide system. This in turn might lead to a better understanding of the ^{205}Tl and ^{203}Tl lineshape phenomena.

7.2.2 Measurements.

Extensive measuremnts were made on a degassed sample of thallium(I) ethoxide that was sealed in a 5mm NMR tube. ^{205}Tl R_1 values were measured at ^{205}Tl frequencies of 21.95MHz, 51.84MHz and 231.5MHz and ^{203}Tl R_1 values were measured at ^{203}Tl frequencies of 21.74MHz and 229.2MHz. All measurements were made as a function of temperature.

Later, a second pure thallium(I) ethoxide sample was made and this was found to give significantly less broad linewidths for both ^{205}Tl and ^{203}Tl spectra. The measurement of R_1 for both nuclei at high field and as a function of temperature, indicated that the R_1 behaviour was the same in both samples, and this was confirmed by ^{205}Tl and ^{203}Tl R_1 measurements, at selected temperatures,

at low field. Therefore, the ^{205}Tl and ^{203}Tl R_1 values for the initial sample were retained and used in the analysis presented in later sections, whilst, for the discussion on ^{205}Tl and ^{203}Tl linewidth behaviour at high and low field, the linewidths of the new pure sample were taken to reflect the true linewidth behaviour.

The width of the ^{205}Tl and ^{203}Tl spectra make it impossible to observe either fully at 21.95MHz since the sweep width is restricted to 5000Hz. As noted, the observed spectra show five and seven lines respectively and the spacing between these is equal to $J(^{205}Tl-^{203}Tl)/2$, which is approximately 1280Hz. Hence sweep widths in the order of 10,000 Hz are necessary to observe the full spectra. Thus it was only possible to observe the central three features of the spectrum for each nucleus. This procedure led to a distortion of the baseline by peak folding of the outer peaks, and this, coupled with the problems associated with observing the broad linewidths in the spectrum of both nuclei made analysis difficult. However experimental errors were within ± 10% for both ^{205}Tl and ^{203}Tl R_1 values measured at this field strength.

Each component of the multiplet spectra for either nucleus appeared to relax at the same rate and so signal intensities required for calculation of the R_1 values were measured from the central feature of each spectrum. The results are given in tables {7 -2 } to {7 - 5}.

Table (7 - 2) Temperature dependence of ^{205}Tl R_1 at 21.95MHz.

Temperature (K)	R_1 (s^{-1})
285.1	23.3
289.8	19.8
294.8	17.8
301.8	14.8
307.5	11.9
311.0	12.0
322.2	10.0
330.9	7.2
341.0	6.0

Table (7 - 3) Temperature dependence of ^{203}Tl R_1 at 21.74MHz.

Temperature (K)	R_1 (s^{-1})
281.7	78.2
285.5	58.7
291.6	47.7
292.6	40.4
300.0	32.1
303.6	27.6
314.0	16.6

Table (7 - 4) Temperature dependence of ^{205}Tl R_1 at at 61.84MHz.

Temperature (K)	R_1 (s^{-1})
302.8	41.7
314.9	28.9
322.1	24.3
326.8	26.4
331.7	18.2
336.1	16.2
340.5	18.2
349.3	15.1
353.5	14.0

Table (7 - 5) Temperature dependence of ^{205}Tl and ^{203}Tl at 231.5MHz and 229.2MHz respectively.

Temperature (K)	$^{205}R_1$ (s^{-1})	$^{203}R_1$ (s^{-1})
299.7	——	523
301.0	482	——
310.5	401	407
320.0	321	322
329.6	261	261
339.9	212	213
349.1	190	176

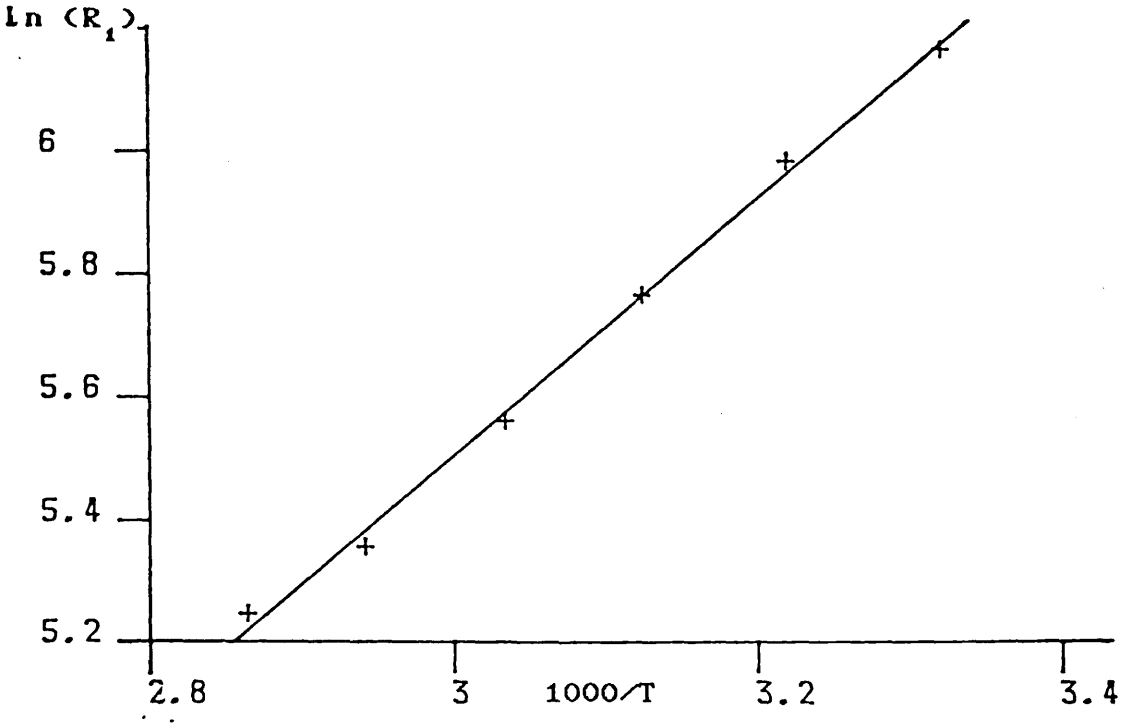

Figure (7-2) Temperature dependence of ^{205}Tl R_1 at 231.5MHz. (neat $[TlOC_2H_5]$)

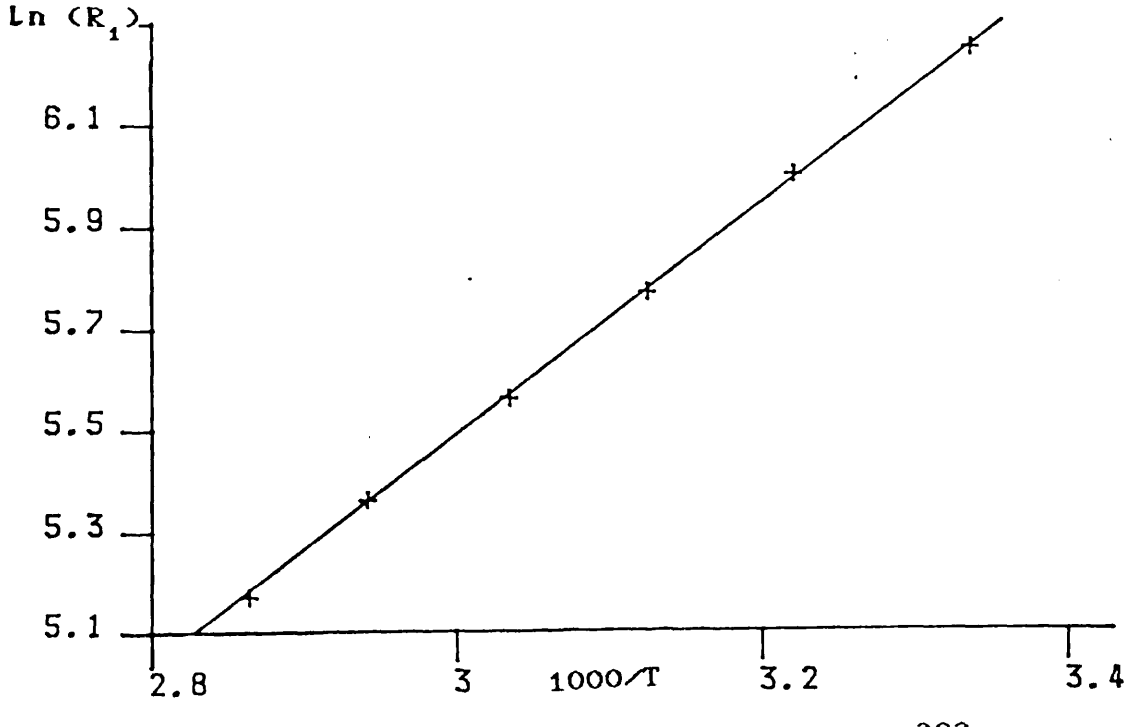

Figure (7-3) Temperature dependence of ^{203}Tl R_1 at 229.2MHz. (neat $[TlOC_2H_5]$)

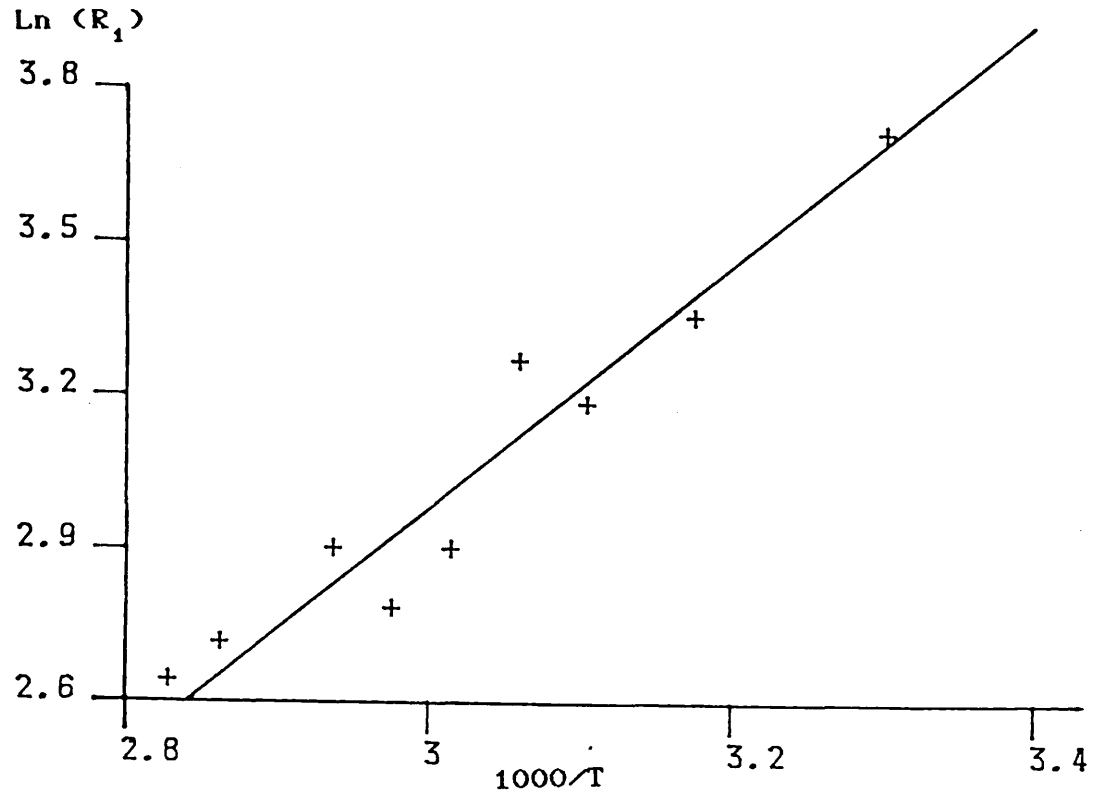

Figure (7-4) Temperature dependence of ^{205}Tl R_1 at 51.84MHz. (neat $[TlOC_2H_5]$)

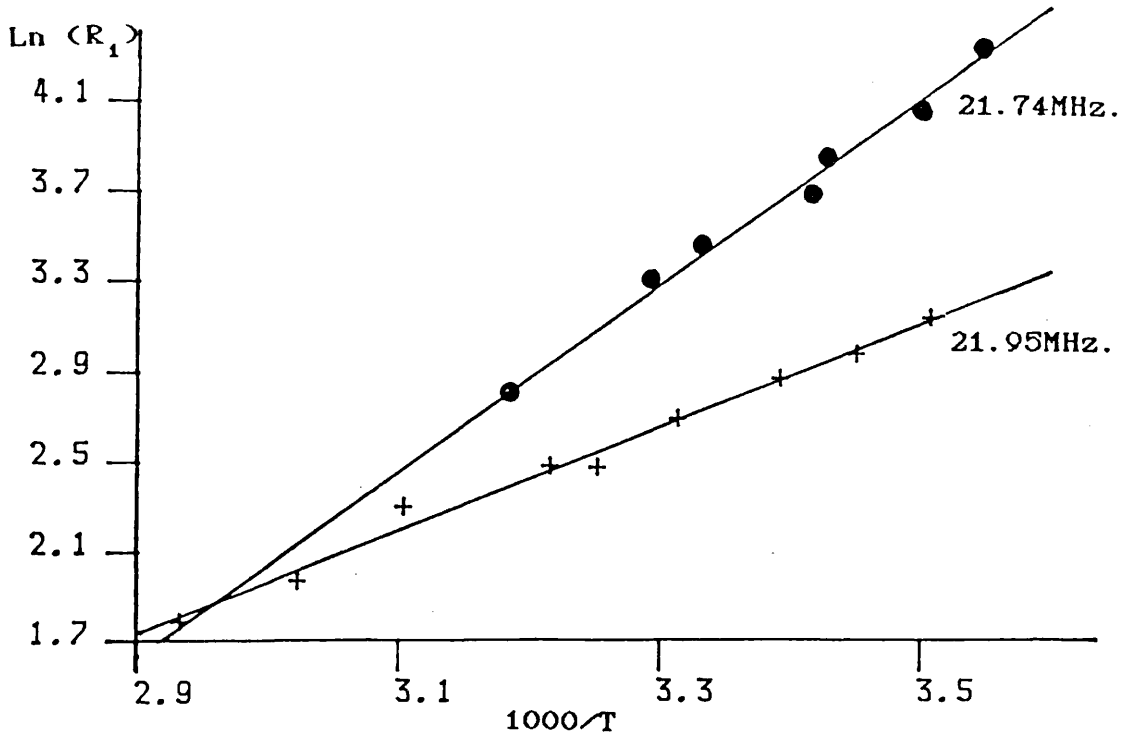

Figure (7-5) Temperature dependence of ^{205}Tl and ^{203}Tl R_1 at 21.95MHz. and 21.74MHz. respectively (neat $[TlOC_2H_5]$)

At temperatures greater than 314.0K, the ^{203}Tl spectra became very broad due to coalescence of the central features. The broad line could not be distinguished from the baseline using a maximum sweep width of 5000Hz and therefore measurements of the ^{203}Tl R_1 values at 21.74MHz are restricted to the temperatures at which the central features are resolved. ^{203}Tl R_1 values at a frequency of 51.74MHz could not be measured with existing pulse lengths (see section (3 - 1)) and so measurements at intermediate field strength are restricted to ^{205}Tl R_1 values alone.

Figures (7 - 2) to (7 - 5) show the plots of ln R_1 against inverse temperature for the data presented in the tables above.

7.2.3 Field dependent analysis of pure thallium(I) ethoxide R_1 data.

7.2.3.1 High field data.

Considering the ^{205}Tl and ^{203}Tl R_1 data obtained at high field, it is noticeable that the large relaxation rates observed are consistent with the dominance of the CSA relaxation mechanism for both nuclei. The rates are observed to be equal and this is as expected, for the ^{205}Tl and ^{203}Tl nuclei should have the same shielding anisotropy, similar resonance frequencies and have the same reorientational correlation times. The relaxation behaviour thus appears to be well defined and may be explained by the Bloch equations[8].

The linear plots of ln R_1 against inverse temperature

It has been noted in section (3.1) that at a frequency of 51.33MHz, the ^{203}Tl R_1 values are too large to be measured on the Jeol FX90Q spectrometer system with the necessary pulse lengths required for the observation of thallium nuclei. However, ^{205}Tl R_1 measurements were performed routinely, and so this suggests qualitatively that the R_1 values for each isotope are still different at this frequency.

The plots of ln R_1 against inverse temperature for both ^{205}Tl and ^{203}Tl R_1 values obtained at low and intermediate field strengths, shown in figures (7 - 4) and (7 - 5), are linear and the subsequent fitting procedure to equation (7 - 2) gave the following best fit parameters.

At 21.95MHz,

$$^{205}R_{1(298)} = 16.2 \pm 0.2\ s^{-1} \qquad (7 - 7)$$

$$^{*205}E_a = 19.2 \pm 0.8\ kJ\ mol.^{-1} \qquad (7 - 8)$$

At 21.74MHz,

$$^{203}R_{1(298)} = 34 \pm 2\ s^{-1} \qquad (7 - 9)$$

$$^{*203}E_a = 35 \pm 2\ kJ\ mol.^{-1} \qquad (7 - 10)$$

At 51.84MHz,

$$^{205}R_{1(298)} = 46.5 \pm 3\ s^{-1} \qquad (7\ \ 11)$$

$$^{*205}E_a = 20 \pm 2\ kJ\ mol^{-1}. \qquad (7 - 12)$$

By assuming that the CSA mechanism dominates the relaxation at high field and the reorientational motion is at extreme narrowing, the CSA contribution

to the total rate at any given field strength may be calculated by applying the simplified CSA R_1 expression in the fast motional limit, given in section (2.3.1) and repeated here for convenience.

$$R_{1CSA} = \frac{2}{15} \gamma^2 B_0^2 \Delta\sigma^2 \left(1 + \frac{\eta^2}{3} \right) \tau_c \ , \quad (7 - 13)$$

where all the symbols have their usual meaning.

It is noticeable that the rates are directly dependent upon τ_c and not the product $\omega_0\tau_c$, as in the full rate equation. Therefore the CSA contribution at each field strength may be calculated, without the need to assume a value for the shielding anisotropy, but simply by scaling the high field data by the squared ratio of the resonance frequencies. The results of this scaling procedure are presented in tables (7 - 6) to (7 - 8).

* The differences in E_a for ^{205}Tl and ^{203}Tl nuclei suggest that more than one motional process is significant for relaxation and so a single activation energy may not be presumed.

Table (7 - 6) Predicted contributions of R_{1CSA} and R_{1other} to the total low field ^{205}Tl R_1 at 21.95MHz.

Temperature (K)	$^{205}R_{1CSA}(s^{-1})$	$^{205}R_{1other}(s^{-1})$
298.0	4.6	11.6
299.7	4.4	11.0
301.0	4.3	9.8
310.5	3.6	8.3
320.0	2.9	6.6
329.6	2.3	5.4
339.6	1.9	4.4
349.1	1.7	3.5

Table (7 - 7) Predicted contributions of R_{1CSA} and R_{1other} to the total ^{203}Tl R_1 at 21.74MHz.

Temperature (K)	$^{203}R_{1CSA}(s^{-1})$	$^{203}R_{1other}(s^{-1})$
298.0	4.6	28.9
299.7	4.4	26.5
301.0	4.3	24.8
310.5	3.7	15.6
320.0	2.9	10.1
329.6	2.3	6.6
339.6	1.9	4.2
349.1	1.6	2.8

Table (7 - 8) Predicted contributions of R_{1CSA} and R_{1other} to the total ^{205}Tl R_1 at 51.84MHz.

Temperature (K)	$^{205}R_{1CSA}(s^{-1})$	$^{205}R_{1other}(s^{-1})$
298.0	25.6	20.9
299.7	24.6	19.8
301.0	24.2	18.7
310.5	20.1	13.5
320.0	16.1	10.6
329.6	13.1	8.3
339.6	10.6	6.7
349.1	9.5	4.8

The results clearly show that the CSA mechanism is not dominant for either nucleus at lower field strengths and it is therefore necessary to account for the residual rate contribution.

7.2.4 Other relaxation contributions.

The residual R_1, (R_{1other}) observed at the low and intermediate field strengths may arise from either a single or a number of contributory mechanisms.

The observed temperature dependence of R_{1other} discounts the possibility of a significant spin-rotation contribution and therefore the rate must be accounted for by a dipole-dipole and/or scalar mechanism.

The contribution of the dipole-dipole relaxation mechanism arising from inter and intramolecular $^{205/203}Tl - {}^1H$, interactions was tested by performing $^{205}Tl - \{^1H\}$ and $^{203}Tl - \{^1H\}$ nuclear Overhauser enhancement experiments at the low and intermediate field strengths at 294.6K and 332.8K. No enhancement was observed and so the mechanism was discounted.

The intramolecular Tl - Tl dipole-dipole mechanism may itself provide a contribution to R_{1other}. The equation for the relaxation of a spin $\frac{1}{2}$ nucleus I interacting with nuclei S in the motional extreme narrowing limit is given by[9]

$$R_{1DD} = \left(\frac{\mu_0}{4\pi} \right)^2 \frac{2}{15} \frac{N_S \gamma_I^2 \gamma_S^2 \hbar^2 \tau_c}{r_{IS}^6}, \quad (7 - 14)$$

where r_{IS} is the internuclear distance and N_S is the number of S spins.

In this limit the condition $\omega_0 \tau_c << 1$ holds and therefore, for the most favourable situation for dipolar relaxation, a maximum correlation time of 500ps is assumed. This value may be inserted into equation (7 - 14), together with the reported value[3] for r_{IS} of 3.84×10^{-10}m, to give the maximum contribution of the dipole-dipole mechanism. This is calculated to be 0.01 s^{-1} and hence this mechanism may be neglected.

It is apparent that the efficiency of the dipole-dipole mechanism is severely impaired by the large internuclear distance observed in the thallium(I) ethoxide tetramer. In a similar manner, the Tl-Tl intermolecular dipole-dipole mechanism may also be assumed to be inefficient. In the structure proposed by previous workers[1,3] the thallium nucleus is surrounded by a tetrahedron of oxygen atoms and thus it is unlikely that the two interacting thallium species may become close enough together to give rise to a significant intermolecular interaction. Further evidence is provided by noting that for the intermolecular mechanism, the Tl-H dipolar interaction is likely to be greater than the Tl-Tl interaction due to the higher magnetogyric ratio of the ^1H

nucleus, and no Tl-H interaction has been observed.

A further suggested experiment to provide corroborative evidence for the lack of a contribution from the dipole-dipole mechanism would be a $^{205}Tl - \{ ^{203}Tl \}$ nOe experiment. For a full contribution of this mechanism the signal enhancement is given by,

$$nOe = 1 + \frac{\gamma_{^{203}Tl}}{2\,\gamma_{^{205}Tl}}, \qquad (7\text{-}15)$$

and on the basis of the previous discussion one would expect to observe no positive signal enhancement.

The assumed lack of any dipolar contribution suggests that the scalar mechanism provides the dominant contribution to the residual rate at low and intermediate field strengths. It is apparent from the coupling observed in both ^{203}Tl and ^{205}Tl spectra, that there is a strong scalar interaction between the two nuclei and it is possible that a modulation of this coupling will lead to a relaxation pathway. In addition, the particularly small difference in resonance frequencies of the ^{205}Tl and ^{203}Tl nuclei may be favourable for the efficiency of this mechanism.

The modulation of the scalar coupling may occur via a chemical exchange process or by the rapid relaxation of a coupled nucleus. If we initially consider the effects of the latter, the maximum observed ^{205}Tl R_1 of 23.3 s^{-1} and ^{203}Tl R_1 of 78.3 s^{-1} at low field suggest that the

relaxation of one nucleus is not rapid enough to cause an appreciable effect on the other. Thus the scalar mechanism of the second kind may be discounted. Therefore it appears that the relaxation arises from a chemical exchange process. The observation of chemical exchange processes in this system is discussed in conjunction with the linewidth behaviour presented in section (7.4).

Typically, for the scalar relaxation mechanism, the chemical exchange time τ_e is in the fast limit such that the condition,

$$\frac{1}{\tau_e} >> J \qquad (7 - 16)$$

holds, where J is the scalar coupling constant in Hz. In this limit the multiplet structure collapses and the scalar relaxation rates R_{1Sc} and R_{2Sc} are given by[10]:

$$R_{1Sc} = \frac{8\,\pi^2\,J^2\,S(S+1)}{3}\left[\frac{\tau_{Sc2}}{1 + (\omega_I - \omega_s)^2\,\tau_{Sc2}^2}\right] \qquad (7 - 17)$$

$$R_{2Sc} = \frac{4\,\pi^2\,J^2\,S(S+1)}{3}\left[\tau_{Sc1} + \frac{\tau_{Sc2}}{1 + (\omega_I - \omega_S)^2\tau_{Sc2}^2}\right] \qquad (7 - 18)$$

However, by observation, it is noticeable that the ^{205}Tl and ^{203}Tl spectra show that the Tl-Tl coupling is

preserved up to a temperature of ~ 335K at high field and a temperature of ~ 355K at low field. Clearly as the multiplet structure in either spectra is not collapsed at ambient temperature, the timescale is such that $\frac{1}{\tau} < J$ and the equations for scalar relaxation {7 - 17} and {7 - 18} do not apply.

The low field relaxation behaviour will now be discussed qualitatively in terms of a dominant scalar mechanism.

The first observation is the difference in the ^{205}Tl and ^{203}Tl R_1 observed at low and intermediate field strengths. It is significant that the less abundant ^{203}Tl spin relaxes more efficiently than the ^{205}Tl spin. Although this behaviour has not been noted previously for spin-lattice relaxation, analogous behaviour arising from a difference in nuclear spin abundances has been noted by Bloembergen and Rowland[11] for the linewidths of ^{205}Tl and ^{203}Tl resonances in solid thallium and thallic oxide. The spectra of both thallium nuclei were observed as a function of the isotopic abundance of each nucleus and it was noted that as one isotope was enriched, its resonance linewidth became sharper whilst the linewidth of the coupled, unlike nucleus became broad. Thus it was concluded that the scalar interaction between unlike spins contributed to the linewidth whilst the interaction between like spins had no effect.

Hinton and Metz[12] similarly found that the ^{203}Tl

solid state powder pattern of thallium(I) nitrate was significantly broader than that given by the ^{205}Tl nucleus and this behaviour was also rationalised on the basis of ^{203}Tl-^{205}Tl scalar interaction.

The difference in R_1 behaviour may be rationalised in a similar manner. If ^{205}Tl and ^{203}Tl relaxation occurs through modulation of the scalar coupling to an inequivalent nucleus then clearly the less abundant ^{203}Tl nucleus will relax more efficiently, as it has more inequivalent neighbours to which it can couple and effect relaxation.

7.2.5 Cross relaxation.

In tables (7 -6) to (7 - 8), the non-CSA relaxation rate, R_{1other}, for both nuclei, is observed to increase with increase in field strength, which is otherwise indicative of a CSA contribution. There is no obvious explanation for this in terms of simple scalar relaxation.

The reason may originate in the presence of multiple spins and the phenomenon of cross relaxation.

The cross-relaxation process may occur between two unlike spins that are coupled via a scalar or dipolar relaxation mechanism and clearly may be operative in this system.

Any relaxation process requires a time dependent interaction Hamiltonian. The Hamiltonian describing the scalar interaction of two spins is given by,

$$\hat{\mathcal{H}}_{SC} = J (\hat{I}_Z \hat{S}_Z + \tfrac{1}{2} (\hat{I}_+ \hat{S}_- + \hat{I}_- \hat{S}_+)) \quad (7 - 19)$$

The modulation of this Hamiltonian by a changing of the number of coupling partners gives rise to a "flip-flop" transition, this links states with the same quantum number m_t.

As discussed by Noggle and Schirmer[13] such a transition can exchange Z magnetisation between two spins.

The argument for a positive field dependence in R_{1other} is simplified by reference to figure (7 - 6).

Figure (7 - 6) Schematic representation of the loss of Z magnetisation from ^{205}Tl and ^{203}Tl spins.

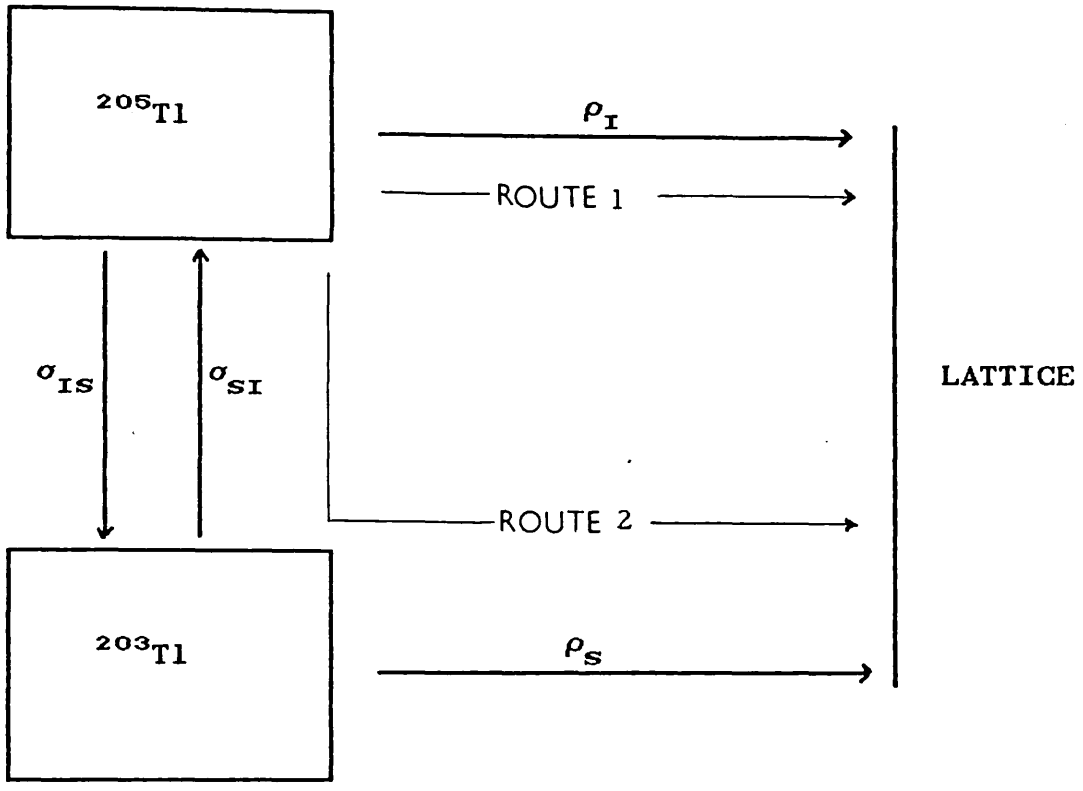

Here it is observed that the relaxation of either nucleus may proceed via two routes. Firstly by the loss of Z magnetisation directly to the lattice via the usual spin-lattice relaxation processes, ρ_I and ρ_S and secondly by an indirect transfer of Z magnetisation to the lattice through a coupled, inequivalent spin, σ_{IS} , σ_{SI}. If we consider the ^{205}Tl nucleus, then as the field strength is increased, the transfer of ^{205}Tl Z magnetisation to the lattice via the ^{203}Tl nucleus (route 2) will be enhanced by the faster relaxation of the ^{203}Tl nucleus due to the increased contribution of the CSA mechanism at this field.

The similar argument holds for the ^{203}Tl nucleus, though this behaviour remains to be verified by ^{203}Tl R_1 measurements at 51.33MHz.

When cross-relaxation provides a significant contribution to the total relaxation rate, the Bloch equations prove to be inadequate for explaining the overall relaxation behaviour. This situation is best represented by the Solomon equations[14].
For two spins I and S,

$$\frac{d\langle I_z\rangle}{dt} = -\rho_I [\langle I_z\rangle - I_o] - \sigma_{IS} [\langle S_z\rangle - S_o], \qquad (7-20)$$

$$\frac{d\langle S_z\rangle}{dt} = -\rho_S [\langle S_z\rangle - S_o] - \sigma_{SI} [\langle I_z\rangle - I_o], \qquad (7-21)$$

where $\langle I_z\rangle$ and $\langle S_z\rangle$ correspond to the intensities of the spins I and S respectively and I_o, S_o are the values of $\langle I_z\rangle$ and $\langle S_z\rangle$ at thermal equilibrium. The parameters ρ_S, ρ_I are the direct relaxation terms, and thus

$$\rho_I = \frac{1}{T_1^{II}}, \qquad (7-22)$$

$$\rho_S = \frac{1}{T_1^{SS}}. \qquad (7-23)$$

The parameters σ_{IS} and σ_{SI} correspond to the cross relaxation terms, where,

$$\sigma_{IS} = \frac{1}{T_1^{IS}}, \qquad (7 - 24)$$

$$\sigma_{SI} = \frac{1}{T_1^{SI}}. \qquad (7 - 25)$$

Thus the equations may be seen to be the simple Bloch equations with added terms that reflect the cross relaxation contribution.

If cross relaxation is significant, then for a two site model, the equation that describes the return to equilibrium of the perturbed magnetisation following a 180^{o} inverting pulse is characterised by a double, rather than a single, exponential function. Thus if cross-relaxation is important in this system, then by treating the intensity : τ time data obtained from the inversion recovery experiment, in the usual manner, one is fitting a best fit curve based on a single exponential model to a double exponential recovery function. Thus the calculated R_1 values may only be a crude representation of the true R_1. In the situation for thallium(I) ethoxide, the model is more complex and the recovery curve would be predicted to be multiexponential.

To fully characterise the inversion-recovery curve, it is necessary to have several, very accurate, intensity : τ time data points. Unfortuately, the number of data points available to characterise the inversion-recovery curves at low and intermediate field strengths are not sufficient to verify multiexponential behaviour.

Further work involving double resonance experiments could better characterise the cross-relaxation behaviour in this system. A saturation of one resonance would give rise to a time dependent decrease in the other resonance. For a full contribution of the scalar mechanism the final intensity would be,

$$I = 1 - \frac{\gamma_{IRRADIATED}}{\gamma_{OBSERVED}} . \qquad (7 - 26)$$

In addition, inversion of either ^{205}Tl or ^{203}Tl leads to a time dependent decrease in the intensity of the other spin which relaxes in time, back to equilibrium.

Section 7.3 ^{205}Tl and ^{203}Tl Relaxation study on thallium(I) ethoxide diluted with cyclohexane.

7.3.1 Measurements.

As a further study on the dependence of the ^{205}Tl and ^{203}Tl R_1 on the chemical exchange processes occuring in thallium(I) ethoxide, a relaxation study on a diluted sample was proposed.

^{205}Tl and ^{203}Tl R_1 measurements were made on a degassed sample of 17 mole% thallium(I) ethoxide in cyclohexane, at ^{205}Tl frequencies of 21.95 MHz and 231.5 MHz and ^{203}Tl frequencies of 21.74 MHz and 229.2 MHz. The measurements were made as a function of temperature and the results are shown in tables (7 - 9) and (7 -10)

Table (7 - 9) Temperature dependence of ^{205}Tl R_1 and ^{203}Tl R_1 in diluted thallium(I) ethoxide at 21.95MHz and 21.74MHz respectively

Temperature (K)	$^{205}R_{1CSA}(s^{-1})$	$^{203}R_{1CSA}(s^{-1})$
292.3	74.0	75.3
307.6	60.8	61.1
315.7	46.1	57.5
325.0	37.2	33.7
337.3	23.1	——

Table (7 - 10) Temperature dependence of ^{205}Tl R_1 and ^{203}Tl R_1 in diluted thallium(I) ethoxide at 231.5MHz and 229.2MHz respectively.

Temperature (K)	$^{205}R_{1CSA}(s^{-1})$	$^{203}R_{1CSA}(s^{-1})$
299.1	72.7	75.3
308.0	62.1	64.4
317.4	56.3	55.6
326.9	49.0	44.3
338.0	42.3	42.2
348.7	33.8	34.2

7.3.2 Discussion.

The Arrhenius plots of the R_1 data are shown in figures (7 - 7) to (7 - 10). A non linear least squares fitting procedure to equation (7 - 2) for the data obtained for each nucleus at high and low field, gave the best fit estimates for R_1 at 298K and the activation energy. These parameters are presented in tables (7 - 11) and (7 - 12).

Table (7 - 11) $R_{1(298)}$ and E_a parameters for ^{205}Tl and ^{203}Tl nuclei at 21.95MHz. and 21.74MHz. respectively.

	^{205}Tl	^{203}Tl
$R_{1(298)}$ (s^{-1})	67 ± 5	69 ± 8
E_a (kJ mol^{-1})	18 ± 3	15 ± 7

Table (7 - 12) $R_{1(298)}$ and E_a parameters for ^{205}Tl and ^{203}Tl nuclei at 231.5MHz. and 229.2MHz respectively.

	^{205}Tl	^{203}Tl
$R_{1(298)}$ (s^{-1})	74 ± 2	77 ± 2
E_a (kJ mol^{-1})	12.3 ± 0.8	13.6 ± 0.9

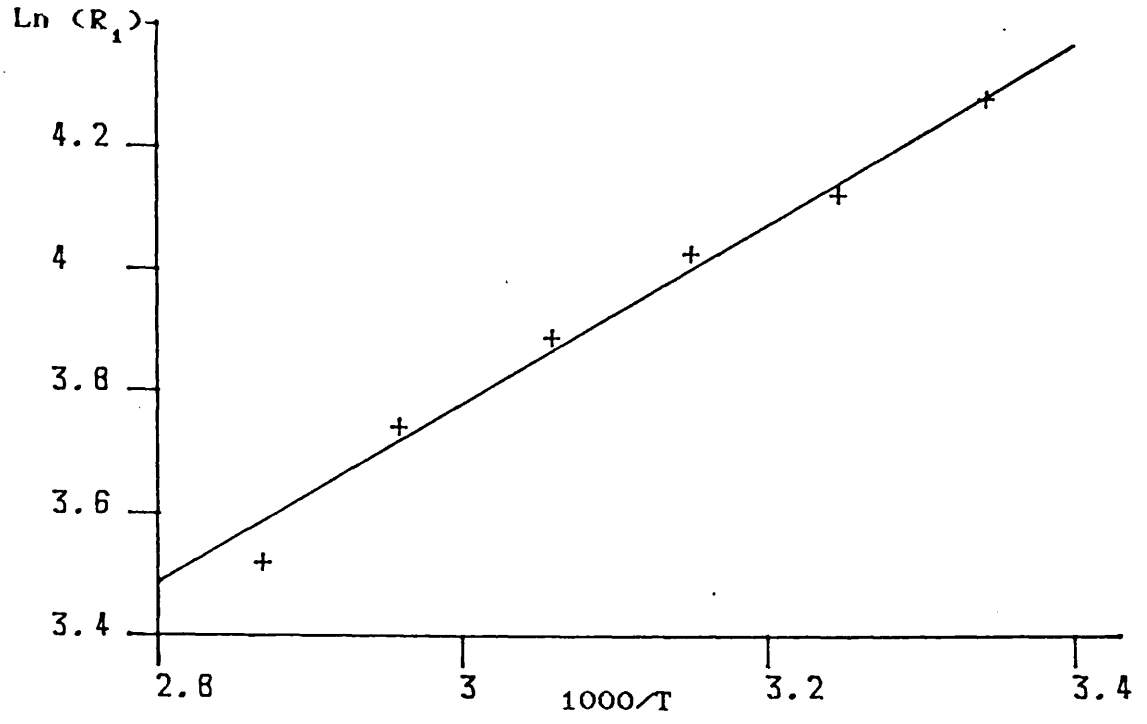

Figure (7-7) Temperature dependence of ^{205}Tl R_1 at 231.5MHz in $[TlOC_2H_5]_4$/Cyclohexane solution.

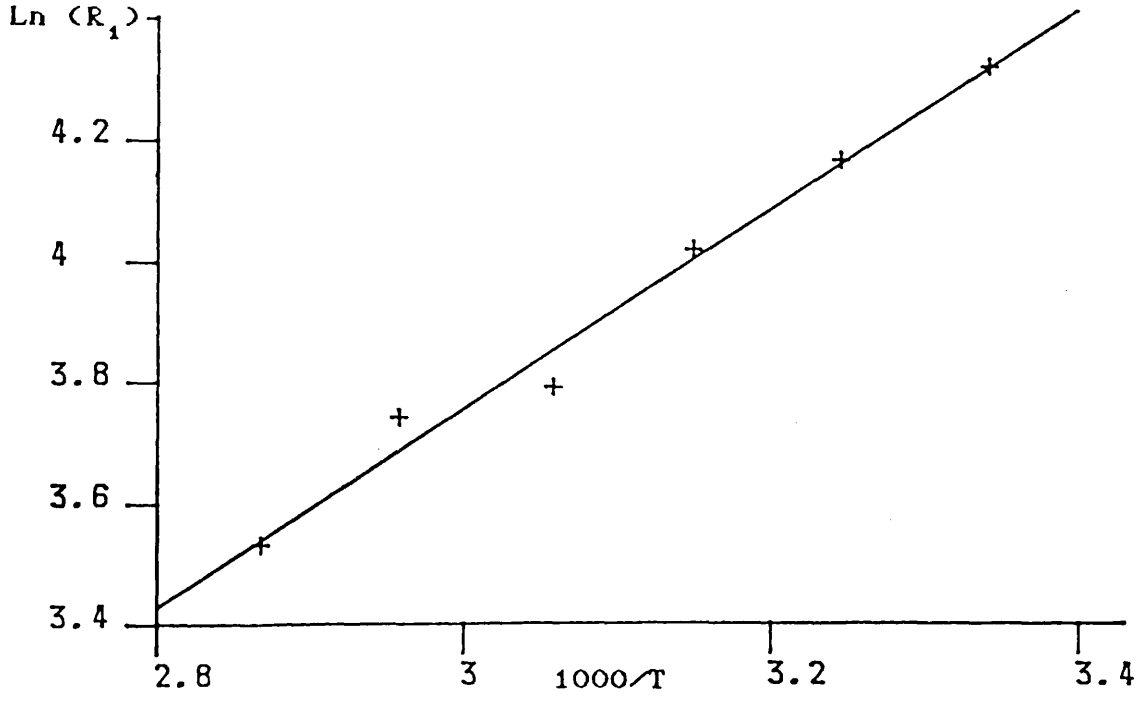

Figure (7-8) Temperature dependence of ^{203}Tl R_1 at 229.2MHz. in $[TlOC_2H_5]_4$/Cyclohexane solution.

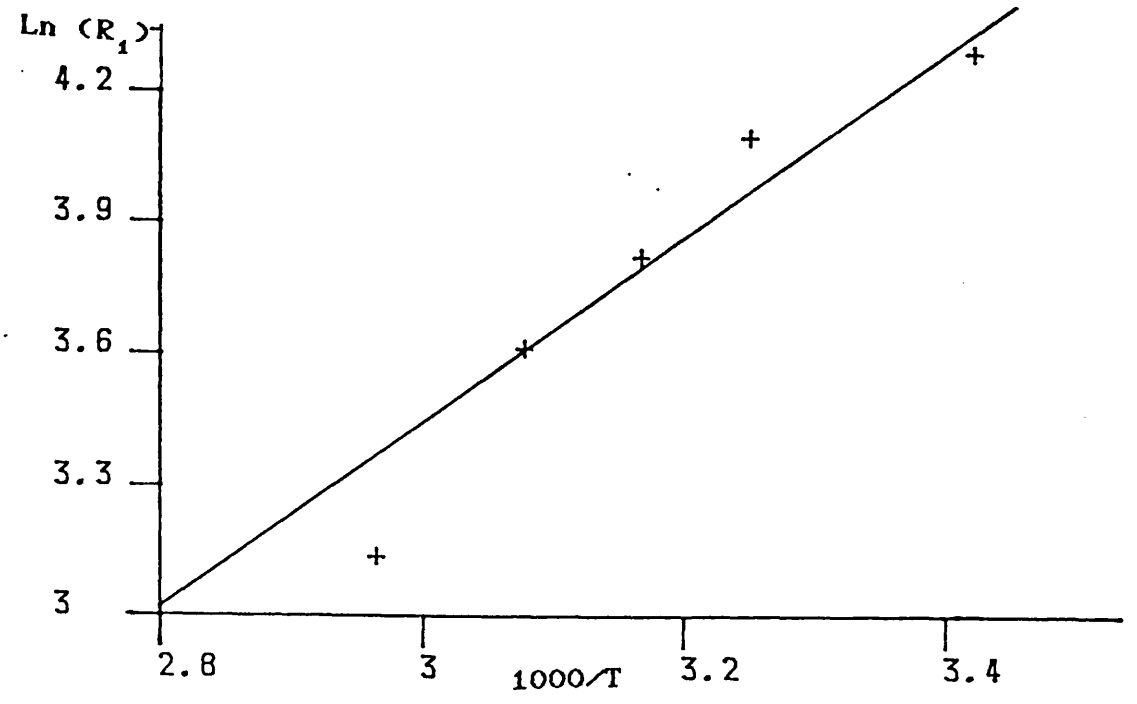

Figure (7-9) Temperature dependence of ^{205}Tl R_1 at 21.95MHz. in $[TlOC_2H_5]_4$/Cyclohexane solution.

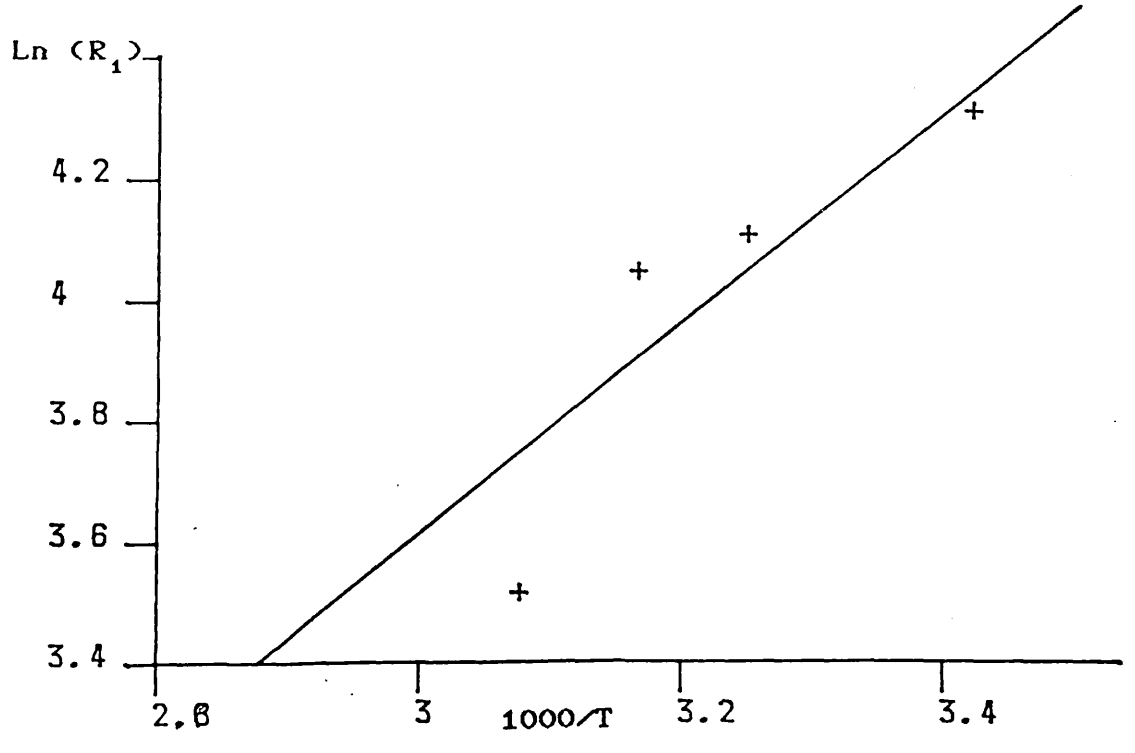

Figure (7-10) Temperature dependence of ^{203}Tl R_1 at 21.74MHz. in $[TlOC_2H_5]_4$/Cyclohexane solution.

No change in the form of either the ^{205}Tl or the ^{203}Tl spectrum was observed on dilution of the pure sample and similarly no shift change was observed. Thus the thallium(I) ethoxide was assumed to maintain its tetrameric structure at both concentrations.

It is apparent that the dilution of thallium(I) ethoxide has a noticeable effect on the R_1 behaviour at both high and low field. At high field, the ^{205}Tl and ^{203}Tl R_1 values are equal, yet significantly lower than those observed at the same field strength in the non-diluted sample.

The low field relaxation behaviour in this system is similarly, significantly different from that observed in the pure sample as both rates are now equalised and are also increased. The rates show only a slight increase with field at higher temperatures, and considering the larger errors in the measured rates at elevated temperatures, there appears to be little, or no field dependence.

Clearly the behaviour of the diluted sample is quite different from the undiluted and the R_1 values obtained in each solution may not be directly compared in a quantitative manner. However, some general effects of dilution may be noted.

The apparent field independent R_1 for both nuclei and the reduction of the high field R_1 on dilution of the pure thallium(I) ethoxide, are both consistent with the fact that the CSA mechanism no longer makes a significant

contribution. This may be rationalised by considering the structure of the thallium(I) ethoxide tetramer. The thallium nucleus has a regular, symmetric environment of oxygen atoms and thus would typically be assumed to show a low shielding anisotropy and hence a negligible contribution from the CSA mechanism. This situation is observed in the diluted sample. However, in the pure thallium(I) ethoxide, the tetramers are very close together and thus undergo many collisions. These collisions may be considered to distort the symmetric environment of the thallium nucleus and thus give rise to the transient CSA mechanism discussed by Schwartz[15].

The equalising of the ^{205}Tl and ^{203}Tl R_1 values at both field strengths shows that the dilution of the neat thallium(I) ethoxide nullifies the effect observed at low field in the pure sample. The reason for this may be seen if we assume that in the pure sample the rate is dominated by a scalar mechanism arising from a chemical exchange process. Dilution significantly impairs the efficiency of the chemical exchange between tetramer units and is thus assumed to reduce the efficiency of the scalar mechanism.

This argument is not fully consistent with the observed results as it is apparent that the relaxation mechanism is more efficient in the diluted sample at low field. However it must be re-iterated here that the pure and diluted samples may not be directly compared quantitatively as they are essentially two different

solutions in which factors such as solvent and viscosity are different. This is clearly seen in the difference in activation energies for the relaxation mechanisms operative in the two samples.

Finally, the apparent field independence of the R_1 values for each nucleus is not explained by the dominance of the scalar mechanism, as the presence of the $(\Delta\omega\ \tau_{SC})^2$ term in the scalar rate expression should lead to a field dependence.

It appears that the field independence may only be explained by a dominant dipole-dipole contribution which is unlikely in view of the discussion in section (7.2.4) and so this anomally remains unexplained.

Section 7.4 ^{205}Tl and ^{203}Tl lineshape behaviour.

Further information on the relaxation behaviour of both thallium nuclei in pure and diluted thallium(I) ethoxide systems may be obtained by observation of the lineshape behaviour.

7.4.1 Line broadening due to chemical exchange.

The spectra have been noted[7] to be resolved at ambient temperature at both high and low field, yet gradually broaden and coalesce as the temperature increases. The Tl-Tl coupling eventually collapses and the single resonance linewidths for both ^{205}Tl and ^{203}Tl nuclei are then observed to become narrower. This

behaviour is indicative of a chemical exchange process.

If we consider the exchange of units of thallium(I) ethoxide molecules; each unit may contain either the ^{205}Tl or ^{203}Tl nucleus. If the chemical exchange results in a ^{205}Tl unit being replaced by a ^{203}Tl unit or vice versa, the tetramer will change to another of the possible tetrameric species outlined in table (7 - 1) and will then exhibit the coupled spectra common to that species. This exchange modulates the ^{205}Tl - ^{203}Tl scalar coupling and leads to a broadening of the thallium resonance.

In addition to the exchange of different isotopes, the exchange may occur between thallium(I) ethoxide units containing the same species. If the incoming unit is different in spin-state to the outgoing unit, the effect felt by the coupled Tl nucleus will be the same as coupling to a fast relaxing nucleus and will similarly modulate the Tl - Tl coupling and give rise to a broadening of the spectra.

Alternatively, the loss of an ethoxide unit does not change the spin system but would be expected to change the coupling pathway and hence the coupling constant.

The observation of different ^{205}Tl and ^{203}Tl linewidths is consistent with the effects of chemical exchange as the less abundant species gives the broader resonance[11,12].

7.4.2 Other line broadening contributions.

If we consider that, at high field the CSA mechanism

makes a dominant contribution to the R_1 in neat thallium(I) ethoxide, then typically one would expect it to make a major contribution to the R_2.

At 298K, at low field the ^{205}Tl and ^{203}Tl linewidths are 82 Hz and 128 Hz respectively and the corresponding high field linewidths are 808 Hz and 1155 Hz respectively. Thus on initial inspection, a strong field dependency that is characteristic of this mechanism, is noted.

By assuming the extreme narrowing limit holds, from the theory presented in Chapter 2, the value of R_{2CSA} is $\frac{7}{6}$ the value of R_{1CSA}. This allows us to calculate a predicted R_2 contribution from the CSA mechanism at both field strengths of interest. Thus for the ^{205}Tl nucleus the contribution at high and low field are 595 s^{-1} and 19 s^{-1} respectively, giving linewidth contributions of 190Hz and 6Hz. The contribution of the ^{203}Tl R_2 at high and low field is 641 s^{-1} and 39.4 s^{-1}, giving linewidth contributions of 204 Hz and 13 Hz. Clearly the dominant contribution to the observed linewidths does not arise from the CSA mechanism and it is unlikely that the scalar mechanism can account for all of the residual contribution.

It is necessary to note at this point the contribution of an additional unknown broadening effect that has been attributed to sample degradation. In the course of this work, two pure thallium(I) ethoxide samples have been studied. The initial study followed that made by

Forster[7] using the same sample described in his work. The ^{205}Tl and ^{203}Tl linewidths were found to be sufficiently broad at high field for the multiplet structure to be unresolved at ambient temperature and the spectral envelope of the ^{205}Tl resonances at 298K was noted to have a linewidth of 3800Hz. A new sample was made and this showed significantly narrower linewidths such that the coupling was still resolved at high field, giving the linewidths mentioned earlier.

It is significant to note this difference in high field linewidth behaviour in reference to the R_1 study presented earlier. The collapsed multiplet observed for the spectrum of both isotopes in the first sample would suggest that the fast exchange limit applied and that the condition (7 - 16) holds. This would lead one to wrongly use equations (7 - 17) and (7 - 18) to describe the R_{1Sc} and R_{2Sc} behaviour.

7.4.3 Effect of dilution on ^{203}Tl and ^{205}Tl linewidths.

Dilution of the pure thallium(I) ethoxide sample to 17mole% gives rise to a small, but noticeable reduction in the low field ^{205}Tl and ^{203}Tl linewidths at 298K to 60Hz and 88Hz respectively. This behaviour is different from that observed by Schneider and Buckingham[5] who suggested that the spectra were invariant to dilution. The relative decrease in linewidth due to dilution is observed to be far greater at high field, where the measured values at

298K are 235Hz and 257 Hz respectively. The coupling is noted to be resolved at all temperatures studied at both high and low field.

The significant reduction in linewidths observed at high field is as predicted, as the dilution of the sample reduces the efficiency of the scalar exchange broadening, and secondly has been noted to reduce the efficiency of the CSA mechanism. Further evidence for the reduction in the efficiency of the scalar mechanism upon dilution is given by noting that the difference between ^{205}Tl and ^{203}Tl linewidths observed in the pure sample is severely reduced in the diluted sample.

Finally, It is apparent that the small reduction in linewidths observed on dilution at low field, suggests that the linewidth at this field is dominated by processes other than the CSA or scalar mechanisms.

References for CHAPTER SEVEN.

1. N.V.Sidgwick and L.E.Sutton, J. Chem. Soc., 1461 (1930).
2. D.C.Bradley, J. Chem. Soc., 4780 (1958).
3. L.F.Dahl, G.L.Davies, D.L.Wampler and R.West, J. Inorg. Nucl. Chem., 24, 357 (1962).
4. V.A.Maroni and J.G.Spiro, Inorg. Chem., 7, 193 (1968).
5. W.G.Schneider and A.D.Buckingham, Disc. Faraday Soc., 34, 147 (1962).
6. P.J.Burke, R.W.Matthews and D.G.Gillies, J. Chem. Soc., Dalton, 1439 (1980).
7. M.J.Forster, Ph.D. Thesis University of London, (1984).
8. F.Bloch, Phys. Rev., 70, 460 (1946).
9. D.M.Grant and J.R.Lyerla Jr., M.T.P. Int. Rev. Series, Vol.4, Chapter 5.
10. A.Abragam, "The Principles of Nuclear Magnetism", O. U. P. (1961).
11. N.Blombergen and T.J.Rowland, Phys. Rev., 97, 1679 (1955).
12. J.F.Hinton and K.R.Metz, J. Amer. Chem. Soc., 104, 6206 (1982).
13. J.H.Noggle and R.E.Schirmer, "The Nuclear Overhauser Effect", Academic Press (1971).
14. I.Solomon, Phys. Rev. 99, 559 (1955).
15. R.N.Schwartz, J. Magn. Reson., 24, 205 (1974).

APPENDIX 1 PGSE Pulse Sequence Microprogram[1].

Address	K	C	B	A	8	7	J	5	4	3	2	1	Command	Parameter No.	Comment
0	•	•	•	•	•	•	•	•	•	•	•	•			
1													TIM	9	INITIAL WAIT
2	•	•	•	•	•	•	•	•	•	•	•	X			
3													TIM	1	PW1 = 90°
4	•	•	•	•	•	•	•	•	•	•	•	•			
5													TIM	11	10μs WAIT
6	•	•	•	•	•	•	•	•	•	•	•	•			
7													TIM	3	PI
8	•	•	•	X	•	•	•	•	•	•	•	•			
9													TIM	4	PD FIELD GRADIENT
10	•	•	•	•	•	•	•	•	•	•	•	•			
11													TIM	11	10μs WAIT
12	•	•	•	•	•	•	•	•	•	•	•	•			
13													TIM	3	PI
14	•	•	•	•	•	•	•	•	•	•	•	X			
15													TIM	2	PW 2 = 180°
16	•	•	•	•	•	•	•	•	•	•	•	•			
17													TIM	11	10μs WAIT
18	•	•	•	•	•	•	•	•	•	•	•	•			
19													TIM	3	PI
20	•	•	•	X	•	•	•	•	•	•	•	•			
21													TIM	4	PD FIELD GRADIENT
22	•	•	•	•	•	•	•	•	•	•	•	•			
23													TIM	11	10μs WAIT
24	•	•	•	•	•	•	•	•	•	•	•	•			
25													TIM	3	PI
26	•	•	•	•	X	•	•	•	X	•	•	•			↑ SCANS
27													TIM	8	
28													PUL		
29													LD2	1	
30	•	•	•	•	X	•	•	X	X	•	•	•			
31													TIM	6	

Address	K	C	B	A	8	7	J	5	4	3	2	1	Command	Parameter No.	Comment
	EXT.IV	EXT.III	EXT.II	HOMO SPOIL	Irradiation gate	AD trigger	EXT.V	Receiver gate	Phase reset	0° or 90° phase	0° or 180° phase	Observation gate	TIM (Table 1) JMP LD1 (Table 2) JC1 LD2 (Table 2) JC2 PUL INT (Table 1)		

Address	K	C	B	A	8	7	J	5	4	3	2	1	Command	Parameter No.	Comment
32	•	•	•	•	X	X	•	X	X	•	•	•			
33													INT	8	SCANS
34	•	•	•	•	X	-	•	X	X	•	•	•			
35													INT	8	
36													JC2		
37	•	•	•	•	•	•	•	•	•	•	•	•			
38													TIM	12	DELAY = $5T_1$
39													JMP	2	
40													JMP	0	
41															
42											•				
43															
44															
45															
46															
47															
48															
49															
50															
51															
52															
53															
54															
55															
56															
57															
58															
59															
60															
61															
62															
63															

Address	K	C	B	A	8	7	J	5	4	3	2	1	Command	Parameter No.	Comment
	EXT.IV	EXT.III	EXT.II	EXT.I	Irradiation gate	AD trigger	EXT.V	Receiver gate	Phase reset	0° or 90° phase	0° or 180° phase	Observation gate	TIM (Table 1) JMP LD1 (Table 2) JC1 LD2 (Table 2) JC2 PUL INT (Table 1)		

REFERENCE

1. D.R.Parkinson, Private Communication.